GLENOHUMERAL CAPSULE SHOULD BE EVALUATED AS A SHEET OF FIBROUS TISSUE: A STUDY IN FUNCTIONAL ANATOMY

by

Susan Marie Moore

BS, University of Kentucky, 2000

Submitted to the Graduate Faculty of

School of Engineering in partial fulfillment

of the requirements for the degree of

Doctor of Philosophy

University of Pittsburgh

2006

UNIVERSITY OF PITTSBURGH

SCHOOL OF ENGINEERING

This dissertation was presented

by

Susan Marie Moore

It was defended on

March 14, 2006

and approved by

Patrick J. McMahon, MD Assistant Professor, Department of Orthopaedic Surgery, University of Pittsburgh Medical Center

David A. Vorp, PhD Associate Professor, Departments of Surgery and Bioengineering

Jeffrey A. Weiss, PhD Associate Professor, Department of Bioengineering, University of Utah

Savio L-Y. Woo, PhD DSc Whiteford Professor, Department of Bioengineering

Dissertation Director: Richard E. Debski, PhD Assistant Professor, Department of Bioengineering

GLENOHUMERAL CAPSULE SHOULD BE EVALUATED AS A SHEET OF FIBROUS TISSUE: A STUDY IN FUNCTIONAL ANATOMY

Susan Marie Moore, PhD

University of Pittsburgh, 2006

Following glenohumeral joint dislocation, surgical repair is often advocated where the glenohumeral capsule is shifted and plicated. However, nearly 25% of patients still experience redislocations. To improve these results, functional evaluations (experimental and computational) of the glenohumeral capsule have been performed whereby isolated, discrete capsuloligamentous regions of the capsule were examined. Specifically, the capsuloligamentous region termed the anterior band of the inferior glenohumeral ligament is often examined in this way since it is frequently injured during dislocations. However, this practice may not be appropriate as recent data suggests that the glenohumeral capsule functions multiaxially. Therefore, the objective of this work was to compare the predicted strain distribution and deformed shape of the anterior band of the inferior glenohumeral ligament to that experimentally measured for two finite element models: 1) composite model including all capsuloligamentous regions and 2) discrete model including only the anterior band of the inferior glenohumeral ligament. The average maximum principal strain for the anterior band of the inferior glenohumeral ligament was 21±14%, 35±14%, and 0±1% for the experimental measurements, composite finite element model, and discrete finite element model, respectively. Thus, the predicted strain distribution in the anterior band of the inferior glenohumeral ligament was similar to that which was experimentally measured for the composite finite element model. Additionally, the predicted deformed shape in the composite finite element model was also similar to experimental data with the anterior band of the inferior glenohumeral ligament clearly

wrapping around the humeral head. However, the predicted strain distribution and shape for the discrete finite element model was drastically different from that observed experimentally with the anterior band of the inferior glenohumeral ligament twisting somewhat along its longitudinal axis and buckling away from the humeral head. These differences may be attributed to neglecting the boundary conditions along the margins of the anterior band of the inferior glenohumeral ligament applied by the remaining capsuloligamentous regions. Thus, the glenohumeral capsule should be evaluated as a sheet of fibrous tissue and composite finite element models may be utilized to evaluate its function in the normal, injured, and surgically repaired state.

TABLE OF CONTENTS

LIST OF TABLES

LIST OF FIGURES

PREFACE

I would like to acknowledge my dissertation advisor, Dr. Richard Debski, for his continual guidance, training, and the numerous opportunities he has bestowed upon me. He has provided an enriching environment within which I have been fortunate enough to cultivate my skills as a researcher. I would also like to acknowledge the clinical advisor to my dissertation, Dr. Patrick McMahon. He has been a wonderful inspiration and exemplifies the attitude that all researchers should aspire to have. Thank you both for your commitment to research, education, and fun. I wish you and your families joy and happiness in the years to come.

Additionally, I would like to thank the remaining members of my dissertation committee, Drs. David Vorp, Jeffrey Weiss, and Savio Woo. Dr. Vorp has been a tremendous complement to the other committee members and has provided a unique perspective to multiple engineering obstacles. Dr. Weiss and his staff, particularly Ben Ellis, have been an intrical part of my dissertation by providing their expertise in computational modeling and multiaxial mechanical testing of soft tissues. Dr. Woo has been a continual influence throughout my dissertation work by teaching the theory and application of fundamental engineering concepts and principles.

I have been blessed with a long list of friends that have been putting up with me for many years, for which I am eternally grateful. You have all kept me sane and reminded me what is most important in life: friends, family, and fun. Jason, hard to believe you are father now. Based on our experiences in Saudi Arabia, your kids are going to be hell raisers and fire starters.

Joey and Kristin, you knew me when having fun meant driving around stealing street signs and hunting for abandoned houses. Stacy, Jenny, and Kate, what can I say? We had some great times, excluding the tree falling on our house and my car, of course. Melissa and Christina, you always kept me in check. Some times the only thing that got me through the week was ordering pizza, Melissa swearing in foreign languages, and watching classics like the Spice Girls' movie. Jessica, between Pittsburgh and Kentucky we have had way too many adventures and mishaps, but I will always remember the bouncer tossing you out on your butt in Lexington and you nearly getting your butt kicked over a taxi in Pittsburgh. Joie and Tiffany, there's nothing like cooking out and listening to the Pirates game. I could always count on you guys for happy hour at Harris Grill on a nice summer day. Eric, Dan, and Danny, we too have had some good happy hours, mostly at Hemmingway's and usually next to a large stack of cups. Eric, you are full of great ideas, like the theme for my 26th birthday. Danny, we could very well have been separated at birth. Thanks for the trip to Japan and for coming up with highly inappropriate nicknames. Hope you liked your Christmas stocking. Jen, I have no idea how you have put up with me (and my 'odd' eating habits, which have been photographed) for so long. We have some great pictures that are highly questionable. Between the three Christmas parties and our birthday parties, we will never be able to run for public office. Alexis, or should I say Shalexis, you have been a great friend through the good times and the difficult times. I will always remember Bernard, 'Christmas', and our conversations in UC and Enrique (I am still nervously waiting for you to use 'the card'). As long as your parents have a pool, and are close personal friends with Santa, I will always visit Lewisberry.

Lastly, to my family, thank you for your continual support, good humor, and brutal honesty. Mom, you have always been and will continue to be my role model in life. Your strength, persistence, perseverance, and love are unwavering and have made me the person I am today. Alex, you are and always will be my 'favorite brother'. Thank you for always being there, kicking my butt when it was warranted (and sometimes when it was not), and never letting my head get too big. You have proven to be a wonderful listener and the protective big brother every farm girl needs. Jackie, I have always considered you to be my sister. You have been there for me and have given solid professional and personal advice. Despite our distances apart, our family has remained close and will always be bonded together. Thank you for everything.

1.0 INTRODUCTION AND BACKGROUND

Glenohumeral stability is maintained through a complex combination of bony contact, muscular restraints, and ligamentous restraints in the form of a capsule. These ligamentous restraints are referred to as the glenohumeral capsule which is the primary focus of this work. The glenohumeral capsule has been divided into various capsuloligamentous regions based upon its variable thickness. (Figure 1.1) The thicker capsuloligamentous regions include the anterior and posterior bands of the inferior glenohumeral ligament (AB-IGHL and PB-IGHL, respectively), superior glenohumeral ligament (SGHL), and the middle glenohumeral ligament (MGHL). However, additional capsuloligamentous regions also exist. These include the tissue residing directly between the anterior and posterior bands of the inferior glenohumeral ligament (axillary pouch) and the tissue superior to the posterior band of the inferior glenohumeral ligament (posterior region). Moreover, since the middle glenohumeral ligament is only present in 40% of shoulders, [1] the tissue superior to the anterior band of the inferior glenohumeral ligament, encompassing the superior glenohumeral ligament has been termed the anterosuperior region. Thus, the capsuloligamentous regions of interest in this current work are the anterior and posterior bands of the inferior glenohumeral ligament, axillary pouch, anterosuperior region, and the posterior region.

The majority of glenohumeral joint dislocations, 80%, occur in the anterior direction [2] resulting in rupture or excessive stretching of the anterior band of the inferior glenohumeral ligament. [3-8] Following the initial episode, subsequent dislocations occur in nearly 90% of shoulders in young patients. [9] Therefore, surgical repair whereby the glenohumeral capsule is plicated and shifted to reduce joint laxity is often advocated. Diagnosis of injury to the capsuloligamentous regions of the glenohumeral capsule is performed for the purpose of surgical planning. However, it is quite subjective and sometimes inconclusive. Following surgical repair, nearly a quarter of shoulders still redislocate. [10] Moreover, following surgical repair, patients experience redislocations, osteoarthritis, pain, and joint stiffness. Therefore, there exists a need to improve patient outcome, which may be possible with better diagnosis and surgical repair procedures.

Changes or modifications to diagnosis or surgical repair procedures should be based upon the function of the glenohumeral capsule. However, in order to gain a better understanding as to the function of the glenohumeral capsule, and each of its capsuloligamentous regions, it may be necessary for researchers to re-evaluate the methodologies by which they elucidate function. A ligament is defined as a band or sheet of fibrous tissue and it is clear that the glenohumeral capsule is a *sheet* rather than a band of fibrous tissue. However, while the structure and function of the glenohumeral capsule has been clinically, experimentally, and computationally evaluated in the past, [11-20] these evaluations did not treat the glenohumeral capsule as a sheet of fibrous tissue. Rather, researchers have evaluated the function of the glenohumeral capsule by transecting the margins of the capsuloligamentous regions such that they could be isolated into discrete entities and evaluated in the direction parallel to their longitudinal axis. [12, 14, 15, 17, 18, 21-35]

This practice allowed for more simplistic experimental and computational analyses. However, recent work has suggested that it may be necessary to evaluate the glenohumeral capsule as a sheet of fibrous tissue instead of using isolated, discrete capsuloligamentous regions. [14, 36, 37] Thus, our current understanding of the function of the glenohumeral capsule, and each of its capsuloligamentous regions, may be inaccurate. While changes or modifications to the methodologies employed to diagnose injuries or surgically repair them may be necessary to improve patient outcome, our current research practices may not be sufficient to provide clinicians with the information necessary to make these changes/modifications. Therefore, there exists a need to better understand the function of the glenohumeral capsule, which may require more sophisticated experimental and computational analyses than those that are currently being used by researchers such that the glenohumeral capsule is evaluated as a sheet of fibrous tissue.

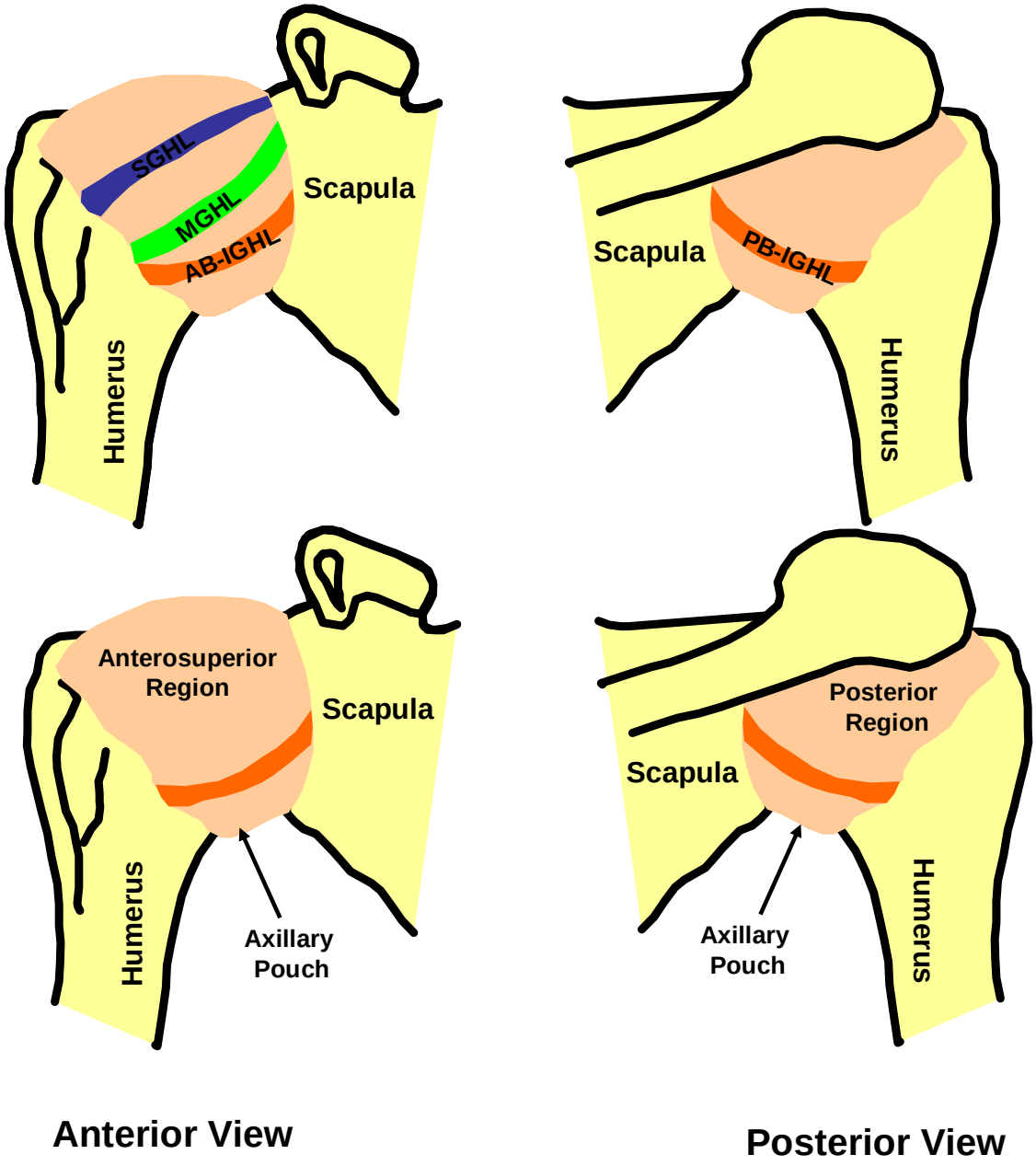

Figure 1.1: Schematic denoting capsuloligamentous regions of the glenohumeral capsule

1.1 DEMOGRAPHICS

The glenohumeral joint is the most commonly dislocated major joint in the body with dislocations frequently occurring with the arm in an abducted and externally rotated position. The majority of these dislocations (greater than 80%) occur in the anterior direction [2, 38] resulting in injury to the anterior band of the inferior glenohumeral ligament. [3-8] Approximately 2% of the general population (~5.6 million in the United States) dislocates their glenohumeral joint between the ages of 18-70 years. [39, 40] Roughly 34,000 shoulder dislocations occur per year in the young adult population between the ages of 15 to 25 years. [40, 41] Moreover, the activity level in this population has increased over the last two decades; especially due to the insurgence of females in sports. This increased activity level has resulted in an increase in the incidence of dislocation in this age range of the population. [42, 43] Therefore, this value serves as a lower bound for the rate of shoulder dislocation.

1.2 CLINICAL TREATMENT

1.2.1 Diagnosis

Anterior shoulder dislocations can be diagnosed with radiographs, which demonstrate anteroinferior displacement of the humeral head relative to the glenoid. However, after reduction, there is often little or no radiographic evidence of the dislocation. Imaging techniques such as magnetic resonance are used to identify an avulsion of the capsuloligamentous regions from the anteroinferior glenoid rim. [44] However, it is much more difficult to identify lesser degrees of instability such as mild subluxation. Therefore, clinical exams have been developed that attempt to generally assess which capsuloligamentous regions are injured and the extent of this injury.

Clinical exams for anterior shoulder instability are performed by applying an anterior load to the humerus with the joint oriented in positions of abduction and external rotation. Since dislocations frequently occur in the anterior direction with the joint oriented in a position of abduction and external rotation, the patient often becomes apprehensive when the joint is returned to this position for clinical exam. This apprehension indicates that there may be injury to the capsuloligamentous regions of the glenohumeral capsule that stabilize the joint in this joint position. If the patient is agreeable, the clinician compares and contrasts the amount of translation observed with respect to the scapula under the applied load in the injured and contralateral shoulder. (Figure 1.2) In addition to diagnosing which capsuloligamentous regions may be injured, clinical exams are also used as a means for surgical planning.

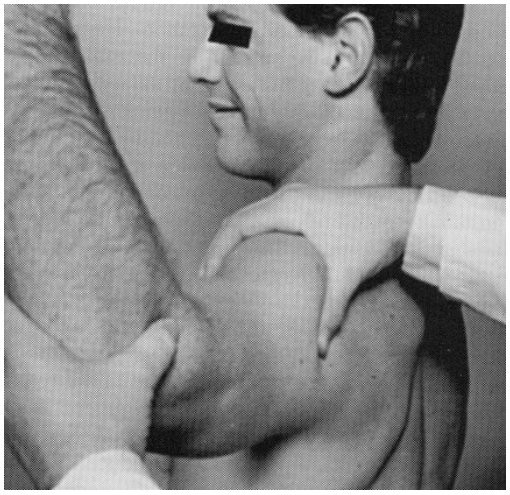

Figure 1.2: Clinical examination where humerus is translated with respect to scapula

However, these clinical exams are quite subjective as the skin and musculature make it difficult to assess the magnitude of the translation observed. Additionally, there is no consensus as to how much external rotation should be applied to the joint when performing these exams. Moreover, these clinical exams can only be utilized to gain a general understanding of which capsuloligamentous regions *may* be injured. It is often assumed that the injury would include damage to the glenoid insertion of the anterior band of the inferior glenohumeral ligament. [44] However, the extent of the injury can not be assessed with these clinical exams. These clinical exams could be improved if the function of the capsuloligamentous regions were more thoroughly understood in these joint positions.

1.2.2 Rehabilitation

Following diagnosis, treatment typically includes an initial immobilization period to allow soft tissue healing. This is followed by a conservative treatment regiment whereby a rehabilitation program that is aimed at strengthening and conditioning the shoulder muscles is prescribed. [45, 46] These muscles include the supraspinatus, infraspinatus, subscapularis, and teres minor aptly named the rotator cuff muscles as they are responsible for rotations of the humerus. In addition to strengthening the rotator cuff muscles, rehabilitation protocols are also aimed at improving strength in the humero-thoracic muscles such as the deltoid, latissimus dorsi, and pectoralis major.

1.2.3 Surgical Repair

However, the patient outcome for conservative treatment has been poor with nearly 90% of shoulders in young patients redislocating. [9] Therefore, surgical repair is often advocated. Surgical repair of anterior dislocations involves plicating and shifting the capsuloligamentous regions and can be performed with open or arthroscopic techniques. A typical surgical repair would first require that the anterosuperior region be incised in the superior-to-inferior direction on either the glenoid or humeral side. [45, 47-49] (Figure 1.3) This is followed by a medial-to-lateral incision, thus resulting in a "T" shape with an upper and lower tissue leaf. The lower leaf is then plicated, shifted in the superior direction, and sutured to the remaining tissue. The upper leaf is then plicated, shifted in the inferior direction, and sutured to the bone and lower leaf. Thus, while evaluations in the direction parallel to the longitudinal axes of capsuloligamentous

regions have been the primary focus of researchers, it is clear that, in general, clinicians treat the glenohumeral capsule as a fibrous sheet and not as a collection of fibrous bands.

However, at this time, it is not clear how much of the tissue should be plicated or how far it should be shifted. Moreover, the effect of making the medial-to-lateral and superior-to-inferior incisions at different locations is also not known. However, nearly a quarter of patients that undergo surgical repair experience redislocations. [10] Therefore, there exists a need to improve patient outcome which may be accomplished by thoroughly understanding the effect that shifting, plicating, and incising the glenohumeral capsule at different locations has on function.

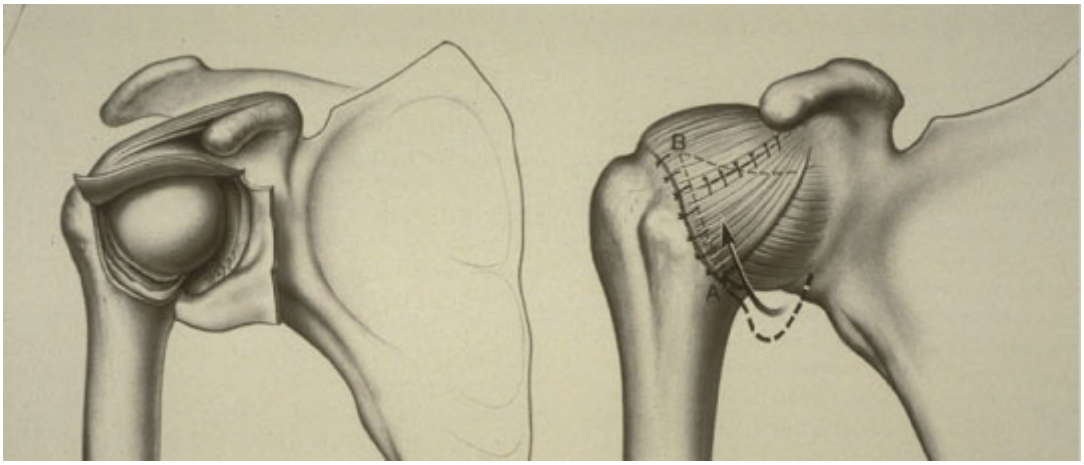

Figure 1.3: Schematic of surgical repair technique illustrating 'T' incision and shift of capsuloligamentous regions

1.3 CLINICAL OUTCOMES

Clinical outcomes for conservative treatment (i.e. rehabilitation) have been extremely poor with redislocations occurring in 60 to 94% of the patients under 25 years of age. [3, 9, 44, 50-53] In the elderly population, nearly 15% suffer weakness, pain, and loss of motion. [54] While surgical repair has improved upon these results, a 12% and 23% recurrence rate are still observed for open and arthroscopic repairs, respectively. [10] In addition to redislocations, 20-25% of patients also suffer from pain, chronic instability, rotator cuff injury, joint stiffness and osteoarthritis. [55-57]

1.4 SHEET VS. DISCRETE

1.4.1 Glenohumeral Capsule should be Evaluated as a Sheet

These poor clinical outcomes may be attributed to our limited understanding as to the biomechanical function of the capsuloligamentous regions since researchers have primarily focused on evaluating them in the direction parallel to their longitudinal axis after isolating them into discrete entities. A recent study by Debski and coworkers [14] found that, with an 89 N anteriorly applied load, approximately 13 N of force was transmitted in the direction perpendicular to the longitudinal axes of the capsuloligamentous regions at four different glenohumeral abduction angles while neutral horizontal abduction and external rotation were maintained. This force is substantial considering that the *in situ* force in the anterior and posterior bands of the inferior glenohumeral ligament was approximately 20 N and 5 N at 60° of glenohumeral abduction, respectively. These data clearly demonstrate the importance of the

capsuloligamentous regions in the directions parallel and perpendicular to their longitudinal axes. Thus, these data provide evidence that the glenohumeral capsule functions multiaxially and should be evaluated as a sheet of fibrous tissue rather than as a collection of discrete capsuloligamentous regions.

A second study has investigated the strain distribution in the anterior band of the inferior glenohumeral ligament and the anterior portion of the axillary pouch with an anteriorly applied translation at 60° of glenohumeral abduction while neutral horizontal abduction and an unknown external rotation was maintained. [36] The direction of the maximum principal strains was oblique to the longitudinal axes of the capsuloligamentous regions. Additionally, the strain distribution pattern was not isolated within each capsuloligamentous region. Rather, the strain distribution pattern was distributed across the margins of the capsuloligamentous regions. Moreover, the magnitude of the average maximum principal strains (~10-15%) was comparable between the anterior band of the inferior glenohumeral ligament and the axillary pouch despite the fact that the anterior band of the inferior glenohumeral ligament is thicker. Thus, these data also imply that the glenohumeral capsule functions multiaxially and should be evaluated as a sheet of fibrous tissue.

1.4.2 Implications for Experimental and Computational Models

Not only do most clinician treat the glenohumeral capsule as a sheet of fibrous tissue during surgical repairs, but recent data suggests that it functions multiaxially and should be evaluated as a sheet of fibrous tissue as well. However, evaluating the glenohumeral capsule as a sheet of fibrous tissue presents itself with a multitude of experimental difficulties. Throughout the range of joint motion, the capsuloligamentous regions actively providing stability have been shown to

change. [24, 30, 31, 33] Additionally, if a capsuloligamentous region is not actively providing stability to the joint, it frequently consists of numerous folds and wrinkles since no tension is being applied. Furthermore, it has recently been suggested that the function of these capsuloligamentous regions may be different within the capsuloligamentous region itself. [58] Therefore, while isolating the glenohumeral capsule into discrete capsuloligamentous regions may be convenient for experiments, it may greatly affect the perceived function as their ability to transfer loads may be greatly altered. Thus, this may not be an appropriate practice when evaluating the overall function of the glenohumeral capsule in providing joint stability.

Due to experimental difficulties and limitations, researchers within our research center have begun to investigate the function of the capsuloligamentous regions via finite element analyses. [21-23] The finite element method is an extremely powerful and versatile tool. Using the finite element method, the function of the capsuloligamentous regions may be evaluated multiaxially at various joint positions or under various loading conditions. A finite element model of the glenohumeral capsule could be used to determine the stress and strain distributions, reaction forces, and contact forces generated between the capsuloligamentous regions and the bones. Moreover, in addition to characterizing the function of the normal glenohumeral capsule, the finite element method may be used to simulate injury to or surgical repair of the glenohumeral capsule. Thus, these data could serve as a basis for improving clinical exams for diagnosis and surgical repairs and may result in approved patient outcome.

Therefore, within our research center, a subject-specific finite element model was previously developed to evaluate the stress and strain distribution in and the forces transmitted by the anterior band of the inferior glenohumeral ligament. [23] However, the anterior band of the inferior glenohumeral ligament was modeled as a discrete capsuloligamentous region while

the remaining capsuloligamentous regions were excluded. Thus, while this finite element model allowed the function of the anterior band of the inferior glenohumeral ligament to be evaluated multiaxially, it did not account for the effect that the other capsuloligamentous regions may have had on this function. Additionally, methodologies to validate the predictions from this finite element model were not developed and the accuracy of the predictions remains unknown.

A second subject-specific finite element model was then developed within our research center that included the anterior and posterior bands of the inferior glenohumeral ligament and the axillary pouch. [21, 22] These three capsuloligamentous regions were modeled as a sheet and the strain distribution in these capsuloligamentous regions, the reaction forces of the capsuloligamentous regions, and the contact force between these capsuloligamentous regions and the humerus was calculated. However, the remaining capsuloligamentous regions were still excluded from the analyses. While the predicted strains and forces compared reasonably well to previous literature, again, no direct validation was performed and the methodologies to do so were not described.

Since neither study included all of the capsuloligamentous regions, the boundary conditions placed on the edges of the modeled capsuloligamentous regions were not representative of that which would be observed *in vivo*. (Figure 1.4) Thus, neglecting to include all of the capsuloligamentous regions may have resulted in inappropriately predicting the deformed shape of the capsuloligamentous regions modeled. The predicted deformed shape greatly affects the predicted stresses, strains, and forces as it governs the mechanism by which the capsuloligamentous regions are loaded. Moreover, it should be noted that the predicted deformed shape may differ depending on the sequence of motions that the bones are moved through when attempting to arrive at a solution for a joint position of interest. The results from

these previous models indicated that arriving at a solution was extremely difficult due to the folding and buckling of the capsuloligamentous regions. Thus, the sequence of motion was altered until a solution could be achieved. The various sequences of motion did affect the predicted deformed shape.

Despite the limitations of these previous finite element models, a tremendous amount of experimental and computational work, elaborate equipment and techniques, and expertise was required for their development. Additionally, these previous studies suggest that finite element models of the glenohumeral capsule must be subject-specific due to the tremendous variation across the population. Thus, incorporating all of the capsuloligamentous regions into such a model would only increase the level of difficulty and the time necessary to evaluate the function of the glenohumeral capsule. This may have a tremendous impact on the area of glenohumeral joint research as fewer investigators would be capable of performing such analyses and the amount of time necessary to address a research question would greatly increase.

Since finite element models allow the multiaxial function of the glenohumeral capsule to be rigorously evaluated (stress, strain, reaction forces, contact forces), it is important that the effect of evaluating only isolated, discrete capsuloligamentous regions with such a model be addressed. Isolating the glenohumeral capsule into discrete capsuloligamentous regions may affect the perceived function of this tissue. Therefore, this information has clinical, experimental, and computational importance. Clinically, it is important to know the effect that changes to the boundary conditions of the capsuloligamentous regions may have on their function especially since surgical repair procedures drastically change these by shifting some capsuloligamentous regions and reattaching them to the glenoid rim. Needing to include all capsuloligamentous regions would have a tremendous impact on experimental designs and

would greatly limit the number of research questions that could be addressed directly by experimental means. Finally, from a computational point of view, the level of complexity, experimental inputs, and time necessary to address research questions would be greatly affected.

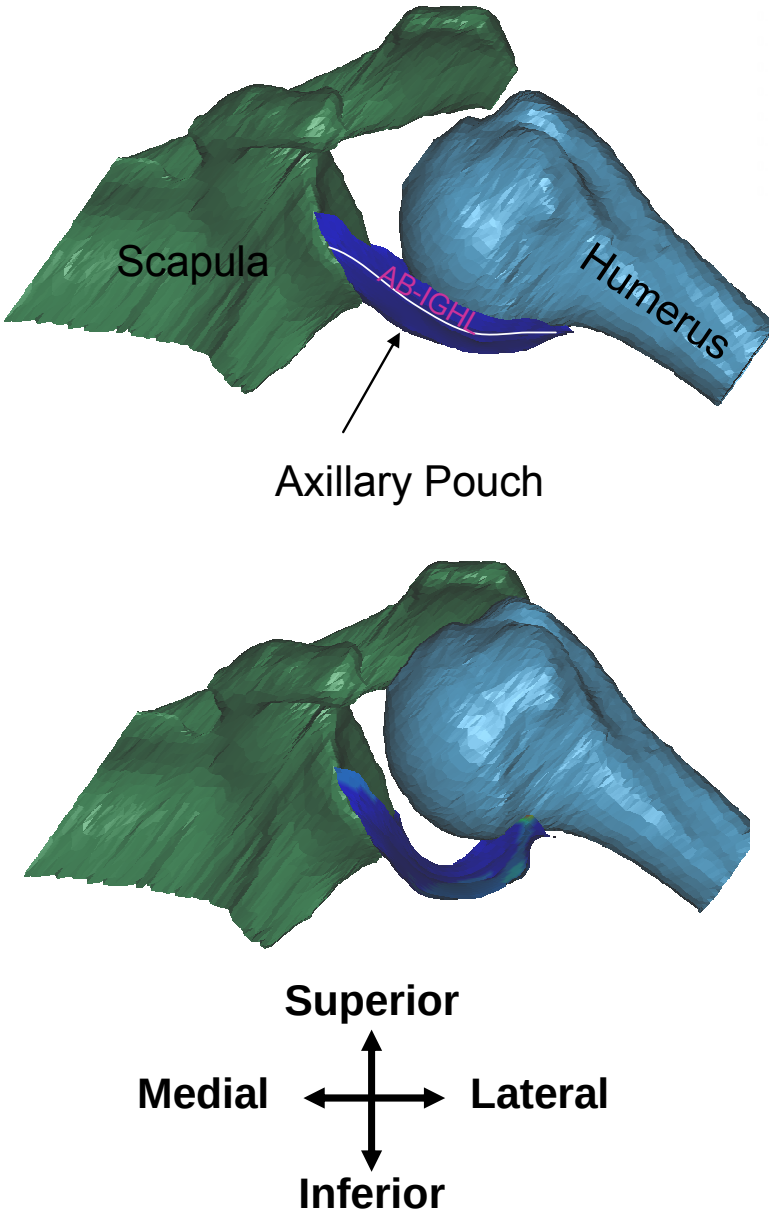

Figure 1.4: Anterior view of glenohumeral joint showing unconstrained superior edge of AB-IGHL

1.5 MOTIVATION: RESEARCH QUESTION AND HYPOTHESIS

The ultimate strain in the anterior band of the inferior glenohumeral ligament and the axillary pouch [15, 17, 28, 29] has previously been measured via bone-capsuloligamentous region-bone complexes. In one study, [28] each capsuloligamentous region was isolated by transecting along their margins. Thus, the boundary conditions at the margins of the capsuloligamentous regions were altered. The average ultimate strain of the capsuloligamentous regions was reported for the tissue midsubstance (10.9±5.5%). A second study, kept all of the capsuloligamentous regions intact thus treating this tissue as a sheet of fibrous tissue. [36] The maximum principal strain in the anterior band of the inferior glenohumeral ligament and axillary pouch were experimentally measured when an anterior translation was applied to the humerus. In this study, the average peak maximum principal strain was reported to be as high as 31±16%. Thus, when treated as a sheet of fibrous tissue, the experimentally measured strains were larger than would be expected based upon the load-to-failure studies previously performed that evaluated the same capsuloligamentous regions individually. The ultimate strain of the capsuloligamentous regions may have been underestimated due to changes in the boundary conditions applied to the capsuloligamentous regions as collagen fibers were transected when they were isolated into discrete capsuloligamentous regions. Therefore, altering the boundary conditions applied to the capsuloligamentous regions may drastically affect the function of these capsuloligamentous regions. Moreover, experimental and computation analyses that evaluate isolated, discrete capsuloligamentous regions may result in a poor predicted deformed shape due to the limited number of boundary conditions applied to the capsuloligamentous regions. As a result, the predicted stress, strain, reaction forces, and contact forces may be inaccurate and false conclusions may be formulated.

1.6 RESEARCH QUESTION

Based on the force transmission characteristics and strain distribution in the capsuloligamentous regions, experimental and computational models that do not treat the glenohumeral capsule as a sheet of fibrous tissue may be inappropriate. The development of finite element models to evaluate the function of the glenohumeral capsule has been advocated and recently utilized. While a tremendous tool, the finite element method must be appropriately applied with adequate boundary conditions. This leads to the following research question: Is it appropriate to evaluate the function of the glenohumeral capsule using isolated, discrete capsuloligamentous regions?

1.7 HYPOTHESIS

The purpose of this research is to determine the effect of evaluating the function of the capsuloligamentous regions of the glenohumeral capsule as isolated, discrete entities has on their perceived function. A parameter commonly measured to investigate the function of ligaments is strain. [17, 23, 28, 29, 36, 37, 59-68]}

Therefore, the hypothesis that was addressed by the current work was:

<u>Hypothesis</u> –Since boundary conditions along the margins of the capsuloligamentous regions are included, a finite element model that is a composite of all ligamentous regions will more closely predict the strain distribution (within 8% strain of that which is experimentally measured) and deformed shape of the anterior band of the inferior glenohumeral ligament than

a finite element model whereby the anterior band of the inferior glenohumeral ligament is modeled as a discrete capsuloligamentous region.

The strain distribution in the anterior band of the inferior glenohumeral ligament was selected as the primary focus of this work since this capsuloligamentous region is commonly injured during anterior dislocations and is also altered during surgical repair. The predicted strain distribution for finite element model could be considered valid if the average difference between the predicted and experimentally measured maximum principal strain values were within 8% strain. The capsuloligamentous regions have been shown to function at strain of more than 30%. Therefore, 8% is an order of magnitude less than the strain levels that the tissue functions within and is larger than the repeatability of a previously described methodology to experimentally measure the strain distribution in the capsuloligamentous regions. [36, 66]

1.8 MOTIVATION: SPECIFIC AIMS

Finite element modeling requires that a constitutive model describing the response of tissues to applied loads or displacements be detailed. While the capsuloligamentous regions have been evaluated extensively in the direction parallel to their longitudinal axes, [12, 17, 20, 27-29, 34]} the mechanical response of this tissue in other directions remains largely unknown. Moreover, discrepancies exist regarding the collagen fiber organization of this tissue with some researchers finding a clear axis of collagen fiber alignment [74] while others have found a certain level of disorganization in capsuloligamentous regions. [69] Therefore, for the current work, there existed a need to determine the appropriate constitutive model for the capsuloligamentous regions.

Once an appropriate constitutive model is determined, it is possible to calculate the predicted strain and deformed shape of tissues under prescribed load or displacement boundary conditions. Previous finite element models of ligamentous tissues have prescribed subject-specific displacement boundary conditions by detailing the orientation of the bones with respect to one another in clinically relevant joint positions. [21-23, 70-72] A clinically relevant joint position can be defined as one where the ligamentous tissue of interest functions to provide joint stability. Thus, for the current work, it was necessary to determine the orientation of the humerus with respect to the scapula in a joint position, such as external rotation, whereby the anterior band of the inferior glenohumeral ligament functions to provide joint stability.

Other major considerations when developing finite element models of ligamentous tissues are the reference strain configuration and geometry of the specimen. Due to the extreme variability across the population, finite element models of ligamentous tissues require subject-specific data. [21-23, 70-72] For the glenohumeral capsule, the reference strain configuration introduces some difficulties as it is not possible to simply apply a pre-load parallel to the longitudinal axes of the capsuloligamentous regions such that they are uniformly loaded. Thus, for the current work, there existed a need to define a repeatable reference strain configuration for the capsuloligamentous regions such that the geometry of these capsuloligamentous regions and the bones may be obtained in this configuration.

For the glenohumeral capsule, a large amount of variability has been demonstrated between specimens for the mechanical properties of the capsuloligamentous regions. [12, 17, 20, 27-29] Therefore, it has been suggested that, for the purpose of finite element modeling, the coefficients to constitutive models may need to be subject-specific. [21] Additionally, large differences exist when comparing data collected from the various capsuloligamentous regions.

[27-29, 73] Therefore, for the current work, there existed a need to determine the subject-specific coefficients to an appropriate constitutive model for each of the capsuloligamentous regions.

A large variability in the strain distribution of the capsuloligamentous regions has also been noted across the population. [36, 66] For the current work, it was necessary to determine whether a composite or discrete finite element model more accurately predicts the strain distribution in the capsuloligamentous regions. Therefore, there existed a need to quantitatively validate the predictions of a composite and discrete finite element model to experimentally measured strains for the same cadaveric joint from which the finite element models were created.

1.9 SPECIFIC AIMS

Based on the data available at the commencement of the current work, the hypothesis was tested with the following specific aims (Figure 1.5):

Specific Aim #1 – Determine the bi-directional mechanical properties and the collagen fiber organization in the axillary pouch as an implication for an appropriate constitutive model

Specific Aim #2 – Determine subject-specific inputs for the finite element models that include:

a. *Determine orientation of the humerus with respect to the scapula in 60° of glenohumeral abduction, neutral horizontal abduction, and 60° of external rotation when an anterior load is applied to the humerus, simulating a joint position utilized to diagnose anterior instability*

b. *Determine the reference strain configuration for the capsuloligamentous regions of the glenohumeral capsule using a repeatable methodology*

c. *Determine the subject-specific geometry of the humerus, scapula, anterior and posterior bands of the inferior glenohumeral ligament, axillary pouch of the inferior glenohumeral ligament, and the anterosuperior and posterior regions while in the reference strain configuration*

d. *Based on the results from Specific Aim #1, determine the coefficients of an isotropic hypoelastic constitutive model for the anterior band of the inferior glenohumeral ligament, posterior band of the inferior glenohumeral ligament, axillary pouch, anterosuperior, and posterior regions that accurately describe the response of these capsuloligamentous regions to applied displacements.*

Specific Aim #3 – For validation, determine the subject-specific strain distribution and deformed shape in the anterior band of the inferior glenohumeral ligament with the joint in the clinically relevant joint position outlined in Specific Aim #2a

Specific Aim #4 – Construct two finite element models from the subject-specific data collected in Specific Aim #2

a. *Model #1 - Composite model whereby the anterior band of the inferior glenohumeral ligament, posterior band of the inferior glenohumeral ligament, axillary pouch, anterosuperior, and posterior regions were included, thus allowing the glenohumeral capsule to be evaluated as a sheet of fibrous tissue*

b. *Model #2 – Model whereby the anterior band of the inferior glenohumeral ligament is the only capsuloligamentous region included, generating a discrete representation of this capsuloligamentous region*

<u>Specific Aim #5</u> – For validation, compare predicted strain distributions and deformed shape from the composite (Model #1) and discrete (Model #2) finite element models to that which was obtained experimentally (Specific Aim #3)

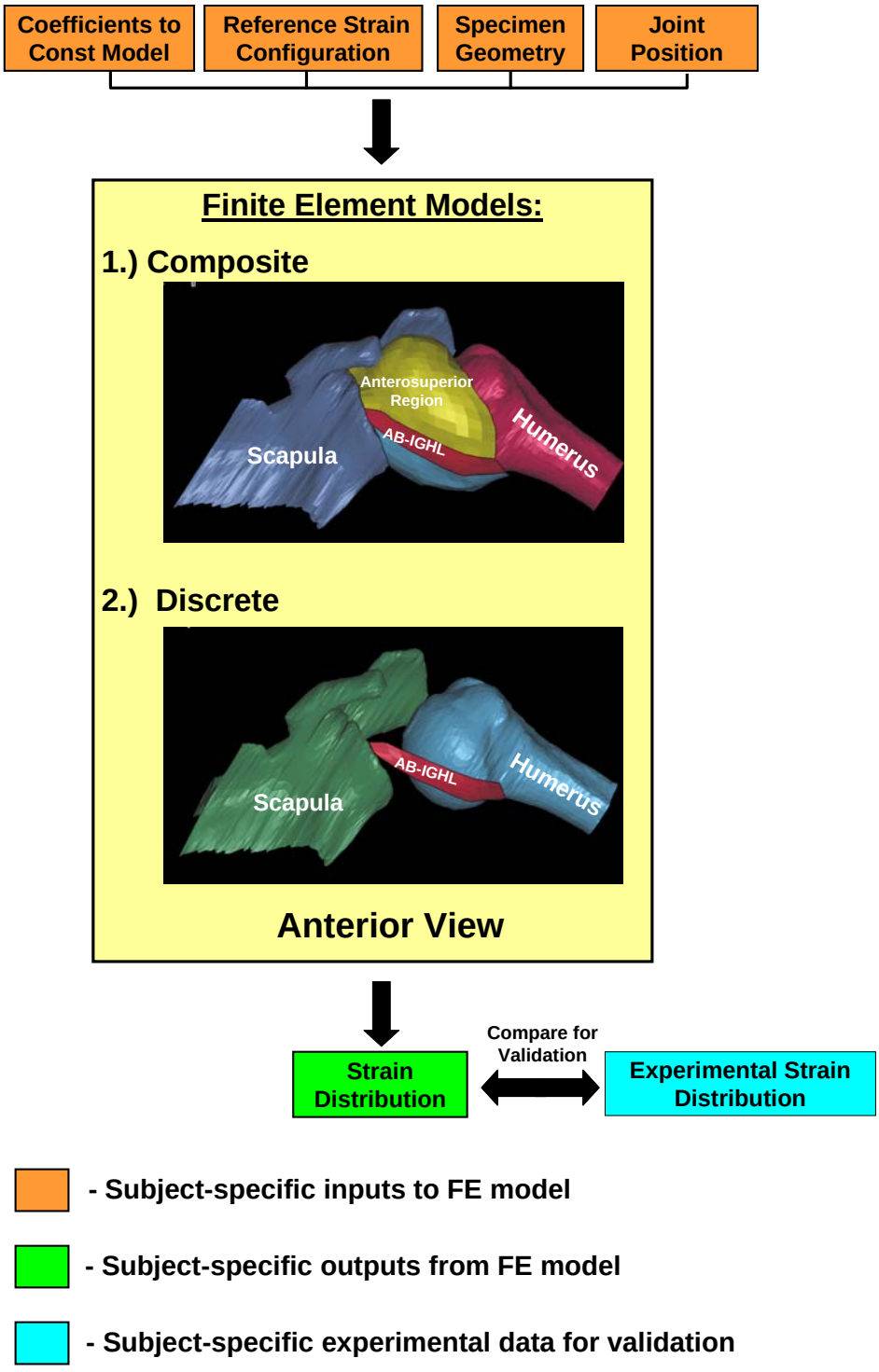

Figure 1.5: Flow chart detailing the subject-specific input and output parameters and the experimentally collected data utilized for validation of the composite and discrete finite element (FE) models

2.0 RATIONALE FOR CONSTITUTIVE MODEL

2.1 INTRODUCTION

Previous research has demonstrated that the anterior and posterior bands of the inferior glenohumeral ligament and the axillary pouch together act as the primary static restraint to anterior translation of the humeral head on the glenoid of the scapula. [24] Therefore, many researchers have investigated the mechanical properties [17, 28, 29] and collagen fiber organization [69, 74] of these capsuloligamentous regions to elucidate function. The current experimental and analytical models have investigated only the uniaxial tensile properties of these capsuloligamentous regions in the direction parallel to the longitudinal axes of its anterior and posterior bands of the inferior glenohumeral ligament. [13, 15, 17, 20, 26, 28] However, substantial loads are transmitted in the direction perpendicular to these axes. [14] Moreover, the direction of the maximum principal strain in the anterior band of the inferior glenohumeral ligament and the anterior portion of the axillary pouch has been shown to be highly variable. [36] In fact, on average, the direction of the maximum principal strains was found to be at an oblique angle (38±36°) to the longitudinal axis of the anterior band of the inferior glenohumeral ligament. These data indicate that significant loads may be transferred in multiple directions. Therefore, a constitutive model utilized to describe the response of the capsuloligamentous regions to loads may need to account for multi-axial function.

The collagen fiber organization of the axillary pouch may provide more insight into an appropriate constitutive model. Previously, the collagen fiber organization of the anterior and posterior bands of the inferior glenohumeral ligament and the axillary pouch has been qualitatively examined utilizing polarized light microscopy. [69, 74] However, while one study reported that the axillary pouch demonstrated a great deal of intermingling of the fibers, [69] a second study observed an organized pattern of collagen fibers in the axillary pouch which were predominately oriented in the direction of the longitudinal axes of the anterior and posterior bands of the inferior glenohumeral ligament.

Since the mechanical properties of the three regions of the anterior and posterior bands of the inferior glenohumeral ligament and the axillary pouch were unknown in response to loading in perpendicular directions, and due to the lack of agreement regarding its collagen fiber organization, there was insufficient information to select a constitutive model. Therefore, the first objective in this section of this work was to determine the mechanical properties of the axillary pouch in the directions parallel and perpendicular to the longitudinal axis of the anterior band of the inferior glenohumeral ligament. The second objective was to quantify the collagen fiber orientation in the axillary pouch. Based on these data, a constitutive model to be used for all capsuloligamentous regions investigated in this work (anterior and posterior bands of the inferior glenohumeral ligament, axillary pouch, anterosuperior, and posterior capsuloligamentous regions) was selected.

The axillary pouch was selected for these objectives since a large volume of experimental data already exists for this capsuloligamentous region, it was large enough in size to allow perpendicular tissue samples to be harvested for mechanical testing, and it represents one of the two capsuloligamentous regions whose stress and strain distribution were investigated with this work.

2.2 METHODS

2.2.1 Bi-directional Mechanical Tests

2.2.1.1 Tissue Sample Procurement

Tissue samples from 10 fresh-frozen cadaveric shoulders (age: 60.6±9.9 years) (mean±SD) were obtained to determine the mechanical properties of the axillary pouch in the directions perpendicular (transverse) and parallel (longitudinal) to the longitudinal axis of the anterior band of the inferior glenohumeral ligament. Pilot data indicated that 10 specimens would be sufficient to detect differences between the transverse and longitudinal tissue samples. The superior margin of the anterior band of the inferior glenohumeral ligament is one of the most identifiable landmarks and has been highly characterized. [1, 69] Furthermore, the anterior band of the inferior glenohumeral ligament is often used as a consistent reference clinically and experimentally. Therefore, the superior margin of the anterior band of the inferior glenohumeral ligament was chosen as the reference for the transverse (perpendicular to the longitudinal axis of the anterior band of the inferior glenohumeral ligament) and longitudinal (parallel to the longitudinal axis of the anterior band of the inferior glenohumeral ligament) axillary pouch tissue samples.

2.2.1.2 Bi-directional Protocol

To minimize end effects from clamping, a hardened steel punch was used to obtain dog-bone shaped tissue samples from each specimen in both directions. (Figure 2.1) One transverse and

one longitudinal tissue sample was excised from each of the 10 specimens. The gauge dimensions of each tissue sample were 12.5 mm x 2.5 mm, which were chosen based on the resolution of the load cell and the average dimensions of the axillary pouch (to allow both a transverse and longitudinal tissue sample to be obtained from each specimen). When possible, the transverse tissue samples were excised from the medial portion of the axillary pouch, whereas the longitudinal tissue samples were excised from the lateral portion of the axillary pouch. However, due to the variability of the size and shape of the axillary pouch, it was not possible to obtain transverse tissue samples from the medial portion of the axillary pouch for three of the ten specimens. Therefore, seven transverse and three longitudinal tissue samples were harvested from the medial portion of the axillary pouch, while the remaining three transverse and seven longitudinal tissue samples were harvested from the lateral portion of the axillary pouch.

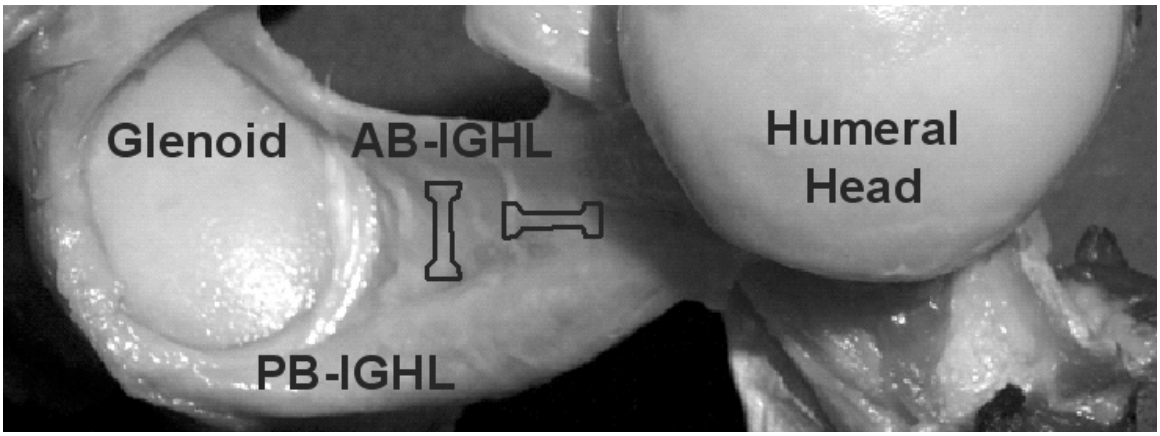

Figure 2.1: Location that dog-bone shaped tissue samples were excised from capsule

The ends of the tissue samples were wrapped with gauze, soaked with 0.9% physiological saline solution, and placed into a set of customized clamps. The faces of the clamps in contact with the tissue samples were designed with teeth to grip the ends of the gauze-wrapped tissue sample. The "teeth" were slightly rounded to ensure that neither the gauze nor the tissue sample was damaged. This clamp-tissue sample-clamp complex was then mounted into a laser micrometer system [75] to determine the cross-sectional area at the center of the sample's gauge length. A rectangular cross-section was assumed. The width and thickness of the tissue sample were represented by the maximum and minimum values obtained by the laser as it rotated 180º, respectively. An average of three measurements was used to represent the sample's cross-sectional area.

A circular punch was used to obtain reflective plastic markers (1.6 mm diameter). [67] Two markers, centered approximately 7 mm apart, were fixed to the midsubstance of each tissue sample using cyanoacrylate as previously described. [67, 76] These markers formed the gauge length for non-contact video strain analysis (Motion Analysis^{TM}, Motion Analysis Corporation, Santa Rosa, CA). During all dissections and determination of the cross-sectional area, the tissue sample was continually kept moist with 0.9% physiological saline solution.

The clamp-tissue sample-clamp complex was then removed from the laser micrometer and mounted in a saline bath that was rigidly fixed to the base of a material testing machine (Instron, Model 4502). Each tissue sample was allowed to equilibrate to the bath temperature (36°-37° C) for three minutes prior to testing.

The zero-load was initially established by allowing the tissue sample to buckle. Subsequently a 0.1 N preload was applied and the tissue samples were cyclically preconditioned between elongation limits of 0-0.3 mm at a rate of 10 mm/min for 10 cycles. The tissue sample

was loaded to failure at a rate of 10 mm/min. Force data was recorded using a load cell (Sensotec Model 34; Columbus, OH) that was accurate to ±0.15 % full scale (±0.07 N). The strain data was recorded by a video camera, and, using Motion Analysis™ software, the edges of the reflective markers were thresholded on the videotape, which allowed the coordinates of their centroids to be calculated and tracked through time. [77, 78] Thus, the midsubstance strain of the tissue sample could be determined throughout the test.

2.2.1.3 Data Analysis

A stress-strain curve was generated for each tissue sample and the tangent modulus, ultimate stress, ultimate strain, and strain energy density were determined. The tangent modulus for each tissue sample was determined by performing a linear regression on each stress-strain curve. The slope of a line fit to the greatest portion of the curve that resulted in an R^2 (squared correlation coefficient) greater than or equal to 0.80 (0.95±0.04) was then defined as the tangent modulus. Paired t-tests were used to detect differences between the transverse and longitudinal axillary pouch tissue samples for each parameter (tangent modulus, ultimate stress, ultimate strain, and strain energy density). The statistical significance was set at $p<0.05$.

Average stress-strain curves were also determined for the transverse axillary pouch and longitudinal axillary pouch tissue samples. These curves were generated by calculating the average stress in the transverse and longitudinal directions at 2.5 % strain increments over the common strain range.

2.2.2 Collagen Fiber Organization

2.2.2.1 Preliminaries

Thirteen fresh-frozen human cadaveric specimens with average age 50.8±11.4 years (mean±SD) were used throughout the course of this study. Six specimens were utilized in preliminary investigations**.** The use of polarized microscopy, as described by Whittaker and Canham, [79] was initially investigated; however, this technique could not readily provide the quantitative structural data that was necessary for this analysis, making visualization of complex patterns difficult. Other methods for analysis of larger samples were then considered. [80, 81] The technique using small angle light scattering (SALS) [81] was chosen due to its angular resolution and accuracy as well as its ability to analyze collagenous tissue with thicknesses up to ~1 mm with a spatial resolution of ±254 μm to an angular resolution of ±1º. Furthermore, the SALS technique provides quantitative information on the collagen fiber angular distribution and predominant fiber direction throughout the tissue. Preliminary studies were also utilized to determine the techniques for acquiring, fixing, and slicing the tissue samples.

2.2.2.2 Tissue Sample Procurement

Three rectangular samples (approx. 11 mm x 6 mm) were excised from the axillary pouch of the seven remaining specimens, totaling 21 tissue samples. (Figure 2.2) Each sample was harvested with one edge parallel to the long axis of the anterior band of the inferior glenohumeral ligament to maintain an orientation reference. As a control, one sample was obtained from the long head of the bicep's tendon in six of the seven specimens. Two *fresh* tissue samples were removed from one rabbit Achilles tendon as an additional control.

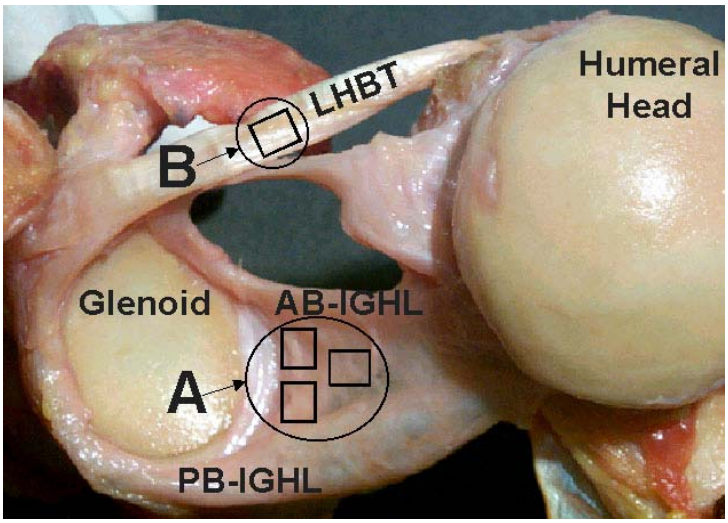

Figure 2.2: Location where SALS tissue samples were excised from capsule

Use of these controls demonstrated that this technique could accurately describe the known fiber alignment in tissue that was frozen prior to being processed by the experimental protocol. Once harvested, each of the samples were fixed while resting on a flat metal surface by immersing the tissue in a beaker of 2-methyl butane, which was surrounded by liquid nitrogen. The metal surface drastically reduced the curling of the samples while the tissue remained in a stress free state. The 2-methyl butane interface decreased the rate at which the liquid nitrogen was able to freeze the tissue, thereby preventing tissue damage. Once frozen, the samples were stored at –80° C until further testing was performed.

2.2.2.3 SALS Protocol

The samples were sliced on a cryostat at 100 μm increments for mounting onto microscope slides. Approximately 10 slices per sample were collected, allowing the variability of the collagen fiber alignment to be compared throughout the depth of the tissue. The slides were kept in a cold room (5° C) until tested within 24 hours. To reduce optical interference with the laser beam of the SALS device, coverslips were not utilized. Therefore, the slides were kept in a covered histology box to prevent any particles from settling on the surface of each tissue slice.

Previous studies have utilized the SALS technique to quantify the orientation of collagenous tissues. [81-83] This technique utilizes the spatial intensity distribution of the scattered light pattern resulting from the sum of the structural information of the tissue in the path of a laser beam. The SALS device passes a 4 mW unpolarized HeNe laser beam, chosen because its wavelength (632.8 nm) is within an order of magnitude of the collagen fiber diameter, through the tissue. For dense fibrous tissues, it has been shown that, optically, the tissue will adhere to the rules of the single slit diffraction theory. When the laser passes through the tissue, light is scattered perpendicular to each collagen fiber axis, thus producing a scattered light intensity.

This distribution of light intensity is a representation of the sum of the structural information throughout the thickness of a tissue at the point of intersection with the laser beam. The maximum intensity of light, therefore, is achieved perpendicular to the angle of predominant alignment of the collagen fibers at a single point in the tissue. The orientation index (OI) [81-85] is then defined as the angle that contains half of the total area under the scattered light intensity vs. fiber angle curve (centered at the predominant fiber angle). Physically, the OI represents the

angular width that half of the fibers are oriented within. As the OI decreases in value, the level of local fiber organization increases. Conversely, an increase in OI indicates a decreased level of fiber alignment.

2.2.2.4 Data Analysis

Each slide was placed individually on the SALS device, and the collagen fiber orientation was measured using the scattered light intensity pattern as previously described. Histograms were generated for each tissue type from multiple specimens. A normal distribution of OI values was found for all samples. From the histograms it was found that the majority of the long head of the biceps tendon, which is known to be highly aligned, was well within an OI of 45° while the axillary pouch ranged from approximately 35°-65°. To demonstrate that the axillary pouch was different from the long head of the biceps tendon, and thus not aligned, the percentage of the area within an OI of 25°-45° was determined for the tissue slices of the axillary pouch and long head of the biceps tendon, and the fresh tissue. The largest area of tissue that could be evaluated for *all* tissue samples was 9.3 mm^2. Statistical analyses were performed to compare the collagen fiber alignment throughout the depth of the axillary pouch as well as between the axillary pouch and long head of the biceps tendon. For the axillary pouch, the percentage of tissue within an OI of 25°-45° was evaluated for slices that represent the bursal, middle, and articular portions of each sample. Each specimen contained three slices of tissue at each depth and these values at a depth were averaged for the three samples. A one factor ANOVA and Student-Newman-Keuls post-hoc tests were used to compare the OI distribution at each depth within the axillary pouch with a significance level $p<0.05$.

The overall percentage of tissue, regardless of depth, within an OI of 25°-45° was then determined in the axillary pouch and long head of the biceps tendon for each specimen. A one factor ANOVA and Student-Newman-Keuls post-hoc tests were also used to compare between these regions of tissue with a significance level $p<0.05$. However, since only six of the seven specimens had long head of the biceps tendon samples, only six specimens were utilized when the long head of the biceps tendon was compared to the axillary pouch. Additionally, a power analysis indicated that the statistical analysis was capable of detecting a 10% difference between the depths of the axillary pouch with a power of 0.80.

2.3 RESULTS

2.3.1 Bi-directional Mechanical Tests

2.3.1.1 Cross-sectional Area

The cross-sectional area for the transverse axillary pouch (n=10) and longitudinal axillary pouch (n=10) tissue samples was 5.7±2.1 mm^2 and 4.8±1.1 mm^2, respectively (2.5 mm width due to hardened steel punch dimensions, mean±SD). No significant differences (p=0.21) could be demonstrated between the cross-sectional area of the transverse axillary pouch and longitudinal axillary pouch tissue samples.

2.3.1.2 Failure Modes

All tissue samples failed in the midsubstance. One longitudinal tissue sample had a partial failure in the midsubstance during loading due to two distinct thickenings. Thus, the tangent

modulus of this tissue sample was determined for the linear region of the stress-strain curve while the entire midsubstance was intact, and the ultimate stress, ultimate strain, and strain energy density are not reported.

2.3.1.3 Mechanical Properties

Representative curves for the transverse and longitudinal axillary pouch tissue samples are shown in Figure 2.3. The stress-strain curves of each tissue sample demonstrated the traditional "toe region" followed by a linear region prior to failure. The average stress-strain curves generated for the transverse axillary pouch and longitudinal axillary pouch tissue samples are depicted in Figure 2.4. The tangent modulus, ultimate stress, ultimate strain, and strain energy density are reported in Table 2.1.

The tangent modulus of the transverse axillary pouch (n=10) tissue samples (5.4±2.9 MPa) was found to be significantly different (p=0.04) from the tangent modulus of the longitudinal axillary pouch (n=10) tissue samples (14.8±13.1 MPa). The ratio of the longitudinal to transverse moduli (n=10) was 3.3±2.8.

Table 2.1: Mechanical properties of axillary pouch in transverse and longitudinal direction. * Significantly different from longitudinal direction ($p<0.05$)

	Modulus (MPa)	Ultimate Stress (MPa)	Ultimate Strain (%)	Strain Energy Density (MPa)
Transverse (n=10)	5.4±2.9*	0.8±0.4*	23.5±11.5	10.8±8.5
Longitudinal (n=10)	14.8±13.1	2.0±1.0	33.3±23.6	21.1±15.4

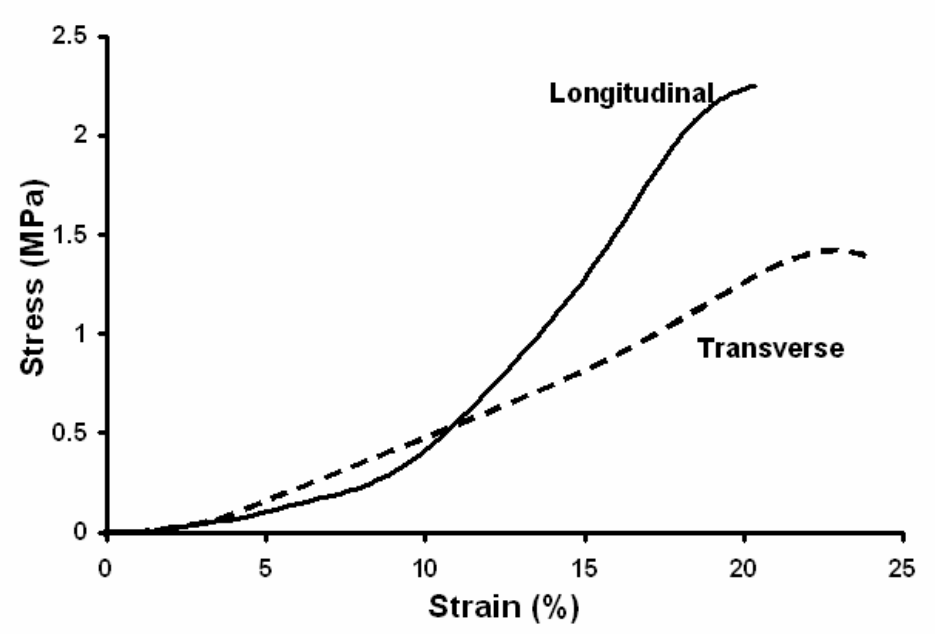

Figure 2.3: Representative stress-strain curves in longitudinal and transverse directions

A significant difference (p=0.01) was demonstrated between the ultimate stress of the transverse (0.8±0.4 MPa) and longitudinal (2.0±1.0 MPa) axillary pouch tissue samples. No significant differences (p=0.29) were found between the ultimate strain of the transverse axillary pouch (23.5 ±11.5%) and longitudinal axillary pouch (33.3±23.6%) tissue samples. Additionally, the strain energy density of the transverse (10.8±8.5 MPa) and longitudinal (21.1±15.4 MPa) axillary pouch tissue samples approached significance (p=0.08).

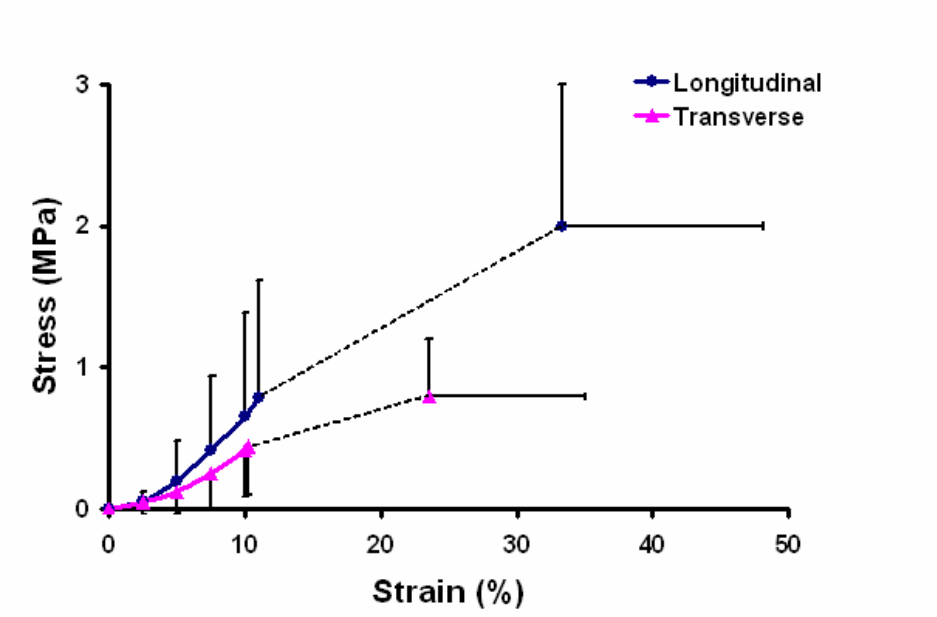

Figure 2.4: Average stress-strain curves for transverse and longitudinal directions (mean±SD)

2.3.2 Collagen Fiber Organization

2.3.2.1 Description of Data

The darker regions of Figures 2.5, 2.6, 2.7, 2.8, and 2.9 represent areas of higher OI values while the white lines illustrate the predominant direction of collagen fiber alignment as determined using the SALS technique. Since the fiber orientation was defined as the predominant fiber angle for 50% of the fibers within the tissue at each point of measurement, the fibers are thus oriented in the direction of the white lines within a range of ± ½ OI. Therefore, the lower the OI value, the lower the overall range of fiber angles, thus depicting an increase in the alignment of the tissue.

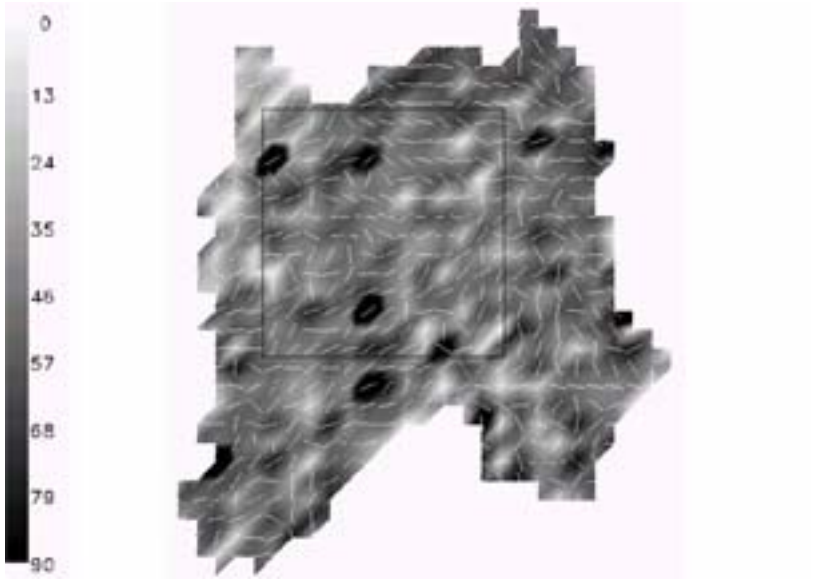

Figure 2.5: OI distribution (°) for axillary pouch issue at 400 µm (bursal slice)

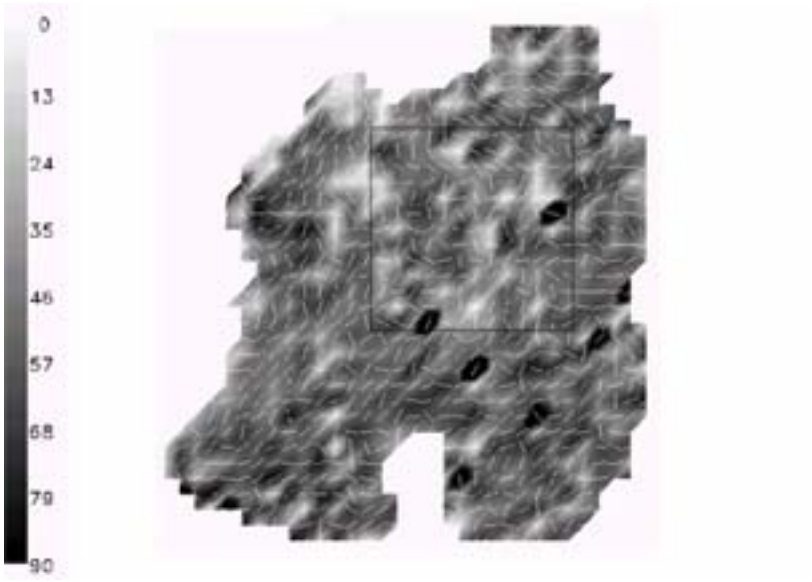

Figure 2.6: OI distribution (°) for axillary pouch issue at 800 µm (middle slice)

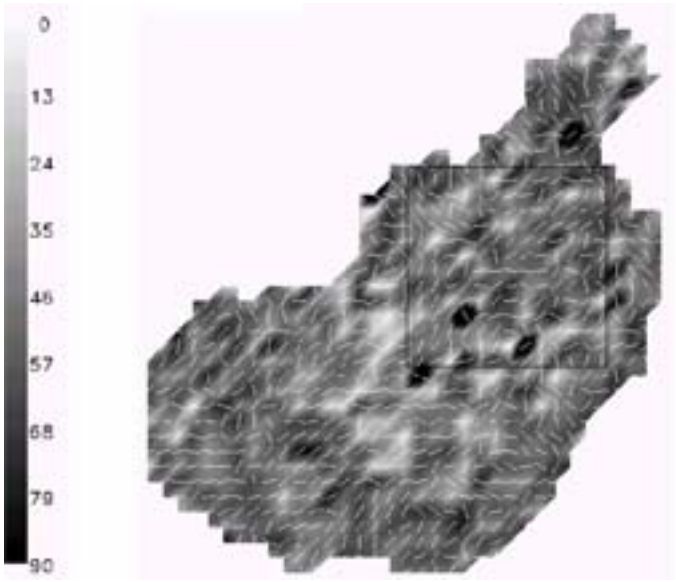

Figure 2.7: OI distribution (°) for axillary pouch issue at 1200 µm (articular slice)

2.3.2.2 Gross Examination of Tissue Samples

A typical distribution of OI values and fiber orientations of the axillary pouch at bursal, middle, and articular depths for one specimen are shown in Figures 2.5, 2.6, and 2.7. Within each slice, there appeared to be no evidence of alignment as indicated by the large percentage of darker regions. While some regions with a low OI were present (regions with lighter color), the fibers within these regions were not organized as indicated by the white lines.

The OI distribution of long head of the biceps tendon tissue clearly demonstrated a high degree of alignment as illustrated by the fact that the long head of the biceps tendon tissue was much lighter in appearance and the fibers were more consistently aligned than that of the axillary pouch. (Figure 2.8) Although the fresh rabbit Achilles tendon is not as aligned as the long head of the biceps tendon, a predominant direction was observed parallel to the long axis of the tendon. (Figure 2.9)

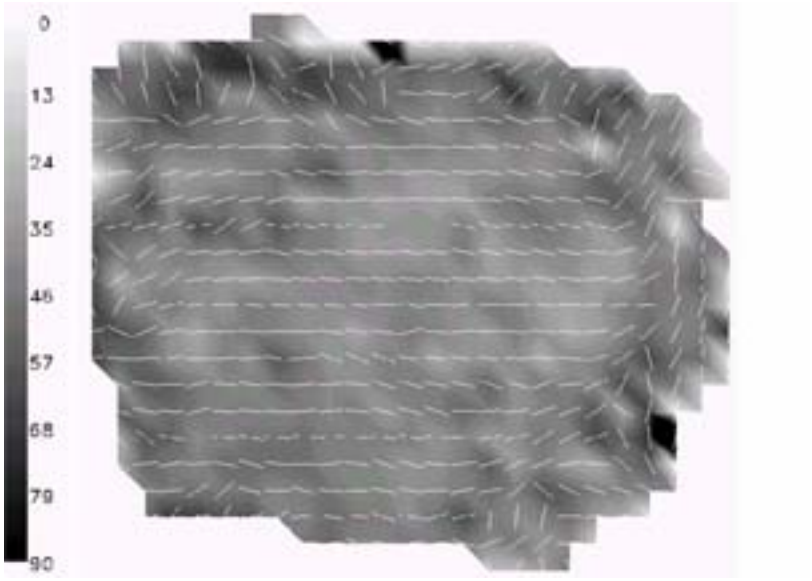

Figure 2.8: OI distribution (°) for long head of biceps tendon

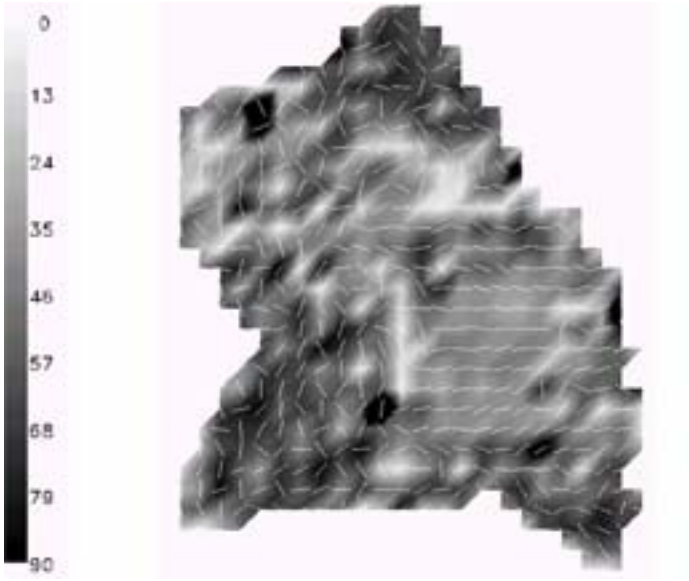

Figure 2.9: OI distribution (°) for rabbit Achilles tendon (fresh tissue) tissue

2.3.2.3 Comparison between Tissue Samples

When comparing the percentage of tissue with each category of OI values a significant difference was found between both the axillary pouch and the long head of the biceps tendon. ($p<0.05$) Overall, the percentage of tissue with an OI of 25°-45° was 23.2±8.5% (mean±SD) for the axillary pouch. (Table 2.2) On the other hand, the percentage of long head of the biceps tendon tissue within this same range was 61.6±15.2%, and the fresh rabbit Achilles tendon was 47.9±7.5%. The bursal, middle, and articular slices of the axillary pouch were found to have similar fiber orientation throughout the depth of the tissue ($p>0.05$). Overall, the percentage of bursal tissue with an OI of 25°-45° was 24.9±10.7% while the middle and articular tissue yielded 22.7±7.2% and 21.7±7.4%, respectively. (Table 2.3)

Table 2.2: Percentage of tissue whose OI is between 25-45 (mean±SD, n=7)

Percentage of AP (OI 25-45)	Percentage of LHBT (OI 25-45)	Percentage of Fresh Rabbit Achilles (OI 25-45)
23.2±%	61.6±15.2%	47.9±7.5%

Table 2.3: Percentage of bursal, middle, and articular axillary pouch tissue whose OI is between 25-45 (mean±SD, n=7)

Percentage of Bursal (OI 25-45)	Percentage of Middle (OI 25-45)	Percentage of Articular (OI 25-45)
24.9±10.7%	22.7±7.2%	21.7±7.4%

2.4 SIGNFICANCE OF RESULTS

2.4.1 Bi-directional Mechanical Properties

2.4.1.1 Discussion of Results

The mechanical properties of the axillary pouch were determined in the transverse and longitudinal directions with respect to the longitudinal axis of the anterior band of the inferior glenohumeral ligament. Significant differences were detected between the ultimate stress and tangent modulus of the transverse and longitudinal tissue samples. No significant differences were observed between the ultimate strain and strain energy density of the transverse and longitudinal tissue samples. Significant differences may not have been detected for the ultimate strain and strain energy density due to variations in the size of the toe region of the stress-strain curves. Although a significant difference was detected between the tangent modulus and ultimate stress of the transverse and longitudinal axillary pouch, the data demonstrate that the transverse properties of the axillary pouch play a substantial role in joint stability. The ratio of the longitudinal to transverse tangent moduli (3.3±2.8), was substantially smaller than the ratio of moduli for ligaments that function *uniaxially* along their length such as the medial collateral ligament (MCL) of the knee (30) [67] and interosseous ligament of the forearm (385. [86] (Table 2.4) This indicates that the axillary pouch functions multiaxially to provide stability and allow a large range of motion at the glenohumeral joint.

Table 2.4: Summary of mechanical properties obtained for various ligaments

Tissue Type	Tangent Modulus (MPa)	Ratio of Tangent Modulus	Ultimate Stress (MPa)	Ultimate Strain (%)
Transverse axillary pouch Longitudinal axillary pouch	5.4±2.9 14.8±13.1	3.3±2.8	0.8±0.4 2.0±1.0	23.5±11.5 33.3±23.6
Transverse medial collateral ligament Longitudinal medial collateral ligament (knee) [67]	11.0±3.6 332.2±58.3	30	1.7±0.5 38.6±4.8	11.7±0.9 17.1±1.5
Transverse interosseous ligament Longitudinal interosseous ligament (forearm) [86]	1.1±1.6 431.3±321.3	385	0.1±0.1 52.7±33.5	N/A
Anterior longitudinal axillary pouch [28] Posterior longitudinal axillary pouch [28]	30.3±10.6 41.9±12.5	N/A	5.5±2.0 5.6±1.9	15.1±5.7 9.9±5.3
Longitudinal hip capsule [87]	Range 76±57 to 286±391	N/A	Range 2.0±1.4 to 6.0±9.0	Range 6.2±1.8 to 25.3±7.5
Anterior and posterior cruciate ligament and lateral collateral ligament [88]	345±22	N/A	36±3	15±1

2.4.1.2 Comparison to Literature

The range of knee motion is significantly limited compared to that of the shoulder due to anatomical constraints that require ligaments to function predominately in a uniaxial direction. Butler et al. [88] reported the ultimate stress for the anterior cruciate (ACL), posterior cruciate (PCL), and lateral collateral (LCL) ligaments lumped together. (Table 2.4) The ultimate strain in the transverse direction of the axillary pouch (23.5±11.5%) was approximately 1.5 times greater than the ultimate strain in the functional direction of knee ligaments. [67, 88] These large multiaxial strains allow the large range of motion at the glenohumeral joint.

The hip joint has a similar anatomical arrangement as the shoulder and is encompassed by a joint capsule. The longitudinal ultimate stress of the hip capsule ranges from 2.0±1.4 MPa to 6.2±8.8 MPa [87] and was similar to the ultimate stress in the longitudinal direction of the axillary pouch. However, the ultimate strain in the longitudinal direction of the hip capsule ligaments ranged from 6.2±1.8% to 10.4±4.7%, which is substantially less than that of the axillary pouch. The longitudinal tangent modulus of the hip capsule was 5-19 times greater than that of the axillary pouch. While the hip joint has a large range of motion, substantially more motion is possible at the glenohumeral joint. This may explain differences in the ultimate strain and tangent modulus of the hip capsule compared to the axillary pouch of the glenohumeral joint. Due to the similarities between the ligamentous restraints at each joint, it may also be necessary to evaluate the bi-directional mechanical properties of the hip capsule.

The results for ultimate stress of the longitudinal axillary pouch tissue samples (2.0±1.0 MPa) were similar to a previous study that reported the average ultimate stress to be 5.5±2.0 MPa. [28] The average midsubstance strain in the longitudinal direction reported by Bigliani and coworkers [28] also correlates well with the ultimate strain presented in the current study. (Table 2.4) The increased variability in the strain values reported in this study may be attributed to the fact that their experimental protocol tested bone-ligament-bone complexes, as opposed to the clamp-tissue sample-clamp complexes tested in this study.

2.4.1.3 Limitations

Excising the tissue samples may have broken the interfiber and transfiber bonds, causing some variation in the mechanical properties. [67] In addition, due to the anatomical arrangement at the glenohumeral joint, the axillary pouch cannot be uniaxially tensile tested in the transverse

direction using a bone-ligament-bone complex. Therefore, in order to determine the bi-directional mechanical properties, it was necessary to excise tissue samples.

It should also be noted that the location of tissue excision was not randomized. To investigate the contribution of this variable, a comparison was performed between the tissue samples harvested from the medial and lateral portions for both the transverse and longitudinal tissue samples. No differences could be detected and based on the grouped data a power analysis revealed that 140 specimens should be tested to detect significant differences with 80% power. However, some bias may still exist in the data and could be addressed in future studies that examine the inhomogeneity throughout the tissue. It should also be noted that while approximately 2% of the population between the ages of 18-70 years dislocates their glenohumeral joint, this percentage increases in individuals participating in sports activities. Therefore, the majority of individuals who suffer dislocations are younger than the average age of the specimens tested in this study.

2.4.1.4 Implications

While previous experimental and computational models have focused on the anterior and posterior bands of the inferior glenohumeral ligament, [13, 15, 17, 20, 26, 28] the axillary pouch has been shown to stabilize the glenohumeral joint in positions of abduction and external rotation. [24] Therefore, the data reported in this study suggests that analytical models that fail to consider the mechanical properties of the axillary pouch in the transverse direction may result in an inaccurate description of the stress and strain distribution. Consequently, regions of high stress that could result in tissue rupture may go undetected and the accurate contributions to joint stability would be unknown. Therefore, these data suggest that experimental and computational

models of the glenohumeral capsule may need to include all of the capsuloligamentous regions, not just those that are thicker. Additionally, while no differences were detected for the ultimate stress and strain energy density when comparing the transverse and longitudinal directions, the tangent modulus and ultimate strain in the longitudinal direction was significantly larger. Therefore, the appropriate constitutive model to describe the tissue remains unclear. While the tissue does not appear to be completely isotropic due to the differences detected, the tissue also does not appear to be completely transversely isotropic (commonly used for ligaments [72, 89]) as differences were not detected for all mechanical properties. Therefore, it was necessary to combine these data with the results from the collagen fiber organization before a constitutive model could be selected.

The data obtained in this study also have clinical implications. Based on the ratio of the tangent moduli, it may be beneficial to investigate surgical repair techniques that result in similar tangent moduli in the transverse and longitudinal directions following surgical repair techniques that plicate and shift the tissue.

2.4.2 Collagen Fiber Organization

2.4.2.1 Discussion of Results

In this study, the collagen fiber organization of the axillary pouch was quantified using the SALS technique. The results indicated that the fiber architecture of the axillary pouch is random. As expected, the long head of the biceps tendon [90] and the fresh tissue demonstrated a high degree of alignment, thus demonstrating the efficacy of our methods. The random organization in the axillary pouch is supported by O'Brien et al.'s [69] qualitative findings that the axillary pouch is less organized with a great deal of intermingling of fibers.

2.4.2.2 Limitations

In this study, only one structural measure was determined for three samples that were excised from each axillary pouch and only three depths were examined for each sample. Moreover, the tissue samples evaluated in this work were not loaded, and this work did not investigate the composition of the tissue, which may vary throughout the tissue. Therefore, future studies should investigate additional structural measures (e.g. collagen fiber diameter) and the composition of the axillary pouch on larger tissue samples, at additional depths, and under load.

2.4.2.3 Implications

Traditional ligaments, such as the medial collateral ligament of the knee, are known to function uniaxially along their length with collagen fibers organized parallel to this direction of loading. [91] However, the collagen fiber organization of the axillary pouch was found to be random

suggesting that the axillary pouch is an isotropic material that functions multiaxially. The multiaxial function of the axillary pouch is also supported by previous studies where substantial forces were found to be transmitted perpendicular to the longitudinal axes of the capsuloligamentous regions [14] and the direction of the maximum principal strain in the anterior band of the inferior glenohumeral ligament and anterior portion of the axillary pouch was found to be highly variable. [36] Similar to the results obtained for the bi-directional mechanical properties of the axillary pouch, its collagen fiber organization also implies that experimental and computational models may need to include all of the capsuloligamentous regions, not just those that are thicker.

The data reported in this study also has clinical implications as it implies that the ability of the axillary pouch to transfer loads across its entire insertion into the glenoid/labrum may be significantly altered during a surgical repairs that shift the tissue. Therefore, clinicians may want to place more emphasis on their placement and fixation of the axillary pouch during repair procedures. Specifically, proper fixation to the rim of the glenoid, in both the medial-to-lateral and superior-to-inferior direction, may be necessary to eliminate the possibility of rendering a portion of a capsuloligamentous region inactive. Moreover, over tightening the axillary pouch may also have adverse effects by significantly increasing peak loads.

3.0 SUBJECT-SPECIFIC INPUTS TO FINITE ELEMENT MODEL

3.1 INTRODUCTION

In order to develop the finite element models, it was necessary to experimentally collect several subject-specific parameters. The parameters utilized in this work were the: joint position; reference strain configuration; geometry of the bones and capsuloligamentous regions; and coefficients to an isotropic hypoelastic constitutive model for each capsuloligamentous region. Since the finite element models were to be kinematically driven, the location of the humerus with respect to the scapula was determined in a clinically relevant joint position. It was also necessary to determine the reference strain configuration of the tissue using a repeatable methodology such that stress and strain predictions could be calculated with respect to this configuration. Once the reference strain configuration was established, the geometry of the bones and capsuloligamentous regions was determined with the tissue in this configuration. Lastly, the coefficients to an isotropic hypoelastic constitutive model were determined for each of the five capsuloligamentous regions to be modeled: anterior band of the inferior glenohumeral ligament; posterior band of the inferior glenohumeral ligament; axillary pouch; anterosuperior; and posterior. Each of these inputs to the finite element models were experimentally collected using the same shoulder specimen, thus yielding subject-specific parameters.

3.2 JOINT POSITION

3.2.1 Clinically Relevant Joint Position

Clinical exams have been developed that attempt to generally assess which capsuloligamentous regions are injured and the extent of this injury. To test for injuries resulting from an anterior dislocation, these exams are typically performed with the humerus at 60° of glenohumeral abduction. The clinician then applies an anterior load to the humerus at various degrees of external rotation. Thus, for the current work, it was desired that the joint position of interest simulated a clinical exam. Before selecting the joint position of interest, several joint positions were investigated. Thus, the joint positions resulting from an applied 50 N anterior load [92, 93] at 60° of glenohumeral abduction, 0° of horizontal abduction, and 0°, 30°, and 60° of external rotation were investigated.

3.2.2 Previous Literature

The robotic/universal force-moment sensor testing system has been utilized previously to investigate kinematics of the glenohumeral joint. [14, 92, 93] In the study by Debski and coworkers [14], all of the skin and musculature was kept intact and the resulting joint kinematics were recorded as an 89 N anterior/posterior load was applied to the humerus which was oriented at various angles of glenohumeral abduction, 0° of horizontal abduction, and 0° of external rotation. A capsuloligamentous region of interest (e.g. anterior band of the inferior glenohumeral ligament) was then removed and the previously recorded joint kinematics were then reproduced as the resulting forces were recorded. Using the principal of superposition, the forces recorded after the capsuloligamentous region was removed were subtracted from the forces obtained

before the capsuloligamentous region was removed. This was then repeated for other capsuloligamentous regions of interest. In this way, the *in situ* forces in various capsuloligamentous regions were obtained. At 60° of glenohumeral abduction, approximately 28 mm of humeral translation in the anterior direction was observed which corresponded to an *in situ* force of approximately 20 N in the anterior band of the inferior glenohumeral ligament.

Based on the *in situ* forces, it is clear that the anterior band of the inferior glenohumeral ligament provided stability to the joint in the position tested. However, this study did not investigate positions of external rotation. Furthermore, this study applied an anterior/posterior load to shoulder specimens with the skin and musculature intact. This was not possible for the current work which required that the shoulder specimen be dissected down to the capsuloligamentous regions in order to experimentally measure the strain in the anterior band of the inferior glenohumeral ligament and axillary pouch. Thus, it was not clear if the loading conditions utilized previously were appropriate for this current work. Therefore, the purpose of this section of the current work was to assess the appropriateness of applying a 50 N [92, 93] anterior load at 60° of glenohumeral abduction, 0° of horizontal abduction, and 0°, 30°, and 60° of external rotation with the only soft tissues present being the capsuloligamentous regions and coracoacromial ligament. The coracoacromial ligament was not removed since it acts to guide motion of the joint in the superior/inferior direction when an anterior load is applied to the humerus. (Figure 3.1)

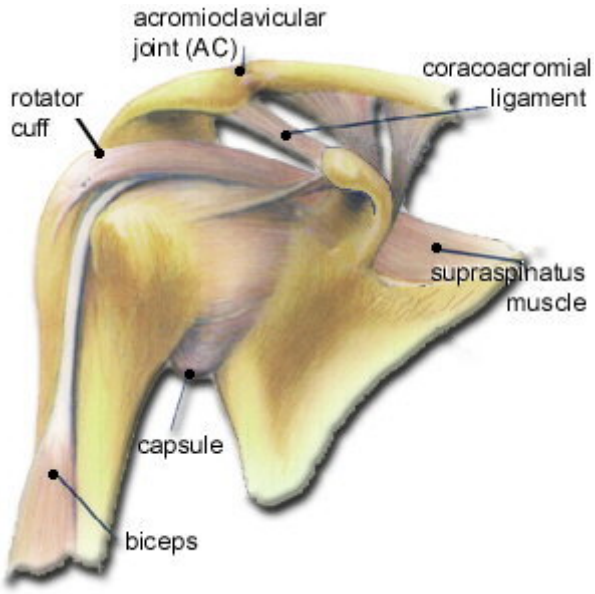

Figure 3.1: Anterior view of glenohumeral joint illustrating coracoacromial ligament

3.2.3 Preliminaries

3.2.3.1 Specimen Preparation

Eight fresh-frozen cadaveric shoulder specimens (52.6 ± 3.5 yrs) were vented and dissected free of all soft tissue except the capsuloligamentous regions and coracoacromial ligament. In order to mount the humerus and scapula within fixtures, epoxy putty was used to generate standard geometry for both. The humerus was fixed within a cylinder of epoxy putty whose longitudinal axis was parallel to the longitudinal axis of the humerus. The scapula was then fixed within a rectangular block of epoxy putty such that the walls of the epoxy putty approximated the scapular plane. [14, 92, 93]

3.2.3.2 Robotic/Universal Force-moment Sensor Testing System

Custom fixtures were previously developed such that the scapula and humerus were rigidly fixed to the end effector and base of the robotic/universal force-moment sensor testing, respectively. (Figure 3.2) The scapular fixture ensured that the plane of the scapula was parallel to the y-z plane of the robotic/universal force-moment sensor testing system. Moreover, the x, y, and z axes of the robotic/universal force-moment sensor testing system were parallel to the anterior/posterior, medial/lateral, and superior/inferior axes of the scapula, respectively. Using these custom fixtures, the humerus and scapula were mounted within a robotic/universal force-moment sensor testing system [14, 91-99] with the joint oriented at a minimal amount of glenohumeral abduction (~0°), 0° of horizontal abduction, and 0° of external rotation.

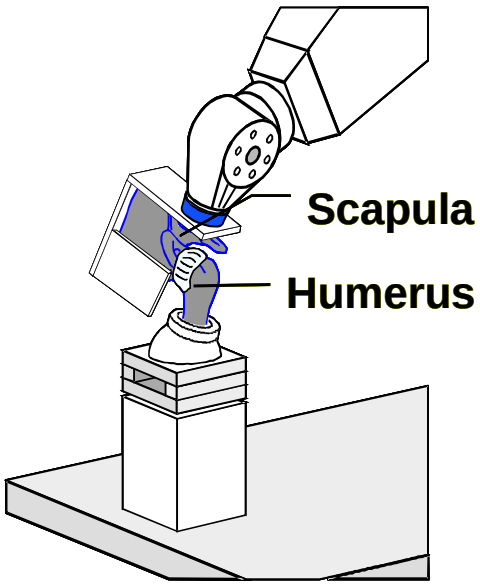

Figure 3.2: Six-degree-of-freedom/universal force-moment sensor testing system

The coordinate system of the robotic/universal force-moment sensor testing system was then translated such that it was coincident with the anatomic coordinate system of the scapula. The relationship between the anatomic coordinate system of the scapula and the coordinate system of the robotic/universal force-moment sensor testing system was established as previously described. [14, 92, 93] The location of the anterior-most and posterior-most aspects of the humeral head was measured with respect to the origin of the coordinate system of the robotic/universal force-moment sensor testing system. The point midway between these two anatomic landmarks represented the origin of the anatomic coordinate system of the scapula and the origin of the robotic/universal force-moment sensor testing system coordinate system was translated to this point.

The path of passive glenohumeral abduction was then determined by minimizing the forces in the anterior/posterior and superior/inferior directions (~0 N) as a 22 N compressive force (medially directed) was held constant. To achieve the force targets, translation of the scapula along the three orthogonal axes was permitted. The path of passive glenohumeral abduction was established in 1° increments from the minimal abduction angle the specimen was initially mounted at to 70° of glenohumeral abduction. The compressive force ensured that the humeral head was then centered within the glenoid cavity throughout all glenohumeral abduction angles.

The joint was then orientated at 60° of glenohumeral abduction and the path of external rotation was established by applying a 3 Nm rotation moment to the scapula while maintaining the 22 N joint compressive force. The joint positions corresponding to 60° of glenohumeral abduction and 0° and 60° of external rotation were then identified. At these joint positions, a 50 N anterior load was applied to the scapula, while maintaining the 22 N compressive force, and the resulting kinematics were recorded.

3.2.3.3 Results

Clinically, joint kinematics of the shoulder are described as motions of the humerus with respect to the scapula. Therefore, the kinematics recorded with the robotic/universal force-moment sensor testing system were transformed such that all joint kinematics and forces are presented as such.

At 0° of external rotation, the humerus subluxed or completely dislocated under 50 N of load making contact with the coracoid process. (Figure 3.3) The force that resulted in dislocation was determined by plotting the anterior force against the resulting anterior translation

of the humerus. (Figure 3.4, Specimen 1) A large increase in translation with minimal increase in force demonstrates that the primary restraint up to that point (i.e. the bony contact) was no longer functioning to stabilize the joint. However, not all specimens dislocated at 0° of external rotation. (Figure 3.4, Specimen 2) Similarly, dislocations were observed for some specimens at 30° of external rotation as well.

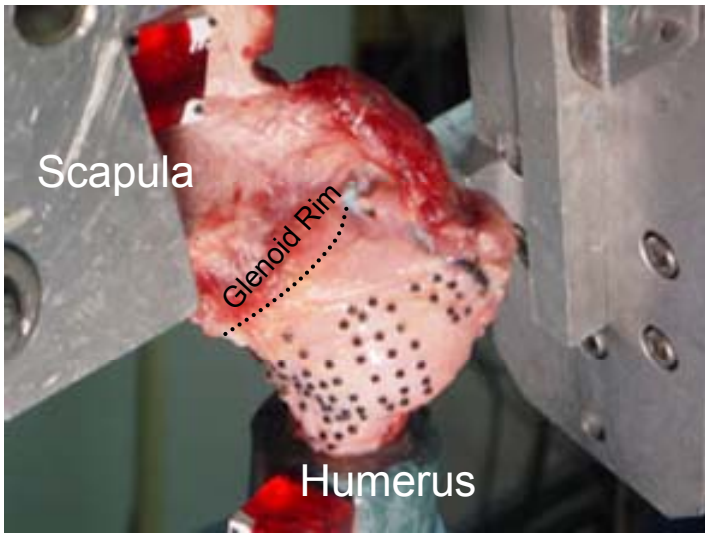

Figure 3.3: Humerus completely dislocated under a 50 N anterior load at 0° of external rotation

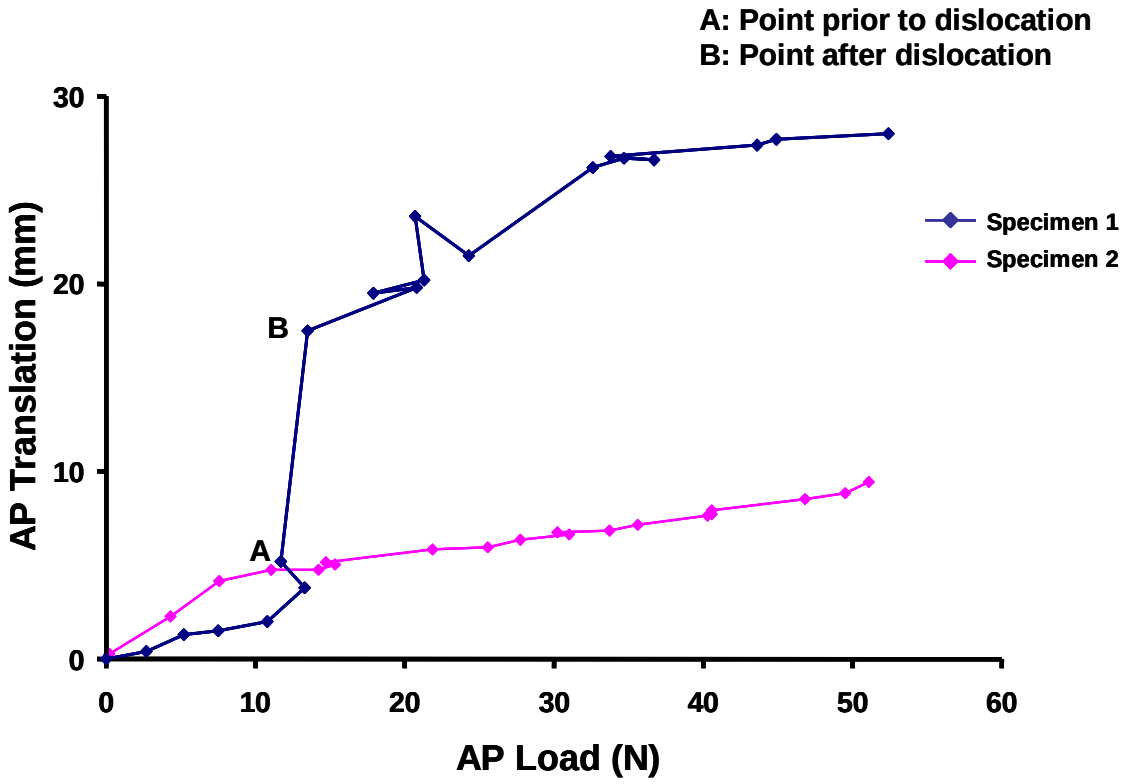

Figure 3.4: Graphs illustrating point prior to dislocation under 50 N anterior load at 0° of external rotation

At 60° of external rotation, the translation of the humeral head was minimized by the capsuloligamentous regions which are the primary static stabilizers in positions of external rotation. [24] Therefore, the humeral head did not make contact with the coracoid process and the capsuloligamentous regions on the anterior side of the joint were taut. As with 0° of external rotation, the anterior force was plotted against the resulting anterior translation for each specimen. (Figure 3.5)

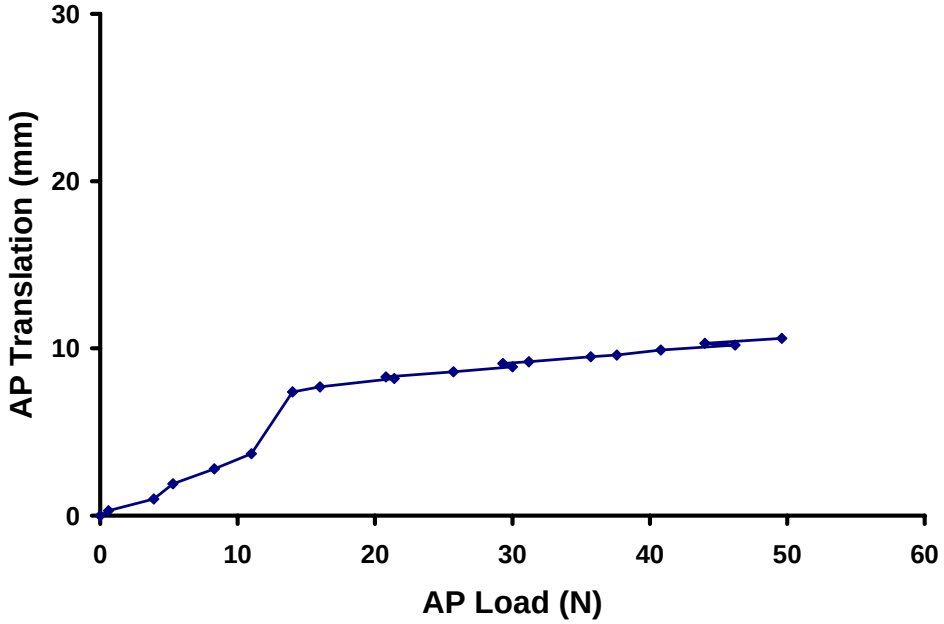

Figure 3.5: Graphs illustrating no dislocation occurred under a 50 N anterior load at 60° of external rotation.

3.2.3.4 Implications

Previous studies using the robotic/universal force-moment sensor testing system applied an anterior/posterior load of 50 N [92, 93] to 89 N. [14] However, the skin and musculature of the specimens utilized in these previous studies were intact as these anterior/posterior loads were applied. In the current work, all skin and musculature were dissected away leaving only the capsuloligamentous regions. Therefore, at 0° of external rotation, applying a 50 N anterior load resulted in joint dislocation. At 60° of external rotation, an anterior load of 50 N did not result in joint dislocation since the some of the capsuloligamentous regions become taught in this position and act as the primary static stabilizers. Another factor affecting the amount of anterior load that results in dislocation was the compressive force applied to the joint (22 N). Therefore, by increasing the compressive force, a larger anterior/posterior load may be applied before

dislocation is observed. However, one must be careful as too high of a compressive force could result in deforming the scapula. The robotic/universal force-moment sensor testing system has been shown to be repeatable to within ±10 N; however, some specimens dislocated with just over 10 N of anterior/posterior load at 0° of external rotation. (Figure 3.4) Therefore, simply decreasing the anterior load applied in this current work may not be sufficient. Instead, it may be necessary to increase the compressive force while the anterior load is applied is decreased to no less than twice the repeatability of the system.

3.2.4 Suggested Methodology: Joint Kinematics

For the current work, several factors were to be satisfied when determining the joint position for which the strain distribution in the capsuloligamentous regions would be evaluated using the finite element models: 1) joint position represented a functional joint position (i.e. no dislocation) and simulates a clinical exam; 2) anterior band of the inferior glenohumeral ligament and the axillary pouch visible during collection of joint kinematics such that strain distribution in these capsuloligamentous regions could be determined; and 3) anterior band of the inferior glenohumeral ligament functions to transfer loads (i.e. taut = transmitting loads). Additionally, while none of the specimens dislocated under an anterior load of 50 N, it may be useful to compare the data from the current work to future studies that evaluate joint positions with less external rotation applied. Therefore, it is suggested that all of the skin and musculature be removed from the specimen and an anterior load of 25 N be applied at 60° of external rotation.

Once in this joint position, the location of the humerus with respect to the scapula must be determined using coordinate systems that can also be utilized by the finite element models since this joint position will be used to kinematically drive the models. Therefore, the same

methodology [100] utilized by previous finite element models [21-23, 70] will be used in this current work. Briefly, registration blocks should be affixed to the scapula and humerus. The registration blocks were merely polished cubes obtained from a company that makes dice. (Midwest Game Supply Company; Polished Blanks size 0.775) In the joint position of interest, three faces of each registration block should be digitized using an external digitizer. The 3D points on each face should then be fit to a plane and the vector normal to this plane will represent the direction of one axis of the coordinate system. The origin of the coordinate system for each registration block should be placed at the corner of the registration block where all three faces intersect. In this way, a coordinate system can be generated for each registration block. The relationship of the humeral registration block with respect to the scapular registration block can then be calculated using transformation matrices.

3.3 REFERENCE STRAIN CONFIGURATION

3.3.1 Previous Literature

A methodology to determine the reference strain configuration of the anterior band of the inferior glenohumeral ligament and anterior portion of the axillary pouch was previously developed by Malicky and coworkers. [36, 37, 66] The authors performed their methodology on a total of eight cadaveric shoulder specimens that were dissected free of all soft tissue except the capsuloligamentous regions. A 6 x 10 grid of strain markers (diameter 0.5 and 0.7 mm) were affixed to the anterior band of the inferior glenohumeral ligament and anterior portion of the axillary pouch using cyanoacrylate. With the joint fixed at 60° of glenohumeral abduction and 15° of horizontal abduction, a small amount of joint distraction was applied. The

capsuloligamentous regions were then inflated to 0.7 kPa and then 4.8 kPa as the humerus was rotated from 15° of external to 15° of internal rotation in 5° increments. For each joint position, the 3D locations of the strain markers were determined at both pressures by taking two stereophotogrammetric images and digitizing the image of the strain markers using an external digitizer. The joint position corresponding to the smallest motion of the strain markers between pressures was then selected. At this joint position the reference strain configuration of the anterior band of the inferior glenohumeral ligament and anterior portion of the axillary pouch was determined by inflating the capsuloligamentous regions to 1.0 kPa and recording the locations of the strain markers.

For the above described methodology, the authors verified that the cyanoacrylate used to affix the strain markers to the capsuloligamentous regions did not have an affect on the mechanical properties of the tissue. Using this methodology, the authors measured experimental strains in the anterior band of the inferior glenohumeral ligament and anterior portion of the axillary pouch as an anterior translation was applied to the humerus in an externally rotated position while all other degrees of freedom were constrained except motion in the medial/lateral direction. The authors reported that the repeatability of their methodology was 2.8%.

3.3.2 Preliminaries

In this current work, a subject-specific finite element model that was a composite of all ligamentous regions was to be constructed. Therefore, it was important to establish the reference strain configuration for all capsuloligamentous regions. Since previous work was performed to determine the reference strain configuration of the anterior band of the inferior glenohumeral ligament and the axillary pouch, these capsuloligamentous regions were focused on initially.

Then, it was determined that the methodology used to determine the reference strain configuration of these capsuloligamentous regions also provided a reasonable reference strain configuration for the remaining capsuloligamentous regions. Therefore, a similar protocol to that published previously was performed to determine the reference strain configuration of the anterior band of the inferior glenohumeral ligament and axillary pouch. Additionally, the effect of inflation pressures and repeatability of the methodology was assessed. Moreover, the efficacy of using this methodology to establish the reference strain configuration of the remaining capsuloligamentous regions was also determined.

3.3.2.1 Methodology: Effect of Inflation Pressures

One cadaveric shoulder specimen was dissected free of all soft tissue except the capsuloligamentous regions and the humerus and scapula were fixed within epoxy putty as described in Section 3.2.3.1 of this work. The margins of the anterior and posterior bands of the inferior glenohumeral ligament were identified and a 9 x 5 grid of strain markers (2.0 mm diameter, ~10 mm between strain markers) were adhered to the surface of the tissue using cyanoacrylate. Two columns of strain markers were affixed to each the anterior and posterior band of the inferior glenohumeral ligament and 5 columns of markers were affixed to the axillary pouch. (Figure 3.6) Thus, for each of the reference strain and strained configurations, the same coordinate system was generated and the location of the strain markers was reported with respect to this coordinate system. Therefore, the humerus and scapula were then mounted within a 6-degree of freedom plastic jig at 60° of glenohumeral abduction and neutral horizontal abduction using a goniometer. (Figure 3.7) Neutral internal/external rotation of the humerus was then identified by ensuring that an equal amount of cartilage was on the anterior and posterior sides of

the glenoid. A small amount of joint distraction was then applied. A pressure regulator (resolution: 0.1 psi or 0.7 kPa) was instrumented on an air tank which was used to inflate the capsuloligamentous regions. A needle was placed inside the rotator interval, and the capsuloligamentous regions were inflated to 2.1 kPa, 3.4 kPa, and 6.2 kPa as the humerus was rotated to 0°, ±5°, ±10°, and ±15° of internal/external rotation in a random order. At each joint position, the location of the strain markers were recorded for both pressures using a custom built 3-camera (Adimec®) motion tracking system with tracking software (DMAS®). The camera system had been calibrated for a camera configuration that ensured each strain marker would be visible by at least two cameras at all times. This motion tracking system was determined to be accurate to within ±0.08 mm. The 3D location of each strain marker was measured for each of the three inflation pressures. The vector difference was then computed between the three pressures for the location of each strain marker.

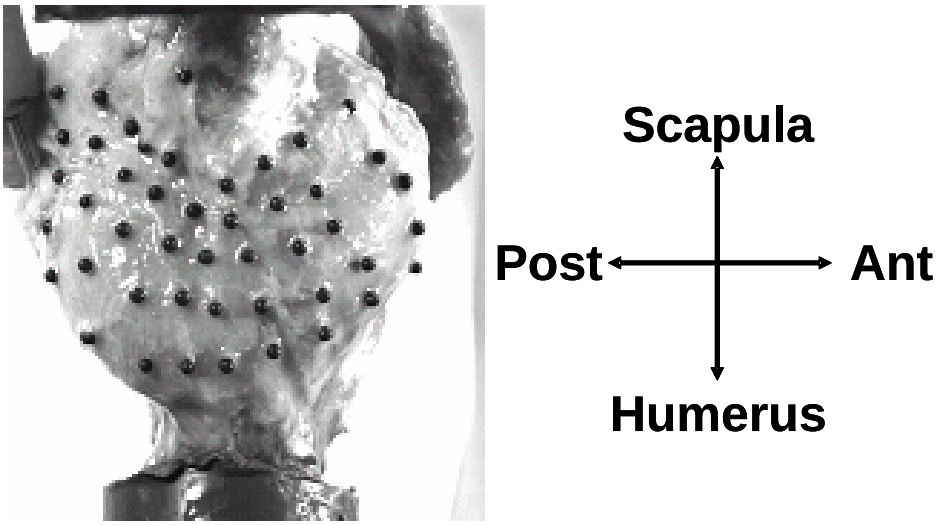

Figure 3.6: Strain markers affixed to anterior and posterior bands of the inferior glenohumeral ligament and axillary pouch

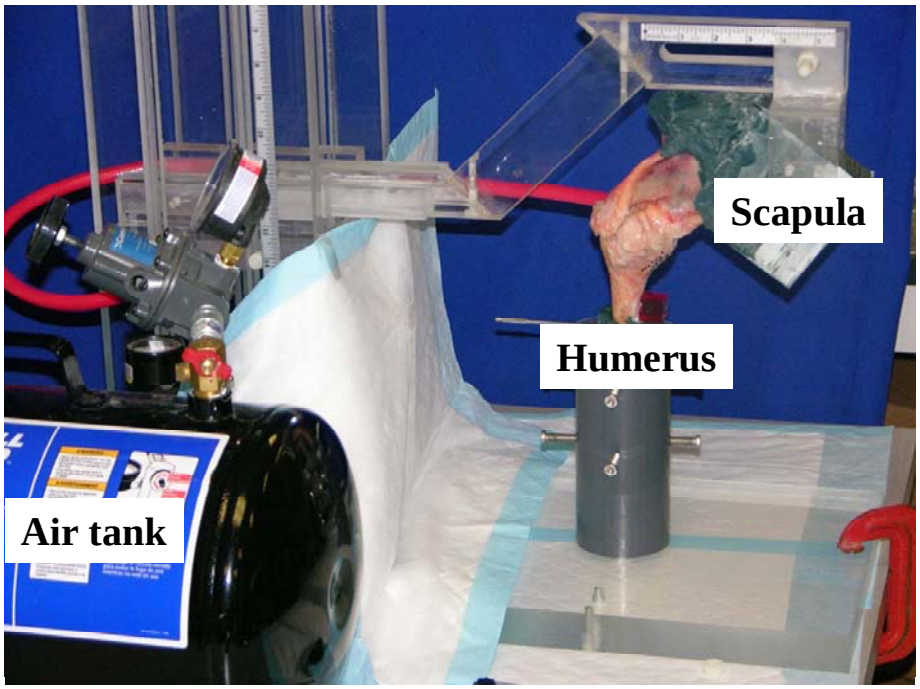

Figure 3.7: Six-degree-of-freedom plastic jig used to establish reference strain configuration

3.3.2.2 Results: Effect of Inflation Pressures

The largest change in the location of any strain marker between 2.1 kPa to 3.4 kPa was 1.16mm and occurred at 10° of internal rotation. This strain marker was located in the axillary pouch near the glenoid insertion site. Between 3.4 kPa to 6.2 kPa, the largest change in location of any strain marker was 5.51 mm and occurred at 10° of external rotation. This strain marker was located on the anterior band of the inferior glenohumeral ligament near the glenoid insertion site. Between 2.4 kPa to 6.2 kPa, the largest change in the location of any strain marker was 4.10 mm and occurred at 15° of external rotation. This marker was located on the anterior band of the inferior glenohumeral ligament near the glenoid insertion.

The magnitude of the average change in location of the strain markers between pressures is shown in Figure 3.8. The largest average change in the location of the strain markers between

2.1 kPa to 3.4 kPa was 0.50±0.17 mm at 10° of external rotation. Between 3.4 kPa to 6.2 kPa, the largest change was 0.50±0.99 mm, which also occurred at 10° of external rotation. Between the lowest (2.1 kPa) and the largest pressure evaluated (6.2 kPa), the largest average change in the location of the strain markers was only 0.46±0.22 mm which occurred at 15° of internal rotation.

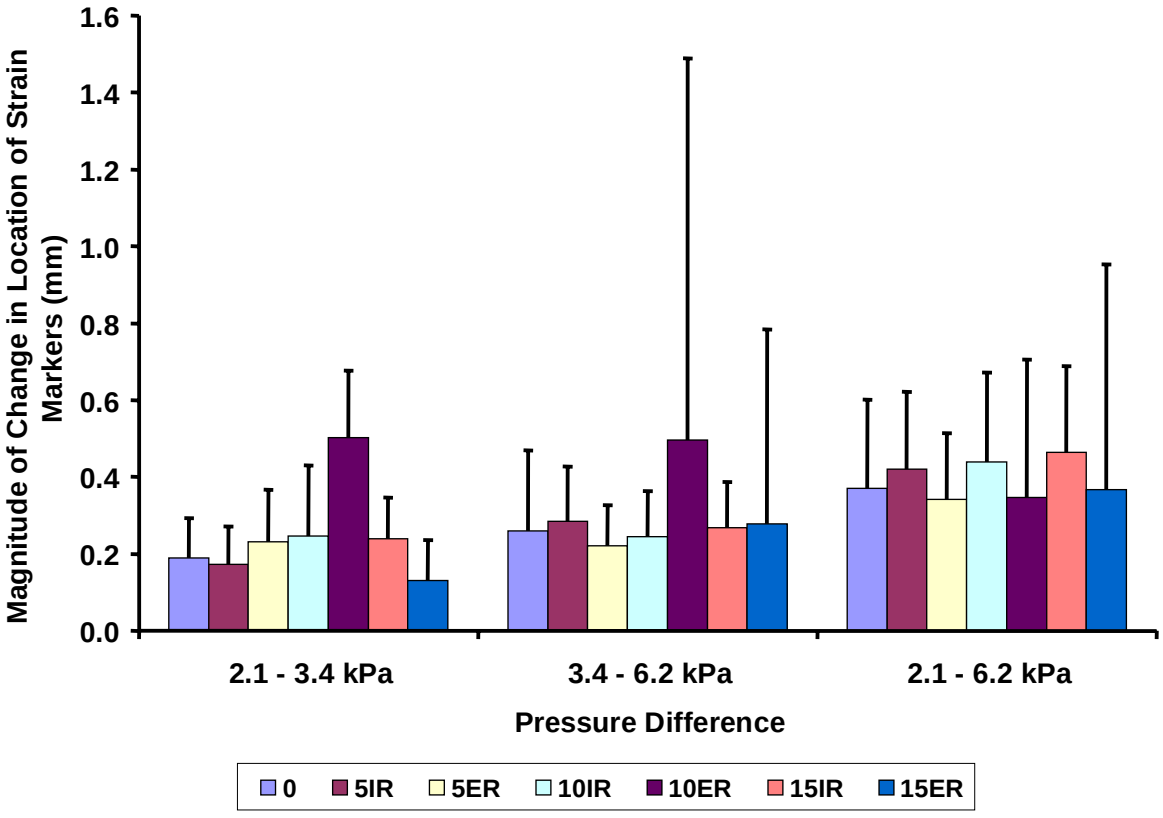

Figure 3.8: Effect of inflation pressures on location of strain markers in reference strain configuration (mean±SD, n=45 strain markers)

3.3.2.3 Implications: Effect of Inflation Pressures

These data indicate that the location of the strain markers is minimally affected by when inflated between pressures of 2.1 kPa to 6.2 kPa. In general, the location of the strain markers changed by less than 0.4 mm. This implies that increasing the pressure in this range (2.1 kPa to 6.2 kPa) does not result in a substantial load being applied to the capsuloligamentous regions. The effect that a difference in strain marker location of approximately 0.4 mm has on the experimentally measured strains will be discussed in a later section of this work.

3.3.2.4 Methodology: Repeatability

One cadaveric shoulder specimen was dissected free of all soft tissue except the capsuloligamentous regions and the humerus and scapula were fixed within epoxy putty as described in Section 3.2.3.1 of this work. A 7x11 grid of strain markers (1.58 mm diameter, ~5 mm between strain markers) was adhered to the anterior and posterior bands of the inferior glenohumeral ligament and axillary pouch using cyanoacrylate. (Figure 3.9) The first column of markers was placed just superior to the anterior band of the inferior glenohumeral ligament and the first and last strain markers in each column were approximately 1cm from the bony insertion sites. Additionally, a registration block was affixed to the humerus and three strain markers were affixed to the corners of one face of the block. This allowed the same coordinate system to be generated regardless of the camera configuration. Therefore, it was possible to compare the location of the strain markers between several different trials.

As was done previously, the joint was mounted within the 6-degree of freedom plastic jig at 60° of glenohumeral abduction and neutral horizontal abduction and internal/external rotation. A small amount of joint distraction was then applied. The capsuloligamentous regions were inflated to 0.7 kPa and 4.8 kPa as the humerus was rotated to 0°, ±5°, ±10°, and ±15° of internal/external rotation in a random order. At each joint position, the location of the strain markers were recorded for both pressures using the motion tracking system which had been calibrated for a camera configuration that ensured each strain marker would be visible by at least two cameras at all times. The joint position corresponding to the smallest average motion of the strain markers between each pressure with no marker moving more than 1 mm, was then selected. At this joint position, the reference strain configuration was determined by inflating the capsuloligamentous regions to 1.0 kPa and recording the position of the strain markers.

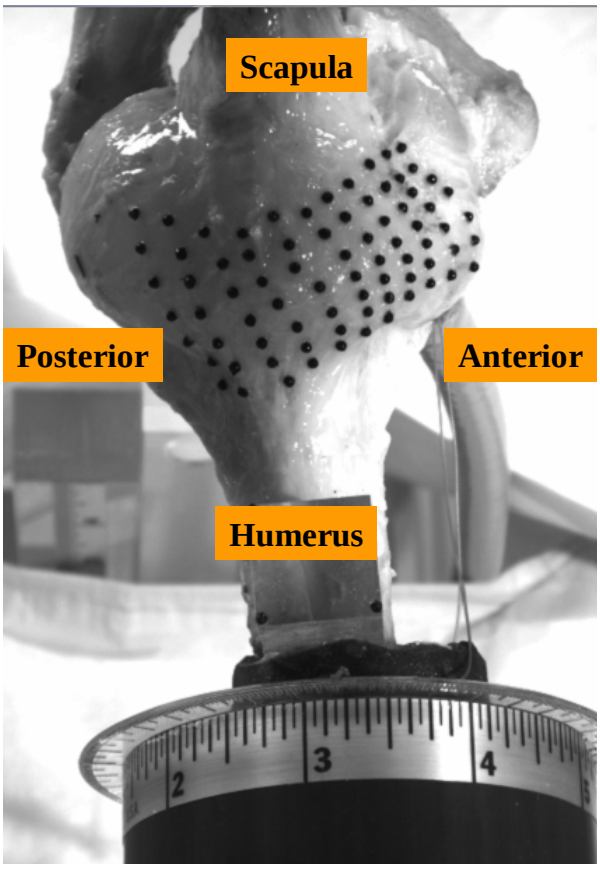

Figure 3.9: Location of strain markers affixed to the anterior and posterior bands of the inferior glenohumeral ligament and axillary pouch

The specimen was then removed from the plastic jig and the cameras were removed from the testing environment. The plastic jig and the camera tripods were then arbitrarily moved in all degrees of freedom. The above described protocol was then repeated two times making a total of three trials. For each trial, the specimen was remounted within the plastic jig, the configuration of the camera system established and calibrated, the joint position with the smallest strain marker

motion between 0.7 kPa and 4.8 kPa identified, and the location of the strain markers at this joint position with an applied 1.0 kPa was determined.

Thus, the 3D location of each strain marker was obtained three times at 1.0 kPa. For each strain marker, a sphere was fit to the three locations measured. The centroid of the sphere was calculated from the three strain marker locations and the radius was defined to be the largest distance between the centroid and the strain marker locations which was a measure of the variability.

3.3.2.5 Results: Repeatability

Several of the strain markers were not visible for at least one of the joint positions of the different trials. Seven, five, and eight strain markers were not visible for at least one joint position for the three trials, respectively. Any strain marker that was not visible in all joint positions was omitted from the analysis for that trial. The joint position with the smallest average strain marker motion between pressures for each of the three trials was 5°, 10°, and 5° of internal rotation, respectively. The average radius of the spheres across the three trials was 1.53 mm. The maximum radius observed was 2.54 mm. The effect of this repeatability on strain calculations is evaluated in a later section of this work.

3.3.2.6 Implications: Repeatability

These data indicate that the methodology described in this work to determine the reference strain configuration had limited variability; however, the effect that this variability has on the experimentally measured strains will be discussed in a later section of this work. The source of the variability was most likely the due to the inflation pressure. In order to inflate the

capsuloligamentous regions, it was necessary to suture the rotator interval. Additionally, cyanoacrylate was also necessary to seal small leaks which were commonly observed where the long head of the biceps tendon entered the joint space.

3.3.2.7 Methodology: Effect on other Capsuloligamentous regions

The above described methodology was evaluated for the anterior and posterior bands of the inferior glenohumeral ligament and axillary pouch. However, in addition to the thicker capsuloligamentous regions, the anterosuperior and posterior regions will be included in the finite element model where the glenohumeral capsule treated as a sheet of fibrous tissue (Model #1). Therefore, it was important to determine whether the reference strain configuration of the anterior and posterior bands of the inferior glenohumeral ligament and axillary pouch provided a suitable reference configuration for the anterosuperior and posterior regions as well.

Additional strain markers (2 x 4 grid) were affixed to the anterosuperior and posterior capsuloligamentous regions of the same specimen utilized in Section 3.3.2.4. Again, the strain markers were placed approximately 5 mm apart and were at least 1 cm from the glenoid and humeral insertion sites. The same experimental setup described in Section 3.3.2.4 was used; however, due to the limited field of view of the 3-camera system, it was not possible to view the anterosuperior or the posterior capsuloligamentous region strain markers with at least 2 cameras simultaneously. Therefore, the plastic jig was rotated about the axis of the humerus such that the anterosuperior strain markers were within the calibrated field of view for the camera system and visible by at least 2 cameras. The capsuloligamentous regions were then inflated to 0.7 kPa and 4.8 at the seven joint positions and the location of the anterosuperior strain markers were measured for both pressures. Then, the plastic jig was again rotated about the axis of the

humerus such that the posterior strain markers were visible by at least 2 cameras and within the calibrated field of view of the camera system. Again, the capsuloligamentous regions were inflated to 0.7 kPa and 4.8 at the seven joint positions and the location of the posterior strain markers were measured for both pressures. For both the anterosuperior and posterior capsuloligamentous regions, the average and maximum motion of the strain markers between pressures was then compared to that which was collected for the anterior and posterior band of the inferior glenohumeral ligament and axillary pouch.

3.3.2.8 Results: Effect on other Capsuloligamentous regions

Shown in Table 3.1 is the motion of each strain marker between 0.7 kPa and 4.8 kPa for the anterosuperior and posterior capsuloligamentous regions. Regardless of the joint position tested, the strain markers in the anterosuperior and posterior capsuloligamentous regions moved more than 0.5 mm. Some strain markers moved as much as 5.0 mm and the average motion of the strain marker was greater than 1.0 mm for all joint positions tested.

Table 3.1: Effect of inflation pressures (0.7 kPa and 4.8 kPa) on anterosuperior and posterior strain markers

Motion of Anterosuperior and Posterior Strain Markers between 0.7 kPa and 4.8 kPa (mm)														
Strain Marker #	0 I/ER		5 ER		5 IR		10 ER		10 IR		15 ER		15 IR	
	Ant	Post	Ant	Post	Ant	Post	Ant	Post	Ant	Post	Ant	Post	Ant	Post
1	1.91	0.40	4.61	0.94	6.23	1.95	4.96	1.56	2.10	0.96	1.36	0.96	1.35	4.15
2	3.22	1.46	2.91	1.15	2.09	3.42	2.68	1.54	1.40	0.72	2.64	2.12	1.65	3.58
3	3.62	1.19	2.85	0.77	5.64	3.75	2.32	1.02	0.70	1.17	1.66	0.55	3.66	3.86
4	2.21	0.77	2.44	1.92	4.79	1.21	2.57	1.77	1.94	1.02	2.38	1.95	0.93	4.17
5	2.89	0.40	4.11	2.61	5.28	2.59	5.01	0.72	1.92	1.21	1.67	1.43	0.41	3.06
6	0.95	0.00	3.80	1.77	4.24	1.91	4.36	0.53	0.93	0.60	1.76	3.88	2.78	5.41
7	1.31	0.37	2.94	1.50	3.94	1.52	1.89	1.75	0.70	1.13	1.05	2.68	2.41	1.99
8	4.75	0.78	2.26	1.95	5.54	2.58	1.56	1.69	1.88	0.93	3.12	0.84	3.82	5.23
Average	2.61	0.67	3.24	1.58	4.72	2.36	3.17	1.32	1.45	0.97	1.95	1.80	2.13	3.93
SD	1.26	0.48	0.836	0.6	1.3	0.89	1.39	0.5	0.59	0.22	0.7	1.11	1.3	1.11
Maximum	4.75	1.46	4.61	2.61	6.23	3.75	5.01	1.77	2.10	1.21	3.12	3.88	3.82	5.41

3.3.2.9 Implications: Effect on other Capsuloligamentous regions

These data indicate that the location of the strain markers on the anterosuperior and posterior capsuloligamentous regions were drastically affected when inflated between pressures of 0.7 kPa to 4.8 kPa. This was true regardless of the joint position tested. Thus, even though a reference strain configuration may be identified for the anterior and posterior bands of the inferior glenohumeral ligament and axillary pouch, this would not correspond to a reference strain configuration for the anterosuperior and posterior capsuloligamentous regions. These data indicated that while the folds and wrinkles of capsuloligamentous regions may have been removed from anterior and posterior bands of the inferior glenohumeral ligament and axillary pouch, they had not been removed from the anterosuperior or posterior capsuloligamentous regions. However, in the current work, joint positions with only neutral horizontal adduction were investigated. As with changes in internal/external rotation, changes to horizontal adduction may also affect the amount of strain marker motion observed.

3.3.2.10 Methodology: Additional Inflation Pressures

The previous results indicated that a large (>1.0 mm) amount of strain marker motion was observed between 0.7 kPa and 4.8 kPa for the anterosuperior and posterior capsuloligamentous regions. However, this was not true for the anterior and posterior bands of the inferior glenohumeral ligament and axillary pouch (~0.2 mm of strain marker motion). Therefore, while inflating the capsuloligamentous regions to 1.0 kPa may provide a good reference strain configuration for the anterior and posterior bands of the inferior glenohumeral ligament and axillary pouch, it did not provide a good reference strain configuration for the anterosuperior and

posterior capsuloligamentous regions. However, the previous results also indicated that increasing the inflation pressure up to 6.2 kPa did not result in an increase in deformation of the capsuloligamentous regions when compared to an inflation pressure of 4.8 kPa. Therefore, the motion of strain markers affixed to the anterosuperior and posterior capsuloligamentous regions was investigated between 4.8 kPa and 6.2 kPa.

One cadaveric shoulder specimen was dissected free of all soft tissue except the capsuloligamentous regions and the humerus and scapula were fixed within epoxy putty. A 2 x 4 grid was adhered to the anterosuperior and posterior regions as described previously. Again the specimen was mounted within the 6-degree of freedom plastic jig and the location of the strain markers were determined or the anterosuperior and posterior capsuloligamentous regions as they were inflated to 4.8 kPa and 6.2 kPa. The average and maximum motion of the strain markers between pressures was then calculated for the anterosuperior and posterior capsuloligamentous regions.

3.3.2.11 Results: Additional Inflation Pressures

Shown in Table 3.2 is the motion of each strain marker between 4.8 kPa and 6.2 kPa for the anterosuperior and posterior capsuloligamentous regions. The largest motion of any strain marker in the anterosuperior capsuloligamentous region was only 0.88 mm and occurred at 10° of internal rotation. For the posterior capsuloligamentous region, the largest motion of any strain marker was only 0.59 mm which occurred at 15° of internal rotation. On average, the motion of the strain markers ranged from 0.14±0.11 mm to 0.60±0.15 mm for the anterosuperior capsuloligamentous region and ranged from 0.13±0.07 mm to 0.44±0.08 mm.

Table 3.2: Effect of inflation pressure (4.8 kPa and 6.2 kPa) on anterosuperior and posterior strain markers

Motion of Anterosuperior and Posterior Strain Markers between 4.8 kPa and 6.2 kPa (mm)														
Strain Marker #	0 I/ER		5 ER		5 IR		10 ER		10 IR		15 ER		15 IR	
	Ant	Post	Ant	Post	Ant	Post	Ant	Post	Ant	Post	Ant	Post	Ant	Post
1	0.33	0.15	0.12	0.22	0.17	0.16	0.45	0.24	0.51	0.16	0.13	0.23	0.27	0.59
2	0.19	0.13	0.07	0.13	0.15	0.10	0.19	0.12	0.49	0.13	0.46	0.26	0.17	0.47
3	0.17	0.04	0.12	0.31	0.35	0.33	0.09	0.03	0.52	0.33	0.43	0.32	0.61	0.38
4	0.15	0.12	0.14	0.12	0.24	0.10	0.15	0.10	0.88	0.17	0.12	0.20	0.40	0.50
5	0.21	0.33	0.41	0.14	0.11	0.29	0.77	0.18	0.50	0.12	0.11	0.30	0.04	0.49
6	0.25	0.26	0.06	0.19	0.14	0.44	0.19	0.20	0.61	0.20	0.24	0.19	0.13	0.36
7	0.49	0.03	0.26	0.18	0.28	0.50	0.41	0.09	0.55	0.19	0.18	0.36	0.16	0.35
8	0.18	0.05	0.12	0.16	0.12	0.25	0.16	0.10	0.79	0.08	0.38	0.22	0.18	0.43
Average	0.14	0.16	0.16	0.18	0.19	0.27	0.30	0.13	0.60	0.17	0.26	0.26	0.24	0.44
SD	0.11	0.12	0.12	0.06	0.09	0.15	0.23	0.07	0.15	0.08	0.15	0.06	0.18	0.08
Maximum	0.33	0.41	0.41	0.31	0.35	0.50	0.77	0.24	0.88	0.33	0.46	0.36	0.61	0.59

3.3.2.12 Implications: Additional Inflation Pressures

These data indicate that the change in location of the strain markers in the anterosuperior and posterior capsuloligamentous regions between 4.8 kPa to 6.2 kPa was minimal. Additionally, in a previous section of this work, it was demonstrated that an inflation pressure of 6.2 kPa did not apply a substantial load to the capsuloligamentous regions. The effect these changes in the location of the strain markers have on experimentally measured strains will be discussed in a later section of this work.

3.3.3 Suggested Methodology: Reference Strain Configuration

Based upon the above preliminary studies, a methodology to obtain the reference strain configuration for the development of subject-specific finite element models was developed. The specimen should be dissected free of all soft tissue except the glenohumeral capsule and a 7x11

grid of strain markers (1.58 mm diameter, ~5 mm between strain markers) should be adhered to the anterior band of the inferior glenohumeral ligament and axillary pouch using cyanoacrylate. The first column of markers should be placed just superior to the anterior band of the inferior glenohumeral ligament and the first and last stain markers in each column were approximately 1cm from the bony insertion sites. Additionally, a 2 x 4 grid of strain markers should be affixed to the anterosuperior and posterior capsuloligamentous regions (these strain markers are only used to verify that only a minimal, ~0.3 mm, of motion is observed for these capsuloligamentous regions in the joint position utilized for the reference strain configuration. Again, these strain markers should be placed approximately 5 mm apart and were at least 1 cm from the glenoid and humeral insertion sites. In order to co-register the location of the strain markers in the reference strain configuration and the strained configurations (Section 4.0), a registration block should be affixed to the humerus just distal to the humeral head and strain markers should be affixed to three corners on one face of the registration block. These strain markers must be visible by at least two of the three cameras. Thus, a common coordinate system can be generated between different camera configurations.

The joint should then be positioned at 60° of glenohumeral abduction and neutral horizontal abduction and internal/external rotation with a small amount of joint distraction applied. The capsuloligamentous regions should then be inflated to 4.8 kPa and then to 6.2 kPa as the humerus is rotated to 0°, ±5°, ±10°, and ±15° of internal/external rotation in a random order. At each joint position, the 3D location of the strain markers should be recorded for both pressures. The joint position corresponding to the smallest average motion of the strain markers on the anterior band of the inferior glenohumeral ligament and axillary pouch between each pressure should be selected. However, no marker should move more than 1 mm. Additionally,

at the selected joint position, it should be verified that the average motion of the strain markers on the anterosuperior and posterior capsuloligamentous regions was no more than 0.3 mm with no strain marker moving more than 1 mm. If these conditions are satisfied, the reference strain configuration should be determined by inflating the capsuloligamentous regions to 5.2 kPa and recording the position of the strain markers on the anterior band of the inferior glenohumeral ligament and axillary pouch.

3.4 SUBJECT-SPECIFIC GEOMETRY

3.4.1 Previous Literature

Previous computational studies have utilized computed tomography and magnetic resonance imaging to obtain subject-specific geometry of the bones and/or soft tissues. [65, 70, 71, 97, 98, 101] Computed tomography allows for easy visualization of the bony geometry. However, with all soft tissues intact, visualization of specific soft tissue structures can be quite difficult. While magnetic resonance imaging allows for easy visualization of specific soft tissue structures amidst other soft tissues, the cost of magnetic resonance imaging is much greater than computed tomography. Therefore, some researchers have excised all soft tissues except those of interest prior to scanning specimens via computed tomography [65, 70, 71] which greatly improved the visualization of the soft tissue structure of interest.

3.4.2 Preliminaries

3.4.2.1 CT Data Acquisition

The stress and strain distribution would be greatly affected by the contact between the capsuloligamentous regions and the cartilage of the humeral head. Therefore, it was important to include the articular cartilage of the humeral head. The geometry of the registration blocks was also necessary since the kinematics of the bones are to be described using coordinate systems generated at these blocks. Thus, in order to co-register the location of the bones in the imaging environment (e.g. CT) and robotic/universal force-moment sensor testing system environments, it was also necessary to visualize the registration blocks that were affixed to each bone. Moreover, since the coefficients to the constitutive model were to be determined for each capsuloligamentous region, it was necessary to obtain the geometry of each capsuloligamentous region. Lastly, all of this information was to be obtained while the capsuloligamentous regions were inflated to the reference strain configuration (i.e. inflation of capsuloligamentous regions while in the imaging environment).

Due to the importance of the bony geometry and the need for the metal air tank to be in the imaging environment, volumetric CT data acquisition was investigated. Additionally, since the only soft tissue of interest was the glenohumeral capsule, all other soft tissues were removed making visualization of the capsuloligamentous regions possible. However, several issues had to be addressed: 1) visualization of registration blocks; 2) distinguishing between the capsuloligamentous regions; 3) assessing where the capsuloligamentous regions insert into the humeral head and glenoid of the scapula; and 4) visualization of humeral head articular cartilage.

To address these issues, four specimens were utilized in preliminary experiments. The specimens were mounted within the CT scanner such cross-sectional views along the length of the humerus were obtained. A soft tissue protocol was used for each of the four specimens which produced good visualization of the registration blocks in all cases. In order to discern the boundaries of the capsuloligamentous regions, several materials were affixed to the boundaries using cyanoacrylate such that the ends of the tube terminated at the insertion sites to the humeral head and glenoid of the scapula. Of these materials (rubber tubing, copper wire, plastic coated wire, and beaded plastic cable), only the rubber tubing was easily visible with the soft tissue protocol without any artifacts. (Figure 3.10) Moreover, it was possible to assess where the capsuloligamentous regions inserted into the humerus and glenoid of the scapula. The rubber tubing could be visualized along the longitudinal axes of the capsuloligamentous regions in successive CT data scans. The last CT data scan where a rubber tube was visible marked the insertion site for the margin of the capsuloligamentous region that the rubber tube marked. Visualization of the humeral head cartilage was also important and presented itself as a "halo" around the cortical bone of the humeral head. (Figure 3.10) A typical field of view was 180 cm and visualization of all necessary features was possible with the following CT scanner settings: 100 kV, 120 mA, 512 matrix, 1 x 1 axial.

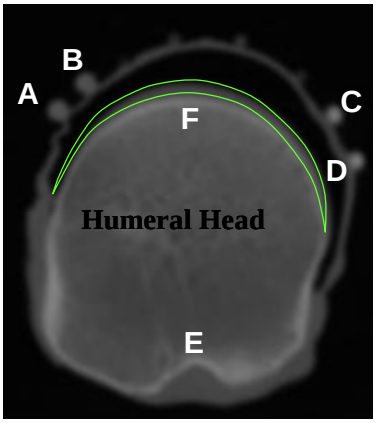

A: Superior margin of PB-IGHL

B: Inferior margin of PB-IGHL

C: Inferior margin of AB-IGHL

D: Superior margin of AB-IGHL

E: Bicipital groove

F: Articular cartilage (outlined in green)

Figure 3.10: CT slice with rubber tubes denoting margins of anterior and posterior bands of the inferior glenohumeral ligament and showing articular cartilage

3.4.2.2 Accuracy: Reconstructed Geometry

Two of the four specimens were then selected to assess the accuracy of generating 3D geometry from CT scans by comparing physical measurements to those of geometry models developed of the humerus, scapula, and registration block. Therefore, it was first necessary to generate the geometry of the humerus, scapula, and a registration block such that they could be used within a computer modeling environment. Thus, their geometries were reconstructed by manually segmenting each CT slice (SURFdriver® Version 3.5.6) which had been converted into bitmap images. (Figure 3.11) The manual segmentations for each slice were then used to generate a polygon mesh of each surface (humerus, scapula, and registration block). This mesh was then smoothed twice to account for user segmentation errors using a built in algorithm within the SURFdriver® software package. The smoothed surfaces were then exported in a .DXF file format which was then imported into a viewing package. (Rhino3D®; Seattle, Washington)

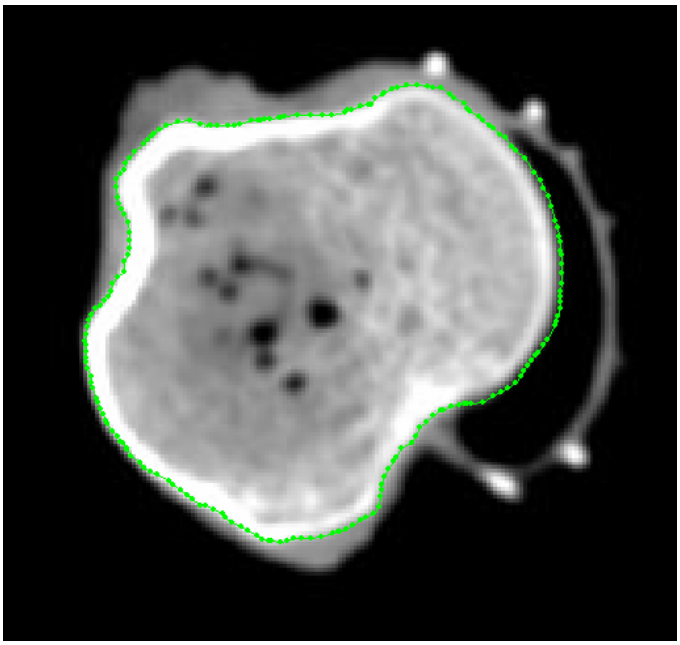

Figure 3.11: Slice from CT scan of humerus which has been segmented (green) for reconstruction

Several measurements were then made using these surfaces which were then compared to physical measurements made on the actual humerus, scapula, and registration block. The measurements used for the comparisons were: 1) superior-to-inferior height of glenoid; 2) anterior-to-posterior width of glenoid; 3) width of the bicipital groove; and 4) width of registration blocks. For both specimens, each measurement, excluding the registration blocks, was made using calipers. This was then repeated four more times yielding a total of five trials. The registration blocks were a standard geometry created with dimension 20 mm x 20 mm x 20 mm. Thus, 20 mm was selected as the "gold standard" to which measurements made from the reconstructed geometry of the registration blocks was compared. For the reconstructed geometry of the humerus, scapula, each measurement was made within Rhino3D® for both specimens. This was then repeated four more times yielding a total of five trials. (Figure 3.12)

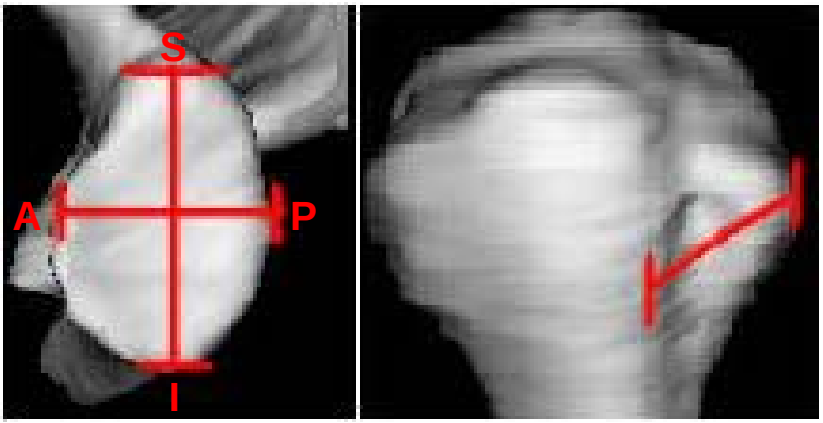

Figure 3.12: Measurements taken on glenoid (left) and bicipital groove of humerus (right)

The average and standard deviation of each measurement was then calculated for each physical measurement and for the measurements made on the reconstructed geometry. (Table 3.3) An f-test, with significance set at $p<0.05$, was then used to compare the repeatability of the physical and reconstructed measurements. A student t-test, with significance set at $p<0.05$, was used to compare the physical and reconstructed measurements.

Table 3.3: Comparison of physical measurements and those made using reconstructed geometry of CT scans

		Superior-to-Inferior Glenoid	Anterior-to-Posterior Glenoid	Bicipital Groove	Registration Block
Specimen #1	Physical Measurement (mm)	39.9±0.5	29.2 ±0.9	8.9±0.8	20.0
	Reconstructed Geometry (mm)	36.8±0.3	30.3 ±0.7	9.0±0.8	19.6±0.2
Specimen #2	Physical Measurement (mm)	33.3±2.6	24.2 ±0.5	8.8±0.9	20.0
	Reconstructed Geometry (mm)	31.5±0.9	24.0 ±0.4	10.7±0.5	19.0 ±0.1

No significant differences between the repeatability of the physical measurements and the reconstructed geometry were detected for any of the measurements made. However, significant differences were detected between the magnitudes of the physical measurements and those made using the reconstructed geometry for the superior-to-inferior glenoid in both specimens. ($p<0.05$) The average superior-to-inferior height of the glenoid was 39.9±0.5 mm and 36.8±0.3 mm for the physical measurement and the reconstructed geometry of the first specimen while they were 33.3±2.6mm and 31.5±0.9 mm, respectively. Additionally, for the second specimen a significant difference was detected for the bicipital groove. (physical measurement: 8.8± 0.9 mm; reconstructed geometry: 10.7± 0.5 mm; $p<0.05$) Significant differences were also detected

for the registration blocks of both specimens with the largest difference between the physical measurement and the reconstructed geometry being 1 mm for the second specimen. ($p < 0.05$)

The significant differences detected for the superior-to-inferior height of the glenoid was most likely due to difficulty discerning the boundary between the glenoid itself and the labrum, a soft tissue layer around the glenoid. (Figure 3.13) Adding additional difficulty is the fact that the long head of the biceps tendon also inserts into the superior margin of the glenoid. Therefore, it was much easier to make the physical measurement of the superior-to-inferior height of the glenoid since the labrum and long head of the biceps tendon were dissected away from the glenoid. However, it is important to note that the superior aspect of the glenoid should have a minimal impact on the results of this current work since the humerus translates inferiorly as an anterior translation is applied, [102] thus minimizing any contact with the superior aspect of the glenoid.

http://www.scoi.com/images/scoi-shoulder-glenoid.jpg

Figure 3.13: Schematic illustrating insertion site of long head of biceps tendon into labrum of glenoid

The significant differences detected for the registration blocks were most likely due to the orientation of the registration block with respect to the axis that the CT scanner took measurements along. (Figure 3.14) Recall that this axis was parallel to the humeral shaft. Since the edges of the registration block were not parallel and perpendicular to the humeral shaft, difficulties were encountered when reconstructing the geometry since the appearance of the corners of the registration block was difficult to observe initially. This problem can be circumvented by ensuring that the edges of the registration block are parallel and perpendicular to the humeral shaft allowing a large portion of the registration block to be viewable instead of a small corner.

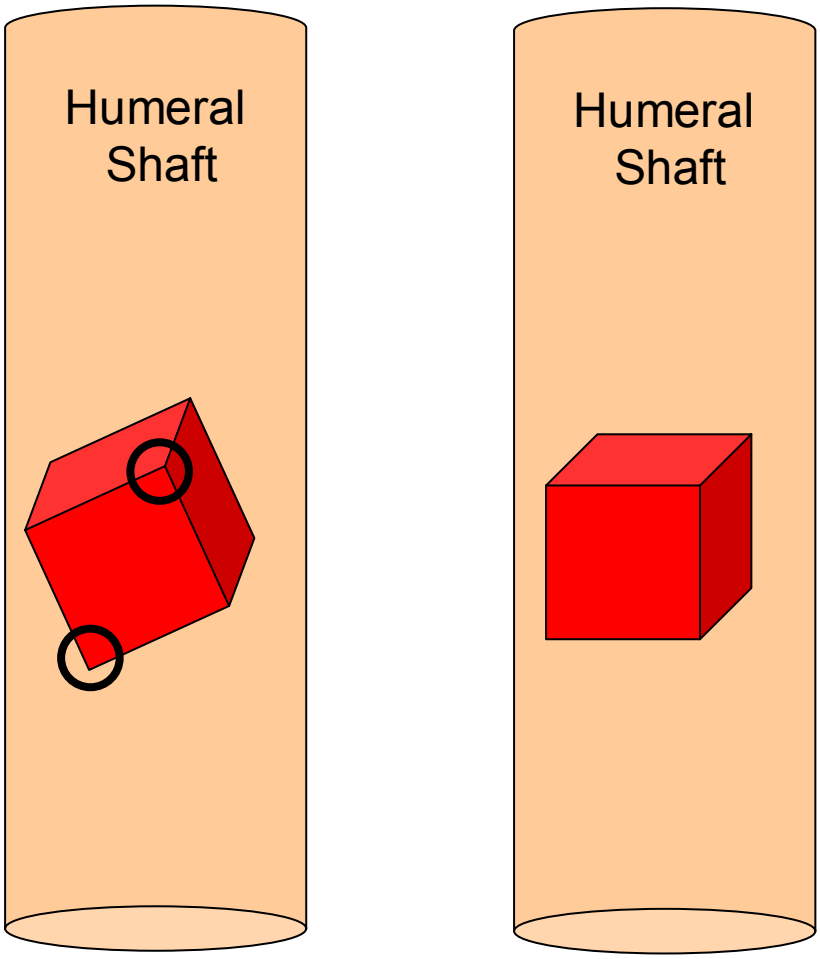

Figure 3.14: Schematic illustrating a bad (left) and good (right) orientation of registration block

3.4.3 Suggested Methodology: Subject-Specific Geometry

Based upon the above preliminary study, a methodology to obtain the subject-specific geometry of the humerus, scapula, capsuloligamentous regions, and registration blocks was established for the development of subject-specific finite element models. Specimens should be dissected such that the only soft tissue remaining is the glenohumeral capsule and the coracohumeral ligament. Registration blocks should be affixed to the humerus and scapula such that their edges are parallel and perpendicular to the humeral shaft. Additionally, rubber tubing is affixed to the

margins of the capsuloligamentous regions using cyanoacrylate. With the joint inflated to the reference strain configuration, a volumetric CT scan should be taken using a soft tissue protocol (100 kV, 120 mA) with a slice increment of at least 1 mm.

3.5 COEFFICIENTS OF CONSTITUTIVE MODEL

3.5.1 Previous Literature

The mechanical properties of the capsuloligamentous regions have been investigated previously. [12, 17, 27-29, 103, 104] However, these previous studies have applied only a uniaxial tensile load to the capsuloligamentous regions to investigate the failure properties of the tissue. Therefore, an aspect ratio of at least five was utilized to allow for a uniform strain distribution across the tissue sample. Based on the collagen fiber organization and the bi-directional mechanical properties previously reported in this work, (Section 2.0) the capsuloligamentous regions may be isotropic.

While the coefficients to an isotropic material may be determined from merely one loading condition, in order to determine the coefficients to a transversely isotropic constitutive model, two loading conditions are required. At this time, the constitutive model that accurately describes the capsuloligamentous regions is moderately uncertain with the results from *Specific Aim #1* suggesting that an isotropic model may be appropriate. However, the majority of tendons and ligaments such as the medial collateral ligament of the knee are considered to be transversely isotropic. [76, 79, 105] Therefore, it was necessary to experimentally collect data that could be used to determine coefficients for either an isotropic or transversely isotropic constitutive model. Moreover, loading conditions in addition to those used to determine the

coefficients to the constitutive model should be applied such that the results of these experiments can be predicted by the coefficients. In this way the accuracy of the determined coefficients can be determined.

Thus, uniaxial tensile test designed to obtain failure properties of the tissue during only one loading condition. Additionally, in order to ensure a uniform distribution of stress across the tissue sample being tested, an aspect ratio of at least five must be utilized. However, this does not allow for information regarding the Poisson's effect to be determined with the tangent modulus, ultimate stress, ultimate strain, and strain energy density being the parameters that can be determined. Previously, a subject-specific finite element model of the anterior and posterior bands of the inferior glenohumeral ligament and the axillary pouch has been developed. [21] In this study, the capsuloligamentous regions were described as isotropic with the tangent modulus obtained from load-to-failure experiments and an assume Poisson's ratio of 0.4. However, based on sensitivity studies performed by the authors, the model was found to be highly sensitive to changes in both tangent modulus and changes in bulk to shear modulus ratio. In fact, changes in the predicted maximum principal strain (16%) and reaction forces (9 N) were shown when the tangent modulus was increased or decreased by 50% of its original value. Similarly, altering the bulk to shear modulus ratio from 1.0 to 10.0 resulted in changes to the predicted maximum principal strain and reaction forces of 43% and 25% of the original value, respectively. These data indicate not only the importance of using subject-specific coefficients to the constitutive model and the tangent modulus but the Poisson's ratio or bulk modulus as well. Therefore, a uniaxial load-to-failure tensile test is not adequate to determine the coefficients of an isotropic constitutive model since information regarding the Poisson's ratio or bulk modulus can not be obtained. Thus, for an isotropic material, one of two testing protocols may be followed: 1)

apply a tensile load to a tissue sample with an aspect ratio of less than five with a grid of strain markers affixed to the midsubstance or 2) apply a shear load to a tissue sample with an aspect ratio of less than five with a grid of strain markers affixed to the midsubstance. [72]

Since most ligamentous tissues are transversely isotropic, with a preferred alignment along their length, [76, 79, 105] researchers have focused on the response of various tissues to tensile loads applied along the length of the tissue. [17, 26, 28, 29, 64, 91, 106, 107] However, this neglects the contribution of the extracellular matrix and the fiber-fiber interactions. A recent study has investigated the response of the medial collateral ligament of the knee, to shear loading. [72] Square tissue samples were excised from the medial collateral ligament. (10 x 25 mm) A shear load was applied along the length of the tissue samples as the elongation and force were recorded. Since the collagen fibers of the medial collateral ligament of the knee are indeed aligned along its length, this experiment largely examined the response of the extracellular matrix. Using finite element analysis, the experiment was then simulated with an assumed transversely isotropic constitutive model. The experimental force-elongation curve was compared to the force-elongation curve obtained from the finite element simulation. The coefficients of the constitutive model that describe the extracellular matrix were then adjusted until these curves matched. The other coefficients were previously obtained from uniaxial load to failure experiments performed in the directions parallel and perpendicular to the longitudinal axis of the ligament.

With this method previously utilized for the medial collateral ligament of the knee, multiple loading conditions (tensile and shear) should be applied to tissue samples harvested from the capsuloligamentous regions when possible. Additionally, the tensile and shear experiments should be performed in the directions parallel and perpendicular to the longitudinal

axes of the capsuloligamentous regions (i.e. total of four loading conditions) such that coefficients to either an isotropic or a transversely isotropic constitutive model may be determined and then used to predict the remaining experiments.

3.5.2 Preliminaries

The experimental protocol to apply tensile and shear loads to tissue samples excised from the five capsuloligamentous regions was established within the thesis work of another graduate student (Eric J. Rainis, BS). Based on the work performed by Mr. Rainis and on previously published work with the MCL [72], the following testing methodology was developed for the five capsuloligamentous regions.

3.5.2.1 Tissue Sample Procurement

The largest square tissue sample size that could be repeatedly excised from the axillary pouch and posterior capsuloligamentous regions was determined to be 25 x 25 mm. A square tissue sample was necessary since tensile and shear loads would be applied in the direction parallel and perpendicular to the longitudinal axis of the capsuloligamentous regions. Although an isotropic material model was assumed, loads were applied in the parallel and perpendicular direction to verify that this assumption was reasonable. In addition to comparing the experimental and finite element simulation force-elongation data, the predicted strain distribution was also compared to that obtained experimentally. Therefore, in order to measure the strain distribution experimentally, a 3 x 3 grid of uniformly placed strain markers (1.6 mm diameter) was fixed to the tissue sample.

The size of the anterior and posterior bands of the inferior glenohumeral ligament and anterosuperior capsuloligamentous regions did not allow for a large square tissue sample to be excised. The size of the anterosuperior region is limited due to the rotator interval and the size of the supraspinatus tendon insertion. The anterior and posterior bands of the inferior glenohumeral ligament have an approximate width of 5 mm, thus also limiting the size of the tissue samples. Therefore, only a 5 x 15 mm rectangular tissue sample was excisable from the anterior and posterior bands of the inferior glenohumeral ligament and anterosuperior capsuloligamentous regions. It was only possible to apply a 3 x 2 grid of strain markers to these tissue samples.

3.5.2.2 Experimental Set-up

Custom clamps were designed to allow for the application of tensile loads and could be reconfigured for the application of shear loads. (Figure 3.15) For both the tensile and shear tests, a load cell (Sensotec, Columbus, OH; Model 31; Capacity 10 lbs.) was used to measure the load along the axis of motion of the materials testing device. For the shear tests, a second load cell (Sensotec, Columbus, OH; Model 31; Capacity 1000 grams) was incorporated into the clamp design to measure the load in the direction perpendicular to the axis of motion of the materials testing device.

The location of the strain markers was recorded throughout the tests using the same custom built camera system described in Section 3.3.2.1. However, for this application, only one camera was necessary since tissue sample remained in the same plane throughout the tests and only the 2D location of the strain markers was necessary.

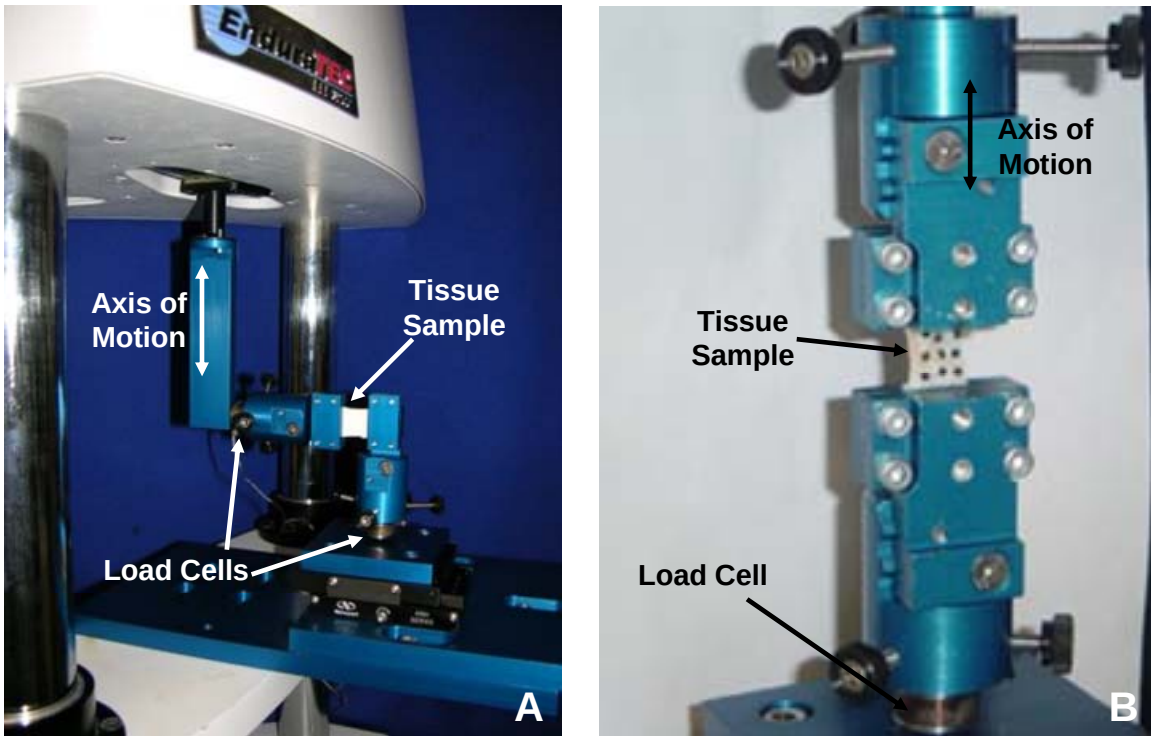

Figure 3.15: Custom fixtures designed for shear (A) and tensile (B) testing

3.5.2.3 Loading Conditions

For the axillary pouch and posterior capsuloligamentous regions, the tissue samples were loaded in tension and in shear in the directions parallel (longitudinal) and perpendicular (transverse) to the longitudinal axes of the capsuloligamentous regions. Based on the clamp design, it was possible to test in tension for the longitudinal direction and in shear for the transverse direction (option A) without clamping a different portion of the tissue sample within the clamps. (Figure 3.16) This was also true for tension in the transverse direction and shear in the longitudinal direction (option B). However, once option A or B was tested, the tissue that was previously clamped had to be removed from the tissue sample so that the tissue sample could be tested for the remaining option. Therefore, it was first necessary to randomly select option A or B and to then randomly choose between the two possibilities within each option. (Figure 3.17)

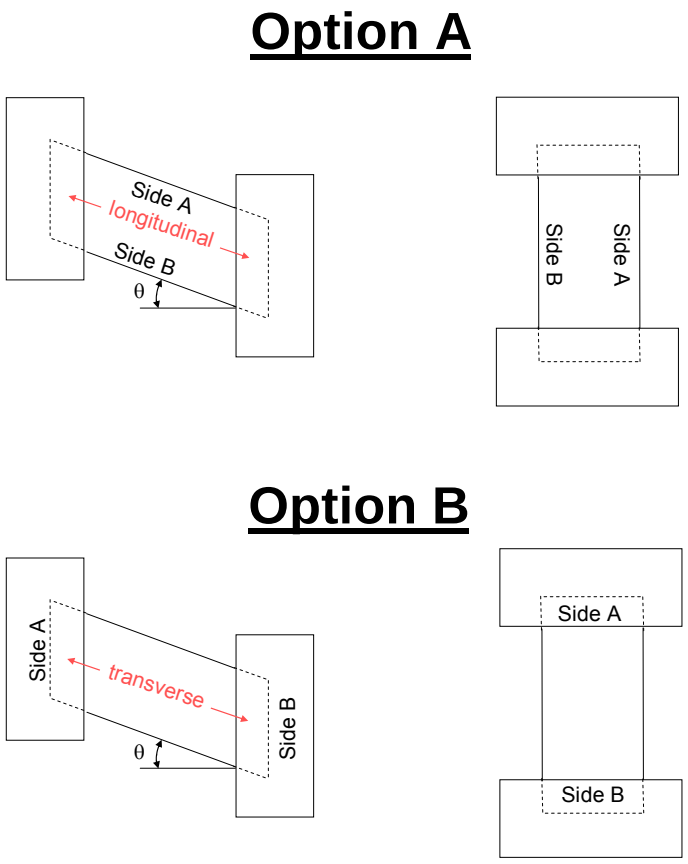

Figure 3.16: Schematic illustrating how clamping affected order of testing

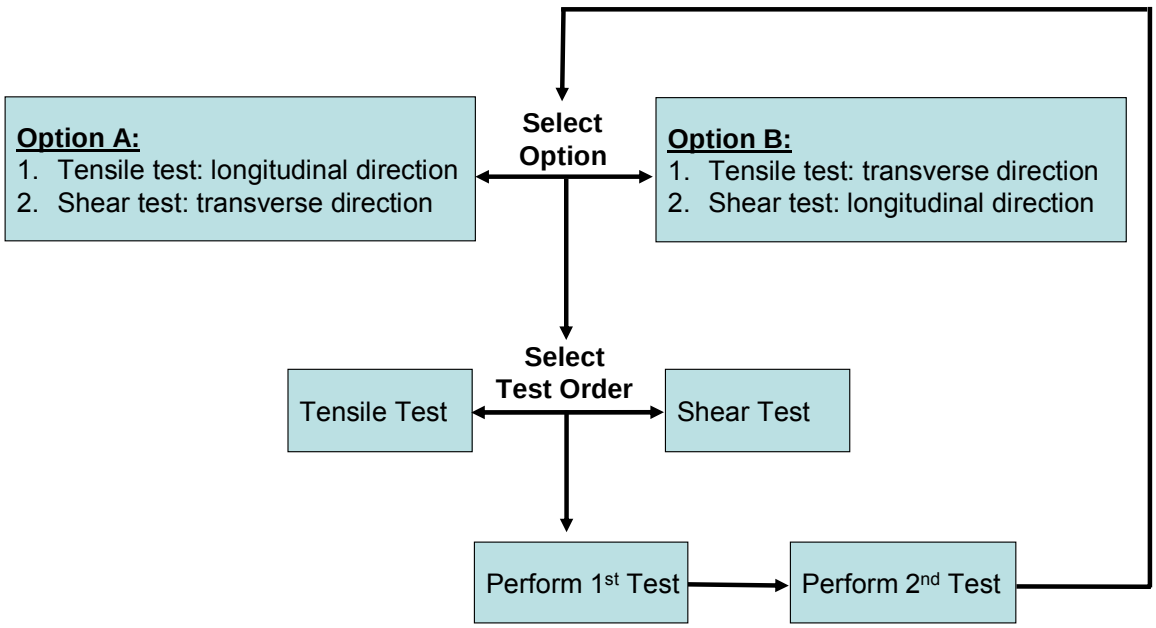

Figure 3.17: Flow chart illustrating order mechanical tests were performed

For tests in tension, a 0.5 N preload was first applied. With this preload applied, the location of the strain markers was recorded using the camera system which represented the reference strain configuration for that experiment. The dimensions of the tissue sample (length between clamps, width, and thickness near both clamps and in the midsubstance) were then measured using digital calipers. The tissue samples were then preconditioned by applying a cyclic elongation from 0-1.5 mm at 10 mm/min for a total of 10 cycles. Preliminary experiments indicated that this would load the tissue samples just beyond the linear region of the load-elongation curve. The preload was then re-established and a 3 mm displacement was applied at 10 mm/min while the location of the strain markers was recorded with the camera system. The 3 mm displacement ensured that the tissue sample would be loaded into the linear region of the load-elongation curve without causing damage. (Figure 3.18)

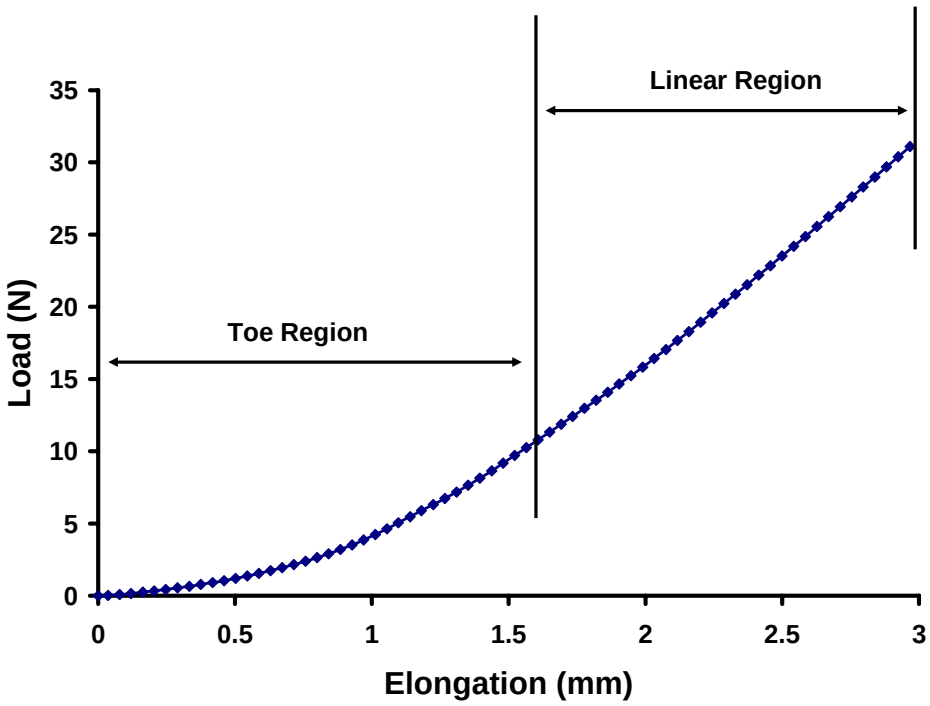

Figure 3.18: Load-elongation curve for Axillary Pouch when 3 mm displacement applied in tension

For tests in shear, a 0.03 N preload as applied in the direction perpendicular to the axis of motion of the materials testing device and a 0.1 N preload was applied parallel to the axis of motion of the materials testing device. With these preloads applied, the location of the strain markers was recorded using the camera system which represented the reference strain configuration for that experiment. The dimensions of the tissue sample (length between clamps, width, and thickness near both clamps and in the midsubstance) were then measured using digital calipers. The tissue samples were then preconditioned by applying a cyclic elongation from 0-2 mm at 10 mm/min for a total of 10 cycles. Preliminary experiments indicated that this would load the tissue samples just beyond the linear region of the load-elongation curve. The preload was then re-established and a displacement was applied at 10 mm/min such that the shear strain

of the clamp-tissue sample-clamp construct was 0.38°. The tangent of 0.38° is 0.4; therefore, the displacement was calculated from $0.4*L_o$ where L_o was the length between the clamps. This displacement ensured that the tissue sample would be loaded into the linear region of the load-elongation curve without causing damage. Again, throughout the test, the location of the strain markers was recorded with the camera system.

For the anterior and posterior bands of the inferior glenohumeral ligament and the anterosuperior capsuloligamentous regions, the tissue samples were loaded in tension in the longitudinal direction. The small size of the tissue samples did not allow for testing in the transverse direction. Therefore, only a tensile load was applied to these capsuloligamentous regions while both shear and tensile loads were applied to the axillary pouch and posterior capsuloligamentous regions.

A preload (anterosuperior: 0.3 N; anterior and posterior bands of the inferior glenohumeral ligament: 0.6 N) was first applied and the location of the strain markers was recorded using the camera system which represented the reference strain configuration for that experiment. The dimensions of the tissue sample (length between clamps, width, and thickness near both clamps and in the midsubstance) were then measured using digital calipers. The tissue samples were then preconditioned by applying a cyclic elongation from 0-1 mm at 10 mm/min for a total of 10 cycles. Preliminary experiments indicated that this would load the tissue samples just beyond the linear region of the load-elongation curve. The preload was then re-established and a 1.5 mm displacement was applied at 10 mm/min while the location of the strain markers was recorded with the camera system. The 1.5 mm displacement ensured that the tissue sample would be loaded into the linear region of the load-elongation curve without causing damage.

Between each test, the tissue sample was allowed 30 minutes to fully recover. Again, this value was chosen based on preliminary experiments performed by Mr. Rainis that demonstrated that load-elongation curves obtained from applying the same loading condition to a tissue sample with a 30 minute recovery period were nearly identical. ($R^2 > 0.99$) Additionally, for all tissue samples and loading conditions, the loading and unloading portions of the load-elongation curves were consistent after 10 cycles of preconditioning.

3.5.2.4 Finite Element Simulation

Once the mechanical testing experiments were completed, they were simulated using finite element analyses. [72] The size of the tissue sample was simulated using the measurements taken during the experiment and the effect of clamping was simulated by assuming that clamping resulted in a 20% compression of the tissue under the clamps. One of the "clamped" ends was fixed while the other moved as prescribed by the displacement of the materials testing device crosshead. The constitutive model utilized to describe the tissue samples response to loading was isotropic hypoelastic. The load-elongation curve obtained from the finite element simulation was then compared to that of the experiment using a nonlinear optimization program that minimized the sum of the square difference between the two load-elongation curves. The coefficients of the constitutive model were then iteratively adjusted until the load-elongation matched.

In this way, for the axillary pouch and posterior capsuloligamentous regions, four loading conditions were performed and could be simulated for each tissue sample. In theory, the coefficients of the constitutive model obtained from the shear test should be the same as that for the tensile test in the same direction (i.e. transverse or longitudinal). Thus, the accuracy of the

coefficients obtained from the finite element simulation could be assessed by using one of the two tests (shear or tensile) to determine the coefficients and then predict the strain distribution for the remaining experiment using those coefficients. The predicted experiment could then be compared directly to the experimental results.

Additionally, for the axillary pouch and posterior capsuloligamentous regions, the accuracy of using an isotropic hypoelastic constitutive model could also be assessed. Since the tissue samples were shear and tensile tested in both the transverse and longitudinal directions, the coefficients obtained for the two perpendicular directions could be compared. Moreover, the coefficients obtained for the longitudinal direction could be used to predict the results of the experiments performed in the transverse direction and vice versa.

3.5.3 Suggested Methodology: Constitutive Model Coefficients

For the axillary pouch and posterior capsuloligamentous regions, tissue samples should be prepared as previously described (Section 3.5.2.1) and then the testing sequence determined. (Figure 3.17)

For the tensile test in the longitudinal direction (Option A), the protocol detailed in Section 3.5.2.3 should be followed. The tissue sample should then be returned to the displacement level corresponding to the preload and a 30 minute recovery period should be allowed. At this point, the load-elongation curve should be evaluated to verify that the tissue sample was loaded into the linear region of the curve. If the load-elongation curve demonstrates that the tissue sample was primarily only loaded within the toe region, the tissue sample should be returned to the displacement level corresponding to the preload and a 30 minute recovery period should be allowed. The protocol should then be repeated; however, the applied

displacement should be increased from 3 mm to 4 mm. Based on the preliminary work by Mr. Rainis, a displacement level of more than 4 mm is not expected. Thus, if more than 4 mm is necessary, one should consider that the tissue sample may be slipping within the clamp set-up.

Following the recovery period, then next loading condition should be applied. For shear loading in the transverse direction the protocol detailed in Section 3.5.2.3 should again be followed. Following the applied shear, the tissue sample should be returned to the displacement level corresponding to the preload and a 30 minute recovery period should be allowed. As with the tensile test, if the load-elongation curve demonstrates that the tissue sample was primarily only loaded within the toe region, the tissue sample should be returned to the displacement level corresponding to the preload and a 30 minute recovery period should be allowed. The protocol should then be repeated; however, the applied displacement should be increased by 1 mm. Again, based on the preliminary work by Mr. Rainis, a displacement level increased by more than 1 mm is not expected. Thus, if this is necessary, one should consider that the tissue sample may be slipping within the clamp set-up.

To accommodate Option B, the tissue sample should be removed from the clamps and the previously clamped tissue should be removed using a scalpel. With the remaining tissue sample, the above protocol should then be followed to test the transverse direction in tension and the longitudinal direction in shear.

For the anterior and posterior bands of the inferior glenohumeral ligament and the anterosuperior capsuloligamentous regions, the tissue samples should be prepared as described in Section 3.5.2.1. As with the axillary pouch and posterior regions of the capsule, if the load-elongation curve demonstrates that the tissue sample was primarily only loaded within the toe region, the tissue sample should be returned to the displacement level corresponding to the

preload and a 30 minute recovery period should be allowed. The protocol should then be repeated; however, the applied displacement should be increased by 0.5 mm. It may be necessary to increase the displacement to 2.5 mm; however, more than 2.5 mm should not be necessary unless if the tissue sample is not slipping within the clamps.

Regarding the finite element simulations, coefficients to an isotropic hypoelastic constitutive model (tangent modulus and Poisson's ratio) should be determined for each loading condition applied to the tissue samples. For the axillary pouch and posterior region, four sets of coefficients will be determined (one set per loading condition). Thus, for the composite finite element model, the coefficients should be input as an average over the four loading conditions. For the anterior and posterior bands of the inferior glenohumeral ligament and the anterosuperior region, only one set of coefficients will be determined since only one loading condition was applied. Therefore, these coefficients should be utilized by the finite element models (composite and discrete).

4.0 EXPERIMENTALLY MEASURED STRAINS

4.1 PREVIOUS LITERATURE

In addition to developing a methodology to determine the reference strain configuration for the anterior band of the inferior glenohumeral ligament and the anterior portion of the axillary pouch, Malicky and coworkers [36, 37, 66] also investigated the strain distribution. Once the reference strain configuration was established an anterior translation of 0, 4, 7, 10, 12, 16, and 18 mm (strained configurations) was applied to the humerus of the eight cadaveric shoulder specimens which were oriented at 60° of glenohumeral abduction, 15° of horizontal abduction and externally rotated. During the application on the anterior load, motion of the humerus was allowed in 2-degrees-of-freedom (medial/lateral and anterior/posterior). As was done with the reference strain configuration, the 3D location of the strain markers was determined by taking two stereophotogrammetric images and digitizing the images using an external digitizer.

To determine the strain distribution, the 3D locations of each strain marker in the reference stain configuration and in each of the strained configurations were input into the finite element solver ABAQUS. The location of the strain markers were used to denote coordinates of nodes in membrane elements. Since a 6 x 10 grid of strain markers was utilized experimentally, a total of 45 elements were constructed from the coordinates of these strain markers. A small thickness was prescribed and an arbitrary constitutive model and mechanical properties were utilized as these parameters would have no effect on the strain calculations. The magnitude and

direction of the maximum principal strain in each element was then calculated. Using this methodology, the authors reported an average peak maximum principal strain of 31±16% and 28±14% near the glenoid and humerus, respectively with an 18 mm anterior translation applied.

4.2 PRELIMINARIES

In this current work, strain predictions in the anterior band of the inferior glenohumeral ligament were to be compared to experimentally measured strains in these same capsuloligamentous regions. Therefore, it was important to establish a methodology to not only experimentally measure the location of strain markers in the reference strain configuration (Section 3.3) but also to establish a methodology to experimentally measure the location of the strain markers while the joint is in a clinically relevant joint position that simulated a clinical exam. (strained configuration)

A similar protocol to that published previously [36, 37, 66] was performed to determine the location of the strain markers while the joint was placed in several clinically relevant joint positions via the robotic/universal force-moment sensor testing system. The joint positions tested were those achieved when a 25 N anterior load was applied at 60° of glenohumeral abduction, neutral horizontal abduction, and 0°, 30°, and 60° of external rotation. All three joint positions were investigated to ensure that the joint position associated with 60° of external rotation was still a reasonable joint position to evaluate.

The repeatability of this methodology for determining the strained configurations (0°, 30°, 60° of external rotation with an applied anterior load) was determined. Additionally, since determining the 3D location of the strain markers requires an observer to manually locate the

centroid of each strain marker, the intra- and inter-observer repeatability of this process was determined. Lastly, the effect of the repeatability of both the reference strain configuration and the strained configurations on the calculated strain magnitude was assessed.

4.2.1 Methodology: Repeatability of Strained Configuration

The same specimen utilized to establish the repeatability of the reference strain configuration, (Sections 3.3.2.4-3.3.2.6) was used to establish the repeatability of the strained configuration. It was first necessary to place the joint in clinically relevant joint positions. (Section 3.2) Therefore, the specimen was mounted within a robotic/universal force-moment sensor testing system using the protocol described in Section 3.2.3.2. The camera system previously described in Section 3.3.2.1 was then utilized to measure the 3D location of the 77 strain markers in each of the clinically relevant joint positions. (0°, 30°, and 60° of external rotation with a 50 N anterior load applied) The specimen was then removed from the custom fixtures, the robotic/universal force-moment sensor testing system was returned to its initial robot joint configuration, the cameras were removed from the testing environment, and the camera tripods were arbitrarily moved in all degrees of freedom.

The above described protocol was then repeated two times making a total of three trials. For each trial, the robotic/universal force-moment testing system was recalibrated and the specimen was remounted within this testing system. Additionally, the configuration of the camera system was established and calibrated such that all strain markers were visible by at least two cameras at all times.

Thus, the 3D location of each strain marker was obtained three times for each clinically relevant joint position. For each strain marker, a sphere was fit to the three locations measured. The centroid of the sphere was calculated from the three strain marker locations and the radius was defined to be the largest distance between the centroid and the strain marker locations which was a measure of the variability.

4.2.2 Results: Repeatability of Strained Configuration

The average variability in the strain marker locations of the strained configuration was 0.94 mm and 0.98 mm at 0° and 60° of external rotation, respectively. The maximum variability observed for any strain marker was 1.85 mm and 1.76 mm, respectively.

4.2.3 Implications: Repeatability of Strained Configuration

These data indicate that the methodology described in this work to determine the strained configuration was more repeatable than that of the reference strain configuration (2.54 mm). These differences are most likely due to the variability in the inflation process, which is only necessary for the reference strain configuration. The effect of the repeatability of the reference strain configuration and the strained configurations on the experimentally measured strains will be evaluated in a later section of this work.

4.2.4 Methodology: Intra- and Inter-observer Repeatability

One of the strained configurations obtained in Section 4.2.1 was randomly selected (60° external rotation with a 50 N anterior load). Using the camera system, the intra-observer repeatability

was assessed by having one observer manually determine the centroid of all 77 markers on three separate occasions. For the inter-observer repeatability, three different observers independently located the centroid of all 77 markers using the camera system. Thus, for both the intra- and inter-observer repeatability, three trials of data existed.

For each strain marker, a sphere was fit to the three locations measured. The centroid of the sphere was calculated from the three strain marker locations and the radius was defined to be the largest distance between the centroid and the strain marker locations which was a measure of the variability.

4.2.5 Results: Intra- and Inter-observer Repeatability

For the intra-observer data, the average variability in the location of the strain markers was 0.09 mm while the inter-observer data was only slightly less variable (0.12 mm). The maximum variability in the location of the strain markers was 0.18 mm and 0.34 mm for the intra- and inter-observer variability, respectively.

4.2.6 Implications: Intra- and Inter-observer Repeatability

These data indicate that both the intra- and inter-observer variability of the 3D location of the strain markers was substantially better than that observed for the reference strain configuration and the strained configurations. Thus, these data should have a minimal impact on the calculated strains. Therefore, any efforts to improve the variability should focus first on the reference strain configuration and second on the strained configuration.

4.2.7 Methodology: Repeatability of Entire Strain Protocol

In order to determine the repeatability of the entire protocol that has been described for experimentally measuring strains in the anterior band of the inferior glenohumeral ligament and axillary pouch, data from Sections 3.3.2.4 and 4.2.1 was utilized. In these previous sections, the reference strain configuration and the strained configuration were determined three separate times using the same specimen. Therefore, for the same specimen three trials existed for both the reference strain configuration and for the strained configuration. Each of the three reference strain configuration trials were randomly matched with a strained configuration and the maximum principal strain in each element was calculated using a finite element solver (ABAQUS version 6.4). Recall that not all 77 strain markers were visible for the reference strain configuration. Therefore, those strain markers that were not visible for the reference strain configuration were also omitted from this analysis. The location of the strain markers were used to denote coordinates of nodes in membrane elements, small (0.02 mm) thickness was prescribed, and an arbitrary constitutive model and mechanical properties were assigned.

The magnitude of the maximum principal strain was calculated for the centroid of each element. Since three trials were performed, a total of three strain magnitudes were obtained for each element. The standard deviation of the maximum principal strain was determined for each element across the three trials. To determine the overall variability for the magnitude of the maximum principal strain for the entire methodology, the average standard deviation across all elements was calculated.

The directions of the maximum principal strains were plotted at the integration points yielding four direction vectors per element. Nine elements were randomly selected from the 0° and 60° of external rotation data. Each element was superimposed on itself for the three trials.

One integration point was arbitrarily selected, and the corresponding direction vector was analyzed for each of the elements. Then, for each element, a protractor was used to determine the angle between the direction vectors of the three trials. Thus, for each element evaluated, the difference between the three trial was determined (trial 1 versus trial 2, trial 1 versus trial 3, and trial 2 versus trial 3). The overall variability for the direction of the maximum principal strain for the entire methodology was calculated by determining the average difference between trials across all elements.

4.2.8 Results: Repeatability of Entire Strain Protocol

The strain distribution followed the same trends for all three trials with the highest strains occurring in the anterior aspect near the glenoid. (Figure 4.1) The average strain magnitude at 0° and 60° of external rotation ranged 9.2-12.5% and 9.9-13.7%, respectively. (Table 4.1) The maximum strain occurred in the third trial for both 0° and 60° of external rotation and was 31.2% and 33.6%, respectively. The repeatability of the entire methodology at 0° of external rotation was ±3.0%. However, at 60° of external rotation a minimal increase in this value was observed with a repeatability of ±3.5%. For the maximum principal strain direction, the average difference between trials across all elements was 7±8° and 5±5° for 0° and 60° of external rotation respectively.

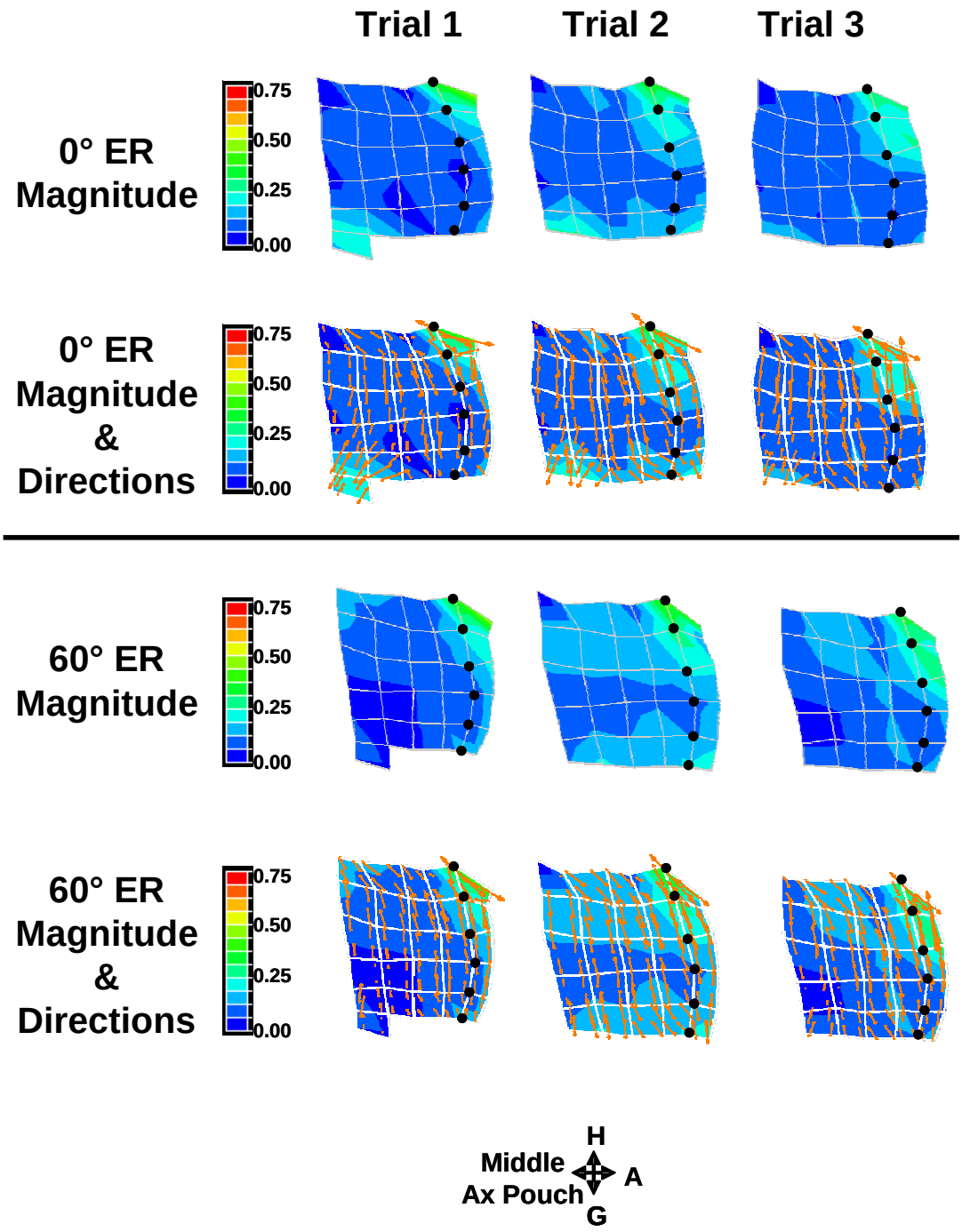

Figure 4.1: Fringe plot of maximum principal strain magnitude and direction for 3 trials. Black circles denote location of anterior band of inferior glenohumeral ligament. Key shows orientation with respect to humerus (H), glenoid (G), middle axillary pouch, and anterior (A)

Table 4.1: Average and peak maximum principal strains for 3 trials of the same specimen (mean±SD, trial 1: n=26 elements, trials 2 and 3: n=25 elements)

		Trial 1	Trial 2	Trial 3
0° ER	Average (%)	9.2±5.9	12.5 ±5.4	10.6 ±6.0
	Peak (%)	23.7	23.3	31.2
60° ER	Average (%)	9.9 ±5.4	13.7 ±5.8	11.6 ±6.5
	Peak (%)	22.0	25.6	33.7

4.2.9 Implications: Repeatability of Entire Strain Protocol

Previously, Malicky and coworkers [36] reported that the repeatability of their methodology to determine the reference strain configuration affected the experimentally measured strains by ±2.8%. In the current work, the repeatability of several additional factors were included: 1) camera calibration and configuration for reference strain configuration; 2) camera calibration and configuration for strained configurations; 3) inflation process; 4) and use of robotic/universal force-moment sensor testing system to determine the joint kinematics. Despite the increased number of factors included in the current work, the repeatability of experimentally measuring the maximum principal strain in the anterior and posterior bands of the inferior glenohumeral ligament and the axillary pouch was ±3.5%. This repeatability was reasonable and acceptable given since it is an order of magnitude less than the values of maximum principal strains to be investigated in this work (>30%). With an applied anterior translation of 18 mm at 60° of glenohumeral abduction 15° of horizontal abduction, and an unknown amount of external

rotation, the peak maximum principal strain has been reported to be 31±16% and 28±14% near the glenoid and humerus, respectively. Additionally, based on tangent modulus obtained from the stress-strain curves presented in an earlier section of this work (Section 2.3.1.3), 5.4±2.9 MPa to 14.8±13.1 MPa, an increase of 3.5% strain would result in only a minimal increase in stress. Therefore, the methodology outlined for experimentally measuring the stain distribution in the anterior band of the inferior glenohumeral ligament and the axillary pouch was acceptable for this current work.

Little is known regarding the direction of the maximum principal strains. However, it was important to verify that the methodology detailed in this current work did not produce drastically different direction vectors. Otherwise, this would be an indication that the methodology was not in fact repeatable. On average, the difference in the direction of the maximum principal strains between trials was less than 10° at both 0° and 60° of external rotation. Previously, the direction of the maximum principal strain in the anterior band of the inferior glenohumeral ligament was found to be oriented at 38±36° with respect to the longitudinal axis of this capsuloligamentous region. [36] Thus, the repeatability of the direction of the maximum principal strain reported in the current work is an order of magnitude less than the variability of measurements that may be made. Therefore, it appears that the methodology outlined in this current work is repeatable for both the magnitude and direction of the maximum principal strains and can therefore be used to experimentally measure strains for comparison to those predicted by finite element models.

4.2.10 Methodology: Experimentally Measure Strain

In order to confirm that the methodology outlined above to experimentally measure strains produced reasonable results, six specimens were tested and compared to literature. These specimens were prepared as described in Section 3.3.2.4. The reference strain configuration and strained configurations were then determined as previously described in Sections 3.3.2.4 and 4.2.1, respectively. Strained configurations were determined for 0°, 30°, and 60° of external rotation with a 25 N anterior load applied. A one-factor repeated measures ANOVA ($p<0.05$) was used to detect significant differences in the magnitude of the maximum principal strain between external rotation values. Since the same elements were utilized for each strained configuration, repeated measures were possible.

4.2.11 Results: Experimentally Measured Strains

The magnitude of the maximum principal strain distribution for each of the six specimens is shown in Figures 4.2 and 4.3. Figure 4.2 is a histogram showing the number of elements within a range of strain magnitudes specified by the x-axis. A normal distribution was not observed for all six specimens. For specimen six, two strain markers were found to no longer be adhered to the axillary pouch during testing. Therefore, for this specimen only 52 elements were evaluated while 60 elements were evaluated for the remaining five specimens. The average maximum principal strain for each specimen is shown in Table 4.2 and ranged from a minimum of 1.4±4.8% to 18.9±14.3%, 7.0±6.7% to 22.4±16.6%, and 8.5±7.9% to 23.0±17.7%, respectively. The average peak maximum principal strain across all specimens increased with external rotation (37.7±12.0%, 48.3±12.4%, and 55.5±19.0%, respectively). The maximum principal strain

measured at 30° of external rotation was significantly larger than that at 0° of external rotation for five of the six specimens. ($p<0.05$) The same was also true for 60° compared to 0° of external rotation. Moreover, the maximum principal strain was found to be significantly larger at 60° of external rotation for three of the six specimens when compared to 30° of external rotation. ($p<0.05$)

Qualitative evaluation of the fringe plots clearly shows that the overall pattern of strain distribution varied greatly among the specimens tested. However, some similarities existed. With increased external rotation, a larger quantity of the tissue was recruited to transmit the loads. This was true on the glenoid and humeral sides. Additionally, the magnitude of strain was generally larger near the glenoid insertion.

The directions of the maximum principal strains are shown in Figure 4.4. At 0° of external rotation, the direction of the maximum principal strains near the glenoid was relatively aligned with the longitudinal axis of the anterior band of the inferior glenohumeral ligament; however, closer to the humerus the direction was at a more oblique angle. At 30° and 60° of external rotation, near both the glenoid and humerus, the direction was clearly aligned with the longitudinal axis of the anterior band of the inferior glenohumeral ligament.

Table 4.2: Average maximum principal strain at 0°, 30°, and 60° of external rotation (ER). *Significantly different from 0° of external rotation. †Significantly different from 30° of external rotation (mean±SD, trials 1-5: n=60 elements, trial 6: n=52 elements)

Maximum Principal Strain (%)			
	0° ER	30° ER	60° ER
Specimen 1	4.3±5.5	7.0±6.7*	8.5±7.9*†
Specimen 2	9.9±12.0	10.9±13.0*	12.0±14.5*†
Specimen 3	14.1±2.3	18.2±15.3*	19.6±16.2*†
Specimen 4	1.4±4.8	13.2±15.3*	15.9±16.9*
Specimen 5	3.7±8.2	8.7±12.3*	8.7±13.0*
Specimen 6	18.9±14.3	22.4±16.6	23.0±17.7

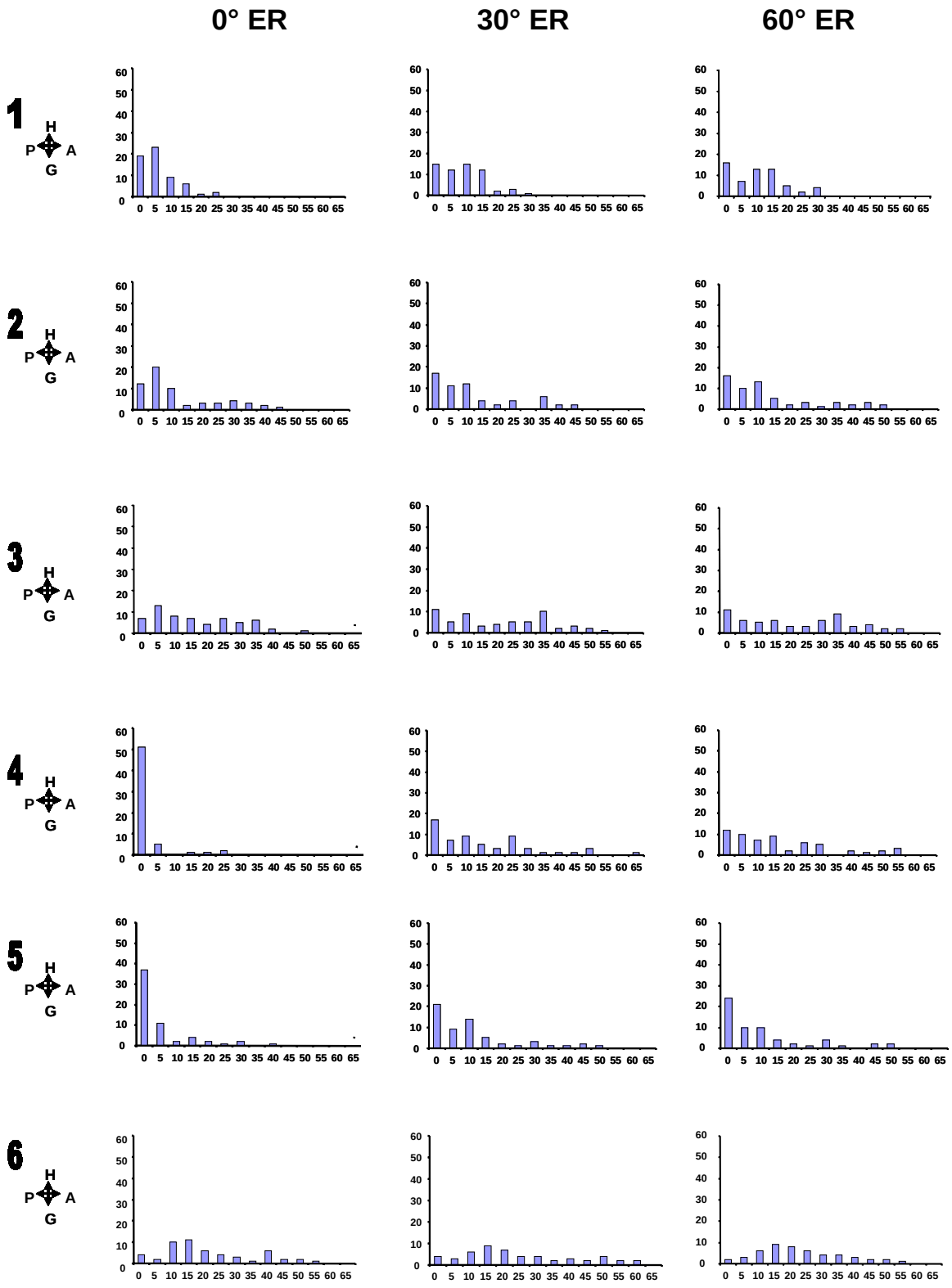

Figure 4.2 Histograms showing number of elements whose maximum principal strains (y-axis-%) were within the range specified by the bin size described on the x-axis for 0°, 30°, and 60° of external rotation

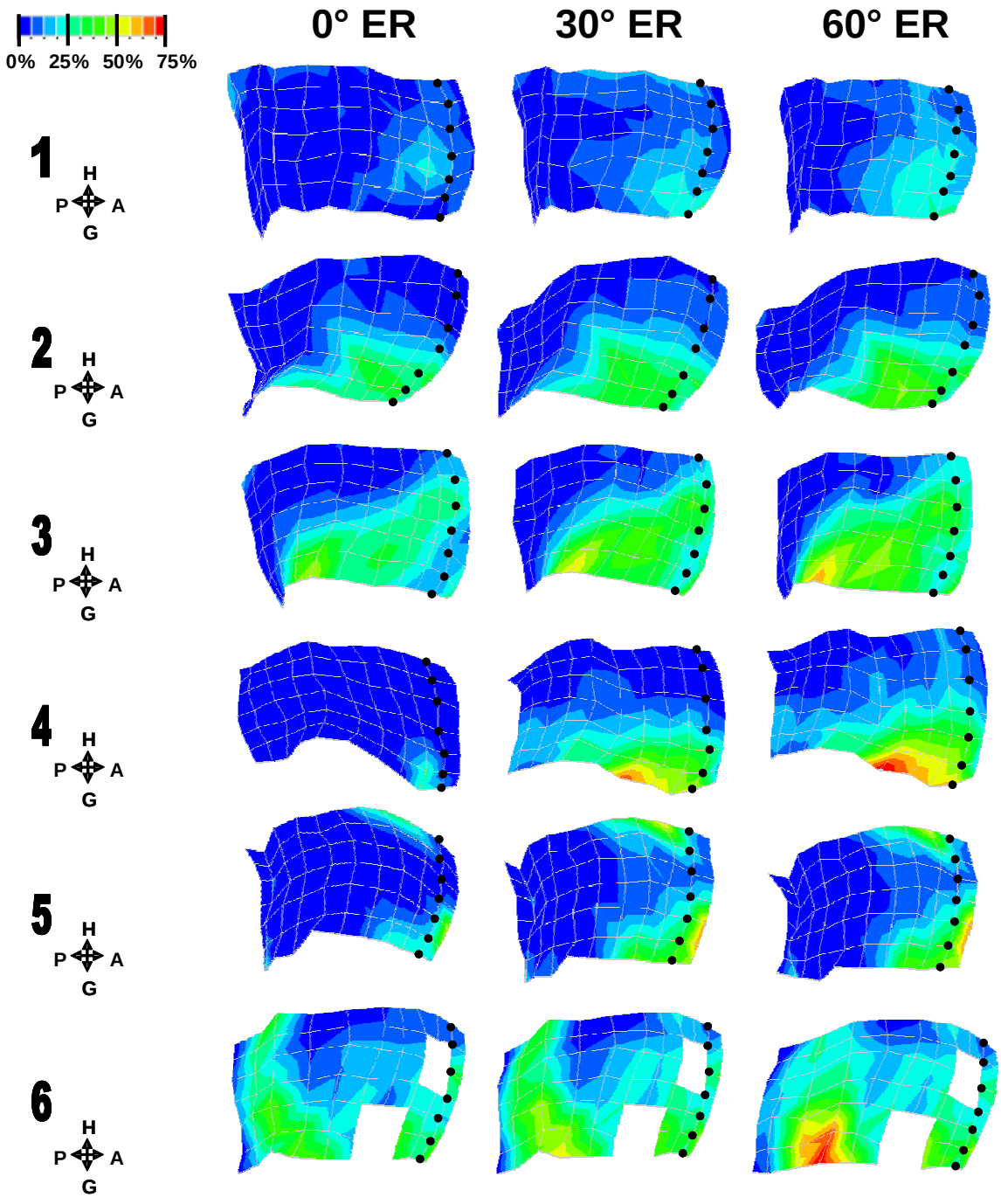

Figure 4.3: Fringe plots for 6 specimens showing maximum principal strain magnitude. Black circles denote location of anterior band of inferior glenohumeral ligament and key indicates the orientation with respect to humerus (H), glenoid (G), anterior (A), and posterior (P)

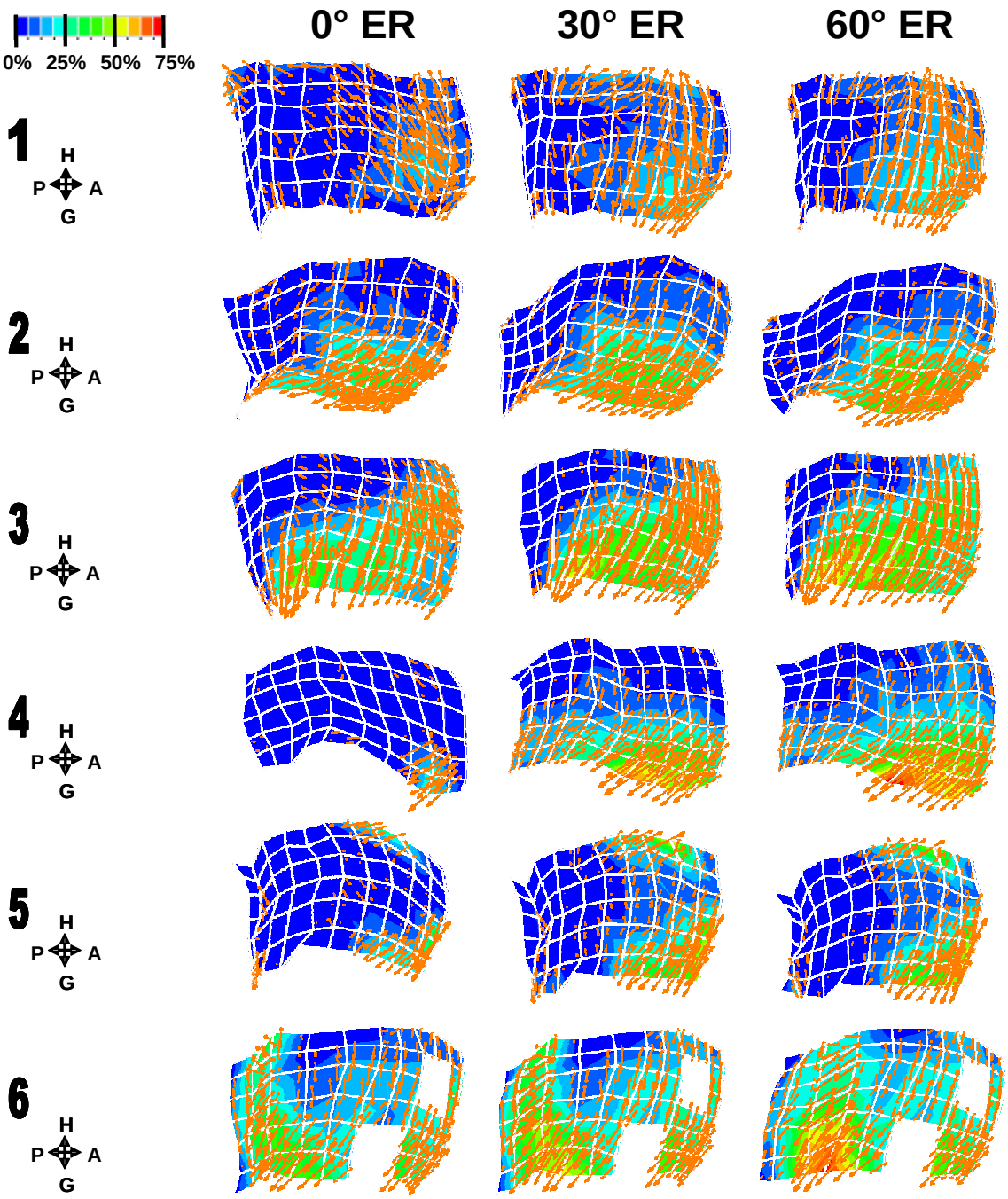

Figure 4.4: Fringe plots for 6 specimens showing maximum principal strain magnitude (color) and direction (arrows). Key indicates orientation with respect to humerus (H), glenoid (G), anterior (A), and posterior (P)

4.2.12 Implications: Experimentally Measured Strains

These data compare well with a previous study [36] that reported the average maximum principal strain in the anterior band of the inferior glenohumeral ligament and anterior portion of the axillary pouch to be 14±4% and 15±6% near the glenoid and humerus, respectively, when an 18 mm translation was applied to the humerus at 60° of glenohumeral abduction, 15° of horizontal abduction, and an unknown external rotation. Additionally, they reported peak maximum principal strains of 31±16% and 28±14%, respectively.

The good agreement of these data with that of previous studies suggests that the methodology proposed in the current work to experimentally measure the strain distribution in the anterior band of the inferior glenohumeral ligament and axillary pouch may be used for validation of the finite element models in the current work. Additionally, the extreme variability in the pattern of the strain distribution demonstrates the need for subject-specific inputs and validation of finite element models. Furthermore, these data also demonstrate the need for multiple subject-specific finite element models in the future allowing for a more accurate representation of the population.

These obtained for the direction of the maximum principal strains are contradictory to a previous study [36] that constrained more degrees than the current study. Thus, while the previous study did not report an organized pattern for the direction of the maximum principal strains, the current work allowed for more realistic joint motions. The data obtained in the current study indicates that when an anterior load is applied to the joint loads are transmitted along the longitudinal axis of the anterior band of the inferior glenohumeral ligament with and without external rotation. Surgical techniques for anterior dislocations shift and plicate the anterior band of the inferior glenohumeral ligament and the anterior half of the axillary pouch. Therefore, these techniques drastically disrupt the ability of these capsuloligamentous regions to transfer loads which may contribute to the number of recurrent dislocations.

The current work requires the anterior band of the inferior glenohumeral ligament and the axillary pouch to be functioning in the joint position evaluated. Significant differences were detected when comparing the magnitude of the maximum principal strain at 0°, 30°, and 60° of external rotation with 60° yielding the largest strains. However, a normal distribution was not observed with minimal strain in places. Thus, it may be more appropriate to divide the axillary pouch into several smaller portions for evaluation. Therefore, based on the magnitude and direction of the maximum principal strains, the joint position corresponding to 60° of external rotation with a 25 N anterior load applied to the humerus was most appropriate.

4.3 SUGGESTED METHODOLOGY: EXPERIMENTAL STRAINS

Using the robotic/universal force-moment sensor testing system the joint should be placed in a clinically relevant joint position that simulates a clinical exam. (Section 3.2.1) The camera

system should then be calibrated and used to measure the 3D location of the 77 strain markers in the clinically relevant joint position. (60° of external rotation with a 25 N anterior load applied)

The magnitude and direction of the maximum principal strain should then be calculated using the finite element solver ABAQUS. The location of the 77 strain markers in the reference strain configuration and the strained configuration should be input and membrane elements assigned. A minimal thickness (0.02 mm) should be assigned and an arbitrary constitutive model and its coefficients selected. The magnitude of the maximum principal strain should then be calculated at the centroid of each element while the direction is calculated at each node.

5.0 DATA COLLECTED FOR CONSTRUCTION OF FINITE ELEMENT MODELS

5.1 SPECIMEN PREPARATION

One cadaveric shoulder specimen (male, 45 years old, left) was allowed to thaw at room temperature overnight. Radiographs were taken to verify that no osteoarthritis or bony traumas had occurred. All soft tissues were dissected away except for the glenohumeral capsule and the coracohumeral ligament and the bones were scraped clean of all soft tissue remnants. Throughout the dissection and all experimental data collection, special care was taken to ensure that the glenohumeral capsule remained hydrated with a 0.9% physiologic saline solution. An experienced orthopaedic surgeon identified the margins and insertion sites of the anterior and posterior bands of the inferior glenohumeral ligament. A 7x11 grid of black plastic strain markers (1.58 mm diameter, ~5 mm between strain markers) was adhered to the capsule using cyanoacrylate. (Figure 5.1) The first column of markers was placed just superior to the anterior band of the inferior glenohumeral ligament and the first and last stain markers in each column were approximately 1cm from the bony insertion sites. Due to the size of the axillary pouch, the 11th column of strain markers was just below the inferior margin of the posterior band. A 2x4 grid of strain markers were then affixed to the anterosuperior and posterior capsuloligamentous regions. Again, the strain markers were placed approximately 5 mm apart and were at least 1 cm from the glenoid and humeral insertion sites.

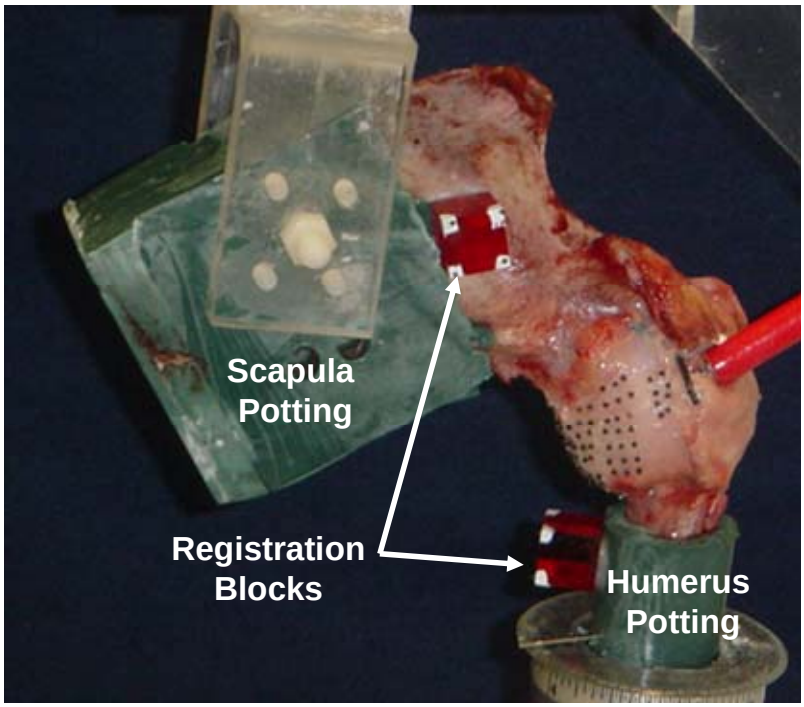

Figure 5.1: Picture showing strain markers, registration blocks, and potted humerus and scapula

Registration blocks were then affixed to the humerus and scapula using a cyanoacrylate and baking soda compound. The humeral registration block was oriented such that its edges were parallel and perpendicular to the humeral shaft. The scapular registration block was oriented such that its edges were 30° from being parallel and perpendicular to the medial margin of the scapula. This was necessary such that the edges of the registration blocks were parallel and perpendicular to the axis of the CT data since the CT would be taken at 60° of glenohumeral abduction (~60° between the axis of the humeral shaft and the medial margin of the scapula. Three black plastic markers (1.58 mm diameter) were then affixed to three of the corners of the humeral registration block which were used to co-register the locations of the strain markers for

the reference strain configuration and the strained configurations since the camera system would be set-up in different configurations with a different calibration for the two environments.

The humerus was then potted in a cylinder of epoxy putty such that the central axis of the cylinder was parallel to the humeral shaft. The scapula was potted in epoxy putty using a rectangular mold such that the medial margin of the scapula was parallel to one side while the scapular plane was parallel to the other. This allowed the humerus and scapula to fit into standard fixtures.

5.2 REFERENCE STRAIN CONFIGURATION

5.2.1 Methods

The joint was mounted within the 6-degree of freedom plastic jig at 60° of glenohumeral abduction and neutral horizontal abduction and internal/external rotation. A small amount of joint distraction was then applied. The capsuloligamentous regions were inflated to 4.8 kPa and 6.2 kPa as the humerus was rotated to 0°, ±5°, ±10°, and ±15° of internal/external rotation in a random order. At each joint position, the location of the strain markers were recorded for both pressures using the motion tracking system which had been calibrated for a camera configuration that ensured each strain marker would be visible by at least two cameras at all times.

Snapshots from the camera system were taken for each joint orientation for the 4.8 kPa and 6.2 kPa pressures. These snapshots were then overlaid on each other and joint orientations that showed a large amount of strain marker motion via visual inspection were excluded from further analysis. (Figure 5.2) With this method only three joint orientations remained (5° of internal rotation, 5° of external rotation, and 10° of external rotation). The 3D location of all 77

strain markers was then determined for these three joint orientations at 4.8 kPa and 6.2 kPa. The joint orientation corresponding to the smallest average motion of the strain markers between each pressure with no marker moving more than 1 mm, was then selected. At this joint orientation, the reference strain configuration was determined by inflating the capsule to 5.2 kPa and recording the location of the strain markers.

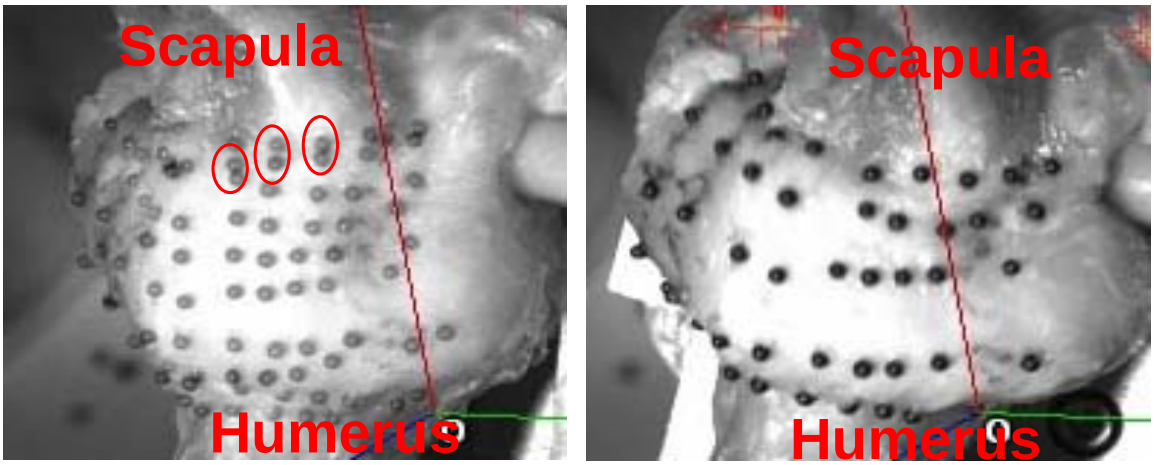

Figure 5.2: Overlaid snapshots at two different joint positions showing large (left) and non-visible (right) strain marker motion between a low and high pressure. Red ovals highlight used to highlight the same strain markers at two different pressures.

Due to the limited field of view of the 3-camera system, it was not possible to view the strain markers affixed to the anterosuperior or the posterior capsuloligamentous regions. Therefore, the plastic jig was rotated about the axis of the humerus such that the anterosuperior strain markers were within the calibrated field of view for the camera system and visible by at least 2 cameras. The capsuloligamentous regions were then inflated to 4.8 kPa and 6.2 kPa at the seven joint orientations and the location of the anterosuperior strain markers were measured for

both pressures. Then, the plastic jig was again rotated about the axis of the humerus such that the strain markers affixed to the posterior capsuloligamentous region were visible by at least 2 cameras and within the calibrated field of view of the camera system. Again, the capsuloligamentous regions were inflated to 4.8 kPa and 6.2 kPa at the seven joint orientations and the location of the posterior strain markers were measured for both pressures. For both the anterosuperior and posterior capsuloligamentous regions, the average and maximum motion of the strain markers was then determined.

5.2.2 Results

The magnitude of the strain marker motion between 4.8 kPa and 6.2 kPa for anterior band of the inferior glenohumeral ligament and axillary pouch is shown in Table 5.1. The smallest average strain marker motion was 0.17 mm and was observed for 5° and 10° of external rotation. The maximum strain marker motion was less than 1.0 mm for both joint orientations measuring 0.48 mm for both. However, the minimum strain marker motion was 0.05 mm and 0.02 mm, respectively. Therefore, 10° of external rotation was selected as the joint orientation to be used to obtain the reference strain configuration. (i.e. location of strain markers with 5.2 kPa inflation pressure applied)

Table 5.1: Magnitude of strain marker motion for anterior band of inferior glenohumeral ligament and axillary pouch between 4.8 kPa and 6.2 kPa (n=77 strain markers)

	Strain Marker Motion (mm)		
	5° Internal Rotation	5° External Rotation	10° External Rotation
Average	0.18	0.17	0.17
SD	0.16	0.08	0.09
Max	0.90	0.48	0.48

For the anterosuperior and posterior capsuloligamentous regions, the strain marker motion between 4.8 kPa and 6.2 kPa measured at 10° of external rotation is shown in Table 5.2. For both capsuloligamentous regions, the average strain marker motion was less than 0.30 mm. In fact, the average and maximum strain marker motion was less than that of the anterior band of the inferior glenohumeral ligament and axillary pouch.

Table 5.2: Magnitude of strain marker motion on anterosuperior and posterior regions of capsule between 4.8 kPa and 6.2 kPa (n=8 strain markers)

	Strain Marker Motion 10° of External Rotation (mm)	
	Anterosuperior Region	Posterior Region
Average	0.14	0.08
SD	0.07	0.03
Max	0.29	0.13

5.3 SPECIMEN GEOMETRY

5.3.1 Methods

Once the reference strain configuration was determined, rubber tubes were then affixed to the margins of the anterior and posterior band of the inferior glenohumeral ligament using cyanoacrylate such that the ends of the tubes terminated at the insertion sites. The joint was then fixed in 6-degree of freedom plastic jig at the joint orientation corresponding to the reference strain configuration. The plastic jig was laid on its side such that it fit within the scanning area of the CT scanner. (Figure 5.3) A field of view (180 mm) was selected such that the registration blocks were included in the viewing area. The nozzle was then reinserted into the rotator interval and the glenohumeral capsule was inflated to 5.2 kPa. A CT scan was then taken (100 kV, 120 mA) with a slice increment of 1 mm. The rubber tubes, registration blocks, humerus, articular cartilage of the humerus, scapula, and capsuloligamentous regions were all visible.

The geometry of the humerus, scapula, registration blocks, anterior and posterior bands of the inferior glenohumeral ligament, axillary pouch, anterosuperior, and posterior capsuloligamentous regions were manually segmented on each slice from the CT dataset. (SURFdriver version 3.5.6, Hawaii) However, several issues were encountered: 1) insertion of posterior band of the inferior glenohumeral ligament and posterior region inserted directly into the labrum which was not modeled in the current work and 2) anterosuperior and posterior regions were not visible in those CT data slices near the glenoid insertion.

Two types of insertion sites exist for the capsuloligamentous regions at the glenoid. [16] The capsuloligamentous regions can either insert into the labrum directly or an indirect insertion into the labrum and glenoid exists. It is important to note that, in the current study, experimental strains were not collected near the insertion sites of the glenoid or humerus. Thus, no strain comparisons or predictions are to be made near either insertion site. Since very little information is available for the labrum, it was excluded from the current study. Therefore, it was assumed that the capsuloligamentous regions inserted into the glenoid directly. However, the labrum of the specimen from which the experimental data was collected was large at the posterior glenoid and small at the anterior glenoid. (Figure 5.4)

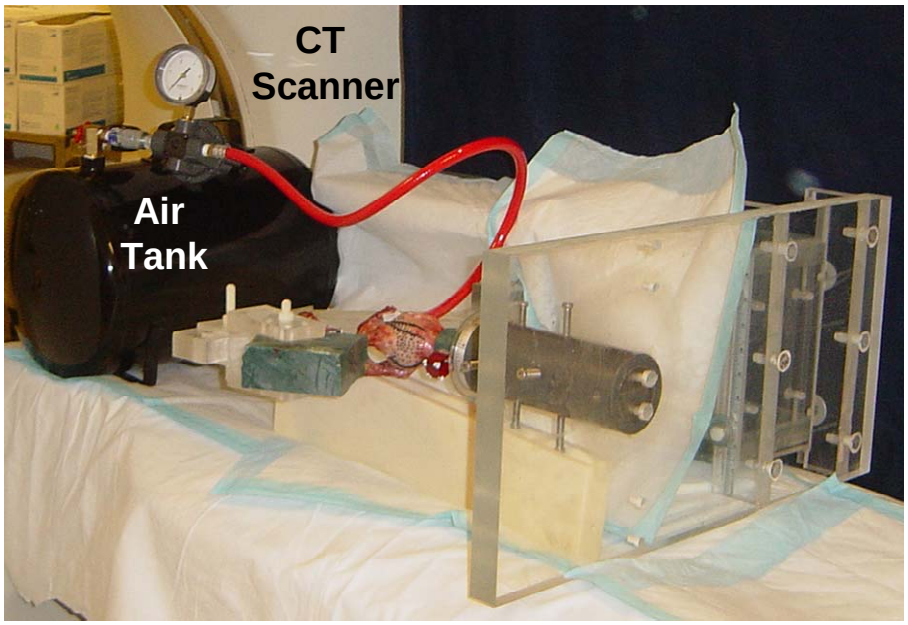

Figure 5.3: CT data acquisition of specimen geometry

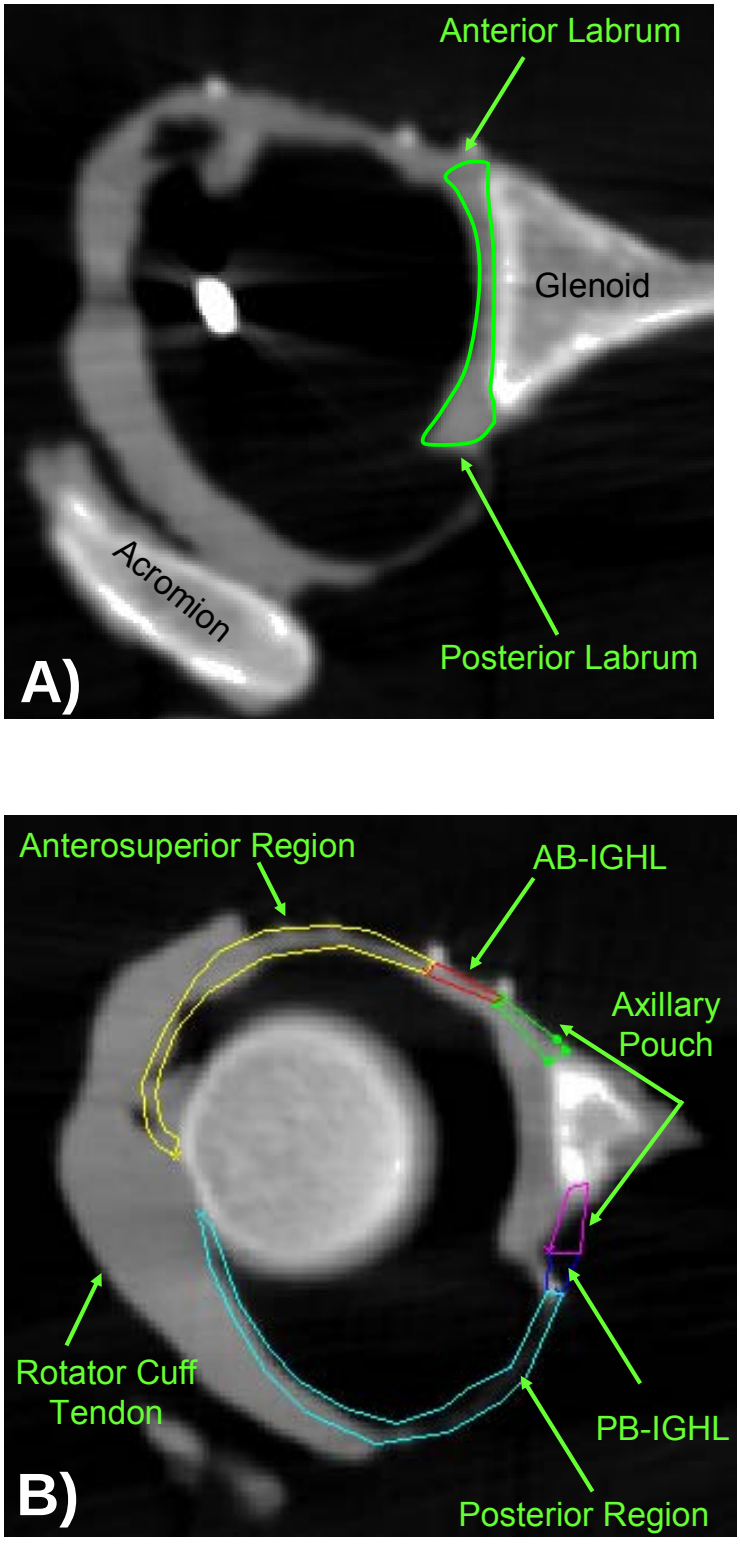

Figure 5.4: Slice from CT data set showing A) size of and B) approximated insertion to labrum

In addition to the problems encountered with the labrum, some difficulties occurred when segmenting the anterosuperior and posterior capsuloligamentous regions. When approaching the glenoid insertion site from the midsubstance of the capsuloligamentous regions, visibility of the anterosuperior and posterior capsuloligamentous regions was diminished. (Figure 5.5) Therefore, the position in space of these capsuloligamentous regions were approximated based on knowledge of the anatomy. (Figure 5.6) Changes to the CT data acquisition protocol may be necessary to improve visibility of these capsuloligamentous regions in the future.

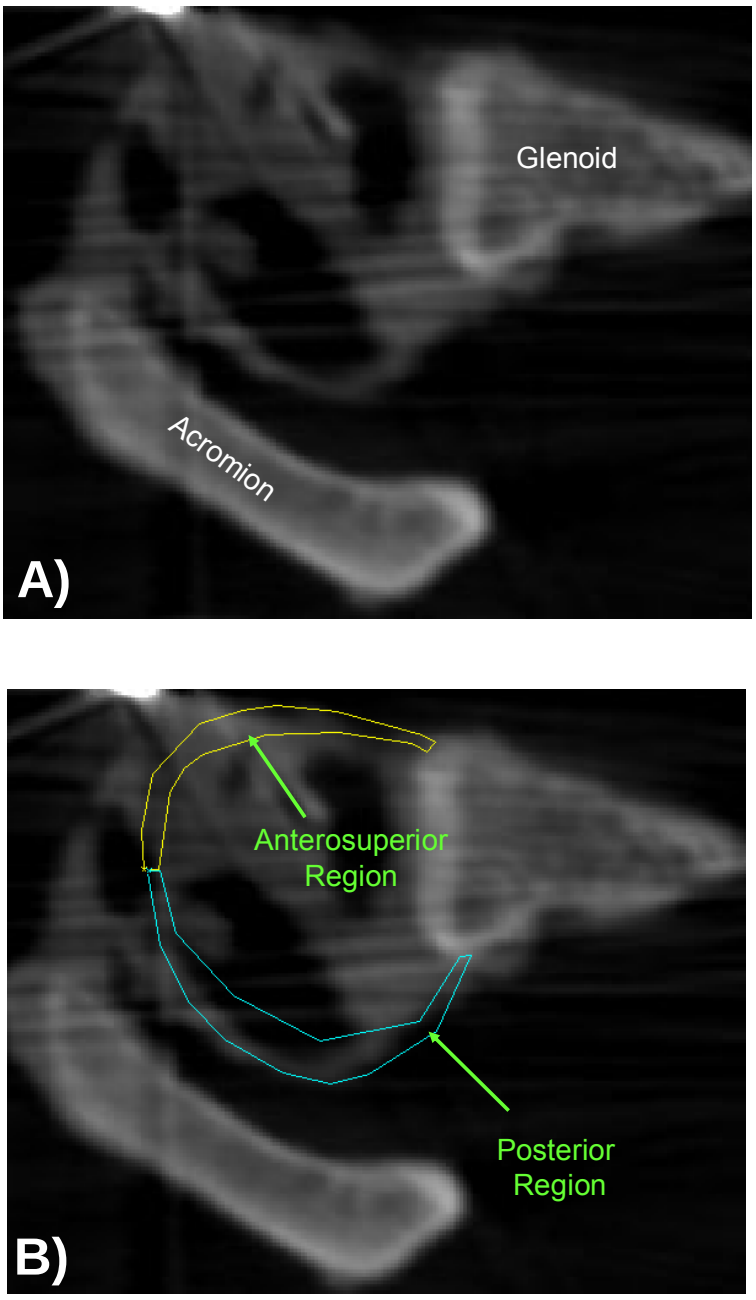

Figure 5.5: Slice from CT data set showing A) visual loss and B) approximation of capsuloligamentous regions

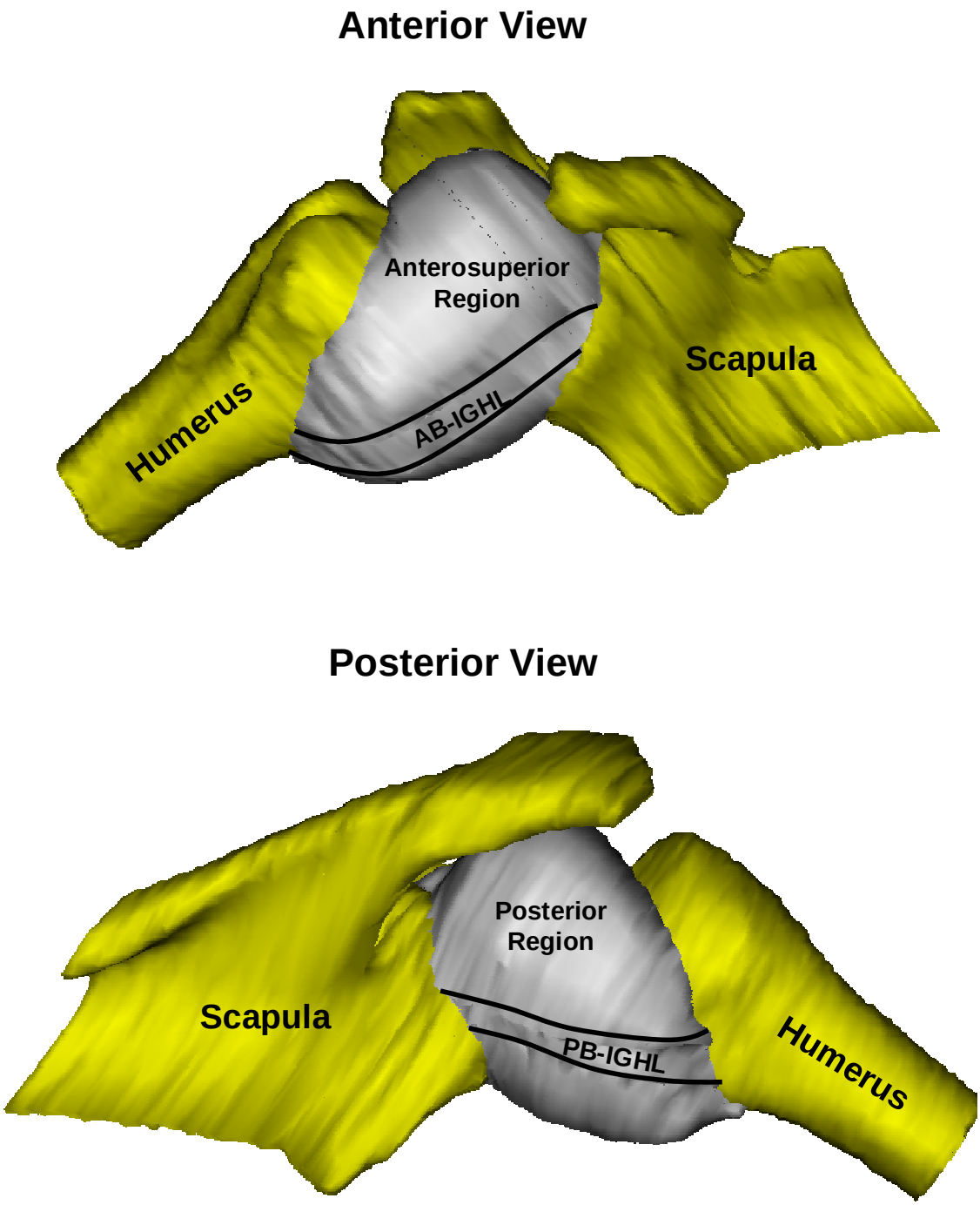

Figure 5.6: Surfaces generated for anterosuperior and posterior capsuloligamentous regions

5.4 JOINT KINEMATICS

5.4.1 Methods

The scapula and humerus were rigidly fixed to the end effector and base of the robotic/universal force-moment sensor testing, respectively, using custom fixtures such that the scapular fixture ensured that the plane of the scapula was parallel to the y-z plane of the robotic/universal force-moment sensor testing system. Moreover, the x, y, and z axes of the robotic/universal force-moment sensor testing system were parallel to the anterior/posterior, medial/lateral, and superior/inferior axes of the scapula, respectively. At this initial position, the joint was oriented at 49° of glenohumeral abduction, 0° of horizontal abduction, and 0° of external rotation. (Figure 5.7)

Figure 5.7: Joint mounted in robotic/universal force-moment sensor testing system

The coordinate system of the robotic/universal force-moment sensor testing system was then translated such that it was coincident with the anatomic coordinate system of the scapula. The relationship between the anatomic coordinate system of the scapula and the coordinate system of the robotic/universal force-moment sensor testing system was established as previously described. [14, 92, 93] The location of the anterior-most and posterior-most aspects of the humeral head was measured with respect to the origin of the coordinate system of the robotic/universal force-moment sensor testing system. The point midway between these two anatomic landmarks represented the origin of the anatomic coordinate system of the scapula and the origin of the robotic/universal force-moment sensor testing system coordinate system was translated to this point.

The path of passive glenohumeral abduction was then determined by minimizing the forces in the anterior/posterior and superior/inferior directions (~0 N) as a 22 N compressive force (medially directed) was held constant. To achieve the force targets, translation of the scapula along the three orthogonal axes was permitted. The path of passive glenohumeral abduction was established in 1° increments from the abduction angle the specimen was initially mounted (49°) at to 70° of glenohumeral abduction. The compressive force ensured that the humeral head was then centered within the glenoid cavity throughout all glenohumeral abduction angles.

The joint was then orientated at 60° of glenohumeral abduction and the path of external rotation was established by applying a 3 Nm rotation moment about the longitudinal axis of the humerus while maintaining the 22 N joint compressive force. The joint position corresponding to 60° of glenohumeral abduction and 60° of external rotation were then identified. At this joint position, a 25 N anterior load was applied, while maintaining the 22 N compressive force, and

the resulting kinematics, which simulated a clinical exam, were recorded via the robotic/universal force-moment sensor testing system. With the joint at 60° of glenohumeral abduction and 60° of external rotation with a 25 N anterior load applied, an external digitizer (Microscribe 3DX) was used to digitize the faces of the registration blocks. The transformation matrix describing the location of the humeral registration block with respect to the scapular registration block was then determined.

5.4.2 Results

The path of passive abduction was obtained from 49° to70° of glenohumeral abduction. The external rotation torque, applied at 60° of glenohumeral abduction, resulted in a maximum of 52° of external rotation. Therefore, the 25 N anterior load was applied to the humerus at 52° of external rotation. Since motion at the glenohumeral joint is commonly described as motion of the humerus with respect to the scapula, the data was processed in this manner. Thus, the anterior translation of the humerus with respect to the scapula in response to the loading conditions is shown in Figure 5.8 for 52° of external rotation. At 52° of external rotation an anterior translation of 3.9 mm was observed with a 25 N anterior load applied.

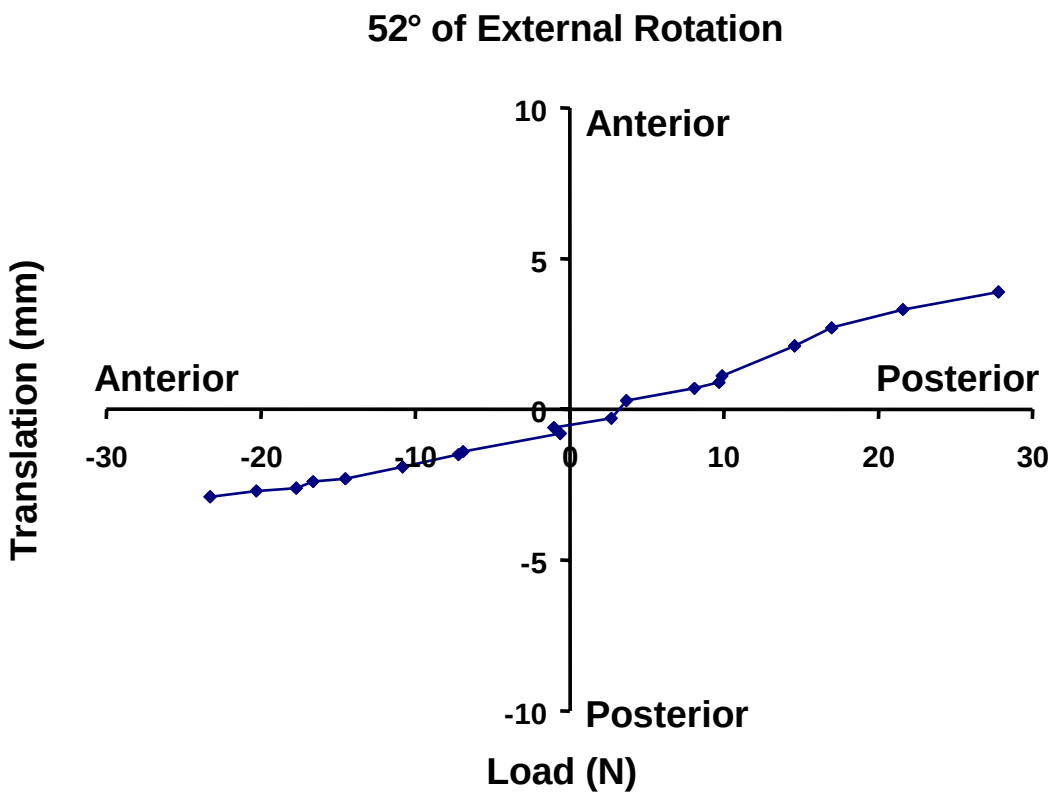

Figure 5.8: Anterior translation--humerus with respect to scapula at 52° of external rotation

A coupled motion in the superior-inferior direction was observed as a result of the applied anterior load. (Figure 5.9) When externally rotated from 0° to 52°, the humeral head was in a posterior position. Thus, when the anterior load was applied at 52° of external rotation, the humerus moved in the anterior direction from this position. Additionally, the humeral head was in an inferior position after being rotated from 0° to 52° of external rotation. At 52° of external rotation with an applied 25 N anterior load, the coupled inferior translation was 2.9 mm.

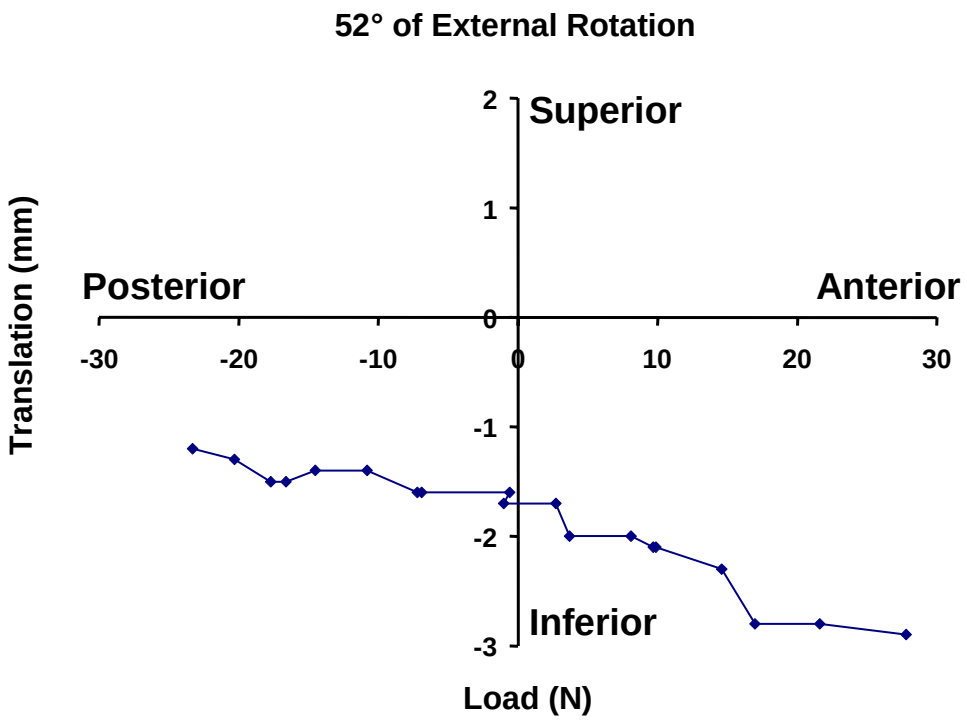

Figure 5.9: Superior translation--humerus with respect to scapula at 52° of external rotation

5.5 EXPERIMENTAL STRAINS

5.5.1 Methods

Using the robotic/universal force-moment sensor testing system the joint was positioned at 52° of external rotation with a 25 N anterior load applied. The camera system was calibrated for the working volume the 3D location of the 77 strain markers in the clinically relevant joint position. (strained configuration)

The magnitude and direction of the maximum principal strain was then calculated using ABAQUS®. The location of the 77 strain markers in the reference strain configuration and the strained configuration were input and membrane elements assigned. A minimal thickness (0.02

mm) was assigned and an arbitrary constitutive model was selected. The magnitude of the maximum principal strain was then calculated at the centroid of each element while the direction is calculated at each node.

5.5.2 Results

It was observed that three strain markers were no longer affixed to the capsuloligamentous regions during testing. These strain markers were located near the glenoid and on the anterior half of the axillary pouch. Thus, the maximum principal strain could only be evaluated for 55 elements. Table 5.3 shows the magnitude of the maximum principal strains measured for 52° of external rotation which were similar to those observed for the previous 6 specimens tested. (Section 4.2.11) Figure 5.10 is a fringe plot illustrating the magnitude and direction of the maximum principal strains. Comparing these data to those previously obtained for the 6 specimens, it appears that some strain markers were no longer affixed to the capsuloligamentous regions, but were not detected. However, the pattern and magnitude of the strain distribution, especially for the anterior band of the inferior glenohumeral ligament and the anterior half of the axillary pouch, was similar to what was previously observed for the 6 specimens. Additionally, in these capsuloligamentous regions, the direction of the maximum principal strains also showed alignment, which was also observed previously.

Table 5.3: Magnitude of maximum principal strains at 52° of external rotation at 25 N (n=55 elements)

	52° External Rotation
	25 N
Average (%)	14.3
SD	15.5
Peak (%)	54.9

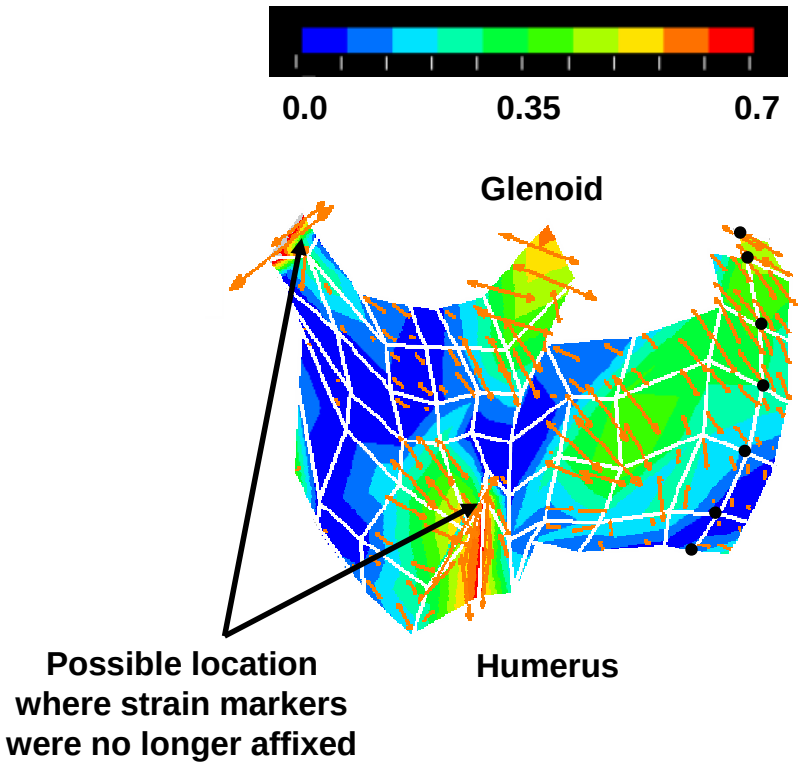

Figure 5.10: Magnitude and direction of maximum principal strains at 52° of external rotation. Black circles denote location of anterior band of inferior glenohumeral ligament.

5.6 COEFFICIENTS TO CONSTITUTIVE MODEL

5.6.1 Methods

The posterior region was tested first followed by the axillary pouch. (Section 3.5.3) For the posterior region, Option B was selected and the tensile load was applied in the transverse direction. A load limit of 34 N was reached before the 3 mm displacement was achieved. The tissue sample was then returned to the displacement level corresponding to the preload and a 30 minute recovery period should be allowed. Following the recovery period, the experimental set-up was altered for shear loading in the longitudinal direction. After the applied shear, the tissue sample should be returned to the displacement level corresponding to the preload and a 30 minute recovery period should be allowed. It was then necessary to load the posterior region based for Option A. Thus, a tensile load was applied in the longitudinal direction. A recovery period of 30 minutes was allowed followed by application of the shear load in the transverse direction. The load-elongation curves were clearly into the linear region, thus testing of the posterior region concluded at this point.

For the axillary pouch, Option A was selected and the shear load was applied in the transverse direction. A 30 minute recovery period was allowed and a tensile load in the longitudinal direction was then applied. After the recovery period, the clamps were rotated to accommodate Option B and a shear load was applied in the longitudinal direction. This was followed by a 30 minute recovery period and the application of a tensile load in the transverse direction. Evaluating the load-elongation curve for the application of a tensile load in the transverse direction indicated that a larger displacement should be applied to ensure adequate representation of the linear region. Therefore, the applied displacement was increased to 2.0 mm. However, the load limit for the load cell was reached after 1.9 mm.

The anterosuperior region was then tested. After evaluating the load-elongation curve, a 30 minute recover period was allowed and the displacement was increased to 2.0 mm. The anterior band of the inferior glenohumeral ligament was then tested. After evaluating the load-elongation curve, a 30 minute recovery period was allowed and the displacement was increased to 2.5 mm. However, the load limit for the load cell was reached after 2.3 mm. As with the anterosuperior region and anterior band of the inferior glenohumeral ligament, evaluation of the load-elongation curves demonstrated that a larger displacement may be necessary to adequately represent the linear region of the curve. Therefore, the displacement was increased to 2.5 mm. However, the load limit for the load cell was reached after 2.3 mm.

The coefficients to an isotropic constitutive model were determined in each loading condition for each capsuloligamentous region. Please refer to Sections 3.5.2.4 and 3.5.3 for more information.

5.6.2 Results

The load-elongation curves obtained for the anterosuperior region, anterior band of the inferior glenohumeral ligament, and posterior band of the inferior glenohumeral ligament are shown in Figure 5.11. The general shape of the three curves is similar for both the toe and linear regions. Thus, it would be expected that the coefficients to the isotropic hypoelastic constitutive model would also be similar between these three capsuloligamentous regions.

The load-elongation curves obtained for the axillary pouch and posterior region when a tensile load was applied are shown in Figures 5.12 and 5.13, respectively. For both the axillary pouch and the posterior region, the general shape of the curves in the parallel and perpendicular direction was somewhat different. Thus, for both the axillary pouch and posterior region, some differences would be expected between the coefficients to the isotropic hypoelastic constitutive model obtained for the parallel and perpendicular directions.

The load-elongation curves obtained for the axillary pouch and posterior region are shown in Figures 5.14 and 5.15 with a shear load applied, respectively. The general shape of the curves obtained for both the axillary pouch and posterior region was similar between the parallel and perpendicular directions. Thus, small differences would be expected for the coefficients to the isotropic hypoelastic constitutive model in the two directions.

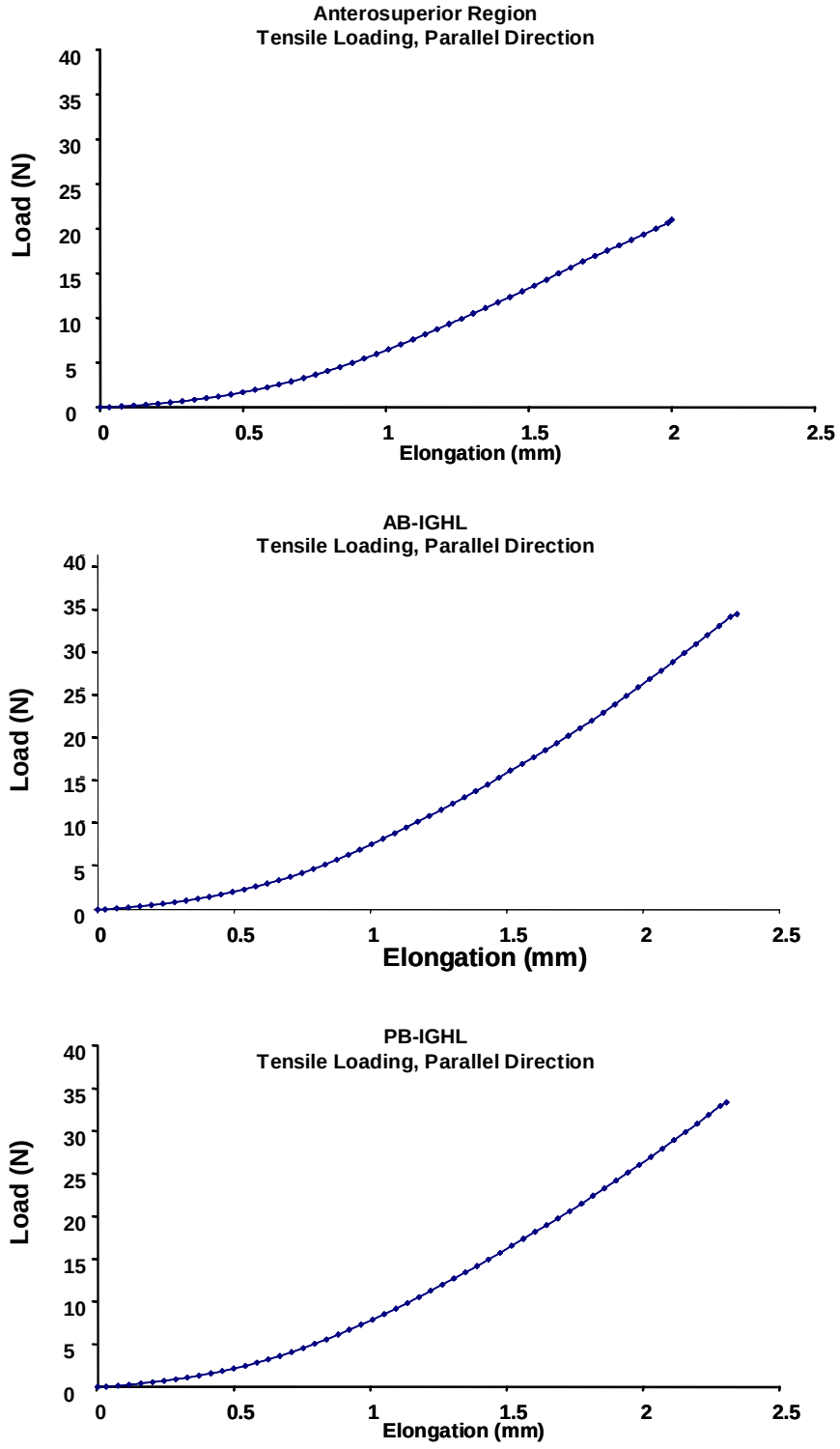

Figure 5.11: Load-elongation curves obtained for anterosuperior region, anterior band of the inferior glenohumeral ligament (AB-IGHL), and posterior band of the inferior glenohumeral ligament (PB-IGHL)

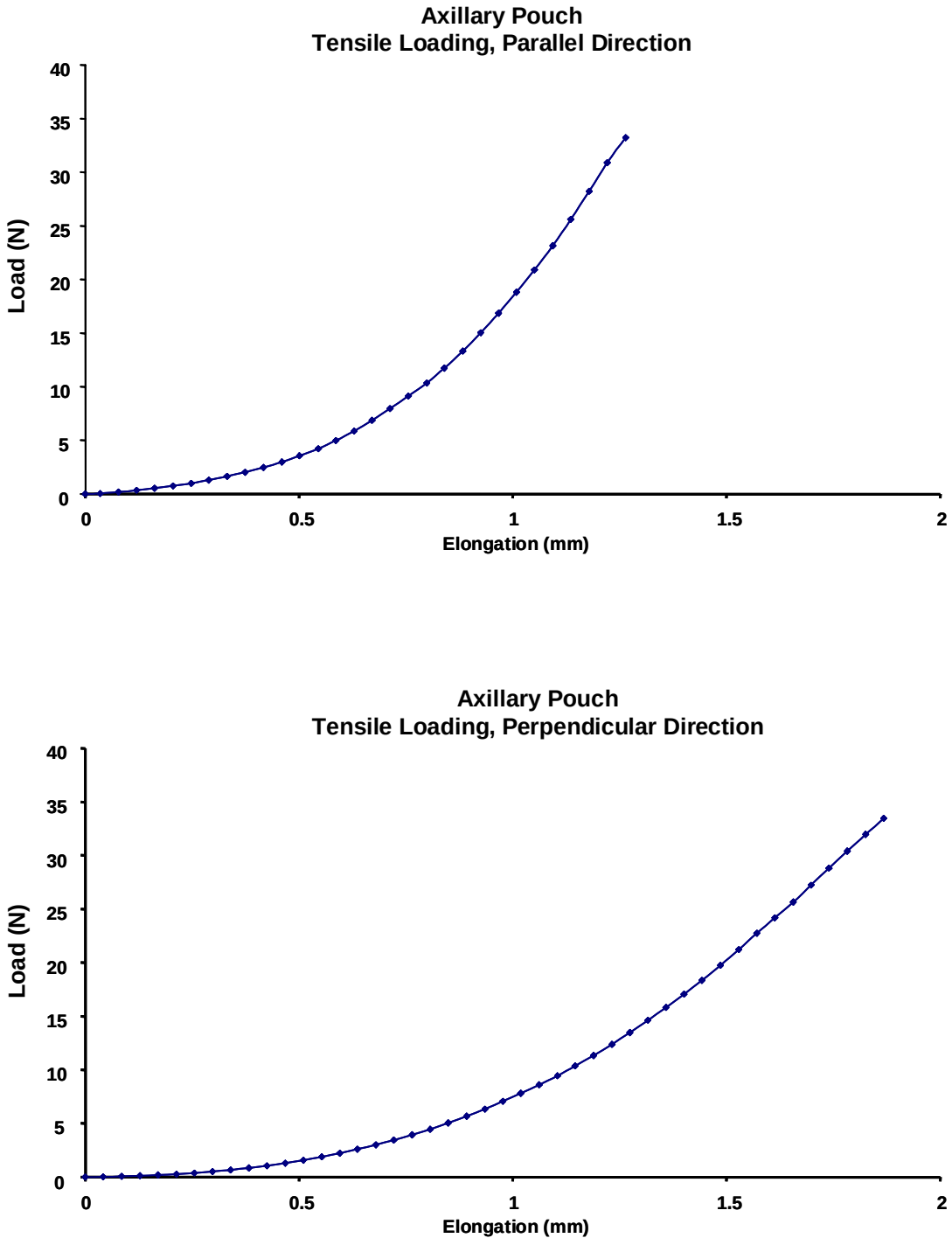

Figure 5.12: Load-elongation curves for the axillary pouch with a tensile load applied in the parallel and perpendicular directions

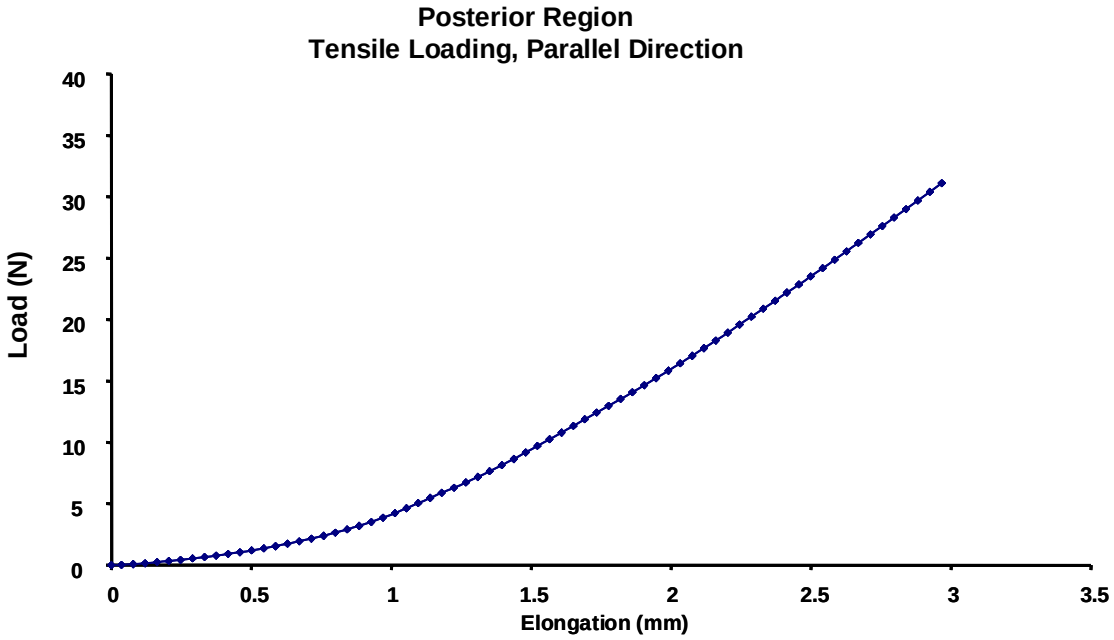

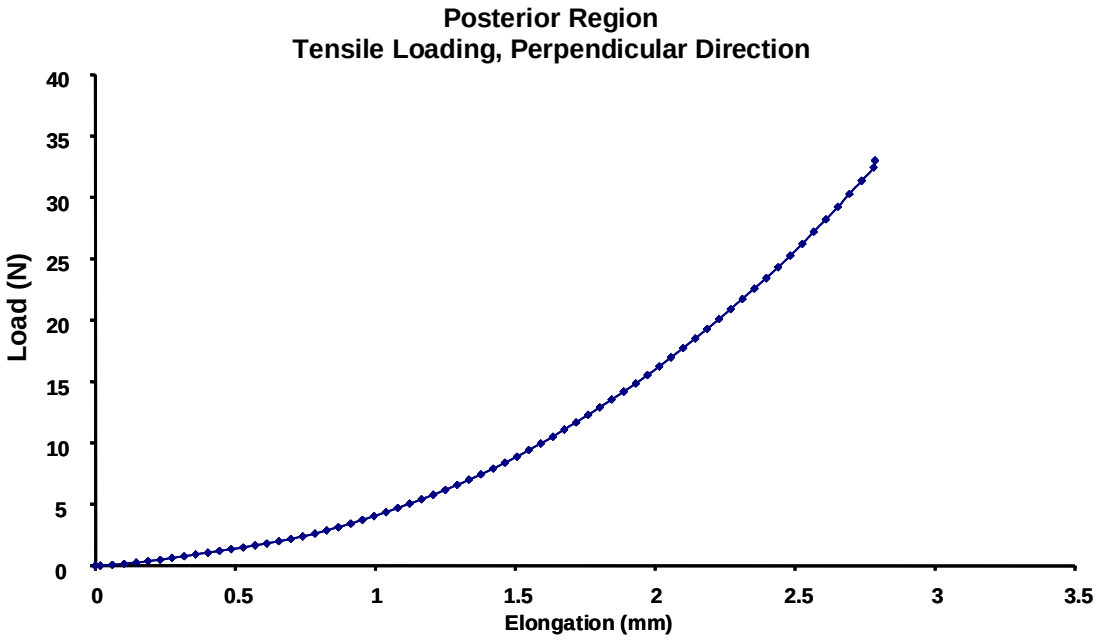

Figure 5.13: Load-elongation curves for posterior region with a tensile load applied in the parallel and perpendicular directions

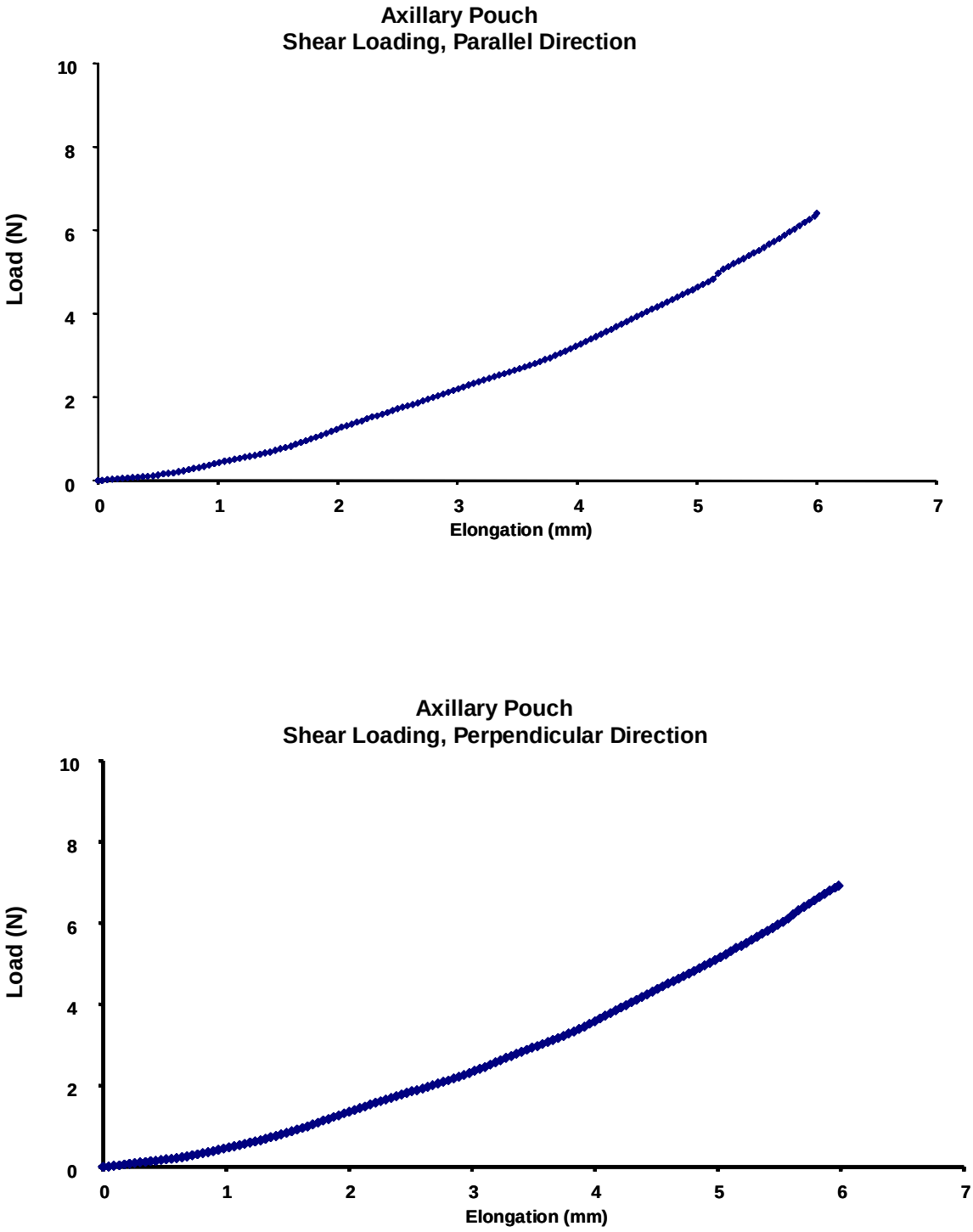

Figure 5.14: Load-elongation curves for axillary pouch with a shear load applied in the parallel and perpendicular directions

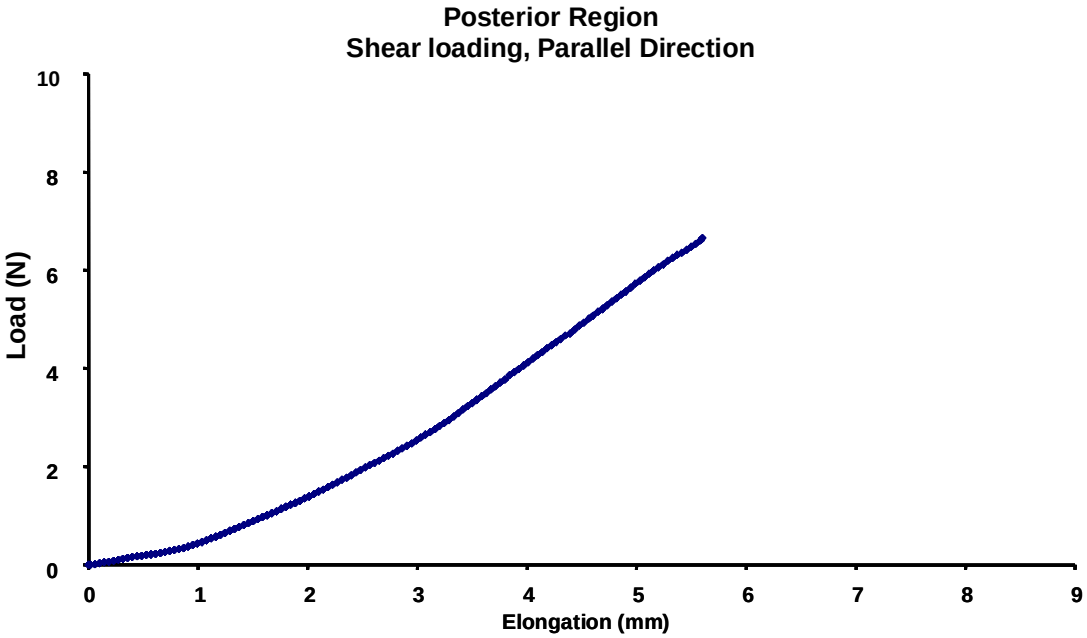

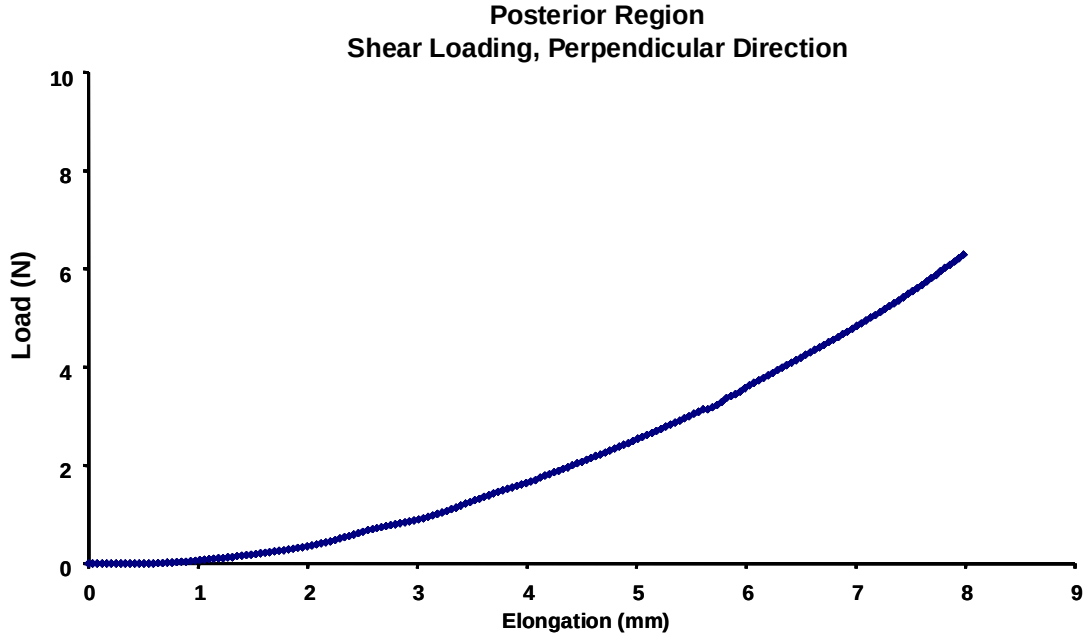

Figure 5.15: Load-elongation curves for posterior region with a shear load applied in the parallel and perpendicular directions

The coefficients to the isotropic hypoelastic constitutive model are shown in Table 5.4. Notice that the tangent modulus (E) was the same order of magnitude for all capsuloligamentous regions and all loading conditions with the only exception being that of the posterior region in the direction parallel to the longitudinal axes of the capsuloligamentous regions. Additionally, the Poisson's ratio was nearly 0.5 for all capsuloligamentous regions regardless of the loading condition. This clearly indicates an incompressible material as would be expected for ligamentous tissues.

As was expected based on the load-elongation curves, small differences exist between the coefficients for the anterior and posterior band of the inferior glenohumeral ligament and the anterosuperior region. The same was true for the axillary pouch and posterior region when a shear load was applied. However, for the axillary pouch and posterior region, differences of approximately 5-8 MPa were obtained for the tangent modulus when comparing the parallel and perpendicular directions. These findings were not surprising based on the qualitative analysis to the general shape of the load-elongation curves for these capsuloligamentous regions.

For the composite and discrete finite element models, only one tangent modulus and one Poisson's ratio are prescribed for each capsuloligamentous region. Therefore, in the case of the axillary pouch and the posterior region, the average across all four loading conditions was calculated: 4.92±2.00 MPa and 5.86±4.60 MPa, respectively. The coefficients to the constitutive model used for the composite and discrete finite element models are described in a later section of this work.

Table 5.4: Coefficients obtained from fitting load-elongation curves from simulated experiments to actual experimental data using an isotropic hypoelastic constitutive model for each capsuloligamentous region under various loading conditions

	Tensile Loading		Shear Loading	
	E (MPa)	ν	E (MPa)	ν
AB-IGHL	2.05	0.4995	N/A	N/A
PB-IGHL	3.73	0.4995	N/A	N/A
Anterosuperior Region	2.12	0.4995	N/A	N/A
Posterior Region (parallel direction)	12.6	0.4995	2.62	0.4995
Posterior Region (perpendicular direction)	4.71	0.4995	3.39	0.495
Axillary Pouch (parallel direction)	4.51	0.4995	5.42	0.4995
Axillary Pouch (perpendicular direction)	7.27	0.4995	2.48	0.4995

6.0 CONSTRUCT FINITE ELMENT MODELS

6.1 PREVIOUS LITERATURE

Until recently, the majority of computational models of the glenohumeral joint neglected the contribution of the glenohumeral capsule [108, 109] or modeled only select capsuloligamentous regions as one-dimensional elements. [13, 18, 25] More recently, a kinematically driven finite element model of the anterior band of the inferior glenohumeral ligament has been developed previously. [23] As with the current study, the geometry of the anterior band of the inferior glenohumeral ligament, scapula, humerus, and articular cartilage of the humerus was segmented from a CT data set. The humerus and scapula were modeled as rigid triangular shell elements while the anterior band of the inferior glenohumeral ligament and articular cartilage of the humeral head were modeled as 8-node hexahedral elements. Kinematics from a clinical exam of a cadaveric joint were collected and used to drive the motions of the scapula and humerus in the finite element model. The finite element mesh of the anterior band of the inferior glenohumeral ligament was attached to the scapula and humerus by specifying rigid node sets at the proximal and distal ends of the mesh to be part of the same rigid material as the corresponding bone. A transversely isotropic hyperelastic constitutive model was utilized for the anterior band of the inferior glenohumeral ligament with coefficients taken from literature. [104] For the articular cartilage of the humeral head, an isotropic Mooney-Rivlin constitutive model with coefficients taken from the literature was utilized. [110] Finally, frictionless contact surfaces were

prescribed between the anterior band of the inferior glenohumeral ligament and articular cartilage of the humeral head using the penalty method. [111]

In additional to being ground breaking work for finite element modeling of the glenohumeral capsule, after which the current study is modeled, several key observations/recommendations were presented by the authors. First, excessive bending or buckling of the mesh was noted as the experimental kinematics were applied because the anterior band of the inferior glenohumeral ligament was not always loaded. Thus, the hexahedral elements tended to "invert" during the non-linear solution procedure. Therefore, the authors recommended that shell elements be utilized in the future since they are essentially 2-dimensional. While a thickness is prescribed for stress and strain analyses, element inversion due to bending is typically not encountered. The authors also noted that excluding the remaining capsuloligamentous regions from the analyses may have an impact on the predicted stresses and strains. Additionally, the effect of the coefficients for the constitutive models of the anterior band of the inferior glenohumeral ligament and the articular cartilage of the humeral head were not investigated.

As a follow-up to their first study, [21, 22] the above authors recently published a second study aimed at utilizing the recommendations from their first analysis and addressing some of their limitations. In this second study, the anterior and posterior bands of the inferior glenohumeral ligament and axillary pouch capsuloligamentous regions were incorporated. These capsuloligamentous regions were modeled as quadrilateral shell elements while all other parameters of the model remained the same. The authors also performed a sensitivity analysis for the mesh density and the coefficients to the constitutive models utilized for the capsuloligamentous regions and the articular cartilage of the humeral head. Utilizing shell

elements proved to be extremely successful eliminating the problem of element "inversion". The mesh density analyses demonstrated that the predicted strains were highly affected by changes in the mesh. This was largely attributed to the elements being forced to bend around the folds that developed in the capsuloligamentous regions as the kinematics were applied. Additionally, it was determined that the articular cartilage of the humeral head could be treated as rigid. Changes to the coefficients of the constitutive model for the capsuloligamentous regions caused only minimal (<8%) changes in the predicted strains when changed by 25% of the initial value.

While the strain and forces predicted by both of these previous models compared well to the literature, neither was validated with experimentally collected data for the specimen modeled. This is a large limitation since the joint kinematics, [102] mechanical properties, [17, 27-29, 103, 104] *in situ* forces in the capsuloligamentous regions, [14] and strain distribution [36, 66] have all been shown to be highly variable between specimens. Additionally, neither study incorporated all capsuloligamentous regions which could greatly affect the predicted stresses and strains as the boundary conditions applied to the capsuloligamentous regions would change and forces could be transmitted between these capsuloligamentous regions. Thus, while being a tremendous advance in the area of finite element modeling of the glenohumeral capsule these previously generated models are not capable of addressing the research question outlined in this current work.

6.2 GLENOHUMERAL CAPSULE AS A SHEET: MODEL #1

6.2.1 Meshing

The surface definitions for the humerus, scapula, anterior and posterior bands of the inferior glenohumeral ligament, axillary pouch, anterior superior, and posterior capsuloligamentous regions, and the registration blocks were imported into a finite element pre-processor. (TrueGrid, XYZ Scientific, Livermore, CA) Triangular surfaces representing the humerus and scapula were converted directly to rigid body shell meshes. [112]

The anterior and posterior band of the inferior glenohumeral ligament, axillary pouch, anterosuperior, and posterior capsuloligamentous regions were each meshed individually with quadrilateral shell elements. The boundaries of each capsuloligamentous region were defined by 3D curves that were projected to the bursal surface of the capsuloligamentous region. The edges of the mesh were then attached to these 3D curves and the mesh was projected to the bursal surface of the capsuloligamentous region. However, the finite element pre-processor occasionally projected the mesh to the articular surface of the capsuloligamentous region in some locations. To circumvent this problem, additional 3D curves were generated in the medial-to-lateral direction. Again, these curves were projected to the bursal surface of the capsuloligamentous regions. The number of partitions of the mesh was then increased to correspond to the number of 3D curves that were added. These new partitions were then attached to their corresponding 3D curves. This methodology forced the partition of the mesh to lie upon a 3D curve that resided on the bursal surface. Thus, this provided additional constraints when the pre-processor projected the mesh to the surface. Thus, a mesh of quadrilateral shell elements was generated for each of the capsuloligamentous regions such that their bursal surface

was represented. The nodes along the edges of two adjacent meshes (e.g. edges of anterior band of the inferior glenohumeral ligament mesh adjacent to that of axillary pouch mesh and anterosuperior mesh) were then merged together. Thus, this was a *composite model* including all of the capsuloligamentous regions. For each of the meshes, a 2 mm uniform thickness was then prescribed. [28]

From the proximal to the distal end of each capsuloligamentous region mesh, a total of 31 elements were prescribed. The number of elements between each partition was varied such that a uniform element size was achieved across all capsuloligamentous regions. Additionally, the resolution of these elements was defined such that the size of the elements was uniform in the medial-to-lateral direction. (Figure 6.1)

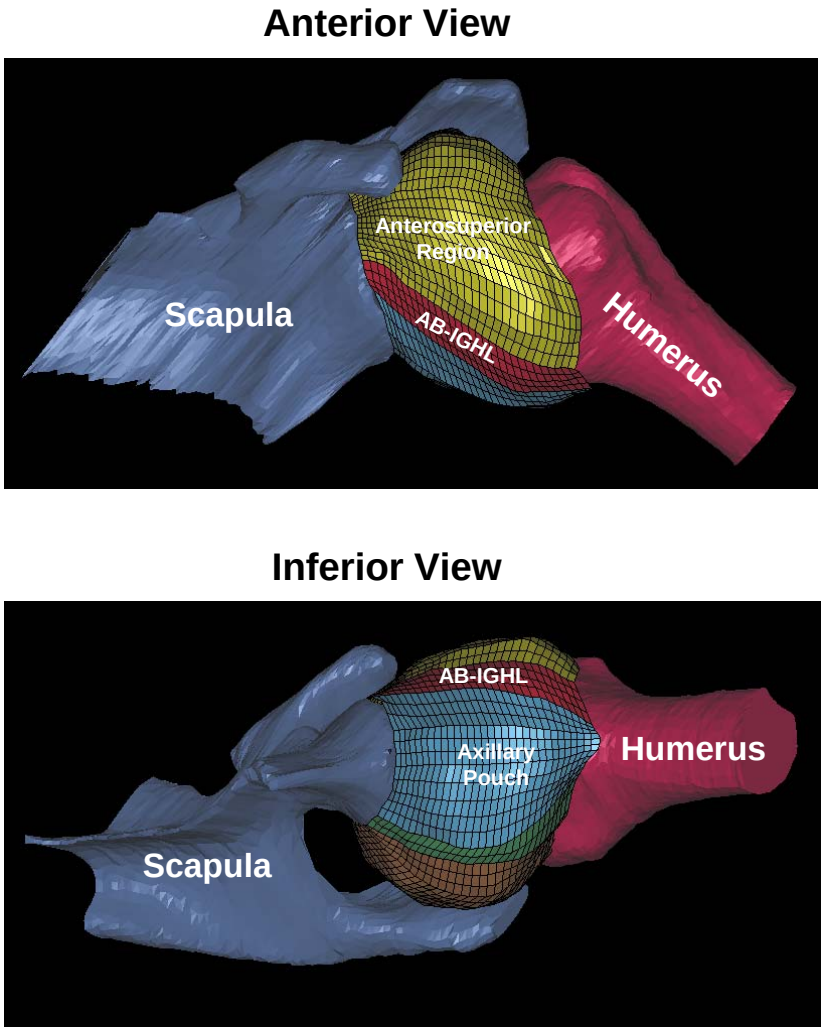

Figure 6.1: Original mesh for composite model showing uniform element size and undeformed shape of capsuloligamentous regions

6.2.2 Boundary Conditions

Since the surfaces were generated from the CT data set, their relative positions with respect to one another were defined by the reference strain configuration and not by the experimentally collected joint position. The surfaces of the registration blocks were then utilized to generate the same coordinate systems that were generated experimentally when determining the joint position

with the external digitizer. Thus, the coordinates of points lying on the same three faces of the registration blocks were identified. Again, an orthogonal coordinate system was generated from these data with its origin at the point where all three planes intersect. Thus, the transformation matrix of the humeral and scapular registration blocks with respect to the global coordinate system of the finite element pre-processor was determined. The transformation matrix of the humeral registration block with respect to the scapular registration block was then calculated. All of the surfaces were then translated and rotated such that the coordinate system at the humeral registration block was aligned with the global coordinate system of the finite element pre-processor while maintaining their relative relationship to one another. The transformation matrix of the humeral registration block with respect to the scapular registration block that was obtained experimentally was then input into the finite element model using a method described by Simo and Qu-Voc [113] whereby transformation matrices are converted into quaternions. [22] Since the registration blocks were rigidly affixed to the bones, the same quaternions could be used to describe the relative motion of the humerus with respect to the scapula. The motion of the humerus in the CT position was then moved to the joint position determined experimentally in incremental steps which were defined using "load curves" in the finite element pre-processor. [22] The nodes at the proximal and distal ends of each mesh were then prescribed to move with the bones.

Contact between the capsuloligamentous regions and the humerus was then prescribed. No contact was observed between the capsuloligamentous regions and the glenoid; therefore, no contact was prescribed. Thus, for the humerus, a frictionless sliding surface was defined and contact was enforced using the penalty method. [21, 22, 111]

6.2.3 Constitutive Model

The non-linear finite element solver NIKE3D is extremely versatile and is convenient for analyses involving large displacements. For this reason, NIKE3D has been utilized extensively in the past to solve for stress and strain distributions in ligaments. [21-23, 65, 72, 89, 101, 114-116]} Both previous models of the capsuloligamentous regions of the glenohumeral capsule utilized NIKE3D. [21-23]

To date, NIKE3D does not include an isotropic hyperelastic constitutive model for shell elements. However, the capabilities exist to augment NIKE3D to include this constitutive model in the near future. Therefore, an isotropic hypoelastic constitutive model was prescribed at this time. In the future, an isotropic hyperelastic constitutive model will be incorporated and meaningful data will be obtained from the predicted stress distributions. However, for the current research question, an isotropic hypoelastic constitutive model is sufficient. The hypoelastic constitutive model would likely result in slightly lower predicted stresses and strains when the tissue is loaded to within the linear region of the stress-strain relationship. However, the regions of high stress or strain would be unaffected by the use of the hyperelastic constitutive model. [21] Thus, for each capsuloligamentous region, the coefficients of the constitutive model that were obtained from the combined experimental and computational approach (Section 5.6) were input. (Table 6.1) For the axillary pouch and posterior region, the coefficients were taken as an average of the coefficients obtained from the four different loading conditions investigated (4.92±2.00 MPa and 5.86±4.60 MPa, respectively).

Table 6.1: Coefficients of constitutive model used for each capsuloligamentous region in the composite finite element model

Coefficients of Isotropic Constitutive Model		
	E (MPa)	ν
AB-IGHL	2.05	0.4995
PB-IGHL	3.73	0.4995
Axillary Pouch	4.92	0.4995
Anterosuperior Region	2.12	0.4995
Posterior Region	5.83	0.4995

6.2.4 Finite Element Analysis

The implicitly integrated finite element code NIKE3D was used for all analyses. An incremental-iterative solution strategy was employed. Iterations were based on a quasi-Newton method [117] and convergence was based on the L_2 displacement and energy norms. [112] The motions of the humerus with respect to the scapula were thus incrementally applied over quasi-time with the time step size being adjusted via an automatic procedure. Computations were carried out on an SGI Origin 3800 with 32 CPUs on a proprietary high-speed shared-memory interconnected with 16 GB of shared memory. The run time was approximately 14 minutes.

6.3 GLENOHUMERAL CAPSULE AS DISCRETE: MODEL #2

6.3.1 Meshing

The anterior band of the inferior glenohumeral ligament was to be modeled as a discrete ligament. The mesh for the anterior band of the glenohumeral ligament that was generated for the composite model (Model #1) was also utilized for Model #2. However, the meshes for the remaining capsuloligamentous regions were excluded. Thus, the nodes along the edges of the mesh were not merged with any other nodes leaving the edges free and unconstrained.

6.3.2 Boundary Conditions

The same boundary conditions prescribed for the composite model (Model #1) were also prescribed for the discrete model of the anterior band of the inferior glenohumeral ligament (Model #2).

6.3.3 Constitutive Model

The same constitutive model prescribed for the composite model (Model #1) was also prescribed for the discrete model of the anterior band of the inferior glenohumeral ligament (Model #2). Additionally, the same coefficients to the constitutive model input for the anterior band of the inferior glenohumeral ligament of the composite model (Model #1) were also input for the discrete model of the anterior band of the inferior glenohumeral ligament (Model #2).

6.3.4 Finite Element Analysis

The same finite element analysis prescribed for the composite model (Model #1) was also prescribed for the discrete model of the anterior band of the inferior glenohumeral ligament (Model #2). Computations were carried out on an SGI Origin 3800 with 32 CPUs on a proprietary high-speed shared-memory interconnected with 16 GB of shared memory. The run time was approximately 6 minutes.

6.4 MODELING DIFFICULTIES ENCOUNTERED

Several difficulties were encountered while attempting to get the two models to run and arrive at a solution for the joint position desired. Since a compressive force was applied when determining the joint position, the humeral head was compressed against the glenoid of the scapula; however, when the CT data was collected, some joint distraction was applied. Thus, when the humerus was moved directly from the CT position to the joint position of interest, the capsuloligamentous regions became lax and were largely unloaded. (Figure 6.2) Thus, an infinite number of solutions could be determined. For the discrete model of the anterior band of the inferior glenohumeral ligament (Model #2), the boundary conditions applied by the remaining capsuloligamentous regions such as the anterosuperior region and axillary pouch were neglected. Since the anterior band of the inferior glenohumeral ligament lies somewhat inferior to the humeral head, it buckled downward as the humerus moved from the CT position to the joint position in the absence of these additional boundary conditions. Thus, a large strain was observed at one corner of the mesh which resulted in the norms growing unbounded and the inability to arrive at a solution for the joint position desired.

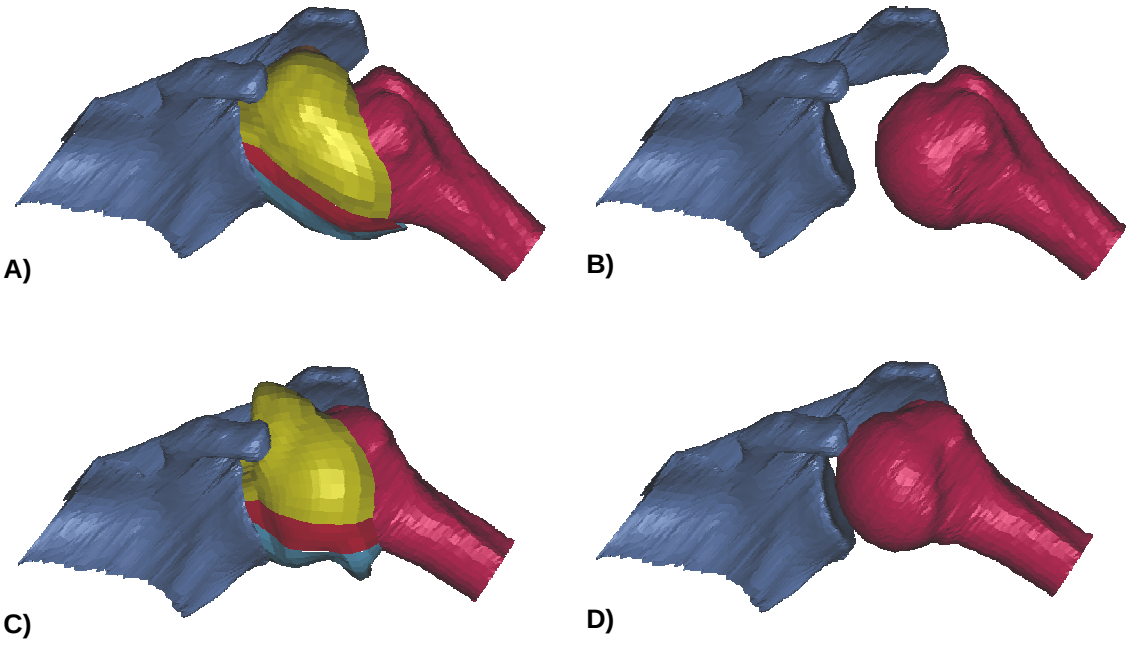

Figure 6.2: Position of humerus with respect to scapula in CT position with (A and B) and in joint position of interest (C and D)

6.4.1 Meshing

The above described problems were observed for the original mesh which consisted of 900 elements that were uniformly sized. Therefore, the sensitivity of this mesh to several parameters was investigated. First, several different mesh densities for the composite model (Model #1) were evaluated. The number of elements was increased and decreased by ⅛, ¼, and ½ of the original mesh. The mesh density was only adjusted in the medial-to-lateral direction with all other parameters consistent (e.g. penalty factor, mechanical properties, etc.) between the variations of the composite model. None of these variations of the composite model were able to arrive at a solution for the joint position desired. (Table 6.2) The best results were obtained when the mesh density was decreased by ½. Further decreasing the mesh density was not investigated since this mesh was already somewhat course and further reduction could result in poor predictions. Therefore, the mesh that was decreased by ½ of the original mesh was used for all further analyses.

Table 6.2: Mesh density analysis for composite model

% of Solution Achieved	
Mesh Density	**Model #1**
Decrease ½	64.8
Decrease ¼	2.5
Decrease ⅛	16.0
Original mesh	24.5
Increase ⅛	20.0
Increase ¼	23.6
Increase ½	25.0

The size of the elements in the medial-to-lateral direction was then adjusted for this mesh density using a scale factor. A scale factor of 1.0 indicates that the size of the elements were uniform. A scale factor of 1.0 was utilized in the above section where the sensitivity of the mesh to mesh density was investigated. A scale factor larger than 1.0 indicates at the size of the elements at the insertion sites was smaller than those at the midsubstance. Thus, a scale factor less than 1.0 indicates that the size of the elements at the insertion sites was larger than those at the midsubstance. Four additional scale factors were initially investigated: 0.80; 0.90; 1.1; and 1.2. Again, all other parameters were consistent between these variations of the mesh. None of these variations resulted in the composite model being able to converge to a full solution. (Table 6.3) The best results were obtained for a scale factor of 0.90; however the results obtained for a scale factor of 0.80 and those obtained previously for a scale factor of 1.0 were similar.

Therefore, three additional scale factors (0.95, 0.93, and 0.83) were also investigated. From the results, larger elements near the insertion sites appeared to be beneficial. Three different scale factors (0.80, 0.90, 0.95, and 1.0) were selected for further analysis as they provided a good distribution within the scale factors that appeared most promising.

Table 6.3: Scale factor for element size in medial-to-lateral direction

% of Solution Achieved	
Element Scale Factor	Model #1
0.80	59.8
0.83	50.0
0.90	71.8
0.93	64.4
0.95	72.3
1.0	64.8
1.1	48.3
1.2	25.0

6.4.2 Boundary Conditions

After adjusting the mesh, it was then necessary to evaluate its sensitivity to the penalty factor used to describe the contact between the humerus and the capsuloligamentous regions. For each of the variations to the mesh of the composite model described above (scale factor: 0.80, 0.90,

0.95, and 1.0) the sensitivity of the mesh to three additional penalty factors was investigated: 0.1, 0.01, and 0.001. The previous analyses for the element scale factor utilized a penalty factor of 1.0. Therefore, a total of four different orders of magnitude were investigated. (Table 6.4) Penalty factors of 0.01 and 0.001 allowed for a greater percent of the solution to be achieved when the element scale factor was 0.80. These variations to the composite model did not result in convergence to a full solution. Therefore, the sensitivity of the mesh to three additional penalty factors was investigated (0.0095, 0.011, and 0.015). However, again the variations to the composite model did not result in convergence to a full solution with the percent of the solution achieved being 50.0%, 94.0%, and 90.1%, respectively.

Table 6.4: Effect of penalty factor to describe contact between humerus and capsuloligamentous regions

% of Solution Achieved				
Penalty Factor	Element Scale Factor			
	0.80	0.90	0.95	1.0
1.0	59.8	71.8	72.3	64.8
0.1	49.1	74.4	62.5	62.5
0.01	95.6	70.0	62.5	50.0
0.001	91.9	65.1	62.5	50.0

In addition to adjusting the penalty factor, the sequences by which the incremental joint motions were applied were an additional boundary condition that could be adjusted in an attempt to converge to a solution. For example, on could choose to apply incremental motions from the

CT position to the joint position of interest such that part or all of the translation along the x-axis was applied *before* any other motions were applied. Once at the desired x-translation, the other motions could then be applied.

Adjusting the sequence in which the joint motions are applied can prove to be extremely beneficial as they can be adjusted in any way such that large strains and poor shape of the elements can be avoided. Thus, it is important to note that the sequence used to apply the joint motions can greatly affect the predicted deformed shape of the capsuloligamentous regions. Therefore, one should consider whether the predicted deformed shape of the capsuloligamentous regions is physically reasonable. Since the previous variations to the composite model did not enable the model to converge to a full solution, it was necessary to find a sequence of joint motions that would increase the percent of the solution achieved.

Therefore, it was necessary to determine whether a specific translation along or rotation about the axes defined by the registration block was the primary cause for the problems. The most successful variation of the composite model (scale factor 0.80; penalty factor 0.01) was used for these analyses. (Figure 6.3) Six different sequences of motion were initially investigated. The first sequence prescribed only the translation along the x-axis while the remaining degrees-of-freedom were excluded. The second sequence prescribed only the translation along the y-axis while the remaining degrees-of-freedom were excluded. Likewise, this was done for the translation along the z-axis and rotations about the x-, y-, and z-axes. While each of these six sequences resulted in convergence, it appeared that it was much more difficult (i.e. more time necessary) to converge to a full solution for the sequence prescribing the translation along z-axis and for the sequence prescribing the rotation about the z axis. (Table 6.5)

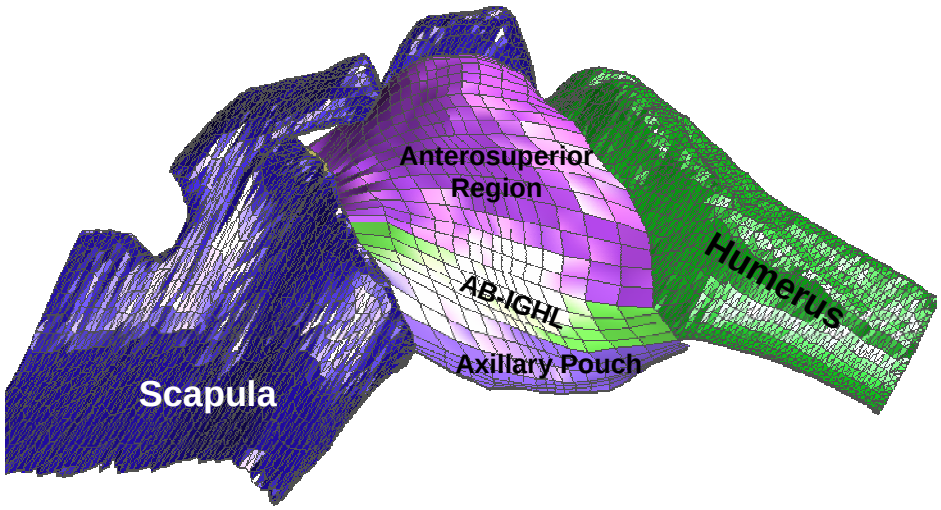

Anterior View

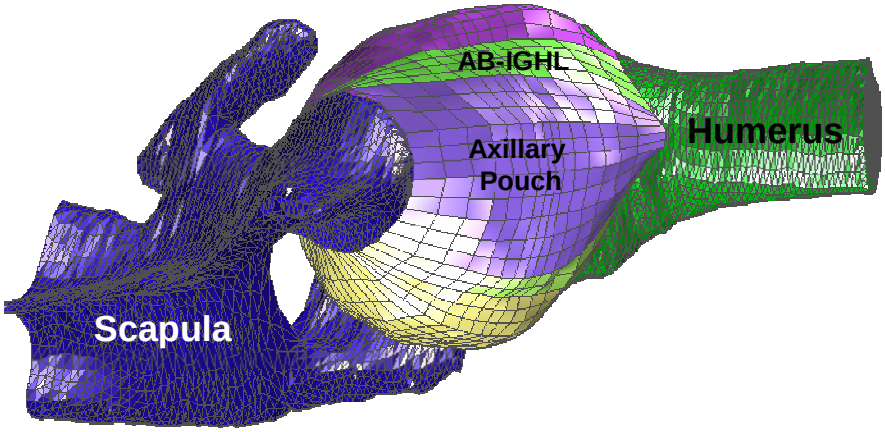

Inferior View

Figure 6.3: Mesh density where largest percentage of solution was achieved showing larger elements at insertion sites and smaller elements at the midsubstance (element scale factor 0.80)

Table 6.5: Percent to solution achieved when only one motion is applied (composite model)

% of Solution Achieved	
Only Motion Applied	**Model #1**
x translation	100.0
y translation	100.0
z translation	100.0
x rotation	100.0
y rotation	100.0
z rotation	100.0

Next, the behavior of the composite model when only the translations and only the rotations were applied was investigated. The percent of the solution achieved for these two analyses was 100.0% and 72.5%, respectively. Based on the results from the six different sequences whereby only one translation or rotation was applied, it appeared that the rotation about the z-axis was a limiting factor. Recall that these axes correspond to the axes of the humeral registration block. Therefore, no direct physical meaning may be interpreted. However, the rotation about the z-axis was largely responsible for externally rotating the humerus while translations along the y-axis were largely responsible for the applied anterior translation.

It was necessary to find a motion along or about the other axes that would avoid deforming the mesh in an undesirable way while applying the rotation about the z-axis. Therefore, the rotation about the z-axis and the translation along the x-axis were applied while

the other degrees of freedom were neglected. For this sequence of joint motion, the composite model obtained full convergence. Therefore, an attempt was made to first apply the rotation about the z-axis and translation along the x-axis *followed* by the motions in the remaining degrees of freedom. After several minor variations in this sequence of joint motions, 100.0% of the solution was achieved. (Figure 6.4)

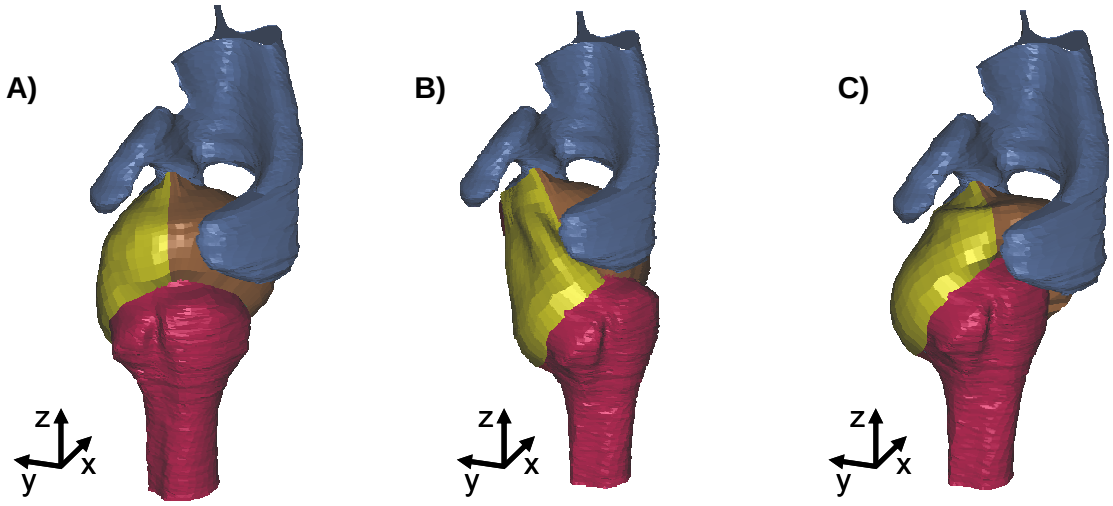

Figure 6.4: Sequence of joint motions applied in order to achieve convergence to a full solution where position of bones are shown for A) initial position based on CT data, B) after rotation about z-axis and translation along x-axis, and C) after remaining motions were applied

7.0 PREDICTED STRAIN DISTRIBUTION

7.1 GLENOHUMERAL CAPSULE AS A SHEET: COMPOSITE MODEL

For the composite model, the maximum principal strain was determined for each capsuloligamentous region for the joint position of interest. (Table 7.1) The largest peak (58.8%) and average (33.5±14.9%) strains were noted for the anterior band of the inferior glenohumeral ligament. While the axillary pouch and anterosuperior capsuloligamentous regions also exhibited large peak strains (44.2% and 40.6%, respectively), their average strains were only 8.9±10.6% and 12.0±8.7%, respectively. Thus, this indicated that a large portion of the axillary pouch and anterosuperior capsuloligamentous regions were unloaded. For both the anterior band of the inferior glenohumeral ligament and the axillary pouch, the peak strains were located in the midsubstance closer to the glenoid than the humerus. The peak strains in the posterior band of the inferior glenohumeral ligament and the posterior capsuloligamentous region were less 15%.

Evaluating the fringe plots clearly demonstrated that the strains were primarily observed in the anterior band of the inferior glenohumeral ligament, the anterior half of the axillary pouch, and the inferior half of the anterosuperior region. (Figure 7.1) The maximum principal strain across the anterior band of the inferior glenohumeral ligament and the axillary pouch was 16.2±16.4%. The strains that arose were not only due to tensile loads being applied to the capsuloligamentous regions, but also due to the capsuloligamentous regions wrapping around the

humeral head. The predicted deformed shape of the anterior band of the inferior glenohumeral ligament, axillary pouch, and inferior half of the anterosuperior capsuloligamentous regions resembled their shape observed experimentally. (Figure 7.2) However, the predicted deformed shape for the superior half of the anterosuperior and the posterior capsuloligamentous regions did not correlate with what was observed experimentally. Specifically, near the 12 o'clock position on the glenoid, both of the anterosuperior and posterior capsuloligamentous regions buckled out, away from the joint space, in the superior direction. Realistically, gravity acts to pull these capsuloligamentous regions in the inferior direction. The deformed shape of the capsuloligamentous regions may be greatly affected by the sequence in which the motions are applied during the finite element analysis. Therefore, it may be possible to obtain a more realistic deformed shape for the anterosuperior and posterior regions if the motions were able to be applied in a more realistic sequence.

Table 7.1: Strains predicted by composite model for each capsuloligamentous region (AB-IGHL: n=60 elements, Axillary pouch: n=165 elements, PB-IGHL: n=30 elements, Anterosuperior region: n=285 elements, Posterior region: n=360 elements)

	Maximum Principal Strain (%)			
	Peak	Minimum	Average	SD
AB-IGHL	58.8	2.1	33.5	14.9
Axillary Pouch	44.2	0.0	8.9	10.6
PB-IGHL	6.7	0.0	2.8	1.9
Anterosuperior	40.6	0.0	12.0	8.7
Posterior	14.9	0.0	3.4	2.9

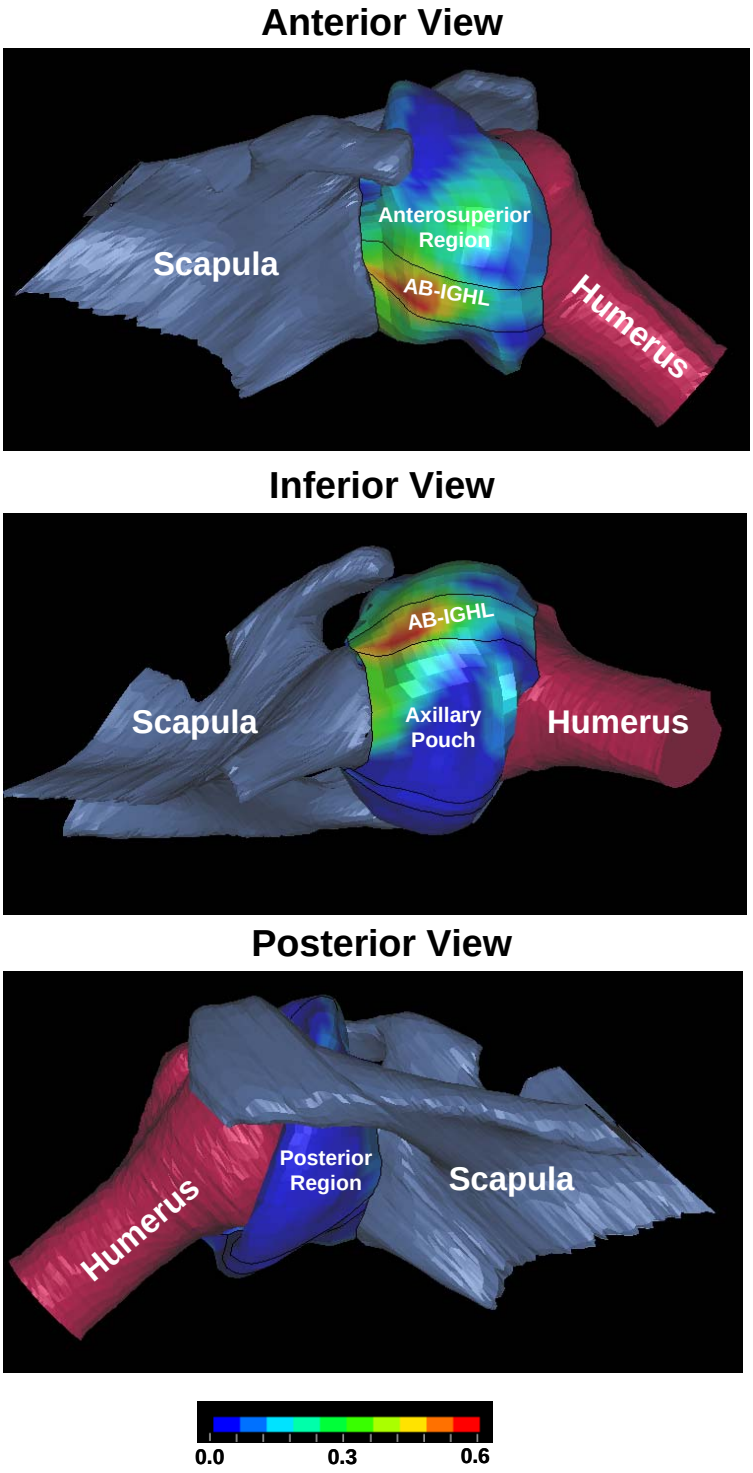

Figure 7.1: Fringe plot of composite finite element model at 60° of external rotation with 25 N anterior load applied showing predicted locations of high strain (unitless) and deformed shape of capsuloligamentous regions

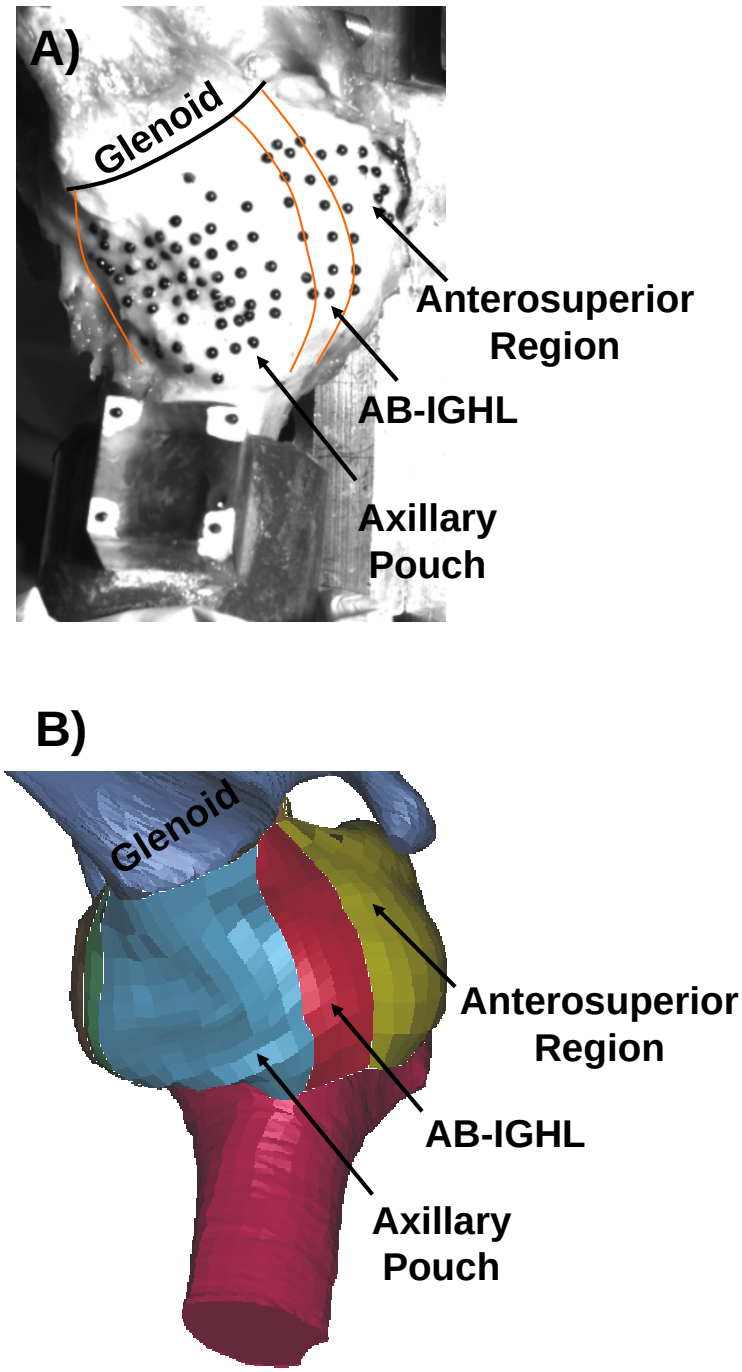

Figure 7.2: Inferior view showing shape of capsuloligamentous regions obtained A) experimentally and B) from the composite finite element model at 60° of external rotation with a 25 N anterior load applied

7.2 EFFECT OF MESH REFINEMENT

Since the mesh utilized for these analyses was somewhat coarse (i.e. minimal elements), it was necessary to determine whether or not a finer mesh (i.e. increased mesh density) would affect the predicted strains. However, as described previously, increasing the mesh density resulted in the model failing to converge to a solution. Therefore, in order to investigate the effect of the mesh density on the predicted strains, comparisons were made at the maximum time step to which both meshes were able to converge. Therefore, the mesh that resulted in convergence to a full solution (coarse mesh: 900 elements) and the original mesh (fine mesh: 3,069 elements) were compared. (Figure 7.3) The original, i.e. finer, mesh may not have been able to converge to a full solution since the mesh appeared to be sensitive to the size of the elements near the insertion sites. This was most likely due to the contact between the capsuloligamentous regions and the articular cartilage of the humeral head which was modeled as a rigid body.

The maximum percentage of the solution achieved for the finer mesh was 40%. Thus, at this time step the average maximum principal strain in the anterior band of the inferior glenohumeral ligament and axillary pouch was 13.7±10.9% and 11.8±10.2% for the coarse and fine mesh, respectively. Thus, a slight decrease in strain was observed when the number of elements was increased. A point-by-point comparison was not possible since the number of elements was different between the fine and coarse meshes. The peak maximum principal strains for the coarse and fine mesh were 38.9% and 43.2%, respectively, and were in the same approximate location. (Figure 7.4) Moreover, the fringe plots for the two meshes demonstrated that the strain distribution and the predicted deformed shape of the anterior band of the inferior glenohumeral ligament and axillary pouch looked similar between the coarse and fine meshes.

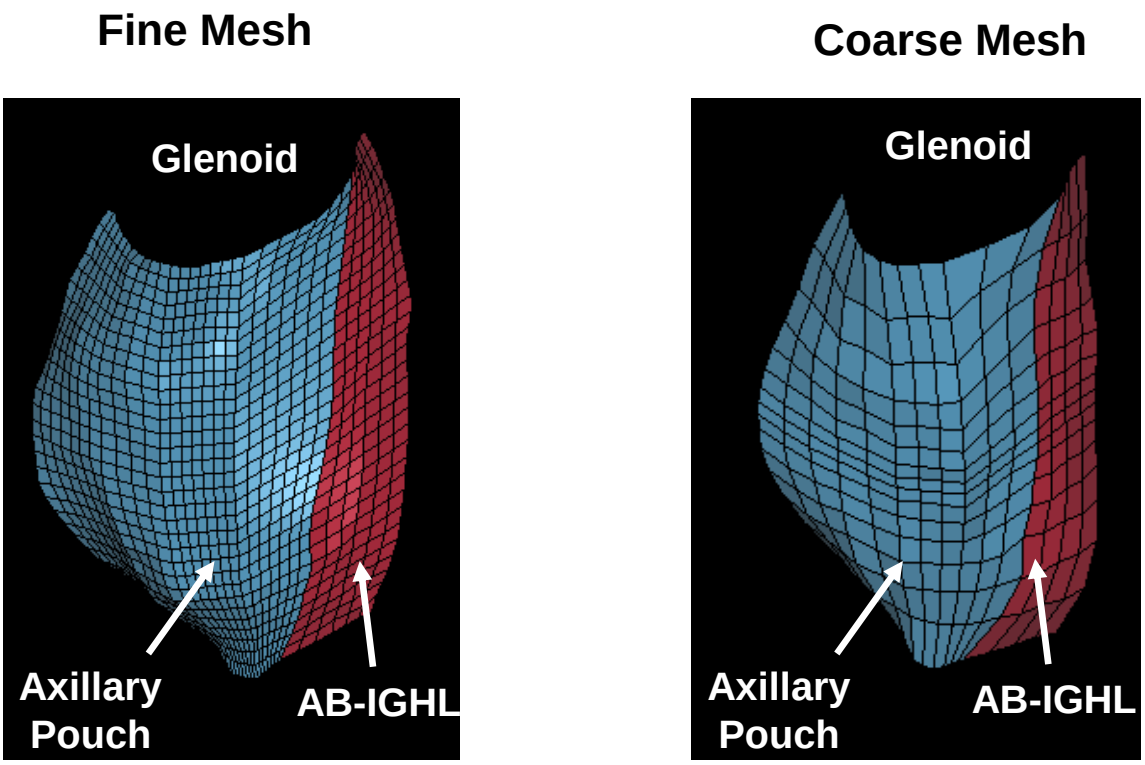

Figure 7.3: Inferior view of plots showing fine mesh with approximately three times as many elements as the coarse meshes of anterior band of inferior glenohumeral ligament (AB-IGHL) and axillary pouch

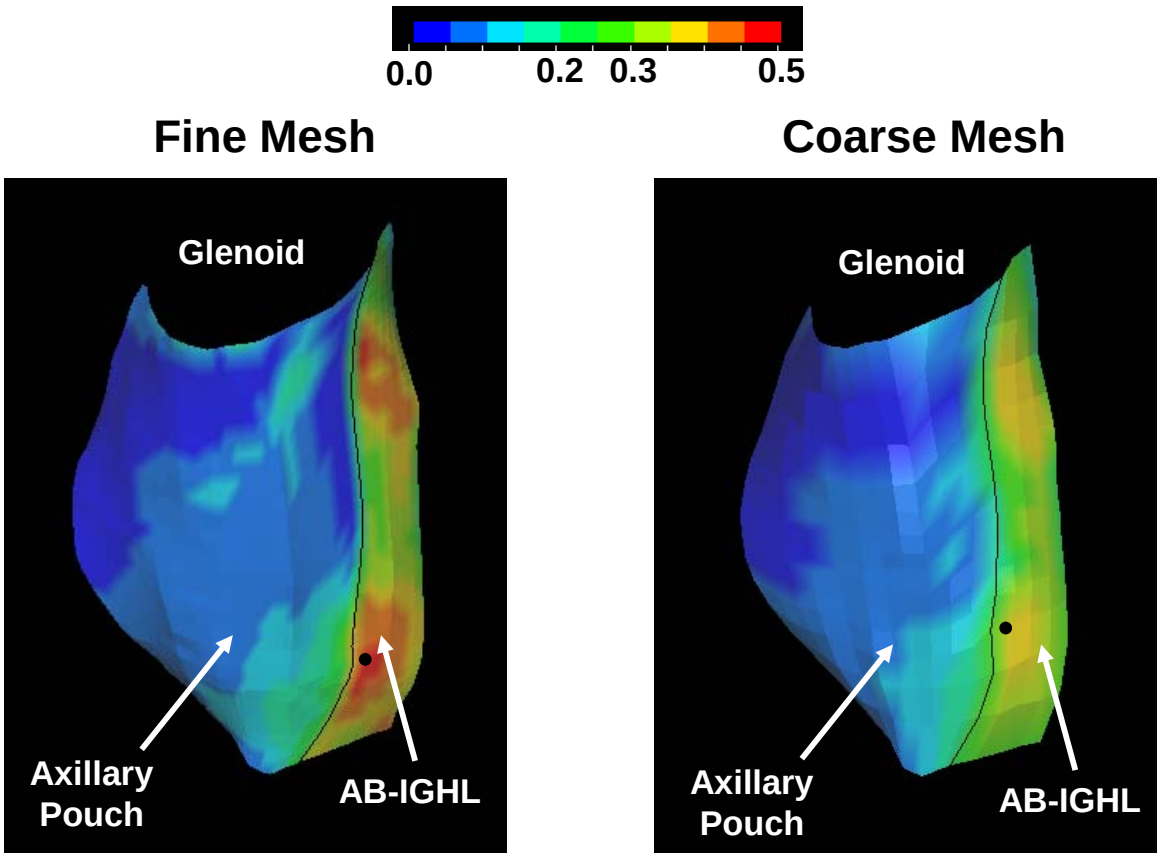

Figure 7.4: Inferior view of maximum principal strain fringe plots for the fine and course meshes showing similar strain distributions. Black circle denotes location of peak maximum principal strain.

7.3 GLENOHUMERAL CAPSULE AS DISCRETE: DISCRETE MODEL

For the discrete model of the anterior band of the inferior glenohumeral ligament, the peak maximum principal strain was only 5.5%. Overall, the maximum principal strain was 0.8±1.1%. The predicted deformed shape of the anterior band of the inferior glenohumeral ligament was not representative of that which was observed experimentally. (Figure 7.5) In fact, it twisted away from the humeral head resulting in no contact between the two. Therefore, strains were only observed at the insertion sites while the midsubstance remained unloaded. This was contrary to what was observed for the composite finite element model for peak strains.

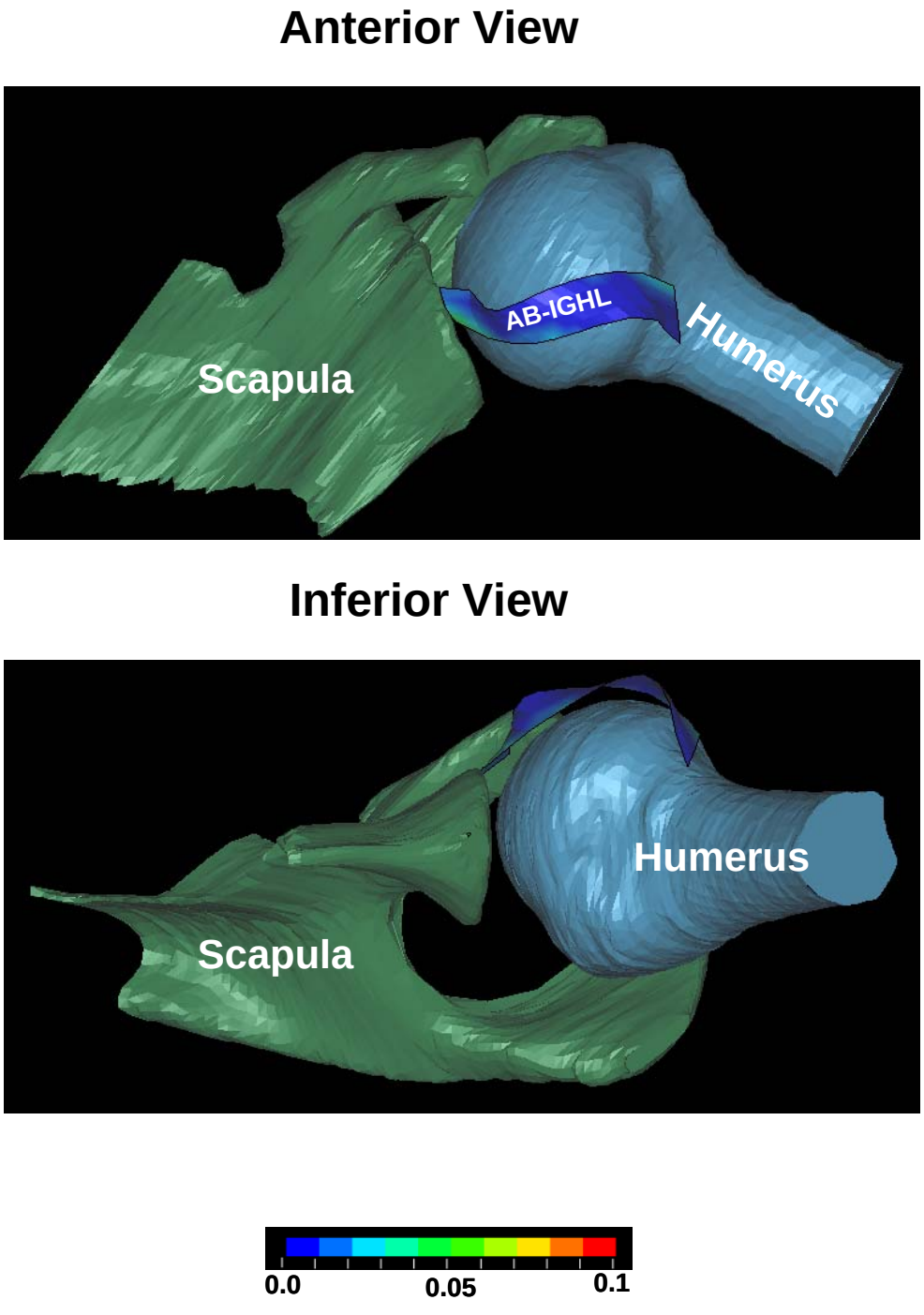

Figure 7.5: Fringe plot of discrete model of anterior band of the inferior glenohumeral ligament (AB-IGHL) at 60° of external rotation with a 25 N anterior load applied showing predicted strain (unitless) distribution and deformed shape

7.4 SIGNIFICANCE

The predicted maximum principal strains and the predicted deformed shape of the capsuloligamentous regions were vastly different between the composite and discrete finite element models. The predicted maximum principal strains for the composite finite element model resembled that which was observed experimentally while the discrete finite element model was clearly different. However, the accuracy of the strains predicted by the composite finite element model will be determined in a latter section of this current work.

For the composite finite element model (Model #1), the predicted deformed shape, where the capsuloligamentous regions were loaded, compared well to what was observed experimentally. However, in the locations where the capsuloligamentous regions were not loaded (i.e. the superior half of the anterosuperior region) the predicted deformed shape did not compare well to experiments. This was most likely due to the fact that the force of gravity acting on the tissue samples was not included as a boundary condition in the model. Thus, future finite element models aimed at evaluating the function of the anterosuperior or posterior capsuloligamentous regions will have to incorporate the force of gravity into their boundary conditions.

For the discrete finite element model of the anterior band of the inferior glenohumeral ligament (Model #2), the predicted strains were an order of magnitude less than that predicted by the composite model. Moreover, the predicted deformed shape of the anterior band of the inferior glenohumeral ligament was different with the discrete finite element model producing an unrealistic shape. Thus, neglecting to include the boundary conditions imposed by the remaining

capsuloligamentous regions drastically affects both the predicted strain distribution within the capsuloligamentous regions and the deformed shape of the capsuloligamentous regions.

Previously, the anterior band of the inferior glenohumeral ligament was discretely modeled. [23] In this previous study, the predicted deformed shape of the anterior band of the inferior glenohumeral ligament was more realistic than that observed for the current work. However, it is important to note that in the previous study, the joint position investigated did not include external rotation. Moving from a minimally rotated position, i.e. CT position, to an externally rotated position, as was done in the current work, yields substantially more interaction between the humeral head and the anterior band of the inferior glenohumeral ligament. Moreover, the position of the bones and capsuloligamentous regions in the reference strain configuration would also play a role since the CT data was acquired in the reference strain configuration. In this previous study, the reference strain configuration was obtained by simply palpating the anterior band of the inferior glenohumeral ligament and assessing an approximate zero-load configuration for this capsuloligamentous region. Therefore, the previous study may have also resulted in a poorly predicted deformed shape of the anterior band of the inferior glenohumeral ligament if an externally rotated joint position was investigated or a more rigorous reference strain configuration were determined.

In a different study, the anterior and posterior bands of the inferior glenohumeral ligament and the axillary pouch were modeled together, while the remaining capsuloligamentous regions were excluded. [21, 22] In this study, the authors investigated the strain distribution with the joint at 0°, 30°, and 60° of external rotation. Again, the predicted deformed shape of the capsuloligamentous regions modeled was more realistic in this previous study than what was found in the current work. This may be attributed to the fact that three of the five

capsuloligamentous regions were included in this previous study while only one capsuloligamentous region was included in the discrete finite element model for the current work. Thus, more boundary conditions were included in the previous model. However, examination of the predicted deformed shape of the capsuloligamentous regions for this previous study reveals that the predicted deformed shape of the capsuloligamentous regions did not differ between the different joint positions investigated. Thus, despite the fact that external rotation was applied, the absence of the anterosuperior capsuloligamentous region, and possibly the posterior capsuloligamentous region, resulted in the capsuloligamentous regions failing to wrap extensively around the humeral head. However, despite the extreme variability in the to the geometry of the capsuloligamentous regions, wrapping of these capsuloligamentous regions around the humeral head, as external rotation is applied, has been previously documented. [69]

In the current work, the humerus was moved from the CT position to the joint position of interest arbitrarily, meaning that the capsuloligamentous regions deformed based on motions that were not representative of what would be observed *in vivo*. However, despite the arbitrary sequence of motions, the composite finite element model was successfully able to predict the deformed shape of the capsuloligamentous regions that were loaded in the joint position of interest. Thus, these data indicate that, in order to appropriately predict the deformed shape of the capsuloligamentous regions, a composite finite element model, whereby all capsuloligamentous regions are included, should be utilized.

8.0 VALIDATION OF FINITE ELEMENT MODELS

8.1 SUMMARY OF ASSUMPTIONS AND VALIDATION CRITERIA

Several assumptions were made when constructing the composite and discrete finite element models in the current work. An isotropic hypoelastic constitutive model was assumed for the capsuloligamentous regions while the humerus, scapula, and articular cartilage of the humerus were modeled as rigid bodies. Also, it was assumed that the capsuloligamentous regions inserted directly into both the humerus and scapula and that the labrum could be neglected and was, therefore, excluded from the analyses. Additionally, it was assumed that the capsuloligamentous regions could be modeled using shell elements due to their small thickness. With these assumptions in place, the predictions from the composite and discrete finite element models are to be considered valid if the average difference between the experimental and predicted results is less than 8% strain. This criteria was selected since it is at least twice the repeatability of the methodology for measuring the experimental strains (±3.5%) while still being an order of magnitude less than the functional range of the glenohumeral capsule (30%-60%). [36, 37, 66]

8.2 METHODOLOGY

The meshes for the composite model (Model #1) and the discrete model of the anterior band of the inferior glenohumeral ligament (Model #2) were generated from the CT data of the capsuloligamentous regions in their reference strain configuration. Thus, the humeral registration block could be used to co-register the location of the 77 strain markers to the nodes of the mesh that correspond to the same location in space with respect to the humeral registration block. Thus, the experimental strain for each strain marker could be directly compared to the predicted strains at the corresponding node and the average difference between the experimental and predicted strains could be determined for both models.

However, the coordinates of the mesh nodes with respect to the coordinate system created at the humeral registration block in the finite element pre-processor did not correspond to the coordinates of the strain markers with respect to the coordinate system created at the humeral registration block from the experimental data collected with the camera system. Since the coordinate system at the humeral registration block was created the same way in both environments (finite element pre-processor and experimental), this indicated that the position of the capsuloligamentous regions was not the same in the two environments. The reference strain configuration was determined using the custom built camera system with the medial-to-lateral axis of the joint being vertical. (Figure 8.1) However, due to the size limitations of the CT scanner, the CT data was acquired with the anterior-to-posterior axis of the joint being vertical. Thus, gravity was acting along a different axis. Upon further investigation of coordinates of the nodes in the mesh, it appeared that the differences resided in the coordinate that corresponded with the anterior-to-posterior direction. Thus, gravity caused the reference strain configuration of the capsuloligamentous regions to shift when the CT scan was taken. Therefore, the proposed methodology to compare the experimental and predicted strains was not possible.

Camera System

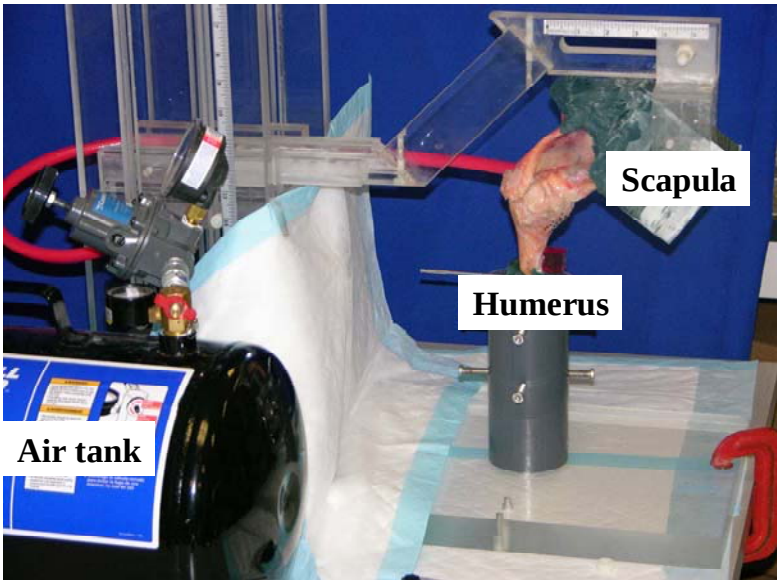

CT Scanner

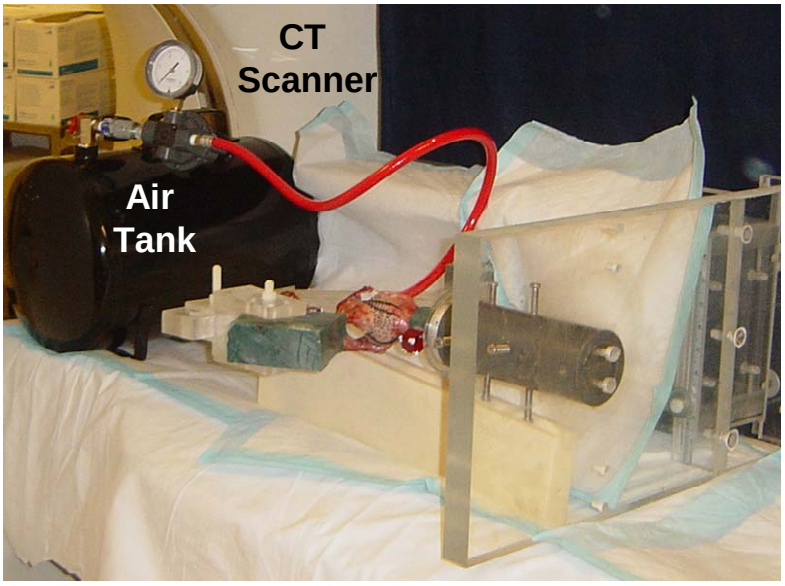

Figure 8.1: Orientation of joint with respect to gravity different for camera system and CT scanner

An alternative methodology was then utilized to compare the experimental and predicted strains. As was done with the scapula, humerus, registration blocks, and capsuloligamentous regions, the strain markers were manually segmented and surfaces were generated. However, since the CT images were acquired with 1 mm slice increments, and the diameter of the strain markers was 1.6 mm, not all of the strain markers were visible during segmentation. Moreover, since not all the strain markers were visible, it was difficult to identify them. Therefore, it was not possible to utilize all of the strain markers even if it was possible to segment them. However, it was possible to interpolate where some of the strain markers would have been once some of the other strain markers were identified. The strain at the nodes that approximated the centroid of elements generated by the strain markers was then compared to the experimentally measured strains. (Figure 8.2) Comparisons were possible for eleven elements that were located near the anterior band of the inferior glenohumeral ligament. The average difference between the predicted and experimental maximum principal strains was then calculated for the composite (Model #1) and discrete (Model #2) models.

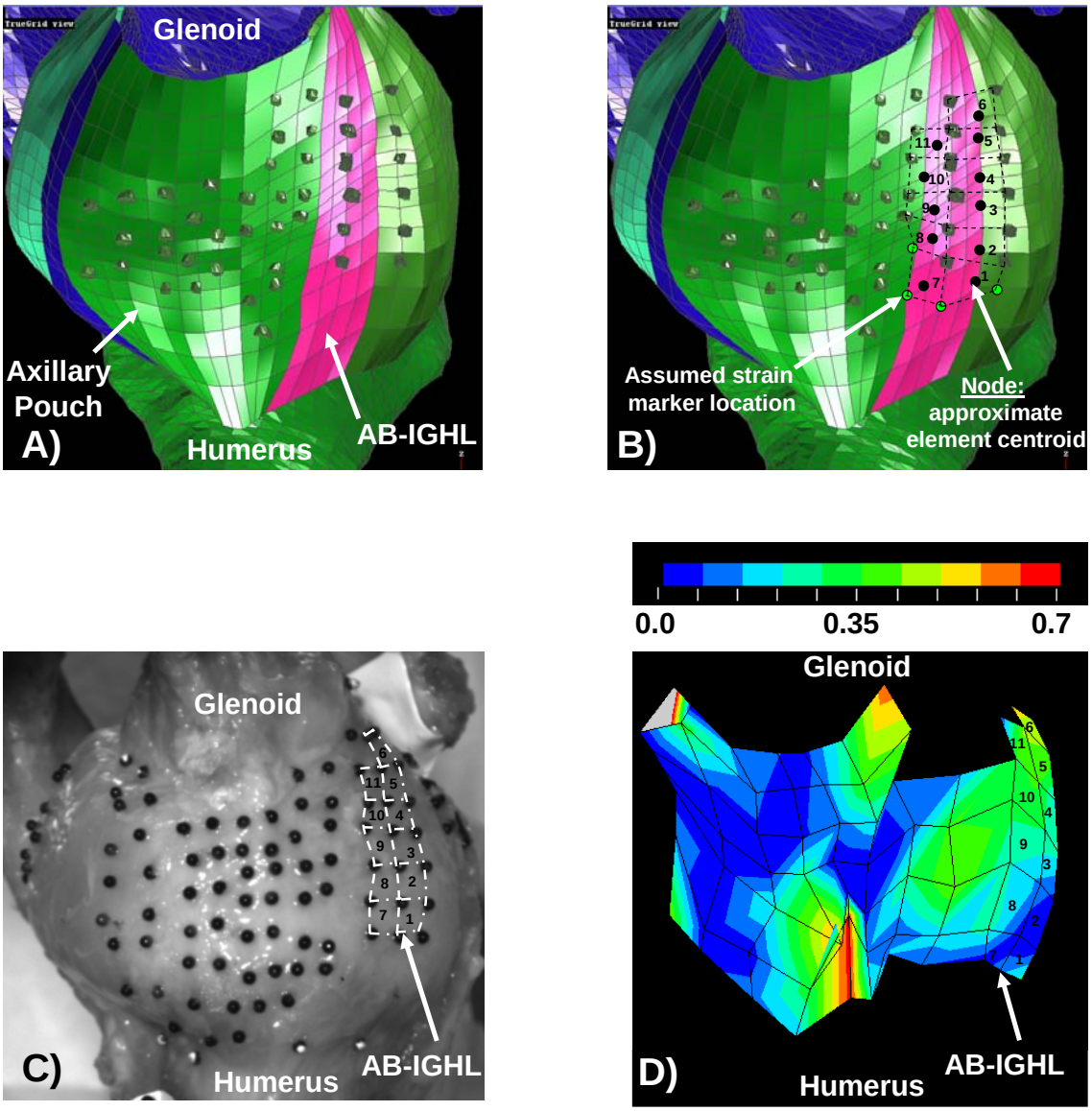

Figure 8.2: Inferior view of glenohumeral joint showing A) segmented strain markers, B) nodes used to approximate element centroids, C) experimental strain markers used to make elements, and D) elements from experimental strains compared. Note that experimental strains compared were within functional areas of the capsuloligamentous regions.

8.3 RESULTS

The experimental strains and those predicted by the composite finite element model (Model #1) compared very well for four of the eleven elements with the difference between the two being 8% or less. (Table 8.1, Figure 8.3) However, for four other elements the difference between the experimental and predicted strains was 17% or more. The largest difference was 31% for one of the elements near the glenoid (element #11); however, the smallest difference was noted for its neighboring element (element #10) with a difference of only 1%. In general, the largest differences were noted for elements in the middle of the tissue evaluated (i.e. elements #3, 4, 8, 9). The average difference between the experimental and predicted strains of the composite finite element model was 14±9%.

For the discrete finite element model it was clear that extreme differences between the experimental and predicted strains existed. (Table 8.2) In fact, the only elements that compared well between the discrete finite element model and experimental data were those where little to no strain was observed experimentally. The good agreement for these elements (elements #2, 3, and 7) did not represent accurate predictions; however, since the overall pattern of the strain distributions was grossly different.

Table 8.1: Comparison of experimental strains and those predicted by composite finite element (FE) model

	Maximum Principal Strain (%)		
Element	Experimental	Composite FE Model	Difference
1	11	13	2
2	7	22	15
3	8	35	27
4	28	41	14
5	36	43	8
6	38	45	7
7	0	17	17
8	12	30	18
9	24	43	19
10	41	40	1
11	28	59	31

Average	14
SD	9

Table 8.2: Comparison of experimental strains to the predicted by discrete finite element (FE) model

	Maximum Principal Strain (%)		
Element	Experimental	Discrete FE Model	Difference
1	11	1	10
2	7	1	6
3	8	0	8
4	28	0	28
5	36	0	36
6	38	0	38
7	0	0	0
8	12	0	12
9	24	0	24
10	41	2	39
11	28	1	37

Average	21
SD	14

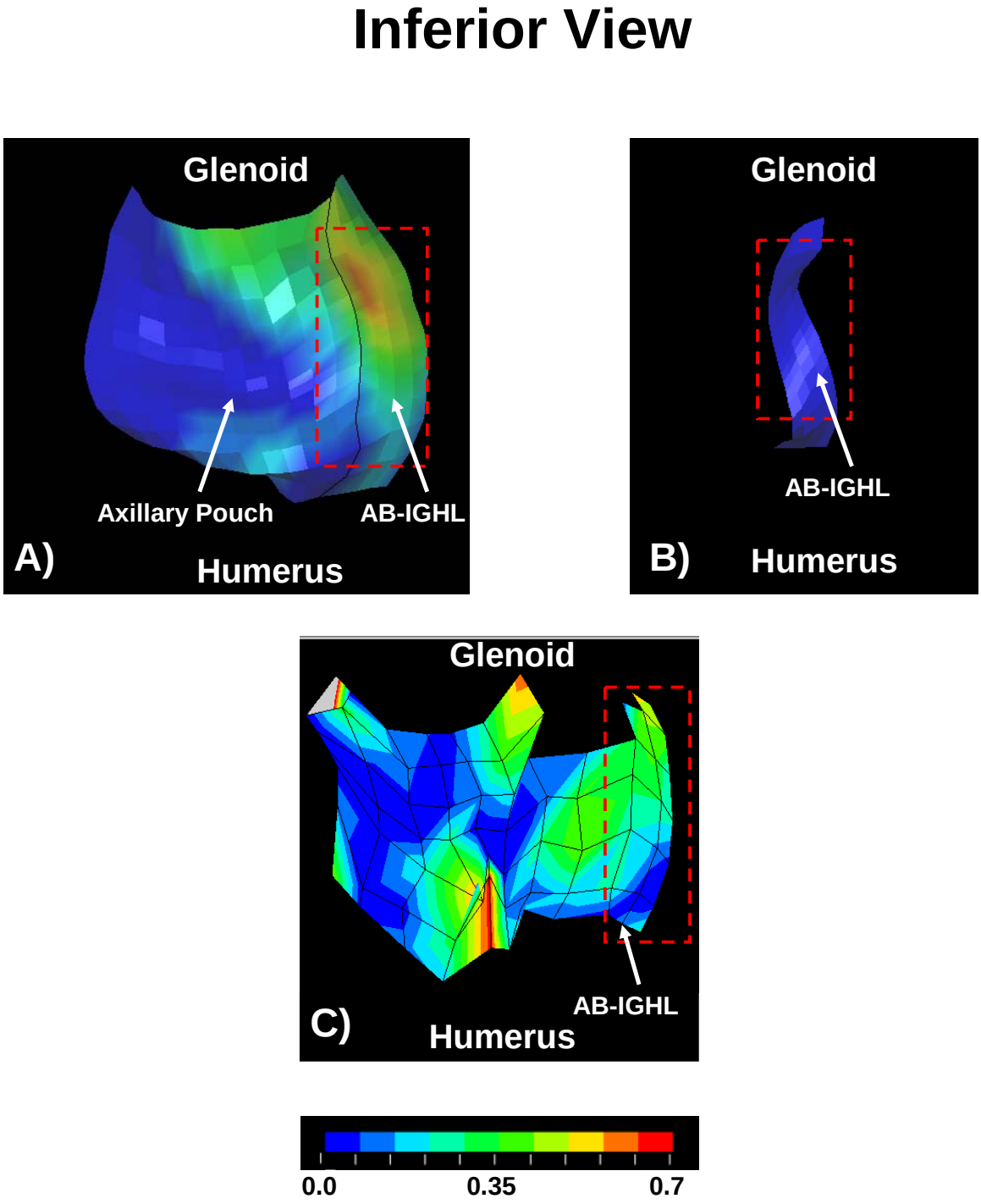

Figure 8.3: Maximum principal strains for A) composite finite element model, B) discrete finite element model, and C) experiment. Red box denotes approximate region where experimental strains were compared.

8.4 IMPLICATIONS

The difference between the experimental maximum principal strains and those predicted by the composite finite element model was 14%. Ideally, this difference should be approximately 8%, since the repeatability of the experimentally measured strains was ±3.5% and the functional range of the capsuloligamentous regions is approximately 30-50% strain.

It is important to note that many difficulties were encountered while experimentally measuring the strains since the specimen was utilized for over 20 hours of testing at that time. Thus, in order to ensure that the capsuloligamentous regions remained hydrated, physiological saline solution was continually applied. Unfortunately, this resulted in poor adherence of the strain markers to the capsuloligamentous regions. Some strain markers were found to no longer be affixed to the capsuloligamentous regions and were thus excluded from the analyses. However, it was possible that the adherence of other strain markers may have been affected. Qualitatively comparing the strain distribution for the composite finite element model to that experimentally collected for the 6 specimens in Section 4.2.11, demonstrates that the strain distribution predicted by the composite finite element model are extremely similar. The same pattern is observed with high strains near the glenoid side of the anterior band of the inferior glenohumeral ligament and the axillary pouch.

Additionally, the magnitudes of the maximum principal strains (16.2±16.4%) of the anterior band of the inferior glenohumeral ligament and the axillary pouch were quite comparable to these previous specimens. (Table 8.3) The maximum principal strain for these previous specimens ranged from 8.5±7.9% to 23.0±17.7% when the joint was positioned at 60° of external rotation with a 25 N anterior load was applied. These data indicate that the composite finite element model produces a reasonable strain distribution. Thus, a robust mesh must be generated such that a rigorous sensitivity study could be performed to determine which parameters may be resulting in the differences between the experimental and predicted strains.

Table 8.3: Comparison of maximum principal strains experimentally measured for 6 specimens and predicted by the composite finite element (FE) model for anterior band of the inferior glenohumeral ligament and axillary pouch when the joint was positioned at 60° external rotation with a 25 N anterior load applied (Specimens 1-5: n=60 elements, Specimen 6: n=52 elements, Composite FE model: n=225 elements)

		Maximum Principal Strain (%)
Experimental Data	Specimen 1	8.5±7.9
	Specimen 2	12.0±14.5
	Specimen 3	19.6±16.2
	Specimen 4	15.9±16.9
	Specimen 5	8.7±13.0
	Specimen 6	23.0±17.7
	Composite FE Model	16.2±16.4

However, for the current mesh of the composite finite element model, even small changes to the parameters resulted in failure to converge to a solution. Previously, quadrilateral shell elements were chosen to model the capsuloligamentous regions [21] since they undergo large amounts of bending and folding. [23] A finer mesh would more easily accommodate the large bending and folding. Therefore, it was surprising that the composite model in the current work was only able to converge to a full solution when a coarse mesh was utilized.

The difficulties observed for the finer mesh may be attributed to the fact that the capsuloligamentous regions were wrapping around the humeral head, which was modeled as rigid. Thus, triangulated surfaces were used to represent the articular cartilage, thus resulting in an unsmooth surface with ridges. Thus, contact between the capsuloligamentous regions and the articular cartilage, modeled in this way, would be a difficult contact problem to resolve. The articular cartilage was modeled as rigid in the current work based upon the results from a previous study in our research center. [21] In this study, it was concluded that the articular cartilage of the humeral head could be treated as rigid since changes to the bulk:shear modulus ratio of the articular cartilage, over several orders of magnitude, had little effect on the predicted strain distribution. In this previous study, the articular cartilage was modeled using hexahedral elements. Additionally, the articular cartilage was then changed from a deformable body to a rigid body which also had little effect. While convergence was still possible with this previous study, it is important to note that only three capsuloligamentous regions were modeled: the anterior and posterior bands of the inferior glenohumeral ligament and the axillary pouch. Therefore, in the current study, substantially more contact was modeled. Thus, the articular cartilage of the humeral head may need to be modeled with hexahedral elements due to the contact with the capsuloligamentous regions. However, based on the results from the previous

study [21], subject-specific properties may not be necessary. Therefore, it is recommended that future investigations initially model the articular cartilage as a deformable body, which may allow them to utilize a finer mesh which is more robust. Thus, the sensitivity of the composite finite element model to the mesh density, penalty factor, and mechanical properties could be rigorously investigated. The results of such a sensitivity analysis may help determine which parameters should be altered to allow for only an 8% difference in the experimental and predicted strains.

However, since the magnitude of the maximum principal strains did not vary much between the coarse and fine meshes, for the time point evaluated, parameters other than the mesh density may have a greater effect on the predicted strains. The comparisons to the experimental strains demonstrated some areas of good agreement and some areas of poor agreement which were located in the midsubstance. Thus, while a rigorous sensitivity study should be performed, the differences noted may not be due to the coefficients to the constitutive model or the constitutive model itself. Instead, these differences may be due to the effect of gravity on the reference strain configuration obtained from the CT data as the capsuloligamentous regions would be more constrained near their insertion sites and less constrained near the midsubstance. Thus, the strain markers near the insertion sites (area of better agreement) may not have been as affected by gravity as those strain markers near the midsubstance (area of poor agreement). Additional factors are the motion sequence prescribed, which may have 'twisted' the capsuloligamentous regions in such a manner as to affect the midsubstance strains.

9.0 DISCUSSION

9.1 IMPLICATIONS OF FINDINGS

9.1.1 Engineering

The data presented in the current work have engineering relevance as there are many implications for experimental and computational analyses. When assessing the function of the glenohumeral capsule, utilizing isolated, discrete capsuloligamentous regions is not advised. Instead, the glenohumeral capsule should be evaluated as a sheet of fibrous tissue.

Isolating the glenohumeral capsule into discrete capsuloligamentous regions drastically alters the boundary conditions applied. Thus, the loads transmitted by the capsuloligamentous region being investigated would not be representative of that observed when all capsuloligamentous regions are included. Altering the load transmission characteristics of the capsuloligamentous region would also result in inaccurate stress and strain distributions. The end result of utilizing isolated, discrete capsuloligamentous regions could be misrepresenting the functional role of the capsuloligamentous region in providing joint stability.

For simplicity, past experimental and computational studies have utilized isolated, discrete capsuloligamentous regions. [12, 14, 15, 17, 18, 21-35] Therefore, additional analyses should be performed with composite and discrete finite element models as a means for assessing the impact this may have on their results. Cutting studies [24, 118-121] sequentially cut and

remove the capsuloligamentous regions and measure the resulting change in joint position. The mechanism by which the capsuloligamentous regions provide stability was altered by limiting the ability to transmit loads between capsuloligamentous regions. Therefore, the resulting joint position may be greatly altered with displacements and rotations being over estimated for those capsuloligamentous regions that were not removed first.

The data obtained in the current work also have implications for studies that determine the mechanical or structural properties of the capsuloligamentous regions at failure by isolating them into discrete regions with a high aspect ratio. To determine the biomechanical properties at failure (e.g. ultimate stress), a uniform distribution of stress across the cross-section is assumed. However, this may not be a valid assumption when the glenohumeral capsule is isolated into discrete capsuloligamentous regions. The results from the current work (collagen fiber organization, direction of maximum principal strains, composite finite element model) demonstrated that interactions exist between the capsuloligamentous regions allowing loads to be transmitted multiaxially. To allow for the complex strain distributions observed experimentally and in the composite finite element model, the capsuloligamentous regions may be highly heterogenous. Thus, a uniform stress distribution may not be possible.

The current work clearly suggests that the glenohumeral capsule should not be evaluated as isolated, discrete capsuloligamentous regions. However, experimentally evaluating the glenohumeral capsule as a sheet of fibrous tissue poses many experimental difficulties. Despite these difficulties, a thorough understanding as to the function of the glenohumeral capsule and its capsuloligamentous regions is necessary to improve patient outcomes. Thus, there exists a need to continue to develop and validate subject-specific composite finite element models. Multiple models should be developed that are representative across the population. These validated

subject-specific composite finite element models should then be utilized to evaluate the mechanisms by with the capsuloligamentous regions transmit loads at various joint positions to provide joint stability.

9.1.2 Clinical

The data presented in the current work have clinical relevance in addition to engineering relevance. The strain distribution pattern observed in the joint positions evaluated experimentally and computationally was complex with larger strains near the glenoid of the anterior band of the inferior glenohumeral ligament, anterior portion of the axillary pouch, and the inferior portion of the anterosuperior region. Thus, our current description of the anatomy [69]does not correlate with the function of the glenohumeral capsule observed in the current work. Researchers have described the anatomy based upon the variable thickness of the glenohumeral capsule and have thus defined the capsuloligamentous regions. However, based upon the strain distribution pattern observed in the current work, one can clearly see that the function of the glenohumeral capsule is not defined by these boundaries.

The strain distribution observed in the experimental portion of the current work also has implications for clinical exams used for diagnosis and surgical planning. The strain distribution pattern remained unchanged through various amounts of external rotation. This implies that clinical exams may be performed at various external rotations to assess the function of the glenohumeral capsule. Additionally, the strain distribution pattern was quite complex indicating that surgical repairs must account for complex injury patterns. Moreover, surgical repairs may need to focus on the anterior band of the inferior glenohumeral ligament, anterior portion of the axillary pouch, and the inferior portion of the anterosuperior region as this is where injury is likely to occur due to the higher strain magnitudes.

Currently, surgical repairs to the glenohumeral capsule plicate and shift the capsuloligamentous regions. Therefore, they drastically alter the boundary conditions for not only the capsuloligamentous regions being repaired, but the remaining capsuloligamentous regions as well since the glenohumeral capsule functions as a sheet of fibrous tissue. Thus, despite the fact that the capsuloligamentous regions may be isotropic, plicating and shifting the capsuloligamentous regions would alter the functional role of the capsuloligamentous regions in providing joint stability. This may explain the high` redislocation rate observed following surgical repair. [10]

Dislocations of the glenohumeral joint can result in rupture or excessive stretching of the capsuloligamentous regions. Thus, surgical repair techniques plicate and shift the capsuloligamentous regions such that the joint laxity in the injured joint is similar to that of the contralateral joint. However, the data presented in this current work suggest that surgeons may be better served to attempt restoring the boundary conditions that existed in the uninjured state.

These concepts could also be investigated via multiple validated subject-specific composite finite element models whereby, in addition to the strain distribution, future studies on the stress distribution within the glenohumeral capsule could also be performed. The stress distributions would provide a means for identifying locations within the glenohumeral capsule that are at risk for injury and could be assessed for various joint positions. Moreover, these models could be utilized to simulate the effect of diminished mechanical properties of the capsuloligamentous regions due to aging [7], disease, or surgical repair procedures that alter the mechanical properties of the capsuloligamentous regions such as thermocapsular shrinkage. [122, 123] Thus, utilizing these models may to simulate the normal, injured, and repaired state, would provide scientific rationale to improve clinical exams for diagnosis and surgical planning, surgical repair techniques, and would enhance our understanding of normal function.

9.2 ADVANCEMENTS AND LIMITATIONS

9.2.1 Advancements

In the current work, a comprehensive analysis was presented whereby experimental methodologies to construct subject-specific composite finite element models of the glenohumeral capsule during a simulated clinical exam were developed. Previously, mechanical testing of the glenohumeral capsule has been performed by isolating the capsuloligamentous regions into discrete entities and then applying a tensile load in the direction parallel to their longitudinal axes. [12, 17, 27-29] However, in the current work, the mechanical response of the capsuloligamentous regions were evaluated bi-directionally and under the application of shear loads. Moreover, a quantitative analysis to the collagen fiber organization of the

capsuloligamentous regions was provided while previous studies were only qualitative with contradictory findings. [69, 74]

Additionally, a methodology to determine the reference strain configuration for all of the capsuloligamentous regions was developed and experimental strains were determined for various positions of external rotation. Moreover, a rigorous evaluation of the repeatability of this methodology was provided whereby the effect of inflation, specimen alignment, equipment calibration, loading protocol, and observer were investigated. The effect of these parameters was evaluated for both the magnitude and direction of the maximum principal strains. Previously, a methodology to determine the reference strain configuration existed for only the anterior band of the inferior glenohumeral ligament and the anterior half of the axillary pouch. [36, 66] The repeatability of this methodology was known for only the magnitude of the maximum principal strains and experimental strains were only collected for one joint position. Thus, the current work was a significant contribution to the literature.

While subject-specific geometry has been obtained utilizing CT scans in previous studies that developed finite element models [21-23, 70-72], in the current work, a detailed comparison between the dimensions of the actual geometry and those generated via segmenting was performed. These data had a direct impact on the methodology for determining the geometry of the registration blocks and demonstrated that the accuracy of measurements decreases where soft tissues insert into the bone.

In addition to experimental advancements, the current work also demonstrated significant advances to computational analyses as well. In the current work, a composite finite element model was generated whereby *all* of the capsuloligamentous regions were included. Additionally, subject-specific mechanical properties were input into the constitutive model for

each of the capsuloligamentous regions. Moreover, the effect of modeling only isolated, discrete capsuloligamentous regions was evaluated. Previous finite element models of the glenohumeral capsule included only select capsuloligamentous regions and utilized average material properties from the literature. [21-23] Based on the finding of this current work, composite finite element models are necessary to accurately predict the strain distribution and shape of the capsuloligamentous regions. Thus, the composite finite element model generated in the current work was novel and demonstrated a significant engineering advance and may be used as a powerful tool to enhance our knowledge of the function of the capsuloligamentous regions in the normal, injured, and repaired states.

9.2.2 Limitations

Despite the multitude of engineering and clinical advancements presented in the current work, several limitations should also be noted. Data from the bi-directional mechanical tests and collagen fiber organization analysis was used to justify the selection of an isotropic constitutive model. However, these analyses were only performed for the axillary pouch, which may not be representative of the other capsuloligamentous regions. However, since these data were collected, bi-directional mechanical tests for the posterior region [103] and a collagen fiber organization analysis for the anterior band of the inferior glenohumeral ligament [124] have been performed using the same methodologies. These studies came to the same conclusion as was found in the current work.

Moreover, while an isotropic hypoelastic constitutive model was assumed, a non-linear stress-strain response was observed. At 60° of external rotation with a 25 N anterior load applied, maximum principal strains of >30% were measured experimentally and predicted by the composite finite element model for the anterior band of the inferior glenohumeral ligament and the axillary pouch. Therefore, it is clear that these capsuloligamentous regions were loaded into the linear region of the stress-strain curve. Since a hypoelastic relationship assumes a linear response throughout the entire stress-strain curve, the tangent modulus would be underestimated. Thus, the hypoelastic constitutive model employed in the current work most likely resulted in slightly underestimating the magnitude of the predicted strains. However, utilizing a hyperelastic material model would not affect the pattern of the strain distribution. It is important to note that the data collected in the current work could be easily used to obtain coefficients to an isotropic hyperelastic constitutive model or even a transversely isotropic constitutive model. However, the finite element solver does not currently allow for these constitutive models when utilizing shell elements.

Subject-specific experimental data were collected for the validation of the predicted maximum principal strains of the composite and discrete finite element models. However, some difficulties were experienced and comparisons between the predicted and experimentally measured strains were only possible for the anterior band of the inferior glenohumeral ligament. Despite the limited quantitative validation, the predicted pattern and magnitude of the maximum principal strains compared quite well to those of six previous specimens.

The labrum was excluded since little is known about its structure and function. However, the labrum acts to provide stability at the joint by increasing the depth of the glenoid concavity. In the specimen utilized for the construction of the finite element models in the current work, the

labrum was large. Additionally, based on the CT data, the posterior band of the inferior glenohumeral ligament and the posterior region both inserted into the labrum directly. It was not possible to confirm this via specimen examination since the capsuloligamentous regions were excised for mechanical testing to determine the coefficients to the constitutive model. All of the insertion sites of the capsuloligamentous regions into the glenoid were modeled as a direct insertion into the bone. McMahon and coworkers [16] have shown that two types of insertion site exist at the glenoid: 1) direct insertion site into the labrum and 2) indirect insertion site into the labrum and glenoid. Moreover, a direct insertion site into the humerus was also modeled. However, a broad insertion site exists for all capsuloligamentous regions at the humerus. Since shell elements were necessary to model the buckling and creasing of the capsuloligamentous regions, only a direct insertion site was possible. Therefore, the assumption that the capsuloligamentous regions directly inserted into the glenoid and humerus may have an impact on the predicted strains, especially near the insertion sites of the capsuloligamentous regions. However, the high strains observed near the glenoid correlate well with previous studies. [16, 17] Since the insertion sites of the capsuloligamentous regions are often injured when the joint is dislocated, an attempt to include a more accurate description of their insertion sites should be made in the future.

Only one joint position was investigated in the current work. The joint position selected was clinically relevant as injury frequently occurs in this joint position and clinical exams for instability are frequently performed in this joint position. However, the function of the capsuloligamentous regions has been shown to vary with joint position. [13, 14, 21, 24, 102, 125, 126] Thus, the effect of excluding boundary conditions, i.e. discrete finite element model, may be greatly dependent upon the capsuloligamentous regions discretely evaluated and the joint position tested.

Finally, the sensitivity of the composite or discrete finite element models to various inputs such as coefficients to the constitutive model and mesh density were not evaluated. These analyses are important as they would allow for a rigorous methodology to determine which parameters (e.g. mesh density, coefficients to constitutive model, etc.) have the largest effect on the predicted strains and deformed shape. These data could be utilized to provide insight to future composite finite element models of the glenohumeral capsule.

9.3 SUMMARY

The anatomy of the glenohumeral capsule is extremely complex; thus, researchers have evaluated its function by examining isolated, discrete capsuloligamentous regions in response to various loading conditions. However, the assumption that there are no interactions between capsuloligamentous regions could have a significant impact on the results. Therefore, the objective of this work was to determine the effect of using composite and discrete finite element models on the predicted strain distribution in the capsuloligamentous regions for a clinically relevant joint position. Methodologies to construct and validate subject-specific finite element models of the glenohumeral capsule were developed. These methodologies were then used to construct two subject-specific finite element models for one cadaveric shoulder: 1) composite model whereby all capsuloligamentous regions are included and 2) discrete model whereby only the anterior band of the inferior glenohumeral ligament was included.

The predicted strain distribution and deformed shape of the composite finite element model resembled that which was obtained experimentally. Based on the strain distribution, the anterior band of the inferior glenohumeral ligament, anterior half of the axillary pouch, and inferior half of the anterosuperior region were responsible for transferring loads between the humerus and scapula. The magnitude of the strains predicted by the composite model differed from the experimental strains by less than 15% strain. However, the predicted strain distribution and shape for the discrete finite element model was drastically different from that observed experimentally with the anterior band of the inferior glenohumeral ligament twisting somewhat along its longitudinal axis and buckling away from the humeral head. In the discrete finite element model, the boundary conditions applied by the remaining capsuloligamentous regions were neglected resulting in poor agreement to the experimentally collected data.

These data indicate the glenohumeral capsule should be evaluated as a sheet of fibrous tissue experimentally and computationally. Based on the finding in the current work, it is necessary to develop subject-specific *composite* finite element models to appropriately evaluate the function of the glenohumeral capsule. In the future, subject-specific composite finite element models of the glenohumeral capsule may be used to more appropriately describe its anatomy and function in the normal, injured, and surgically repaired state.

APPENDIX A

INPUT FILE FOR ABAQUS TO DETERMINE EXPERIMENTAL STRAINS

```
**LOADING CONDITION
*Heading
** Job name: CapsularStrain Model name: SPECIMEN ID
*Preprint, echo=NO, model=NO, history=NO, contact=NO
**
** PARTS
**
*Part, name=Capsule
*End Part
**
** ASSEMBLY
**
*Assembly, name=Assembly
**
*Instance, name=CapsuleInstance, part=Capsule
*Node
1       ,       -36.20761134 ,       29.84211242  ,       -49.19294939
2       ,       -37.61080668 ,       28.99004829  ,       -53.44713949
3       ,       -38.1606632  ,       27.39374383  ,       -58.3235587
4       ,       -37.49834046 ,       25.86860974  ,       -63.03286672
5       ,       -36.97500454 ,       24.96866513  ,       -67.72852853
```

6	,	-35.59055759	,	24.31737959	,	-73.93809936
7	,	-33.50102128	,	21.31037902	,	-78.46984154
8	,	-34.77619759	,	26.18511252	,	-47.67728974
9	,	-35.99175736	,	24.82310825	,	-51.72480875
10	,	-36.47359447	,	23.4339036	,	-56.50365914
11	,	-36.26852864	,	21.95247108	,	-61.42483444
12	,	-36.01810765	,	20.95439796	,	-65.64770131
13	,	-35.04772084	,	20.66977217	,	-71.35861474
14	,	-33.78751776	,	19.0735555	,	-76.10809862
15	,	-33.14499192	,	22.08352554	,	-46.43218743
16	,	-34.04182309	,	20.16646421	,	-50.01520617
17	,	-34.8529055	,	19.66228959	,	-55.13247413
18	,	-34.65965495	,	17.76257166	,	-60.00219502
19	,	-34.8605641	,	17.90478763	,	-64.01600696
20	,	-34.14724417	,	16.71622275	,	-68.91785785
22	,	-28.06664247	,	18.9243799	,	-40.88902994
23	,	-29.44618093	,	17.50353712	,	-43.10116587
24	,	-30.97524425	,	14.30651467	,	-49.6068322
25	,	-31.76031257	,	13.89883981	,	-53.63400529
26	,	-32.24033545	,	12.9089286	,	-58.33360283
29	,	-25.78164336	,	15.90507326	,	-40.03454633
30	,	-27.57938318	,	14.73983055	,	-42.73112053
31	,	-28.85695638	,	12.5595552	,	-47.87114916
32	,	-29.57096874	,	11.52707849	,	-52.00968095
33	,	-29.27542906	,	9.208874884	,	-55.31160615
34	,	-29.97660401	,	9.37820818	,	-60.27121617
35	,	-29.81338963	,	8.726196315	,	-64.51569957
36	,	-22.85143071	,	18.34395248	,	-37.37871848
37	,	-23.39427556	,	14.34776236	,	-39.61258335
38	,	-24.96143193	,	11.36849561	,	-43.37169825
39	,	-25.63417388	,	9.620066791	,	-47.28609228

40 , -26.89725203 , 8.529728868 , -50.88774112
41 , -27.10766194 , 7.186011744 , -52.85186376
42 , -27.73976999 , 6.021496287 , -57.22530886
43 , -20.04062175 , 16.05624397 , -36.2601031
44 , -20.43907763 , 12.83677277 , -38.63993695
45 , -21.96147646 , 9.835559175 , -42.84761938
46 , -22.98589476 , 7.726045573 , -46.84029944
47 , -23.75224956 , 6.641338007 , -50.25337349
48 , -24.04504336 , 4.944038036 , -52.49578136
49 , -24.86961873 , 3.73395545 , -55.89693854
50 , -15.79043835 , 17.68003978 , -33.88313312
51 , -16.91120029 , 14.56539826 , -36.29649345
52 , -17.69296677 , 9.950555582 , -40.05629033
53 , -18.90415283 , 7.442457713 , -44.43677293
54 , -20.29016992 , 5.46335972 , -48.36762991
55 , -21.15777265 , 3.68917357 , -52.44767982
56 , -20.83492695 , 2.403320532 , -56.38437781
57 , -11.18354054 , 17.85192999 , -34.28976434
58 , -12.02663573 , 12.56203571 , -36.9019026
59 , -13.87847414 , 8.414919438 , -40.48068349
60 , -15.32264072 , 6.535419952 , -43.68695676
61 , -16.47165539 , 4.392911528 , -47.96371396
62 , -17.95947514 , 2.570969572 , -51.52081903
63 , -17.68827175 , 0.736822159 , -55.40150282
64 , -6.416280845 , 16.27628421 , -37.04906839
65 , -7.780807333 , 10.4417179 , -38.99639753
66 , -9.009520962 , 5.851199468 , -43.86021858
67 , -10.1871752 , 4.456820784 , -46.80958245
68 , -11.94751402 , 1.854192657 , -51.17452684
69 , -11.53661953 , -0.360549167 , -56.04968817
70 , -12.93812267 , -0.513377858 , -61.15196926

71 , -2.342956884 , 10.7793938 , -41.09469263
72 , -3.579364127 , 5.806068268 , -45.26710018
73 , -2.661498996 , 4.144935457 , -48.40342737
74 , -5.42589213 , 1.773321988 , -52.06203989
75 , -6.578545712 , -0.004447496 , -55.65247366
76 , -8.426088992 , -1.233906012 , -61.36611597
77 , -7.092024028 , -0.48587425 , -64.37474386
*Element, type=M3D4
1 , 8 , 9 , 2 , 1
2 , 9 , 10 , 3 , 2
3 , 10 , 11 , 4 , 3
4 , 11 , 12 , 5 , 4
5 , 12 , 13 , 6 , 5
6 , 13 , 14 , 7 , 6
7 , 15 , 16 , 9 , 8
8 , 16 , 17 , 10 , 9
9 , 17 , 18 , 11 , 10
10 , 18 , 19 , 12 , 11
11 , 19 , 20 , 13 , 12
13 , 22 , 23 , 16 , 15
14 , 23 , 24 , 17 , 16
15 , 24 , 25 , 18 , 17
16 , 25 , 26 , 19 , 18
19 , 29 , 30 , 23 , 22
20 , 30 , 31 , 24 , 23
21 , 31 , 32 , 25 , 24
22 , 32 , 33 , 26 , 25
25 , 36 , 37 , 30 , 29
26 , 37 , 38 , 31 , 30
27 , 38 , 39 , 32 , 31
28 , 39 , 40 , 33 , 32

29 , 40 , 41 , 34 , 33
30 , 41 , 42 , 35 , 34
31 , 43 , 44 , 37 , 36
32 , 44 , 45 , 38 , 37
33 , 45 , 46 , 39 , 38
34 , 46 , 47 , 40 , 39
35 , 47 , 48 , 41 , 40
36 , 48 , 49 , 42 , 41
37 , 50 , 51 , 44 , 43
38 , 51 , 52 , 45 , 44
39 , 52 , 53 , 46 , 45
40 , 53 , 54 , 47 , 46
41 , 54 , 55 , 48 , 47
42 , 55 , 56 , 49 , 48
43 , 57 , 58 , 51 , 50
44 , 58 , 59 , 52 , 51
45 , 59 , 60 , 53 , 52
46 , 60 , 61 , 54 , 53
47 , 61 , 62 , 55 , 54
48 , 62 , 63 , 56 , 55
49 , 64 , 65 , 58 , 57
50 , 65 , 66 , 59 , 58
51 , 66 , 67 , 60 , 59
52 , 67 , 68 , 61 , 60
53 , 68 , 69 , 62 , 61
54 , 69 , 70 , 63 , 62
55 , 71 , 72 , 65 , 64
56 , 72 , 73 , 66 , 65
57 , 73 , 74 , 67 , 66
58 , 74 , 75 , 68 , 67
59 , 75 , 76 , 69 , 68

60 , 76 , 77 , 70 , 69

** Region: (Section-1:Picked)
*Elset, elset=_PickedSet2, internal, generate
1, 1500, 1
** Section: Section-1
*Membrane Section, elset=_PickedSet2, material=Material-1
0.02,
*End Instance
**Nset, nset=_PickedSet4, internal, instance=CapsuleInstance, generate
**1551, 1581, 1
**Elset, elset=_PickedSet4, internal, instance=CapsuleInstance, generate
**1471, 1500, 1
**Nset, nset=_PickedSet5, internal, instance=CapsuleInstance, generate
**1, 31, 1
**Elset, elset=_PickedSet5, internal, instance=CapsuleInstance, generate
**1, 30, 1
*NSET, nset=node1, internal, instance=CapsuleInstance
1
*NSET, nset=node2, internal, instance=CapsuleInstance
2
*NSET, nset=node3, internal, instance=CapsuleInstance
3
*NSET, nset=node4, internal, instance=CapsuleInstance
4
*NSET, nset=node5, internal, instance=CapsuleInstance
5
*NSET, nset=node6, internal, instance=CapsuleInstance
6
*NSET, nset=node7, internal, instance=CapsuleInstance
7

*NSET, nset=node8, internal, instance=CapsuleInstance
8
*NSET, nset=node9, internal, instance=CapsuleInstance
9
*NSET, nset=node10, internal, instance=CapsuleInstance
10
*NSET, nset=node11, internal, instance=CapsuleInstance
11
*NSET, nset=node12, internal, instance=CapsuleInstance
12
*NSET, nset=node13, internal, instance=CapsuleInstance
13
*NSET, nset=node14, internal, instance=CapsuleInstance
14
*NSET, nset=node15, internal, instance=CapsuleInstance
15
*NSET, nset=node16, internal, instance=CapsuleInstance
16
*NSET, nset=node17, internal, instance=CapsuleInstance
17
*NSET, nset=node18, internal, instance=CapsuleInstance
18
*NSET, nset=node19, internal, instance=CapsuleInstance
19
*NSET, nset=node20, internal, instance=CapsuleInstance
20
*NSET, nset=node22, internal, instance=CapsuleInstance
22
*NSET, nset=node23, internal, instance=CapsuleInstance
23
*NSET, nset=node24, internal, instance=CapsuleInstance

24
*NSET, nset=node25, internal, instance=CapsuleInstance
25
*NSET, nset=node26, internal, instance=CapsuleInstance
26
*NSET, nset=node29, internal, instance=CapsuleInstance
29
*NSET, nset=node30, internal, instance=CapsuleInstance
30
*NSET, nset=node31, internal, instance=CapsuleInstance
31
*NSET, nset=node32, internal, instance=CapsuleInstance
32
*NSET, nset=node33, internal, instance=CapsuleInstance
33
*NSET, nset=node34, internal, instance=CapsuleInstance
34
*NSET, nset=node35, internal, instance=CapsuleInstance
35
*NSET, nset=node36, internal, instance=CapsuleInstance
36
*NSET, nset=node37, internal, instance=CapsuleInstance
37
*NSET, nset=node38, internal, instance=CapsuleInstance
38
*NSET, nset=node39, internal, instance=CapsuleInstance
39
*NSET, nset=node40, internal, instance=CapsuleInstance
40
*NSET, nset=node41, internal, instance=CapsuleInstance
41

*NSET, nset=node42, internal, instance=CapsuleInstance
42
*NSET, nset=node43, internal, instance=CapsuleInstance
43
*NSET, nset=node44, internal, instance=CapsuleInstance
44
*NSET, nset=node45, internal, instance=CapsuleInstance
45
*NSET, nset=node46, internal, instance=CapsuleInstance
46
*NSET, nset=node47, internal, instance=CapsuleInstance
47
*NSET, nset=node48, internal, instance=CapsuleInstance
48
*NSET, nset=node49, internal, instance=CapsuleInstance
49
*NSET, nset=node50, internal, instance=CapsuleInstance
50
*NSET, nset=node51, internal, instance=CapsuleInstance
51
*NSET, nset=node52, internal, instance=CapsuleInstance
52
*NSET, nset=node53, internal, instance=CapsuleInstance
53
*NSET, nset=node54, internal, instance=CapsuleInstance
54
*NSET, nset=node55, internal, instance=CapsuleInstance
55
*NSET, nset=node56, internal, instance=CapsuleInstance
56
*NSET, nset=node57, internal, instance=CapsuleInstance

57
*NSET, nset=node58, internal, instance=CapsuleInstance
58
*NSET, nset=node59, internal, instance=CapsuleInstance
59
*NSET, nset=node60, internal, instance=CapsuleInstance
60
*NSET, nset=node61, internal, instance=CapsuleInstance
61
*NSET, nset=node62, internal, instance=CapsuleInstance
62
*NSET, nset=node63, internal, instance=CapsuleInstance
63
*NSET, nset=node64, internal, instance=CapsuleInstance
64
*NSET, nset=node65, internal, instance=CapsuleInstance
65
*NSET, nset=node66, internal, instance=CapsuleInstance
66
*NSET, nset=node67, internal, instance=CapsuleInstance
67
*NSET, nset=node68, internal, instance=CapsuleInstance
68
*NSET, nset=node69, internal, instance=CapsuleInstance
69
*NSET, nset=node70, internal, instance=CapsuleInstance
70
*NSET, nset=node71, internal, instance=CapsuleInstance
71
*NSET, nset=node72, internal, instance=CapsuleInstance
72

```
*NSET, nset=node73, internal, instance=CapsuleInstance
73
*NSET, nset=node74, internal, instance=CapsuleInstance
74
*NSET, nset=node75, internal, instance=CapsuleInstance
75
*NSET, nset=node76, internal, instance=CapsuleInstance
76
*NSET, nset=node77, internal, instance=CapsuleInstance
77
*End Assembly
**
** MATERIALS
**
*Material, name=Material-1
*Hyperelastic, mooney-rivlin
 0.02, 0.02,   0.
** ----------------------------------------------------------------
**
** STEP: Step-1
**
*Step, name=Step-1, nlgeom=YES
*Static
0.05, 1., 1e-05, 1.
**
** BOUNDARY CONDITIONS
**
** Name: BC-1 Type: Displacement/Rotation
*Boundary
node1  ,        1       ,       1       ,       7.598140151
node1  ,        2       ,       2       ,       -6.547103498
```

node1 , 3 , 3 , 2.900088029
node2 , 1 , 1 , 9.076635915
node2 , 2 , 2 , -7.210062876
node2 , 3 , 3 , 4.529495851
node3 , 1 , 1 , 10.34583704
node3 , 2 , 2 , -7.709896341
node3 , 3 , 3 , 5.259413967
node4 , 1 , 1 , 11.07451549
node4 , 2 , 2 , -6.999632172
node4 , 3 , 3 , 5.485811491
node5 , 1 , 1 , 13.17119805
node5 , 2 , 2 , -7.930424813
node5 , 3 , 3 , 6.692366786
node6 , 1 , 1 , 13.98103333
node6 , 2 , 2 , -7.930921617
node6 , 3 , 3 , 9.069775917
node7 , 1 , 1 , 15.17680776
node7 , 2 , 2 , -6.535518323
node7 , 3 , 3 , 12.61700172
node8 , 1 , 1 , 9.682520573
node8 , 2 , 2 , -5.945401245
node8 , 3 , 3 , 3.713570042
node9 , 1 , 1 , 10.66968541
node9 , 2 , 2 , -6.003683491
node9 , 3 , 3 , 4.512460589
node10, 1 , 1 , 11.72578671
node10, 2 , 2 , -6.774698026
node10, 3 , 3 , 4.898945479
node11, 1 , 1 , 13.13209377
node11, 2 , 2 , -6.495674051
node11, 3 , 3 , 5.355213119

node12, 1 , 1 , 15.40717314
node12, 2 , 2 , -6.566353058
node12, 3 , 3 , 6.167017071
node13, 1 , 1 , 17.88097606
node13, 2 , 2 , -7.479089079
node13, 3 , 3 , 8.299931139
node14, 1 , 1 , 18.70224278
node14, 2 , 2 , -6.314083597
node14, 3 , 3 , 12.08748949
node15, 1 , 1 , 10.38115092
node15, 2 , 2 , -3.440959744
node15, 3 , 3 , 3.512889845
node16, 1 , 1 , 12.45091945
node16, 2 , 2 , -3.026125032
node16, 3 , 3 , 5.232013715
node17, 1 , 1 , 14.31178923
node17, 2 , 2 , -5.027578971
node17, 3 , 3 , 4.884443531
node18, 1 , 1 , 16.63329189
node18, 2 , 2 , -5.34416021
node18, 3 , 3 , 5.509032463
node19, 1 , 1 , 17.86330043
node19, 2 , 2 , -5.862775676
node19, 3 , 3 , 5.680936207
node20, 1 , 1 , 20.04731889
node20, 2 , 2 , -5.090233324
node20, 3 , 3 , 7.794507908
node22, 1 , 1 , 10.51453424
node22, 2 , 2 , -0.275834753
node22, 3 , 3 , 1.621189622
node23, 1 , 1 , 12.01195684

node23, 2 , 2 , -0.736982068
node23, 3 , 3 , 1.667366003
node24, 1 , 1 , 14.46862356
node24, 2 , 2 , 0.180511836
node24, 3 , 3 , 4.703329223
node25, 1 , 1 , 18.21181469
node25, 2 , 2 , -1.339703646
node25, 3 , 3 , 5.225440931
node26, 1 , 1 , 19.96968711
node26, 2 , 2 , -2.123411671
node26, 3 , 3 , 5.935405025
node29, 1 , 1 , 11.77445677
node29, 2 , 2 , 2.31653844
node29, 3 , 3 , 1.828513357
node30, 1 , 1 , 13.50269853
node30, 2 , 2 , 2.690463358
node30, 3 , 3 , 3.01410927
node31, 1 , 1 , 16.56751005
node31, 2 , 2 , 1.90200276
node31, 3 , 3 , 4.499266526
node32, 1 , 1 , 18.87005497
node32, 2 , 2 , 1.104768227
node32, 3 , 3 , 5.217488341
node33, 1 , 1 , 21.9573045
node33, 2 , 2 , 2.405682469
node33, 3 , 3 , 6.602790144
node34, 1 , 1 , 23.16805064
node34, 2 , 2 , 1.006462814
node34, 3 , 3 , 6.884600564
node35, 1 , 1 , 26.66516007
node35, 2 , 2 , 1.702825362

node35, 3 , 3 , 8.492085721
node36, 1 , 1 , 7.889846977
node36, 2 , 2 , 1.615806227
node36, 3 , 3 , 2.593184609
node37, 1 , 1 , 10.7602311
node37, 2 , 2 , 4.019522239
node37, 3 , 3 , 2.182842324
node38, 1 , 1 , 14.01949973
node38, 2 , 2 , 5.873805317
node38, 3 , 3 , 3.541098926
node39, 1 , 1 , 16.69693801
node39, 2 , 2 , 5.298481933
node39, 3 , 3 , 4.763866042
node40, 1 , 1 , 19.09254289
node40, 2 , 2 , 4.540273367
node40, 3 , 3 , 5.584875831
node41, 1 , 1 , 21.91850996
node41, 2 , 2 , 4.658011709
node41, 3 , 3 , 5.844010524
node42, 1 , 1 , 25.73733264
node42, 2 , 2 , 5.337888209
node42, 3 , 3 , 7.937111436
node43, 1 , 1 , 7.393972984
node43, 2 , 2 , 2.018769946
node43, 3 , 3 , 3.445286252
node44, 1 , 1 , 10.82665583
node44, 2 , 2 , 4.130485545
node44, 3 , 3 , -0.137896028
node45, 1 , 1 , 13.25518939
node45, 2 , 2 , 6.861443584
node45, 3 , 3 , 2.308988386

node46, 1 , 1 , 16.54465819
node46, 2 , 2 , 8.447199575
node46, 3 , 3 , 4.811486425
node47, 1 , 1 , 18.49337973
node47, 2 , 2 , 7.53906846
node47, 3 , 3 , 6.095870533
node48, 1 , 1 , 21.56923611
node48, 2 , 2 , 7.970790051
node48, 3 , 3 , 6.83387306
node49, 1 , 1 , 25.04333324
node49, 2 , 2 , 8.816894866
node49, 3 , 3 , 8.782559613
node50, 1 , 1 , 5.46860348
node50, 2 , 2 , 2.925283211
node50, 3 , 3 , 5.058204813
node51, 1 , 1 , 7.598826159
node51, 2 , 2 , 3.714520926
node51, 3 , 3 , 4.476158655
node52, 1 , 1 , 7.581067472
node52, 2 , 2 , 7.415654146
node52, 3 , 3 , 3.814627223
node53, 1 , 1 , 13.78229516
node53, 2 , 2 , 10.53345984
node53, 3 , 3 , 3.766457412
node54, 1 , 1 , 16.83798399
node54, 2 , 2 , 11.09064161
node54, 3 , 3 , 5.62503612
node55, 1 , 1 , 20.39951766
node55, 2 , 2 , 11.16912147
node55, 3 , 3 , 7.256066044
node56, 1 , 1 , 22.63344799

node56, 2 , 2 , 11.79099399
node56, 3 , 3 , 9.45683027
node57, 1 , 1 , 5.303066781
node57, 2 , 2 , 2.616304675
node57, 3 , 3 , 4.445553004
node58, 1 , 1 , 8.173552803
node58, 2 , 2 , 6.665787703
node58, 3 , 3 , 4.339097574
node59, 1 , 1 , 9.643311929
node59, 2 , 2 , 10.2136183
node59, 3 , 3 , 3.531946734
node60, 1 , 1 , 12.49538029
node60, 2 , 2 , 12.72474174
node60, 3 , 3 , 3.663603951
node61, 1 , 1 , 15.97338757
node61, 2 , 2 , 14.74379979
node61, 3 , 3 , 5.416853952
node62, 1 , 1 , 19.42230562
node62, 2 , 2 , 14.3838188
node62, 3 , 3 , 7.045832837
node63, 1 , 1 , 22.64775881
node63, 2 , 2 , 15.51018098
node63, 3 , 3 , 8.85027208
node64, 1 , 1 , 5.40138452
node64, 2 , 2 , 6.519795004
node64, 3 , 3 , 4.366070717
node65, 1 , 1 , 7.397784003
node65, 2 , 2 , 11.42943638
node65, 3 , 3 , 5.024787204
node66, 1 , 1 , 9.736244401
node66, 2 , 2 , 14.05167359

node66, 3 , 3 , 5.135334518
node67, 1 , 1 , 11.98332109
node67, 2 , 2 , 15.86863498
node67, 3 , 3 , 5.453367809
node68, 1 , 1 , 16.77645267
node68, 2 , 2 , 17.37832741
node68, 3 , 3 , 6.93044802
node69, 1 , 1 , 20.74926937
node69, 2 , 2 , 18.47051804
node69, 3 , 3 , 8.629454391
node70, 1 , 1 , 22.17525446
node70, 2 , 2 , 17.60242834
node70, 3 , 3 , 12.45183785
node71, 1 , 1 , 4.392544214
node71, 2 , 2 , 14.58025787
node71, 3 , 3 , 5.49343293
node72, 1 , 1 , 8.622019189
node72, 2 , 2 , 15.85232736
node72, 3 , 3 , 5.086247918
node73, 1 , 1 , 9.391282857
node73, 2 , 2 , 17.01982621
node73, 3 , 3 , 4.855406932
node74, 1 , 1 , 13.80455359
node74, 2 , 2 , 19.52863277
node74, 3 , 3 , 7.20889358
node75, 1 , 1 , 16.38023779
node75, 2 , 2 , 21.34465876
node75, 3 , 3 , 9.764571641
node76, 1 , 1 , 19.87906788
node76, 2 , 2 , 22.53398687
node76, 3 , 3 , 14.59638378

node77, 1 , 1 , 18.21261918

node77, 2 , 2 , 18.22873494

node77, 3 , 3 , 14.47710018

**

** OUTPUT REQUESTS

**

*Restart, write, frequency=1

*Output, field

*Node Output

COORD, U

*Element Output

3

EE

*Output, history, variable=PRESELECT

*El Print, freq=999999

*Node Print, freq=999999

*End Step

APPENDIX B

INPUT FILE FOR FINITE ELEMENT PRE-PROCESSOR: COMPOSITE MODEL

```
title COMPOSITE FINITE ELEMENT MODEL

    c ... This is a subject-specific model of the glenohumeral capsule ...
    c ... AB-IGHL, PB-IGHL, Axillary pouch, Anterosuperior, and Posterior regions were
    included...
    c ... The articular cartilage of the humeral head was included in the geometry of the
    humerus since it is considered rigid  ...

    c === CONTROL DEFINITIONS ===
    c === POST-TRUEGRID MODIFICATIONS TO NIKE3D INPUT FILE ===
    nikeopts
    c ... CONTROL CARD 3 ...
     auto              c enable automatic timestepping
     nsteps 10           c number of timesteps
     delt 0.1            c initial delta-t
     mnss 1.0e-4           c minimum allowable timestep size
     mxss 0.10           c maximum allowable timestep size (negative = must point
     opnit 20            c optimal number of iterations per timestep
    c ... CONTROL CARD 4 ...
    c grav 7.071 0 -7.071 1
    c ... CONTROL CARD 5 ...
```

```
 iprt 999              c printout interval (keeps n3dhsp from getting huge)
 iplt 2               c plotting interval (plot every step to n3plot files)
 sw3                  c enable sense switch 3 (verbose output of augmented lag
 sw6                  c enable sense switch 6 (verbose output of convergence i
 igapfg 1              c interface gap plot flag
c ... CONTROL CARD 6 ...
 nsmd bfgs             c use bfgs solution method
 bwmo on               c bandwidth minimization on
 nbsr 1               c number of steps between stiffness reforms (every step)
 nbei 1               c number of steps between equilibrium iterations (every
 nibsr 1              c max number of equil (bfgs) iterations between stiffnes
 msrf 50              c maximum number of stiffness reforms per timestep
 dctol -0.01           c displacement norm convergence tolerance
 ectol 0.001          c energy norm convergence tolerance
c ... CONTROL CARD 7 ...
c anal dyn             c analysis type
c ... CONTROL CARD 8 ...
 maxmem 0
 stifcore 1           c store stiffness matrix in core (always do this - defau
 bfgscore             c store bfgs vectors in core (always do this - default i
 bfor 10              c brick element formulation (1 = bbar, 10 = 1 plus incor
 brstif               c enable brick element geometric stiffness
 lsolver fissle        c use fissle linear equation solver (this is default)
 nrest 999            c number of steps between restart file generation
 nsbrr 0              c number of steps between running restart file generatio
c altol 0.01           c set tolerance for augmented lagrangian iterations (ena
;
```

c ===Define Kinematics of Humeral Registration Block (i.e. True Grid Global C.S.) with respect to Scapular Registration Block using Load Curves===

c === LOAD CURVE DEFINITIONS ===

c ... prescribed translation along the global x-axis for humerus ...

include
C:\Truegrid\SubSpecFEM\Kinematics\Joint_Kinematics\60ER\HumwrtScap\dx.txt

c ... prescribed translation along the global y-axis for humerus ...

include
C:\Truegrid\SubSpecFEM\Kinematics\Joint_Kinematics\60ER\HumwrtScap\dy.txt

c ... prescribed translation along the global z-axis for humerus ...

include
C:\Truegrid\SubSpecFEM\Kinematics\Joint_Kinematics\60ER\HumwrtScap\dz.txt

c ... prescribed rotation about global x-axis for humerus (external rotation)...

include
C:\Truegrid\SubSpecFEM\Kinematics\Joint_Kinematics\60ER\HumwrtScap\rx.txt

c ... prescribed rotation about global y-axis for humerus (abduction) ...

include
C:\Truegrid\SubSpecFEM\Kinematics\Joint_Kinematics\60ER\HumwrtScap\ry.txt

c ... prescribed rotation about global z-axis for humerus (extension)...

include
C:\Truegrid\SubSpecFEM\Kinematics\Joint_Kinematics\60ER\HumwrtScap\rz.txt

c ===Move parts such that the Humeral Registration Block is aligned with the True Grid global C.S.===

lev 1 levct 1 v -118.849 22.1506 77.1414 tf rt 0 0 0 rt 0.973839 0.22715 0.00639683 rt 0.0192865 -0.054571 -0.998324;;
pslv 1

c ===Define 1st material (AB-IGHL)===

nikemats 1 1
mhead ABIGHL
shell
shth 2.0
rho 0.0007
e 2.05
pr 0.4995;

c ===Define 2nd material (Axillary Pouch)===

nikemats 2 1
mhead AxPouch
shell
shth 2.0
rho 0.0007
e 4.92
pr 0.4995;

c ===Define 3rd material (PB-IGHL)===

nikemats 3 1
mhead PBIGHL

```
shell
shth 2.0
rho 0.0007
e 3.73
pr 0.4995;

c                ===Define 4th material (Anterosuperior Region)===

nikemats 4 1
mhead AntSup
shell
shth 2.0
rho 0.0007
e 2.12
pr 0.4995;

c                ===Define 5th material (Posterior Region)===

nikemats 5 1
mhead PostCaps
shell
shth 2.0
rho 0.0007
e 5.83
pr 0.4995;

c                ===Define 6th material (Humerus)===

nikemats 6 20
 mhead humerus material - rigid
 shell
```

```
shth 0.5
rho 1000
e 1e4
pr .3
xtrans 1
ytrans 2
ztrans 3
xrot 4
yrot 5
zrot 6
comflg 1  c center-of-mass flag (if "1", you need to provide coords below)
xcom 0
ycom 0
zcom 0
;

readmesh dyna3d
C:\Truegrid\SubSpecFEM\Simplified_Geometry\attempt8\Geometry\humerusv5sm.d
endpart

c                ===Define 7th material (Scapula)===

nikemats 7 20
mhead scapula material - rigid
shell
shth 0.5
rho 1000
e 1e4
pr .3
xtrans -1
ytrans -1
```

ztrans -1

xrot -1

yrot -1

zrot -1

comflg 1 c center-of-mass flag (if "1", you need to provide coords below)

xcom 16.1987

ycom 15.5346

zcom 94.167

;

readmesh dyna3d
C:\Truegrid\SubSpecFEM\Simplified_Geometry\attempt8\Geometry\scapulav6bsm.d

endpart

pplv

c ===Input Geometry of capsuloligamenous regions (AB-IGHL, PB-IGHL, Axillary pouch, Anteriorsuperior, and Posterior regions)===

vpsd 1
C:\Truegrid\SubSpecFEM\Simplified_Geometry\attempt8\Geometry\ABIGHLv9f.cor
C:\Truegrid\SubSpecFEM\Simplified_Geometry\attempt8\Geometry\ABIGHLv9f.elm;

vpsd 2
C:\Truegrid\SubSpecFEM\Simplified_Geometry\attempt8\Geometry\PBIGHLv8c.cor
C:\Truegrid\SubSpecFEM\Simplified_Geometry\attempt8\Geometry\PBIGHLv8c.elm;

vpsd 3
C:\Truegrid\SubSpecFEM\Simplified_Geometry\attempt8\Geometry\AxPouchv9f.cor
C:\Truegrid\SubSpecFEM\Simplified_Geometry\attempt8\Geometry\AxPouchv9f.elm;

vpsd 4
C:\Truegrid\SubSpecFEM\Simplified_Geometry\attempt8\Geometry\AntSupCapsv10c.cor
C:\Truegrid\SubSpecFEM\Simplified_Geometry\attempt8\Geometry\AntSupCapsv10c.elm;

```
vpsd 5
C:\Truegrid\SubSpecFEM\Simplified_Geometry\attempt8\Geometry\PostCapsv10c.cor
C:\Truegrid\SubSpecFEM\Simplified_Geometry\attempt8\Geometry\PostCapsv10c.elm;

merge

c ===Move surfaces the same amount as bones and registration blocks were moved (See
above)==

lev 1 levct 1 v -118.849 22.1506 77.1414 tf rt 0 0 0 rt 0.973839 0.22715 0.00639683 rt
0.0192865 -0.054571 -0.998324;;
pslv 1

c ===Import Curves used for creating meshes===

include
C:\Truegrid\SubSpecFEM\Simplified_Geometry\attempt8\3Dcurves\ABIGHL3Dcurves.txt
include
C:\Truegrid\SubSpecFEM\Simplified_Geometry\attempt8\3Dcurves\AxPouch3Dcurves.txt
include
C:\Truegrid\SubSpecFEM\Simplified_Geometry\attempt8\3Dcurves\PBIGHL3Dcurves.txt
include
C:\Truegrid\SubSpecFEM\Simplified_Geometry\attempt8\3Dcurves\AntSup3Dcurves.txt
include
C:\Truegrid\SubSpecFEM\Simplified_Geometry\attempt8\3Dcurves\PostCap3Dcurves.txt

c ===Create Mesh for ABIGHL

c ====mesh for ABIGHL===

block 1 3 5; 1 4 7 10 16; -1;
```

89 96.5 104; -96 -90 -65 -43 -39; -55;

c ===Move mesh with respect to the AB-IGHL surface===

tri 1 3; 1 5; -1; v -93.9775 76.4280 56.8798 tf rt 93.9775 -76.4280 -56.8798
rt 94.9616 -76.2571 -56.8315 rt 93.8051 -75.4434 -56.8507;
mbi 1 3; 1 5; -1; xyz 3.75607 2.66348 -1.18632
tri 1 3; 1 5; -1; v -105.448 65.6949 55.1480 tf rt 105.448 -65.6949 -55.1480
rt 106.361 -65.7056 -55.5561 rt 105.424 -64.6984 -55.2287;
mbi 1 3; 1 5; -1; xyz 4.64805 1.00077 -3.85280
mbi 1 3; 1 5; -1; xyz 2.29996 -0.167995 -1.17682
mbi 1 3; 1 5; -1; xyz -2.73335 -0.338181 1.40851
mbi 1 3; 1 5; -1; xyz 0.401512 -0.852127 -0.190453

c ===Attach edges of mesh to curves===

cure 3 1 1 3 2 1 10032
cure 3 2 1 3 4 1 3
cure 3 4 1 3 5 1 10031
curs 2 1 1 2 5 1 1005
cure 1 2 1 1 4 1 1001
cure 1 1 1 1 2 1 100112
cure 1 4 1 1 5 1 100111
curs 1 1 1 3 1 1 1004
curs 1 5 1 3 5 1 1002

c ==Manually move edges of mesh along curves===

pb 2 5 1 2 5 1 xyz 93.2409 -40.3031 -66.6451
pb 2 5 1 2 5 1 xyz 91.7412 -40.0011 -67.3080
pb 1 5 1 1 5 1 xyz 90.5344 -42.4738 -63.4847

pb 2 4 1 2 4 1 xyz 96.7856 -45.3001 -62.3383
pb 2 4 1 2 4 1 xyz 96.0593 -45.0866 -62.8391
pb 2 4 1 2 4 1 xyz 95.5101 -44.3431 -63.1756
pb 2 4 1 2 4 1 xyz 95.1356 -45.7164 -64.1275
pb 2 4 1 2 4 1 xyz 95.3609 -45.6257 -63.8033
pb 2 3 1 2 3 1 xyz 100.696 -60.8594 -60.0477
pb 2 3 1 2 3 1 xyz 100.762 -61.1074 -60.1813
pb 1 2 1 1 2 1 xyz 99.0825 -86.7569 -61.7780
pb 1 1 1 1 1 1 xyz 101.756 -95.1652 -65.7868
pb 2 1 1 2 1 1 xyz 103.606 -91.7460 -64.7023
pb 1 2 1 1 2 1 xyz 99.7349 -91.7329 -63.3302
pb 2 2 1 2 2 1 xyz 102.771 -88.1667 -63.2953
pb 2 2 1 2 2 1 xyz 102.233 -88.4592 -63.6269
pb 2 3 1 2 3 1 xyz 101.080 -68.8745 -60.6802
pb 1 3 1 1 3 1 xyz 96.1207 -72.8853 -58.3479
pb 2 3 1 2 3 1 xyz 101.085 -70.3803 -60.6351
pb 1 4 1 1 4 1 xyz 92.7571 -49.5436 -60.0227
pb 2 4 1 2 4 1 xyz 95.5277 -46.9637 -63.3701
pb 1 4 1 1 4 1 xyz 93.3148 -50.5880 -59.1106
pb 2 4 1 2 4 1 xyz 96.3280 -47.4752 -62.8540
pb 1 3 1 1 3 1 xyz 97.1909 -74.1196 -58.7196
pb 1 3 1 1 3 1 xyz 97.2025 -75.1687 -58.7475
pb 2 3 1 2 3 1 xyz 101.482 -71.6844 -60.5576
pb 2 2 1 2 2 1 xyz 101.750 -86.1421 -62.8927
pb 2 2 1 2 2 1 xyz 101.528 -83.4576 -62.5255
pb 2 3 1 2 3 1 xyz 100.860 -67.8889 -60.6404
pb 2 3 1 2 3 1 xyz 101.521 -68.6602 -60.6843
pb 2 4 1 2 4 1 xyz 96.3818 -45.8749 -62.2893
pb 2 4 1 2 4 1 xyz 96.0484 -44.5162 -62.7031
pb 2 2 1 2 2 1 xyz 101.568 -81.8916 -62.1524
pb 2 2 1 2 2 1 xyz 101.891 -82.9185 -62.2838

c ===Relax the mesh===

relaxi 1 2;4 5; ;50 .01 1

relaxi 1 2;3 4; ;50 .01 1

relaxi 2 3;4 5; ;50 .01 1

relaxi 2 3;3 4; ;50 .01 1

relaxi 1 2;2 3; ;50 .01 1

relaxi 2 3;2 3; ;50 .01 1

relaxi 1 2;1 2; ;50 .01 1

relaxi 2 3;1 2; ;50 .01 1

c ===Project mesh to surface of AB-IGHL===

sfi 1 2; 1 5; -1; sd 1

sfi 2 3; 4 5; -1; sd 1

sfi 2 3; 1 2; -1; sd 1

c ===scale elements in Medial-to-lateral direction such that elements near insertions sites are larger than those at midsubstance===

drs 1 1 1 3 5 1 j 0.8 0.8

c ===Assign ABIGHL to a Material Number===

mate 1

c ===This command flips direction of shell normals===

orpt flip

N 1 1 1 3 5 1

endpart

c ===Create mesh for axillary pouch===

c ===Mesh for Axillary Pouch===

block -1; 1 4 7 8 10 16; 1 4 6 9 12;
120; -88 -75 -62 -50.5 -41 -36; -98 -93.1 -83.3 -78.4 -63.7;

tri -1; 1 6; 1 5; v -120.447 35.8938 82.0004 tf rt 120.447 -35.8938 -82.0004 rt
121.426 -35.6905 -82.0144 rt 120.243 -34.9148 -82.0071;
tri -1; 1 6; 1 5; v -122.082 55.0150 96.3992 tf rt 122.082 -55.0150 -96.3992 rt
123.079 -55.0224 -96.4724 rt 122.088 -54.0151 -96.4151;
mbi -1; 1 6; 1 5; xyz -5.10420 -4.08356 0.563126
mbi -1; 1 6; 1 5; xyz -3.91766 6.24924 8.12576
tri -1; 1 6; 1 5; v -127.135 60.3896 62.6813 tf rt 127.135 -60.3896 -62.6813 rt
128.027 -60.3298 -62.2323 rt 127.020 -59.4010 -62.5843;
mbi -1; 1 6; 1 5; xyz -2.09879 4.74929 1.00466

cure 1 1 5 1 2 5 10032
cure 1 2 5 1 5 5 3
cure 1 5 5 1 6 5 10031
curs 1 1 4 1 1 5 1013
curs 1 1 3 1 1 4 12
curs 1 1 2 1 1 3 1011

pb 1 1 2 1 1 2 xyz 114.642 -77.3042 -84.3960

curs 1 1 1 1 1 2 1010

pb 1 1 1 1 1 1 xyz 111.354 -81.9808 -89.6369

curs 1 1 4 1 6 4 1014
curs 1 1 3 1 6 3 1015
curs 1 1 2 1 6 2 1016
cure 1 5 1 1 6 1 10091
cure 1 2 1 1 5 1 1009
cure 1 1 1 1 2 1 10092
curs 1 6 3 1 6 5 6
curs 1 6 1 1 6 3 8

pb 1 6 4 1 6 4 xyz 93.2139 -35.9489 -74.4809
pb 1 6 3 1 6 3 xyz 94.9597 -37.8927 -80.2797
pb 1 6 3 1 6 3 xyz 94.8199 -37.5748 -79.8665
pb 1 6 2 1 6 2 xyz 94.9751 -40.1662 -81.2644
pb 1 6 2 1 6 2 xyz 94.5931 -38.1831 -80.2884
pb 1 5 4 1 5 4 xyz 100.248 -37.1112 -75.3713
pb 1 5 4 1 5 4 xyz 97.6363 -38.2528 -74.4917
pb 1 5 3 1 5 3 xyz 102.791 -35.7502 -80.7380
pb 1 5 3 1 5 3 xyz 100.311 -37.2878 -79.5961
pb 1 5 2 1 5 2 xyz 104.460 -38.6193 -84.9063
pb 1 5 2 1 5 2 xyz 101.489 -38.2680 -83.7881
pb 1 5 2 1 5 2 xyz 100.636 -39.9708 -83.2114
pb 1 4 4 1 4 4 xyz 105.105 -43.8204 -72.3855
pb 1 4 3 1 4 3 xyz 107.004 -42.9719 -79.0657
pb 1 4 3 1 4 3 xyz 106.293 -43.7141 -78.8937
pb 1 4 3 1 4 3 xyz 106.512 -44.2694 -78.9869
pb 1 4 2 1 4 2 xyz 107.412 -44.8565 -86.0929
pb 1 4 2 1 4 2 xyz 106.327 -44.3733 -85.3942
pb 1 5 4 1 5 4 xyz 96.6530 -37.9294 -74.2007
pb 1 5 3 1 5 3 xyz 98.7405 -38.0712 -79.0902

pb 1 5 2 1 5 2 xyz 99.8011 -39.3778 -82.5212
pb 1 5 2 1 5 2 xyz 98.9061 -39.8738 -82.5665
pb 1 6 4 1 6 4 xyz 93.0052 -35.6546 -74.7800
pb 1 6 3 1 6 3 xyz 93.9590 -35.0609 -77.6632
pb 1 6 2 1 6 2 xyz 94.2669 -37.8551 -80.1240
pb 1 3 4 1 3 4 xyz 108.736 -54.0537 -71.0281
pb 1 3 4 1 3 4 xyz 110.319 -54.8494 -70.1941
pb 1 3 3 1 3 3 xyz 111.740 -54.5896 -79.1039
pb 1 3 2 1 3 2 xyz 111.678 -55.3371 -86.7412
pb 1 3 2 1 3 2 xyz 111.530 -54.7493 -86.7582
pb 1 2 4 1 2 4 xyz 112.677 -69.0060 -70.3767
pb 1 2 3 1 2 3 xyz 115.591 -66.8486 -78.3129
pb 1 2 2 1 2 2 xyz 115.887 -67.0405 -85.6614
pb 1 4 4 1 4 4 xyz 103.350 -42.6827 -72.2501
pb 1 4 3 1 4 3 xyz 105.279 -41.4093 -79.4632
pb 1 4 3 1 4 3 xyz 105.183 -42.7402 -79.1923
pb 1 4 2 1 4 2 xyz 104.729 -43.3712 -85.2720
pb 1 2 4 1 2 4 xyz 113.857 -75.1227 -70.0603
pb 1 2 4 1 2 4 xyz 112.390 -72.5500 -70.6209
pb 1 2 3 1 2 3 xyz 116.314 -71.3286 -78.0179
pb 1 2 2 1 2 2 xyz 116.142 -72.5538 -83.4486
pb 1 2 2 1 2 2 xyz 115.756 -73.3836 -84.9074
pb 1 5 4 1 5 4 xyz 98.7266 -40.8225 -73.2214
pb 1 5 3 1 5 3 xyz 100.154 -40.7053 -78.7668
pb 1 5 2 1 5 2 xyz 100.397 -41.6327 -82.7121
pb 1 4 4 1 4 4 xyz 104.439 -44.5747 -72.0633
pb 1 4 4 1 4 4 xyz 107.306 -46.6952 -70.9215
pb 1 4 4 1 4 4 xyz 107.929 -48.3183 -70.7999
pb 1 3 4 1 3 4 xyz 112.147 -56.4337 -69.7016
pb 1 3 3 1 3 3 xyz 112.400 -54.8227 -78.9746
pb 1 4 3 1 4 3 xyz 109.865 -45.5758 -78.7865

pb 1 4 2 1 4 2 xyz 108.910 -46.9918 -83.8058
pb 1 3 2 1 3 2 xyz 113.710 -56.1617 -86.4523
pb 1 3 4 1 3 4 xyz 111.247 -58.1977 -70.1068
pb 1 3 4 1 3 4 xyz 111.671 -59.5173 -70.1115
pb 1 3 4 1 3 4 xyz 110.819 -58.8944 -70.1815
pb 1 3 3 1 3 3 xyz 112.760 -56.2647 -78.4713
pb 1 3 3 1 3 3 xyz 112.456 -56.3476 -79.1808
pb 1 3 2 1 3 2 xyz 112.923 -57.7285 -86.4392
pb 1 4 2 1 4 2 xyz 109.429 -49.2426 -86.3612
pb 1 4 3 1 4 3 xyz 109.365 -48.6507 -79.1483
pb 1 4 3 1 4 3 xyz 109.001 -48.2634 -79.0281
pb 1 4 4 1 4 4 xyz 108.404 -50.6103 -70.3842

relaxi ;5 6;4 5;50 .01 1
relaxi ;5 6;3 4;50 .01 1
relaxi ;5 6;2 3;50 .01 1
relaxi ;5 6;1 2;50 .01 1
relaxi ;4 5;4 5;50 .01 1
relaxi ;4 5;3 4;50 .01 1
relaxi ;4 5;2 3;50 .01 1
relaxi ;4 5;1 2;50 .01 1
relaxi ;3 4;4 5;50 .01 1
relaxi ;3 4;3 4;50 .01 1
relaxi ;3 4;2 3;50 .01 1
relaxi ;3 4;1 2;50 .01 1
relaxi ;2 3;4 5;50 .01 1
relaxi ;2 3;3 4;50 .01 1
relaxi ;2 3;2 3;50 .01 1
relaxi ;2 3;1 2;50 .01 1
relaxi ;1 2;4 5;50 .01 1
relaxi ;1 2;3 4;50 .01 1

relaxi ;1 2;2 3;50 .01 1

relaxi ;1 2;1 2;50 .01 1

sfi -1; 5 6; 4 5;sd 3

sfi -1; 5 6; 1 2;sd 3

sfi -1; 1 2; 4 5;sd 3

sfi -1; 2 3; 1 3;sd 3

sfi -1; 2 3; 3 4;sd 3

sfi -1; 4 5; 2 3;sd 3

sfi -1; 3 4; 2 3;sd 3

sfi -1; 3 4; 1 2;sd 3

sfi -1; 4 5; 1 2;sd 3

drs 1 1 1 1 6 5 j 0.8 0.8

c ===Assign Axillary Pouch to a Material Number===

mate 2

c ===This command flips direction of shell normals===

orpt flip

N 1 1 1 1 6 5

endpart

c ===create mesh for PBIGHL===

c ====mesh for PBIGHL===

block 1 2 3; 1 4 6 7 10 16; -1;
94 100 105; -85 -83 -77 -66 -50 -41; -115

tri 1 3; 1 6; -1; v -96.3523 48.9756 117.953 tf rt 96.3523 -48.9756 -117.953
rt 97.3076 -48.6865 -118.016 rt 96.0647 -48.0183 -117.922;
tri 1 3; 1 6; -1; v -105.506 60.9310 116.725 tf rt 105.506 -60.9310 -116.725
rt 104.868 -61.4810 -117.263 rt 104.941 -60.1211 -116.882;
mbi 1 3; 1 6; -1; xyz 2.01991 0.517258 11.8227
mbi 1 3; 1 6; -1; xyz 2.71159 -3.69324 1.18745

cure 1 5 1 1 6 1 10091
cure 1 2 1 1 5 1 1009
cure 1 1 1 1 2 1 10092
curs 2 1 1 2 6 1 1022
cure 3 1 1 3 2 1 10191
cure 3 2 1 3 5 1 19
cure 3 5 1 3 6 1 10192

pb 2 6 1 2 6 1 xyz 97.3775 -37.6621 -92.6625
pb 2 6 1 2 6 1 xyz 93.1251 -37.6483 -87.2323
pb 3 6 1 3 6 1 xyz 95.0622 -39.1954 -95.9348
pb 3 6 1 3 6 1 xyz 92.0778 -42.7351 -91.1813

curs 1 6 1 3 6 1 1018

pb 2 1 1 2 1 1 xyz 115.167 -84.5306 -92.6534
pb 2 1 1 2 1 1 xyz 113.694 -85.4483 -91.1462
pb 3 1 1 3 1 1 xyz 114.087 -84.8014 -93.7202
pb 3 1 1 3 1 1 xyz 113.608 -86.6956 -92.8124
pb 3 1 1 3 1 1 xyz 112.922 -87.0840 -91.9949

pb 2 1 1 2 1 1 xyz 113.101 -85.2762 -90.8199

curs 1 1 1 3 1 1 1020

pb 2 5 1 2 5 1 xyz 102.407 -47.2588 -99.1236
pb 3 5 1 3 5 1 xyz 100.262 -47.5818 -101.158
pb 2 5 1 2 5 1 xyz 101.082 -45.9979 -96.1860
pb 2 4 1 2 4 1 xyz 109.866 -63.7720 -98.7474
pb 3 2 1 3 2 1 xyz 112.782 -78.6422 -97.1785
pb 3 2 1 3 2 1 xyz 113.381 -80.3407 -96.8204
pb 2 2 1 2 2 1 xyz 113.278 -77.9512 -94.7142
pb 2 3 1 2 3 1 xyz 111.612 -73.6430 -96.0395
pb 2 4 1 2 4 1 xyz 110.887 -63.2626 -98.9521
pb 3 4 1 3 4 1 xyz 109.002 -63.7895 -100.212
pb 2 4 1 2 4 1 xyz 110.090 -62.2503 -99.3487
pb 3 5 1 3 5 1 xyz 98.7584 -48.3133 -99.1875
pb 3 5 1 3 5 1 xyz 97.7137 -48.1568 -98.2237
pb 2 5 1 2 5 1 xyz 99.6376 -46.3814 -94.8731
pb 2 5 1 2 5 1 xyz 99.0424 -45.6912 -93.8777
pb 2 5 1 2 5 1 xyz 99.3205 -47.1737 -93.4309
pb 3 4 1 3 4 1 xyz 109.388 -62.2898 -101.092
pb 2 4 1 2 4 1 xyz 110.360 -61.6382 -99.6644
pb 2 4 1 2 4 1 xyz 110.323 -61.5573 -99.7520
pb 3 3 1 3 3 1 xyz 111.974 -73.9936 -97.6350
pb 2 3 1 2 3 1 xyz 112.320 -72.7713 -96.3744
pb 3 3 1 3 3 1 xyz 111.619 -72.9761 -98.3642
pb 3 3 1 3 3 1 xyz 111.955 -73.2307 -98.3157
pb 3 2 1 3 2 1 xyz 111.208 -77.9598 -95.7547
pb 2 2 1 2 2 1 xyz 112.459 -77.3567 -94.7573
pb 2 2 1 2 2 1 xyz 112.689 -77.1433 -94.8596
pb 3 4 1 3 4 1 xyz 109.987 -63.2975 -101.108

```
pb 2 4 1 2 4 1 xyz 111.128 -62.6068 -99.7336
pb 3 4 1 3 4 1 xyz 110.089 -63.7183 -100.740
pb 3 3 1 3 3 1 xyz 111.906 -74.6669 -97.8913
pb 2 3 1 2 3 1 xyz 112.606 -73.7374 -96.1338
pb 3 3 1 3 3 1 xyz 112.224 -75.4132 -97.3794
pb 2 3 1 2 3 1 xyz 112.603 -74.3448 -95.8257
pb 2 3 1 2 3 1 xyz 112.524 -74.2816 -96.1194
pb 3 2 1 3 2 1 xyz 111.649 -79.0272 -95.8265
pb 2 2 1 2 2 1 xyz 112.932 -77.8327 -94.4723
pb 2 2 1 2 2 1 xyz 112.629 -77.6203 -94.6840

relaxi 1 2;5 6; ;50 .01 1
relaxi 2 3;5 6; ;50 .01 1
relaxi 1 2;4 5; ;50 .01 1
relaxi 2 3;4 5; ;50 .01 1
relaxi 1 2;3 4; ;50 .01 1
relaxi 2 3;3 4; ;50 .01 1
relaxi 1 2;2 3; ;50 .01 1
relaxi 2 3;2 3; ;50 .01 1
relaxi 1 2;1 2; ;50 .01 1
relaxi 2 3;1 2; ;50 .01 1

sfi 1 2; 1 6; -1; sd 2
sfi 2 3; 3 6; -1; sd 2

drs 1 1 1 3 6 1 j 0.8 0.8

c                    ===Assign PBIGHL to a Material Number===

mate 3
```

c ===This shell normals===

N 1 1 1 3 6 1

endpart

c ===create mesh for AntSup===

c ====mesh for AntSup===

block -1; 1 2 7 10 13 16; 1 3 5 7 9 12 14 16 18 20;
120; -88 -75 -62 -50.5 -41 -36; -100 -95 -90 -85 -80 -75 -70 -65 -60 -55;

tri -1; 1 6; 1 10; v -118.590 39.7391 77.1956 tf rt 118.590 -39.7391 -77.1956
rt 119.468 -39.2601 -77.1882 rt 118.111 -38.8613 -77.1924;
tri -1; 1 6; 1 10; v -128.965 55.9695 64.3746 tf rt 128.965 -55.9695 -64.3746
rt 129.025 -56.5624 -65.1776 rt 128.487 -55.2801 -64.9193;
mbi -1; 1 6; 1 10; xyz -33.4324 -18.2178 13.2019
tri -1; 1 6; 1 10; v -138.013 82.3475 62.9894 tf rt 138.013 -82.3475 -62.9894
rt 139.011 -82.3806 -63.0462 rt 138.051 -81.3523 -62.8993;
tri -1; 1 6; 1 10; v -60.6149 72.1447 40.5616 tf rt 60.6149 -72.1447 -40.5616
rt 61.2909 -72.1447 -39.8247 rt 60.4641 -71.1659 -40.4233;
mbi -1; 1 6; 1 10; xyz -16.7127 -7.08531 -11.6468
mbi -1; 1 6; 1 10; xyz 5.62075 -1.58540 -14.5993
tri -1; 1 6; 1 10; v -78.7730 66.1364 47.2190 tf rt 78.7730 -66.1364 -47.2190
rt 79.7295 -66.0840 -46.9320 rt 78.6887 -65.1450 -47.1190;
tri -1; 1 6; 1 10; v -85.9853 106.300 50.2903 tf rt 85.9853 -106.300 -50.2903
rt 86.9768 -106.178 -50.3360 rt 85.8672 -105.310 -50.2152;
tri -1; 1 6; 1 10; v -78.9972 75.3193 78.2645 tf rt 78.9972 -75.3193 -78.2645
rt 79.9786 -75.1565 -78.1623 rt 78.8517 -74.3427 -78.4226;
mbi -1; 1 6; 1 10; xyz -3.66074 -2.79346 -5.60698

cure 1 1 1 1 2 1 100331

cure 1 2 1 1 5 1 10033

cure 1 5 1 1 6 1 100332

curs 1 1 2 1 6 2 10041

curs 1 1 3 1 6 3 10036

curs 1 1 4 1 6 4 10042

curs 1 1 5 1 6 5 10039

curs 1 1 6 1 6 6 10037

curs 1 1 7 1 6 7 10043

curs 1 1 8 1 6 8 10038

curs 1 1 9 1 6 9 10040

curs 1 1 1 1 1 9 322

cure 1 1 10 1 2 10 100112

cure 1 2 10 1 5 10 1001

cure 1 5 10 1 6 10 100111

curs 1 6 1 1 6 6 10034

curs 1 6 6 1 6 10 10035

pb 1 6 2 1 6 2 xyz 68.2319 -77.8539 -80.7488

pb 1 6 3 1 6 3 xyz 67.7948 -75.4228 -74.2097

pb 1 6 4 1 6 4 xyz 67.8628 -74.6035 -71.6923

pb 1 6 4 1 6 4 xyz 68.1904 -73.2091 -71.6737

pb 1 6 5 1 6 5 xyz 68.3423 -72.3750 -66.5282

pb 1 6 7 1 6 7 xyz 74.8349 -55.9083 -59.9143

pb 1 6 7 1 6 7 xyz 75.0687 -55.5157 -60.2063

pb 1 6 8 1 6 8 xyz 79.3625 -48.9093 -59.2097

pb 1 6 8 1 6 8 xyz 80.0650 -49.2664 -60.8007

pb 1 6 9 1 6 9 xyz 85.4810 -46.1826 -61.6824

pb 1 6 9 1 6 9 xyz 84.3619 -45.3063 -62.0976

pb 1 1 2 1 1 2 xyz 93.2291 -107.125 -79.5811

pb 1 1 3 1 1 3 xyz 93.6882 -104.128 -77.0874
pb 1 1 4 1 1 4 xyz 95.2172 -102.248 -76.1272
pb 1 1 5 1 1 5 xyz 94.8203 -102.214 -75.7431
pb 1 1 6 1 1 6 xyz 94.7017 -103.538 -72.5905
pb 1 1 7 1 1 7 xyz 96.1449 -101.246 -70.2275
pb 1 1 8 1 1 8 xyz 97.3217 -100.193 -69.2480
pb 1 1 8 1 1 8 xyz 98.4439 -98.6055 -69.3691
pb 1 1 9 1 1 9 xyz 99.2866 -96.3526 -67.7567
pb 1 1 9 1 1 9 xyz 99.9709 -96.3541 -66.0459
pb 1 2 2 1 2 2 xyz 83.4877 -106.776 -74.7091
pb 1 2 3 1 2 3 xyz 80.1905 -104.020 -72.3349
pb 1 2 4 1 2 4 xyz 81.7304 -103.046 -68.2886
pb 1 2 5 1 2 5 xyz 85.9849 -100.662 -64.7347
pb 1 2 6 1 2 6 xyz 89.4060 -97.6667 -60.1887
pb 1 2 7 1 2 7 xyz 92.8592 -96.6771 -60.0165
pb 1 2 8 1 2 8 xyz 94.0606 -92.8131 -59.8558
pb 1 2 9 1 2 9 xyz 97.1143 -90.4271 -62.5367
pb 1 4 2 1 4 2 xyz 65.9871 -92.9967 -77.8169
pb 1 5 2 1 5 2 xyz 64.9565 -83.6766 -78.6430
pb 1 3 2 1 3 2 xyz 71.3240 -99.0210 -75.4489
pb 1 5 8 1 5 8 xyz 81.7657 -61.1329 -54.2861
pb 1 5 8 1 5 8 xyz 81.0857 -58.2198 -54.5307
pb 1 5 9 1 5 9 xyz 86.9351 -50.4310 -58.8272
pb 1 5 8 1 5 8 xyz 80.4929 -55.7167 -56.8895
pb 1 5 7 1 5 7 xyz 75.9712 -63.2500 -57.3777
pb 1 5 7 1 5 7 xyz 75.6611 -61.9000 -57.2308
pb 1 5 3 1 5 3 xyz 64.9870 -80.1670 -72.5175
pb 1 4 9 1 4 9 xyz 90.7582 -66.4446 -53.6418
pb 1 2 3 1 2 3 xyz 84.8517 -103.802 -73.4411
pb 1 2 4 1 2 4 xyz 86.0508 -101.912 -69.6976
pb 1 2 5 1 2 5 xyz 88.5452 -100.287 -69.2233

pb 1 2 6 1 2 6 xyz 90.0094 -97.2504 -65.8767

pb 1 2 8 1 2 8 xyz 94.1238 -92.5640 -63.6347

pb 1 3 2 1 3 2 xyz 73.7652 -99.7877 -77.5665

pb 1 3 3 1 3 3 xyz 73.2422 -98.7369 -71.3419

pb 1 3 4 1 3 4 xyz 75.8032 -95.6866 -66.3028

pb 1 3 5 1 3 5 xyz 78.0950 -93.3446 -62.5786

pb 1 3 6 1 3 6 xyz 83.1148 -88.1169 -59.3747

pb 1 3 7 1 3 7 xyz 85.6617 -84.8997 -58.9786

pb 1 3 8 1 3 8 xyz 88.6142 -82.6535 -57.3131

pb 1 3 9 1 3 9 xyz 93.6224 -77.7721 -56.9393

pb 1 4 2 1 4 2 xyz 69.9356 -94.8959 -76.8944

pb 1 4 3 1 4 3 xyz 70.1866 -93.3878 -70.8382

pb 1 4 4 1 4 4 xyz 72.9159 -89.9179 -66.7865

pb 1 4 4 1 4 4 xyz 70.1969 -90.3154 -65.6442

pb 1 4 5 1 4 5 xyz 74.2726 -84.7649 -62.9101

pb 1 4 6 1 4 6 xyz 78.2945 -81.7354 -56.9539

pb 1 4 6 1 4 6 xyz 76.7043 -80.7809 -56.7899

pb 1 4 7 1 4 7 xyz 81.6249 -76.2807 -56.5081

pb 1 4 8 1 4 8 xyz 86.2436 -74.9760 -53.1988

pb 1 4 8 1 4 8 xyz 84.6516 -72.9152 -53.8070

pb 1 4 5 1 4 5 xyz 73.0475 -86.6945 -61.1030

pb 1 2 4 1 2 4 xyz 86.7476 -102.013 -71.5460

pb 1 2 3 1 2 3 xyz 85.6509 -102.816 -74.0423

pb 1 2 2 1 2 2 xyz 85.6012 -104.725 -79.1638

pb 1 5 3 1 5 3 xyz 65.6560 -82.3726 -72.3306

pb 1 5 4 1 5 4 xyz 67.1797 -79.8715 -68.2769

pb 1 5 5 1 5 5 xyz 69.4397 -77.2701 -64.2293

pb 1 5 6 1 5 6 xyz 72.7505 -70.1355 -57.9586

pb 1 5 7 1 5 7 xyz 76.3092 -64.5250 -55.5483

pb 1 5 8 1 5 8 xyz 80.8319 -56.3562 -55.5271

pb 1 5 9 1 5 9 xyz 86.8022 -51.1950 -57.3324

pb 1 5 8 1 5 8 xyz 81.7599 -56.9206 -54.5974

pb 1 5 9 1 5 9 xyz 87.9710 -53.7101 -56.0604
pb 1 5 8 1 5 8 xyz 81.4270 -58.3158 -54.3941
pb 1 5 8 1 5 8 xyz 81.6084 -58.9068 -54.2826
pb 1 5 8 1 5 8 xyz 81.3783 -59.0320 -54.5124
pb 1 5 7 1 5 7 xyz 76.6403 -65.6793 -55.6329
pb 1 5 6 1 5 6 xyz 73.5144 -71.2719 -57.5435
pb 1 5 2 1 5 2 xyz 66.0757 -85.4502 -78.0865
pb 1 5 3 1 5 3 xyz 65.1196 -83.2465 -72.1899
pb 1 5 4 1 5 4 xyz 67.1712 -80.5184 -67.5701
pb 1 5 5 1 5 5 xyz 69.0491 -77.7809 -63.7929
pb 1 4 9 1 4 9 xyz 91.3654 -68.0779 -54.6735
pb 1 4 8 1 4 8 xyz 85.3091 -73.9809 -54.3436
pb 1 4 8 1 4 8 xyz 85.3570 -74.3661 -54.8279
pb 1 4 7 1 4 7 xyz 81.4821 -78.6464 -55.9869
pb 1 4 6 1 4 6 xyz 78.1527 -82.8506 -57.2780
pb 1 4 5 1 4 5 xyz 73.7992 -88.2202 -61.1950
pb 1 4 4 1 4 4 xyz 71.4411 -91.1936 -65.3520
pb 1 4 2 1 4 2 xyz 69.4423 -95.9033 -77.2178
pb 1 4 3 1 4 3 xyz 69.7894 -94.3393 -71.4251
pb 1 3 2 1 3 2 xyz 75.6605 -100.160 -77.4948
pb 1 3 3 1 3 3 xyz 75.7497 -99.2438 -72.7004
pb 1 3 4 1 3 4 xyz 77.2575 -96.9218 -67.4710
pb 1 3 5 1 3 5 xyz 79.8196 -93.9782 -63.5205
pb 1 3 6 1 3 6 xyz 83.1735 -89.6165 -59.4387
pb 1 3 7 1 3 7 xyz 85.7459 -86.8837 -57.8390
pb 1 3 8 1 3 8 xyz 88.8495 -83.7124 -57.3877
pb 1 3 9 1 3 9 xyz 92.9823 -78.5965 -57.7351

pb 1 4 9 1 4 9 xyz 91.3287 -69.7517 -55.1326

pb 1 4 8 1 4 8 xyz 85.9316 -76.6608 -55.1192
pb 1 4 7 1 4 7 xyz 82.5465 -80.3487 -56.0952
pb 1 4 6 1 4 6 xyz 79.3802 -84.3052 -57.5671
pb 1 4 5 1 4 5 xyz 75.0517 -90.2814 -61.5611
pb 1 4 5 1 4 5 xyz 74.6668 -89.4261 -61.4788
pb 1 4 4 1 4 4 xyz 72.6537 -92.8515 -66.2406
pb 1 4 4 1 4 4 xyz 72.2810 -92.6374 -65.9620
pb 1 4 3 1 4 3 xyz 70.6308 -95.3150 -71.6066
pb 1 4 2 1 4 2 xyz 70.0549 -96.8863 -77.3289
pb 1 3 9 1 3 9 xyz 93.2976 -79.3814 -57.8383
pb 1 3 8 1 3 8 xyz 89.2774 -84.6517 -57.3359
pb 1 3 7 1 3 7 xyz 86.2682 -88.0881 -57.9083
pb 1 3 7 1 3 7 xyz 86.4996 -88.5544 -58.1529
pb 1 3 6 1 3 6 xyz 84.1699 -90.9772 -60.1115
pb 1 3 5 1 3 5 xyz 80.9217 -94.8261 -63.9969
pb 1 3 4 1 3 4 xyz 77.7635 -97.7869 -68.3064
pb 1 3 3 1 3 3 xyz 76.7314 -100.083 -72.3256
pb 1 3 2 1 3 2 xyz 76.1318 -100.782 -77.8046

relaxi ;5 6;1 2;50 .01 1
relaxi ;5 6;2 3;50 .01 1
relaxi ;5 6;3 4;50 .01 1
relaxi ;5 6;4 5;50 .01 1
relaxi ;5 6;5 6;50 .01 1
relaxi ;5 6;6 7;50 .01 1
relaxi ;5 6;7 8;50 .01 1
relaxi ;5 6;8 9;50 .01 1
relaxi ;5 6;9 10;50 .01 1
relaxi ;1 2;1 2;50 .01 1
relaxi ;1 2;2 3;50 .01 1
relaxi ;1 2;3 4;50 .01 1

relaxi ;1 2;4 5;50 .01 1

relaxi ;1 2;5 6;50 .01 1

relaxi ;1 2;6 7;50 .01 1

relaxi ;1 2;7 8;50 .01 1

relaxi ;1 2;8 9;50 .01 1

relaxi ;1 2;9 10;50 .01 1

relaxi ;2 5;1 2;50 .01 1

relaxi ;2 5;2 3;50 .01 1

relaxi ;2 5;3 4;50 .01 1

relaxi ;2 5;4 5;50 .01 1

relaxi ;2 5;5 6;50 .01 1

relaxi ;2 5;6 7;50 .01 1

relaxi ;2 5;7 8;50 .01 1

relaxi ;2 5;8 9;50 .01 1

relaxi ;2 5;9 10;50 .01 1

sfi ;5 6;1 10;sd 4

sfi ;1 2;1 10;sd 4

sfi ;2 5;1 2;sd 4

sfi ;2 4;2 3;sd 4

sfi ;2 5;3 4;sd 4

sfi ;2 5;4 5;sd 4

sfi ;4 5;5 6;sd 4

sfi ;2 3;5 6;sd 4

sfi ;2 5;6 7;sd 4

sfi ;2 5;7 8;sd 4

c sfi ;2 4;8 9;sd 4

sfi ;3 4;8 9;sd 4

sfi ;2 3;9 10;sd 4

drs 1 1 1 1 6 10 j 0.8 0.8

c ===Assign Anterosuperior to a Material Number===

mate 4

c ===This command flips direction of shell normals===
c orpt flip

c N 1 1 1 1 6 10

endpart

c ===create mesh for Posterior ===

c ====mesh for Posterior ===

block -1; 1 2 7 11 13 16; 1 4 7 10 13 16 18 19 22 25;
120; -88 -75 -62 -50.5 -41 -36; -100 -95 -90 -85 -80 -75 -70 -65 -60 -55;

tri -1; 1 6; 1 10; v -118.590 39.7391 77.1956 tf rt 118.590 -39.7391 -77.1956
rt 119.468 -39.2601 -77.1882 rt 118.111 -38.8613 -77.1924;
tri -1; 1 6; 1 10; v -128.965 55.9695 64.3746 tf rt 128.965 -55.9695 -64.3746
rt 129.025 -56.5624 -65.1776 rt 128.487 -55.2801 -64.9193;
mbi -1; 1 6; 1 10; xyz -33.4324 -18.2178 13.2019
tri -1; 1 6; 1 10; v -138.013 82.3475 62.9894 tf rt 138.013 -82.3475 -62.9894
rt 139.011 -82.3806 -63.0462 rt 138.051 -81.3523 -62.8993;
tri -1; 1 6; 1 10; v -60.6149 72.1447 40.5616 tf rt 60.6149 -72.1447 -40.5616
rt 61.2909 -72.1447 -39.8247 rt 60.4641 -71.1659 -40.4233;
mbi -1; 1 6; 1 10; xyz -16.7127 -7.08531 -11.6468

mbi -1; 1 6; 1 10; xyz 5.62075 -1.58540 -14.5993
tri -1; 1 6; 1 10; v -78.7730 66.1364 47.2190 tf rt 78.7730 -66.1364 -47.2190
rt 79.7295 -66.0840 -46.9320 rt 78.6887 -65.1450 -47.1190;
tri -1; 1 6; 1 10; v -85.9853 106.300 50.2903 tf rt 85.9853 -106.300 -50.2903
rt 86.9768 -106.178 -50.3360 rt 85.8672 -105.310 -50.2152;
tri -1; 1 6; 1 10; v -78.9972 75.3193 78.2645 tf rt 78.9972 -75.3193 -78.2645
rt 79.9786 -75.1565 -78.1623 rt 78.8517 -74.3427 -78.4226;
mbi -1; 1 6; 1 10; xyz -3.66074 -2.79346 -5.60698
mbi -1; 1 6; 1 10; xyz -0.204407 -14.1116 -67.1569
tri -1; 1 6; 1 10; v -61.9846 112.525 137.779 tf rt 61.9846 -112.525 -137.779
rt 62.4697 -113.111 -138.428 rt 61.7054 -111.925 -138.529;
mbi -1; 1 6; 1 10; xyz 11.7808 14.8445 28.0368
tri -1; 1 6; 1 10; v -72.4352 68.2734 63.1115 tf rt 72.4352 -68.2734 -63.1115
rt 73.3942 -68.5516 -63.0580 rt 72.7137 -67.3129 -63.1098;
mbi -1; 1 6; 1 10; xyz 3.83788 4.31287 -0.895767
mbi -1; 1 6; 1 10; xyz 8.10850 12.4390 -2.24456
tri -1; 1 6; 1 10; v -94.1657 67.9249 125.561 tf rt 94.1657 -67.9249 -125.561
rt 94.2409 -68.8390 -125.960 rt 93.2832 -67.7999 -126.015;
tri -1; 1 6; 1 10; v -77.8330 69.0849 52.7634 tf rt 77.8330 -69.0849 -52.7634
rt 78.8136 -69.2779 -52.8001 rt 78.0278 -68.1054 -52.7115;

cure 1 1 1 1 2 1 10191
cure 1 2 1 1 5 1 19
cure 1 5 1 1 6 1 10192
cure 1 1 10 1 2 10 100331
cure 1 2 10 1 5 10 10033
cure 1 5 10 1 6 10 100332
curs 1 1 2 1 6 2 10052
curs 1 1 3 1 6 3 10053
curs 1 1 4 1 6 4 10054
curs 1 1 5 1 6 5 10055

curs 1 1 6 1 6 6 10056

curs 1 1 7 1 6 7 10057

curs 1 1 8 1 6 8 10058

curs 1 1 9 1 6 9 10059

curs 1 6 1 1 6 10 50

curs 1 1 1 1 1 10 10051

pb 1 6 2 1 6 2 xyz 91.8008 -48.0032 -99.9552

pb 1 6 2 1 6 2 xyz 91.2274 -48.2701 -96.6502

pb 1 6 2 1 6 2 xyz 91.1379 -49.0386 -94.4854

pb 1 6 3 1 6 3 xyz 87.0038 -57.4732 -103.632

pb 1 6 4 1 6 4 xyz 83.7420 -63.3680 -103.651

pb 1 6 6 1 6 6 xyz 76.0348 -73.5688 -97.6331

pb 1 6 7 1 6 7 xyz 72.8627 -75.5164 -93.8023

pb 1 6 8 1 6 8 xyz 71.0976 -77.5235 -90.1101

pb 1 6 9 1 6 9 xyz 70.7344 -79.3619 -86.0919

pb 1 1 2 1 1 2 xyz 111.915 -88.7840 -92.2738

pb 1 1 3 1 1 3 xyz 109.740 -92.1213 -92.6000

pb 1 1 3 1 1 3 xyz 109.725 -92.2983 -91.9258

pb 1 1 3 1 1 3 xyz 109.641 -92.0410 -91.9688

pb 1 1 4 1 1 4 xyz 106.398 -95.0702 -92.2149

pb 1 1 5 1 1 5 xyz 105.186 -96.9597 -91.6969

pb 1 1 6 1 1 6 xyz 101.817 -98.9357 -91.0337

pb 1 1 7 1 1 7 xyz 96.4011 -103.729 -87.2441

pb 1 1 8 1 1 8 xyz 96.4328 -103.945 -86.6147

pb 1 1 9 1 1 9 xyz 93.1821 -107.752 -82.1031

pb 1 1 9 1 1 9 xyz 93.4061 -108.427 -82.4516

pb 1 2 2 1 2 2 xyz 110.825 -79.1752 -107.671

pb 1 2 3 1 2 3 xyz 108.680 -83.0216 -109.701

pb 1 2 4 1 2 4 xyz 103.094 -87.6997 -110.085

pb 1 2 5 1 2 5 xyz 97.6441 -91.9609 -109.177

pb 1 2 7 1 2 7 xyz 85.3968 -101.405 -98.0091
pb 1 2 8 1 2 8 xyz 85.7407 -103.492 -95.0397
pb 1 2 9 1 2 9 xyz 84.2652 -105.423 -86.3565
pb 1 2 6 1 2 6 xyz 93.0502 -99.9445 -101.665
pb 1 2 2 1 2 2 xyz 113.146 -83.2372 -102.250
pb 1 3 2 1 3 2 xyz 106.548 -70.3974 -113.299
pb 1 5 2 1 5 2 xyz 94.4212 -53.9933 -102.501
pb 1 5 3 1 5 3 xyz 88.9829 -59.7407 -106.670
pb 1 5 5 1 5 5 xyz 81.2117 -70.8537 -103.549
pb 1 5 8 1 5 8 xyz 71.3633 -79.9574 -93.9094
pb 1 5 7 1 5 7 xyz 73.0915 -78.0402 -95.8946
pb 1 4 9 1 4 9 xyz 68.6416 -89.1945 -89.3439
pb 1 4 7 1 4 7 xyz 74.0769 -85.3018 -101.007
pb 1 3 9 1 3 9 xyz 69.7111 -98.1268 -91.3271
pb 1 3 9 1 3 9 xyz 71.0264 -98.8887 -91.0522
pb 1 4 6 1 4 6 xyz 76.7833 -82.8910 -104.385
pb 1 2 2 1 2 2 xyz 110.812 -84.6390 -97.2442
pb 1 2 3 1 2 3 xyz 110.131 -89.4784 -103.309
pb 1 2 4 1 2 4 xyz 105.333 -92.0935 -104.633
pb 1 2 5 1 2 5 xyz 101.198 -96.5963 -103.910
pb 1 2 6 1 2 6 xyz 93.4441 -99.6737 -101.081
pb 1 2 7 1 2 7 xyz 89.3907 -102.303 -97.6668
pb 1 2 7 1 2 7 xyz 90.7377 -101.958 -95.7561
pb 1 2 8 1 2 8 xyz 89.2338 -104.028 -91.8827
pb 1 2 9 1 2 9 xyz 91.8399 -103.671 -84.3974
pb 1 2 9 1 2 9 xyz 86.5290 -106.722 -83.6037
pb 1 2 9 1 2 9 xyz 87.6070 -105.113 -85.5410
pb 1 2 9 1 2 9 xyz 86.0844 -104.720 -85.6872
pb 1 2 6 1 2 6 xyz 97.7382 -100.875 -97.2212
pb 1 2 7 1 2 7 xyz 92.4418 -102.844 -93.0361
pb 1 2 8 1 2 8 xyz 90.0441 -103.008 -90.5987

pb 1 2 5 1 2 5 xyz 102.343 -97.6020 -99.4401
pb 1 2 4 1 2 4 xyz 104.977 -93.8855 -100.161
pb 1 2 3 1 2 3 xyz 109.191 -89.5245 -98.9645
pb 1 3 2 1 3 2 xyz 107.524 -76.7212 -107.659
pb 1 3 3 1 3 3 xyz 104.389 -80.2054 -111.222
pb 1 3 4 1 3 4 xyz 99.3314 -85.3879 -111.425
pb 1 3 5 1 3 5 xyz 95.7449 -91.7399 -107.857
pb 1 3 5 1 3 5 xyz 93.3992 -90.6763 -109.621
pb 1 3 6 1 3 6 xyz 88.9218 -93.9534 -102.105
pb 1 3 6 1 3 6 xyz 87.2156 -95.7975 -105.470
pb 1 3 6 1 3 6 xyz 87.1144 -95.3762 -105.864
pb 1 3 7 1 3 7 xyz 84.9200 -97.1529 -99.0239
pb 1 3 7 1 3 7 xyz 82.8003 -97.5113 -101.466
pb 1 3 8 1 3 8 xyz 80.2200 -96.5070 -96.6251
pb 1 3 9 1 3 9 xyz 75.5111 -99.8501 -90.5855
pb 1 3 9 1 3 9 xyz 76.6922 -100.842 -89.0067
pb 1 4 2 1 4 2 xyz 101.598 -62.7041 -109.583
pb 1 4 3 1 4 3 xyz 95.6242 -68.7104 -111.918
pb 1 4 3 1 4 3 xyz 96.5344 -70.5694 -112.246
pb 1 4 2 1 4 2 xyz 103.111 -64.5596 -109.590
pb 1 4 4 1 4 4 xyz 91.9882 -76.1530 -111.915
pb 1 4 5 1 4 5 xyz 86.4537 -82.4002 -107.559
pb 1 4 6 1 4 6 xyz 81.5264 -86.9703 -105.070
pb 1 4 7 1 4 7 xyz 79.5808 -90.6664 -103.407
pb 1 4 7 1 4 7 xyz 77.1718 -90.5339 -103.290
pb 1 4 8 1 4 8 xyz 75.0718 -91.1392 -96.4459
pb 1 4 8 1 4 8 xyz 74.6482 -91.4012 -99.2022
pb 1 4 9 1 4 9 xyz 73.8444 -95.5688 -88.6201
pb 1 4 9 1 4 9 xyz 69.9366 -94.9080 -91.4133
pb 1 4 9 1 4 9 xyz 71.2238 -96.7192 -90.9860
pb 1 4 8 1 4 8 xyz 75.7296 -93.0414 -98.9438

pb 1 5 9 1 5 9 xyz 67.4552 -83.6454 -88.4012

pb 1 5 8 1 5 8 xyz 70.9179 -81.1132 -93.7732

pb 1 5 7 1 5 7 xyz 74.1187 -78.7782 -97.1927

pb 1 5 6 1 5 6 xyz 75.8910 -76.6918 -100.434

pb 1 5 5 1 5 5 xyz 80.1257 -73.5860 -104.503

pb 1 5 4 1 5 4 xyz 84.8865 -66.3775 -107.346

pb 1 5 2 1 5 2 xyz 94.6482 -53.1053 -101.515

relaxi ;5 6;1 2;50 .01 1

relaxi ;5 6;2 3;50 .01 1

relaxi ;5 6;3 4;50 .01 1

relaxi ;5 6;4 5;50 .01 1

relaxi ;5 6;5 6;50 .01 1

relaxi ;5 6;6 7;50 .01 1

relaxi ;5 6;7 8;50 .01 1

relaxi ;5 6;8 9;50 .01 1

relaxi ;5 6;9 10;50 .01 1

relaxi ;1 2;1 2;50 .01 1

relaxi ;1 2;2 3;50 .01 1

relaxi ;1 2;3 4;50 .01 1

relaxi ;1 2;4 5;50 .01 1

relaxi ;1 2;5 6;50 .01 1

relaxi ;1 2;6 7;50 .01 1

relaxi ;1 2;7 8;50 .01 1

relaxi ;1 2;8 9;50 .01 1

relaxi ;1 2;9 10;50 .01 1

relaxi ;2 5;1 2;50 .01 1

relaxi ;2 5;2 3;50 .01 1

relaxi ;2 5;3 4;50 .01 1

relaxi ;2 5;4 5;50 .01 1

relaxi ;2 5;5 6;50 .01 1

```
relaxi ;2 5;6 7;50 .01 1
relaxi ;2 5;7 8;50 .01 1
relaxi ;2 5;8 9;50 .01 1
relaxi ;2 5;9 10;50 .01 1

sfi ;5 6;1 9;sd 5
sfi ;1 2;1 10;sd 5
sfi ;2 5;1 2;sd 5
sfi ;2 5;2 3;sd 5
sfi ;2 5;3 4;sd 5
sfi ;2 5;4 5;sd 5
sfi ;2 5;5 6;sd 5
sfi ;2 5;6 7;sd 5
sfi ;2 5;7 8;sd 5
sfi ;2 5;8 9;sd 5
sfi ;2 5;9 10;sd 5

drs 1 1 1 1 6 10 j 0.8 0.8

c                    ===Assign Posterior to a Material Number===

mate 5


endpart

pplv

merge
```

c ===Tolerances between each capsular region (ABIGHL, PBIGHL, Axillary Pouch, Anterosuperior, and Poterior Regions)--used to merge nodes===

bptol 3 4 .8

bptol 5 4 .5

bptol 3 6 .9

bptol 6 7 .6

bptol 5 7 .67

stp 0

c ===Define nodes to be held rigid to scapula--i.e. insertion site===

nset scap = l
6720 6724 6728 6768 6772 6800:6803 6816 6817 6824:6826 6836 6837 6976 6992 7008:7010 7014 7015 7018 7019 7022 7023 7026:7028 7032 7033 7036 7037 7040 7041 7044 7312:7314 7318:7320 7324:7326 7330:7332 7336:7338 7342 7343 7346 7348:7350 7354 7355;

c ===Define nodes to be held rigid to humerus--i.e. insertion site===

nset hum = l
6755 6761 6767 6793 6799 6930:6933 6944 6945 6961:6963 6974 6975 6991 7007 7261:7263 7268 7269 7274 7275 7280 7281 7288:7290 7295 7296 7301 7302 7307 7308 7311 7617:7619 7626:7628 7635:7637 7644:7646 7653:7655 7660 7661 7664 7671:7673 7678 7679;

c ===Assign nodes in above node sets to be held rigid to scapual and humerus, respectively===

rigid scap rgm 7;

```
rigid hum rgm 6;

c ===Write input deck for NIKE3D===

nike3d
write
end
```

APPENDIX C

INPUT FILE FOR FINITE ELEMENT PRE-PROCESSOR: DISCRETE MODEL

```
title COMPOSITE FINITE ELEMENT MODEL

    c ... This is a subject-specific model of the glenohumeral capsule ...
    c ... AB-IGHL, PB-IGHL, Axillary pouch, Anteriorsuperior, and Posterior regions were
    included...
    c ... The articular cartilage of the humeral head was included in the geometry of the
    humerus since it is considered rigid  ...

    c === CONTROL DEFINITIONS ===
    c === POST-TRUEGRID MODIFICATIONS TO NIKE3D INPUT FILE ===
    nikeopts
    c ... CONTROL CARD 3 ...
     auto              c enable automatic timestepping
     nsteps 10           c number of timesteps
     delt 0.1            c initial delta-t
     mnss 1.0e-4           c minimum allowable timestep size
     mxss 0.10           c maximum allowable timestep size (negative = must point
     opnit 20            c optimal number of iterations per timestep
    c ... CONTROL CARD 4 ...
    c grav 7.071 0 -7.071 1
    c ... CONTROL CARD 5 ...
```

```
 iprt 999              c printout interval (keeps n3dhsp from getting huge)
 iplt 2               c plotting interval (plot every step to n3plot files)
 sw3                  c enable sense switch 3 (verbose output of augmented lag
 sw6                  c enable sense switch 6 (verbose output of convergence i
 igapfg 1              c interface gap plot flag
c ... CONTROL CARD 6 ...
 nsmd bfgs             c use bfgs solution method
 bwmo on               c bandwidth minimization on
 nbsr 1               c number of steps between stiffness reforms (every step)
 nbei 1               c number of steps between equilibrium iterations (every
 nibsr 1              c max number of equil (bfgs) iterations between stiffnes
 msrf 50              c maximum number of stiffness reforms per timestep
 dctol -0.01           c displacement norm convergence tolerance
 ectol 0.001          c energy norm convergence tolerance
c ... CONTROL CARD 7 ...
c anal dyn             c analysis type
c ... CONTROL CARD 8 ...
 maxmem 0
 stifcore 1           c store stiffness matrix in core (always do this - defau
 bfgscore             c store bfgs vectors in core (always do this - default i
 bfor 10              c brick element formulation (1 = bbar, 10 = 1 plus incor
 brstif               c enable brick element geometric stiffness
 lsolver fissle        c use fissle linear equation solver (this is default)
 nrest 999            c number of steps between restart file generation
 nsbrr 0              c number of steps between running restart file generatio
c altol 0.01           c set tolerance for augmented lagrangian iterations (ena
;
```

c ===Define Kinematics of Humeral Registration Block (i.e. True Grid Global C.S.) with respect to Scapular Registration Block using Load Curves===

c === LOAD CURVE DEFINITIONS ===

c ... prescribed translation along the global x-axis for humerus ...

include

C:\Truegrid\SubSpecFEM\Kinematics\Joint_Kinematics\60ER\HumwrtScap\dx.txt

c ... prescribed translation along the global y-axis for humerus ...

include

C:\Truegrid\SubSpecFEM\Kinematics\Joint_Kinematics\60ER\HumwrtScap\dy.txt

c ... prescribed translation along the global z-axis for humerus ...

include

C:\Truegrid\SubSpecFEM\Kinematics\Joint_Kinematics\60ER\HumwrtScap\dz.txt

c ... prescribed rotation about global x-axis for humerus (external rotation)...

include

C:\Truegrid\SubSpecFEM\Kinematics\Joint_Kinematics\60ER\HumwrtScap\rx.txt

c ... prescribed rotation about global y-axis for humerus (abduction) ...

include

C:\Truegrid\SubSpecFEM\Kinematics\Joint_Kinematics\60ER\HumwrtScap\ry.txt

c ... prescribed rotation about global z-axis for humerus (extension)...

include

C:\Truegrid\SubSpecFEM\Kinematics\Joint_Kinematics\60ER\HumwrtScap\rz.txt

c ===Move parts such that the Humeral Registration Block is aligned with the True Grid global C.S.===

lev 1 levct 1 v -118.849 22.1506 77.1414 tf rt 0 0 0 rt 0.973839 0.22715 0.00639683 rt 0.0192865 -0.054571 -0.998324;;
pslv 1

c ===Define 1st material (AB-IGHL)===

nikemats 1 1
mhead ABIGHL
shell
shth 2.0
rho 0.0007
e 2.05
pr 0.4995;

c ===Define 2nd material (Axillary Pouch)===

nikemats 2 1
mhead AxPouch
shell
shth 2.0
rho 0.0007
e 4.92
pr 0.4995;

c ===Define 3rd material (PB-IGHL)===

nikemats 3 1
mhead PBIGHL

```
shell
shth 2.0
rho 0.0007
e 3.73
pr 0.4995;

c                ===Define 4th material (Anterosuperior Region)===

nikemats 4 1
mhead AntSup
shell
shth 2.0
rho 0.0007
e 2.12
pr 0.4995;

c                ===Define 5th material (Posterior Region)===

nikemats 5 1
mhead PostCaps
shell
shth 2.0
rho 0.0007
e 5.83
pr 0.4995;

c                ===Define 6th material (Humerus)===

nikemats 6 20
 mhead humerus material - rigid
 shell
```

```
shth 0.5
rho 1000
e 1e4
pr .3
xtrans 1
ytrans 2
ztrans 3
xrot 4
yrot 5
zrot 6
comflg 1  c center-of-mass flag (if "1", you need to provide coords below)
xcom 0
ycom 0
zcom 0
;

readmesh dyna3d
C:\Truegrid\SubSpecFEM\Simplified_Geometry\attempt8\Geometry\humerusv5sm.d
endpart

c                ===Define 7th material (Scapula)===

nikemats 7 20
mhead scapula material - rigid
shell
shth 0.5
rho 1000
e 1e4
pr .3
xtrans -1
ytrans -1
```

ztrans -1
xrot -1
yrot -1
zrot -1
comflg 1 c center-of-mass flag (if "1", you need to provide coords below)
xcom 16.1987
ycom 15.5346
zcom 94.167
;

readmesh dyna3d
C:\Truegrid\SubSpecFEM\Simplified_Geometry\attempt8\Geometry\scapulav6bsm.d
endpart

pplv

c ===Input Geometry of Capsuloligamentous Regions (AB-IGHL, PB-IGHL, Axillary pouch, Anteriorsuperior, and Posterior regions)===

vpsd 1
C:\Truegrid\SubSpecFEM\Simplified_Geometry\attempt8\Geometry\ABIGHLv9f.cor
C:\Truegrid\SubSpecFEM\Simplified_Geometry\attempt8\Geometry\ABIGHLv9f.elm;
vpsd 2
C:\Truegrid\SubSpecFEM\Simplified_Geometry\attempt8\Geometry\PBIGHLv8c.cor
C:\Truegrid\SubSpecFEM\Simplified_Geometry\attempt8\Geometry\PBIGHLv8c.elm;
vpsd 3
C:\Truegrid\SubSpecFEM\Simplified_Geometry\attempt8\Geometry\AxPouchv9f.cor
C:\Truegrid\SubSpecFEM\Simplified_Geometry\attempt8\Geometry\AxPouchv9f.elm;
vpsd 4
C:\Truegrid\SubSpecFEM\Simplified_Geometry\attempt8\Geometry\AntSupCapsv10c.cor
C:\Truegrid\SubSpecFEM\Simplified_Geometry\attempt8\Geometry\AntSupCapsv10c.elm;

vpsd 5
C:\Truegrid\SubSpecFEM\Simplified_Geometry\attempt8\Geometry\PostCapsv10c.cor
C:\Truegrid\SubSpecFEM\Simplified_Geometry\attempt8\Geometry\PostCapsv10c.elm;

merge

c ===Move surfaces the same amount as bones and registration blocks were moved (See above)==

lev 1 levct 1 v -118.849 22.1506 77.1414 tf rt 0 0 0 rt 0.973839 0.22715 0.00639683 rt 0.0192865 -0.054571 -0.998324;;
pslv 1

c ===Import Curves used for creating meshes===

include
C:\Truegrid\SubSpecFEM\Simplified_Geometry\attempt8\3Dcurves\ABIGHL3Dcurves.txt
include
C:\Truegrid\SubSpecFEM\Simplified_Geometry\attempt8\3Dcurves\AxPouch3Dcurves.txt
include
C:\Truegrid\SubSpecFEM\Simplified_Geometry\attempt8\3Dcurves\PBIGHL3Dcurves.txt
include
C:\Truegrid\SubSpecFEM\Simplified_Geometry\attempt8\3Dcurves\AntSup3Dcurves.txt
include
C:\Truegrid\SubSpecFEM\Simplified_Geometry\attempt8\3Dcurves\PostCap3Dcurves.txt

c ===Create Mesh for ABIGHL

c ====mesh for ABIGHL===

block 1 3 5; 1 4 7 10 16; -1;

89 96.5 104; -96 -90 -65 -43 -39; -55;

c ===Move mesh with respect to the AB-IGHL surface===

tri 1 3; 1 5; -1; v -93.9775 76.4280 56.8798 tf rt 93.9775 -76.4280 -56.8798
rt 94.9616 -76.2571 -56.8315 rt 93.8051 -75.4434 -56.8507;
mbi 1 3; 1 5; -1; xyz 3.75607 2.66348 -1.18632
tri 1 3; 1 5; -1; v -105.448 65.6949 55.1480 tf rt 105.448 -65.6949 -55.1480
rt 106.361 -65.7056 -55.5561 rt 105.424 -64.6984 -55.2287;
mbi 1 3; 1 5; -1; xyz 4.64805 1.00077 -3.85280
mbi 1 3; 1 5; -1; xyz 2.29996 -0.167995 -1.17682
mbi 1 3; 1 5; -1; xyz -2.73335 -0.338181 1.40851
mbi 1 3; 1 5; -1; xyz 0.401512 -0.852127 -0.190453

c ===Attach edges of mesh to curves===

cure 3 1 1 3 2 1 10032
cure 3 2 1 3 4 1 3
cure 3 4 1 3 5 1 10031
curs 2 1 1 2 5 1 1005
cure 1 2 1 1 4 1 1001
cure 1 1 1 1 2 1 100112
cure 1 4 1 1 5 1 100111
curs 1 1 1 3 1 1 1004
curs 1 5 1 3 5 1 1002

c ==Manually move edges of mesh along curves===

pb 2 5 1 2 5 1 xyz 93.2409 -40.3031 -66.6451
pb 2 5 1 2 5 1 xyz 91.7412 -40.0011 -67.3080
pb 1 5 1 1 5 1 xyz 90.5344 -42.4738 -63.4847

pb 2 4 1 2 4 1 xyz 96.7856 -45.3001 -62.3383
pb 2 4 1 2 4 1 xyz 96.0593 -45.0866 -62.8391
pb 2 4 1 2 4 1 xyz 95.5101 -44.3431 -63.1756
pb 2 4 1 2 4 1 xyz 95.1356 -45.7164 -64.1275
pb 2 4 1 2 4 1 xyz 95.3609 -45.6257 -63.8033
pb 2 3 1 2 3 1 xyz 100.696 -60.8594 -60.0477
pb 2 3 1 2 3 1 xyz 100.762 -61.1074 -60.1813
pb 1 2 1 1 2 1 xyz 99.0825 -86.7569 -61.7780
pb 1 1 1 1 1 1 xyz 101.756 -95.1652 -65.7868
pb 2 1 1 2 1 1 xyz 103.606 -91.7460 -64.7023
pb 1 2 1 1 2 1 xyz 99.7349 -91.7329 -63.3302
pb 2 2 1 2 2 1 xyz 102.771 -88.1667 -63.2953
pb 2 2 1 2 2 1 xyz 102.233 -88.4592 -63.6269
pb 2 3 1 2 3 1 xyz 101.080 -68.8745 -60.6802
pb 1 3 1 1 3 1 xyz 96.1207 -72.8853 -58.3479
pb 2 3 1 2 3 1 xyz 101.085 -70.3803 -60.6351
pb 1 4 1 1 4 1 xyz 92.7571 -49.5436 -60.0227
pb 2 4 1 2 4 1 xyz 95.5277 -46.9637 -63.3701
pb 1 4 1 1 4 1 xyz 93.3148 -50.5880 -59.1106
pb 2 4 1 2 4 1 xyz 96.3280 -47.4752 -62.8540
pb 1 3 1 1 3 1 xyz 97.1909 -74.1196 -58.7196
pb 1 3 1 1 3 1 xyz 97.2025 -75.1687 -58.7475
pb 2 3 1 2 3 1 xyz 101.482 -71.6844 -60.5576
pb 2 2 1 2 2 1 xyz 101.750 -86.1421 -62.8927
pb 2 2 1 2 2 1 xyz 101.528 -83.4576 -62.5255
pb 2 3 1 2 3 1 xyz 100.860 -67.8889 -60.6404
pb 2 3 1 2 3 1 xyz 101.521 -68.6602 -60.6843
pb 2 4 1 2 4 1 xyz 96.3818 -45.8749 -62.2893
pb 2 4 1 2 4 1 xyz 96.0484 -44.5162 -62.7031
pb 2 2 1 2 2 1 xyz 101.568 -81.8916 -62.1524
pb 2 2 1 2 2 1 xyz 101.891 -82.9185 -62.2838

c ===Relax the mesh===

relaxi 1 2;4 5; ;50 .01 1

relaxi 1 2;3 4; ;50 .01 1

relaxi 2 3;4 5; ;50 .01 1

relaxi 2 3;3 4; ;50 .01 1

relaxi 1 2;2 3; ;50 .01 1

relaxi 2 3;2 3; ;50 .01 1

relaxi 1 2;1 2; ;50 .01 1

relaxi 2 3;1 2; ;50 .01 1

c ===Project mesh to surface of AB-IGHL===

sfi 1 2; 1 5; -1; sd 1

sfi 2 3; 4 5; -1; sd 1

sfi 2 3; 1 2; -1; sd 1

c ===scale elements in Medial-to-lateral direction such that elements near insertions sites are larger than those at midsubstance===

drs 1 1 1 3 5 1 j 0.8 0.8

c ===Assign ABIGHL to a Material Number===

mate 1

c ===This command flips direction of shell normals===

orpt flip

N 1 1 1 3 5 1

```
endpart

merge

c ===Define nodes to be held rigid to scapula--i.e. insertion site===

nset scap = l
 6720 6724 6728 6768 6772;

c ===Define nodes to be held rigid to humerus--i.e. insertion site===

nset hum = l
 6755 6761 6767 6793 6799;


c ===Assign nodes in above node sets to be held rigid to scapual and humerus, respectively===

rigid scap rgm 3;

rigid hum rgm 2;

c ===Write input deck for NIKE3D===

nike3d
write
end
```

BIBLIOGRAPHY

1. DePalma, A.F., G. Callery, and G.A. Bennett, *Variational anatomy and degenerative lesions of the shoulder joint.* American Academy of Orthopaedic Surgery Instructional Course Lecture Series, 1949. **6**: p. 225-81.

2. Cave, E., J. Burke, and R. Boyd, *Trauma Management*. 1974, Chicago, IL: Year Book Medical Publishers. 437.

3. Arciero, R.A., et al., *Arthroscopic Bankart repair versus nonoperative treatment for acute, initial anterior shoulder dislocations.* Am J Sports Med, 1994. **22**(5): p. 589-94.

4. Baker, C.L., J.W. Uribe, and C. Whitman, *Arthroscopic evaluation of acute initial anterior shoulder dislocations.* Am J Sports Med, 1990. **18**(1): p. 25-8.

5. Caspari, R.B., *Arthroscopic reconstruction for anterior shoulder instability.* Techniques in Orthopaedics, 1988. **3**: p. 59-66.

6. Field, L.D., D.J. Bokor, and F.H. Savoie, 3rd, *Humeral and glenoid detachment of the anterior inferior glenohumeral ligament: a cause of anterior shoulder instability.* J Shoulder Elbow Surg, 1997. **6**(1): p. 6-10.

7. Lee, T.Q., et al., *Age related biomechanical properties of the glenoid-anterior band of the inferior glenohumeral ligament-humerus complex.* Clin Biomech (Bristol, Avon), 1999. **14**(7): p. 471-6.

8. Morgan, C.D. and A.B. Bodenstab, *Arthroscopic Bankart suture repair: technique and early results.* Arthroscopy, 1987. **3**(2): p. 111-22.

9. Henry, J.H. and J.A. Genung, *Natural history of glenohumeral dislocation--revisited.* Am J Sports Med, 1982. **10**(3): p. 135-7.

10. Sperber, A., et al., *Comparison of an arthroscopic and an open procedure for posttraumatic instability of the shoulder: a prospective, randomized multicenter study.* J Shoulder Elbow Surg, 2001. **10**(2): p. 105-8.

11. Black, K.P., et al., *Biomechanics of the Bankart repair: the relationship between glenohumeral translation and labral fixation site.* Am J Sports Med, 1999. **27**(3): p. 339-44.

12. Boardman, N.D., et al., *Tensile properties of the superior glenohumeral and coracohumeral ligaments.* J Shoulder Elbow Surg, 1996. **5**(4): p. 249-54.

13. Debski, R.E., et al., *An analytical approach to determine the in situ forces in the glenohumeral ligaments.* J Biomech Eng, 1999. **121**(3): p. 311-5.

14. Debski, R.E., et al., *In situ force distribution in the glenohumeral joint capsule during anterior-posterior loading.* J Orthop Res, 1999. **17**(5): p. 769-76.

15. McMahon, P.J., et al., *The anterior band of the inferior glenohumeral ligament. Assessment of its permanent deformation and the anatomy of its glenoid attachment.* J Bone Joint Surg Br, 1999. **81**(3): p. 406-13.

16. McMahon, P.J., et al., *Variation in the histologic anatomy of the glenoid origin of the anterior band of the IGHL.* Transcripts of the Orthopaedic Research Society, 1999. **24**.

17. McMahon, P.J., et al., *The anterior band of the inferior glenohumeral ligament: biomechanical properties from tensile testing in the position of apprehension.* J Shoulder Elbow Surg, 1998. **7**(5): p. 467-71.

18. Novotny, J.E., B.D. Beynnon, and C.E. Nichols, *Modeling the stability of the human glenohumeral joint during external rotation.* J Biomech, 2000. **33**(3): p. 345-54.

19. O'Connell, P.W., et al., *The contribution of the glenohumeral ligaments to anterior stability of the shoulder joint.* Am J Sports Med, 1990. **18**(6): p. 579-84.

20. Stefko, J.M., et al., *Strain of the anterior band of the inferior glenohumeral ligament during capsule failure.* J Shoulder Elbow Surg, 1997. **6**(5): p. 473-9.

21. Ellis, B.J., et al., *Methodology and Sensitivity Studies for Finite Element Modeling of the Inferior Glenohumeral Ligament Complex.* J Biomech, 2006. **In Press**.

22. Newman, W.J., et al. *Function of the anterior band of the inferior glenohumeral ligament during the load and shift test*. in *ASME Advances in Bioengineering*. 2002.

23. Debski, R.E., et al., *Stress and strain in the anterior band of the inferior glenohumeral ligament during a simulated clinical examination.* J Shoulder Elbow Surg, 2005. **14**(1 Suppl S): p. 24S-31S.

24. Turkel, S.J., et al., *Stabilizing mechanisms preventing anterior dislocation of the glenohumeral joint.* J Bone Joint Surg Am, 1981. **63**(8): p. 1208-17.

25. Miller, M.C., et al., *A mathematical and experimental model of length change in the inferior glenohumeral ligament in the late cocking phase of pitching.* Transcripts of the Orthopaedic Research Society, 1991. **16**: p. 609.

26. McMahon, P.J., et al., *Deformation and strain characteristics along the length of the anterior band of the inferior glenohumeral ligament.* J Shoulder Elbow Surg, 2001. **10**(5): p. 482-8.

27. Itoi, E., et al., *Capsular properties of the shoulder.* Tohoku J Exp Med, 1993. **171**(3): p. 203-10.

28. Bigliani, L.U., et al., *Tensile properties of the inferior glenohumeral ligament.* J Orthop Res, 1992. **10**(2): p. 187-97.

29. Ticker, J.B., et al., *Inferior glenohumeral ligament: geometric and strain-rate dependent properties.* J Shoulder Elbow Surg, 1996. **5**(4): p. 269-79.

30. Kuhn, J.E., et al., *Ligamentous restraints to external rotation of the humerus in the late-cocking phase of throwing. A cadaveric biomechanical investigation.* Am J Sports Med, 2000. **28**(2): p. 200-5.

31. Kuhn, J.E., et al., *External rotation of the glenohumeral joint: ligament restraints and muscle effects in the neutral and abducted positions.* J Shoulder Elbow Surg, 2005. **14**(1 Suppl S): p. 39S-48S.

32. Soslowsky, L.J., D.M. Malicky, and R.B. Blasier, *Active and passive factors in inferior glenohumeral stabilization: a biomechanical model.* J Shoulder Elbow Surg, 1997. **6**(4): p. 371-9.

33. Malicky, D.M., et al., *Anterior glenohumeral stabilization factors: progressive effects in a biomechanical model.* J Orthop Res, 1996. **14**(2): p. 282-8.

34. Reeves, B., *Experiments on the tensile strength of the anterior capsular structures of the shoulder in man.* J Bone Joint Surg Br, 1968. **50**(4): p. 858-65.

35. Curl, L.A. and R.F. Warren, *Glenohumeral joint stability. Selective cutting studies on the static capsular restraints.* Clin Orthop Relat Res, 1996(330): p. 54-65.

36. Malicky, D.M., et al., *Total strain fields of the antero-inferior shoulder capsule under subluxation: a stereoradiogrammetric study.* J Biomech Eng, 2001. **123**(5): p. 425-31.

37. Soslowsky, L.J., et al. *Total and non-recoverable strain fields of the glenohumeral joint capsule under shoulder subluxation*. in *Open Meeting, American Shoulder Elbow Surgeons*. 2000. Orlando, FL.

38. Hawkins, R.J. and N.G. Mohtadi, *Controversy in anterior shoulder instability.* Clin Orthop Relat Res, 1991(272): p. 152-61.

39. Nelson, B.J. and R.A. Arciero, *Arthroscopic management of glenohumeral instability.* Am J Sports Med, 2000. **28**(4): p. 602-14.

40. Hovelius, L., *Incidence of shoulder dislocation in Sweden.* Clin Orthop, 1982(166): p. 127-31.

41. *United States Census 2000*. 2000, United States Census Bureau.

42. Hovelius, L., *Shoulder dislocation in Swedish ice hockey players.* Am J Sports Med, 1978. **6**(6): p. 373-7.

43. Zebas, C.J., et al., *Musculoskeletal injuries in a college-age population during a 1-semester term.* J Am Coll Health, 1995. **44**(1): p. 32-4.

44. Rowe, C.R., B. Zarins, and J.V. Ciullo, *Recurrent anterior dislocation of the shoulder after surgical repair. Apparent causes of failure and treatment.* J Bone Joint Surg Am, 1984. **66**(2): p. 159-68.

45. Warren, R.F., *Subluxation of the shoulder in athletes.* Clin Sports Med, 1983. **2**(2): p. 339-54.

46. Liu, S.H. and M.H. Henry, *Anterior shoulder instability. Current review.* Clin Orthop, 1996(323): p. 327-37.

47. Neer, C.S., 2nd and C.R. Foster, *Inferior capsular shift for involuntary inferior and multidirectional instability of the shoulder. A preliminary report.* J Bone Joint Surg Am, 1980. **62**(6): p. 897-908.

48. Deutsch, A., et al., *Anterior-inferior capsular shift of the shoulder: a biomechanical comparison of glenoid-based versus humeral-based shift strategies.* J Shoulder Elbow Surg, 2001. **10**(4): p. 340-52.

49. Speer, K.P., et al., *Strategies for an anterior capsular shift of the shoulder. A biomechanical comparison.* Am J Sports Med, 1995. **23**(3): p. 264-9.

50. Hovelius, L., *Anterior dislocation of the shoulder in teen-agers and young adults. Five-year prognosis.* J Bone Joint Surg Am, 1987. **69**(3): p. 393-9.

51. McLaughlin, H.L. and D.I. MacLellan, *Recurrent anterior dislocation of the shoulder. II. A comparative study.* J Trauma, 1967. **7**(2): p. 191-201.

52. Simonet, W.T. and R.H. Cofield, *Prognosis in anterior shoulder dislocation.* Am J Sports Med, 1984. **12**(1): p. 19-24.

53. Wheeler, J.H., et al., *Arthroscopic versus nonoperative treatment of acute shoulder dislocations in young athletes.* Arthroscopy, 1989. **5**(3): p. 213-7.

54. Neviaser, R.J., T.J. Neviaser, and J.S. Neviaser, *Anterior dislocation of the shoulder and rotator cuff rupture.* Clin Orthop, 1993(291): p. 103-6.

55. Montgomery, W.H., 3rd and F.W. Jobe, *Functional outcomes in athletes after modified anterior capsulolabral reconstruction.* Am J Sports Med, 1994. **22**(3): p. 352-8.

56. Bigliani, L.U., et al., *Inferior capsular shift procedure for anterior-inferior shoulder instability in athletes.* Am J Sports Med, 1994. **22**(5): p. 578-84.

57. Rockwood, C.A., et al., *The Shoulder*. 2nd ed. 1998, Philadelphia, PA: W. B. Saunders Co.

58. Moore, S.M., et al. *Anatomy and Function of the Inferior Glenohumeral Ligament of the Shoulder: Is our Description Correct?* in *Summer Bioengineering Conference*. 2006. Amelia Island Plantation, Amelia Island, Florida, USA.

59. Beynnon, B., et al., *The measurement of anterior cruciate ligament strain in vivo.* Int Orthop, 1992. **16**(1): p. 1-12.

60. Beynnon, B.D., et al., *Anterior cruciate ligament strain behavior during rehabilitation exercises in vivo.* Am J Sports Med, 1995. **23**(1): p. 24-34.

61. Musahl, V., et al., *The use of porcine small intestinal submucosa to enhance the healing of the medial collateral ligament--a functional tissue engineering study in rabbits.* Journal of Orthopaedic Research, 2004. **22**(1): p. 214-20.

62. Race, A. and A.A. Amis, *The mechanical properties of the two bundles of the human posterior cruciate ligament.* J Biomech, 1994. **27**(1): p. 13-24.

63. Woo, S.L., *Mechanical properties of tendons and ligaments. I. Quasi-static and nonlinear viscoelastic properties.* Biorheology, 1982. **19**(3): p. 385-96.

64. Woo, S.L., K.J. Ohland, and J.A. Weiss, *Aging and sex-related changes in the biomechanical properties of the rabbit medial collateral ligament.* Mech Ageing Dev, 1990. **56**(2): p. 129-42.

65. Gardiner, J.C. and J.A. Weiss, *Subject-specific finite element models can predict strain in the human medial collateral ligament during valgus knee loading.* J Orthop Res, 2002. **In press**.

66. Malicky, D.L., et al., *Total and nonrecoverable strain fields of the glenohumeral joint capsule under shoulder subluxation.* Transcripts of the Orthopaedic Research Society, 1999. **40**: p. 94.

67. Quapp, K.M. and J.A. Weiss, *Material characterization of human medial collateral ligament.* Journal of Biomechanical Engineering, 1998. **120**(6): p. 757-63.

68. Urayama, M., et al., *Function of the 3 portions of the inferior glenohumeral ligament: a cadaveric study.* J Shoulder Elbow Surg, 2001. **10**(6): p. 589-94.

69. O'Brien, S.J., et al., *The anatomy and histology of the inferior glenohumeral ligament complex of the shoulder.* Am J Sports Med, 1990. **18**(5): p. 449-56.

70. Song, Y., et al., *A three-dimensional finite element model of the human anterior cruciate ligament: a computational analysis with experimental validation.* J Biomech, 2004. **37**(3): p. 383-90.

71. Weiss, J.A., et al., *Three-dimensional finite element modeling of ligaments: Technical aspects.* Med Eng Phys, 2005. **27**(10): p. 845-61.

72. Weiss, J.A., J.C. Gardiner, and C. Bonifasi-Lista, *Ligament material behavior is nonlinear, viscoelastic and rate-independent under shear loading.* J Biomech, 2002. **35**(7): p. 943-50.

73. Bey, M.J., et al., *Structural and mechanical properties of the glenohumeral joint posterior capsule.* J Shoulder Elbow Surg, 2005. **14**(2): p. 201-6.

74. Gohlke, F., B. Essigkrug, and F. Schmitz, *The patterns of the collagen fiber bundles of the capsule of the glenohumeral joint.* J Shoulder Elbow Surg, 1994. **3**(3): p. 111-28.

75. Woo, S.L., et al., *The use of a laser micrometer system to determine the cross-sectional shape and area of ligaments: a comparative study with two existing methods.* J Biomech Eng, 1990. **112**(4): p. 426-31.

76. Scheffler, S.U., et al., *Structure and function of the healing medial collateral ligament in a goat model.* Ann Biomed Eng, 2001. **29**(2): p. 173-80.

77. Smutz, W.P., et al., *Accuracy of a video strain measurement system.* J Biomech, 1996. **29**(6): p. 813-7.

78. Ohno, K., et al., *Healing of the medial collateral ligament after a combined medial collateral and anterior cruciate ligament injury and reconstruction of the anterior cruciate ligament: comparison of repair and nonrepair of medial collateral ligament tears in rabbits.* J Orthop Res, 1995. **13**(3): p. 442-9.

79. Whittaker, P. and P.B. Canham, *Demonstration of quantitative fabric analysis of tendon collagen using two-dimensional polarized light microscopy.* Matrix, 1991. **11**(1): p. 56-62.

80. Dickey, J.H., BR; Dumas, GA; Bednar DA, *Measuring collagen fiber orientation: a two-dimensional quantitative macroscopic technique.* J Biomech Eng, 1998. **120**(4): p. 537-40.

81. Sacks, M.S., D.B. Smith, and E.D. Hiester, *A small angle light scattering device for planar connective tissue microstructural analysis.* Ann Biomed Eng, 1997. **25**(4): p. 678-89.

82. Sacks, M.S., C.J. Chuong, and R. More, *Collagen fiber architecture of bovine pericardium.* Asaio J, 1994. **40**(3): p. M632-7.

83. Sacks, M.S. and D.C. Gloeckner, *Quantification of the fiber architecture and biaxial mechanical behavior of porcine intestinal submucosa.* J Biomed Mater Res, 1999. **46**(1): p. 1-10.

84. Hamann, M.C., M.S. Sacks, and T.I. Malinin, *Quantification of the collagen fibre architecture of human cranial dura mater.* J Anat, 1998. **192 (Pt 1)**: p. 99-106.

85. Hiester, E.D. and M.S. Sacks, *Optimal bovine pericardial tissue selection sites. I. Fiber architecture and tissue thickness measurements.* J Biomed Mater Res, 1998. **39**(2): p. 207-14.

86. Stabile, K.J., et al. *Longitudinal and Transverse Mechanical Properties of the Interosseous Ligament of the Forearm*. in *Bioengineering Conference ASME 2001*. 2001.

87. Hewitt, J., et al., *Regional material properties of the human hip joint capsule ligaments.* J Orthop Res, 2001. **19**(3): p. 359-64.

88. Butler, D., M. Kay, and D. Stouffer, *Comparison of material properties in the fascicle-bone units from human patellar tendon and knee ligaments.* J Biomech, 1986. **19**: p. 425-432.

89. Weiss, J.A., B.N. Maker, and S. Govindjee, *Finite element implementation of incompressible, transversely isotropic hyperelasticity.* Comp Meth Appl Mech Eng, 1996. **135**: p. 107-28.

90. Refior, H.J. and D. Sowa, *Long tendon of the biceps brachii: sites of predilection for degenerative lesions.* J Shoulder Elbow Surg, 1995. **4**(6): p. 436-40.

91. Woo, S.L., et al., *Biomechanics of knee ligaments.* Am J Sports Med, 1999. **27**(4): p. 533-43.

92. Burkart, A., et al., *Glenohumeral translations are only partially restored after repair of the type II SLAP lesion.* American Journal of Sports Medicine, 2002. **In press**.

93. Burkart, A.C. and R.E. Debski, *Anatomy and function of the glenohumeral ligaments in anterior shoulder instability.* Clin Orthop, 2002(400): p. 32-9.

94. Rudy, T.W., et al., *A combined robotic/universal force sensor approach to determine in situ forces of knee ligaments.* J Biomech, 1996. **29**(10): p. 1357-60.

95. Livesay, G.A., et al., *Evaluation of the effect of joint constraints on the in situ force distribution in the anterior cruciate ligament.* J Orthop Res, 1997. **15**(2): p. 278-84.

96. Livesay, G.A., et al., *Determination of the in situ forces and force distribution within the human anterior cruciate ligament.* Ann Biomed Eng, 1995. **23**(4): p. 467-74.

97. Li, G., et al., *A validated three-dimensional computational model of a human knee joint.* J Biomech Eng, 1999. **121**(6): p. 657-62.

98. Li, G., J. Suggs, and T. Gill, *The effect of anterior cruciate ligament injury on knee joint function under a simulated muscle load: a three-dimensional computational simulation.* Ann Biomed Eng, 2002. **30**(5): p. 713-20.

99. Zeminski, J., *Development of a combined analytical and experimental approach to reproduce knee kinematics for the evaluation of anterior cruciate ligament function*, in *Mechanical Engineering*. 2001, University of Pittsburgh: Pittsburgh, PA.

100. Fischer, K.J., et al., *A method for measuring joint kinematics designed for accurate registration of kinematic data to models constructed from CT data.* J Biomech, 2001. **34**(3): p. 377-83.

101. Anderson, A.E., et al., *Subject-specific finite element model of the pelvis: development, validation and sensitivity studies.* J Biomech Eng, 2005. **127**(3): p. 364-73.

102. Moore, S.M., et al., *Multidirectional kinematics of the glenohumeral joint during simulated simple translation tests: impact on clinical diagnoses.* J Orthop Res, 2004. **22**(4): p. 889-94.

103. Moore, S.M., et al., *Bi-directional mechanical properties of the posterior region of the glenohumeral capsule.* J Biomech, 2005. **38**(6): p. 1365-9.

104. Moore, S.M., P.J. McMahon, and R.E. Debski, *Bi-directional Mechanical Properties of the Axillary Pouch of the Glenohumeral Capsule: Implications for Surgical Repair.* J Biomech Eng, 2004. **126**(2): p. 284-288.

105. Parry, D.A., *The molecular and fibrillar structure of collagen and its relationship to the mechanical properties of connective tissue.* Biophys Chem, 1988. **29**(1-2): p. 195-209.

106. Woo, S.L., et al., *Tensile properties of the human femur-anterior cruciate ligament-tibia complex. The effects of specimen age and orientation.* Am J Sports Med, 1991. **19**(3): p. 217-25.

107. Woo, S.L.-Y., M.A. Gomez, and W.H. Akeson, *The time and history-dependent viscoelastic properties of the canine medical collateral ligament.* J Biomech Eng, 1981. **103**(4): p. 293-8.

108. Delp, S.L. and J.P. Loan, *A graphics-based software system to develop and analyze models of musculoskeletal structures.* Comput Biol Med, 1995. **25**(1): p. 21-34.

109. Delp, S.L., A.S. Arnold, and S.J. Piazza, *Graphics-based modeling and analysis of gait abnormalities.* Biomed Mater Eng, 1998. **8**(3-4): p. 227-40.

110. Little, R.B., et al., *A three-dimensional finite element analysis of the upper tibia.* J Biomech Eng, 1986. **108**(2): p. 111-9.

111. Maker, B.N., R.M. Ferencz, and J.O. Hallquist, *NIKE3D: A nonlinear, implicit, three-dimensional finite element code for solid and structural mechanics*. 1990, Lawrence Livermore National Laboratory.

112. Maker, B.N., *Rigid bodies for metal forming analysis with NIKE3D*. 1995, University of California, Lawrence Livermore Laboratory. p. 1-8.

113. Simo, J.C., *On the dynamics in space of rods undergoing large motions: A geometrically exact approach.* Comp Meth Appl Mech Eng, 1988. **66**: p. 125-161.

114. Weiss, J.A., D.A. Schauer, and J.C. Gardiner. *Modeling contact in biological joints using penalty and augmented Lagrangian methods*. in *ASME Winter Annual Meeting*. 1996.

115. Weiss, J.A., B.N. Maker, and D.A. Schauer. *Treatment of initial stress in hyperelastic finite element models of soft tissues*. in *ASME Summer Bioengineering Conference*. 1995.

116. Gardiner, J.C. and J.A. Weiss, *Simple shear testing of parallel-fibered planar soft tissues.* Journal of Biomechanics, 2001. **123**: p. 1-5.

117. Matthies, H. and G. Strang, *The solution of nonlinear finite element equations.* Int J Numer Methods Engng, 1979. **14**: p. 1613-26.

118. O'Brien, S.J., et al., *Capsular restraints to anterior-posterior motion of the abducted shoulder: a biomechanical study.* J Shoulder Elbow Surg, 1995. **4**(4): p. 298-308.

119. Ovesen, J. and S. Nielsen, *Stability of the shoulder joint. Cadaver study of stabilizing structures.* Acta Orthop Scand, 1985. **56**(2): p. 149-51.

120. Ovesen, J. and S. Nielsen, *Posterior instability of the shoulder. A cadaver study.* Acta Orthop Scand, 1986. **57**(5): p. 436-9.

121. Ovesen, J. and S. Nielsen, *Anterior and posterior shoulder instability. A cadaver study.* Acta Orthop Scand, 1986. **57**(4): p. 324-7.

122. Chen, S., et al., *The effects of thermal capsular shrinkage on the outcomes of arthroscopic stabilization for primary anterior shoulder instability.* Am J Sports Med, 2005. **33**(5): p. 705-11.

123. Levine, W.N., L.U. Bigliani, and C.S. Ahmad, *Thermal capsulorrhaphy.* Orthopedics, 2004. **27**(8): p. 823-6.

124. Debski, R.E., et al., *The collagen fibers of the anteroinferior capsulolabrum have multiaxial orientation to resist shoulder dislocation.* J Shoulder Elbow Surg, 2003. **12**(3): p. 247-52.

125. Warner, J.J.P., et al., *Dynamic capsuloligamentous anatomy of the glenohumeral joint.* J Shoulder Elbow Surg, 1993. **2**: p. 115-33.

126. Brenneke, S.L., et al., *Glenohumeral kinematics and capsulo-ligamentous strain resulting from laxity exams.* Clin Biomech (Bristol, Avon), 2000. **15**(10): p. 735-42.